



UNIVERSIDADE FEDERAL DE ITAJUBÁ

**PROGRAMA DE PÓS-GRADUAÇÃO EM MEIO AMBIENTE E RECURSOS
HÍDRICOS**

**ENERGIAS HÍDRICA, EÓLICA E SOLAR NO BRASIL: MUDANÇAS
PROJETADAS PELOS MODELOS CLIMÁTICOS DO CMIP6**

Glauber Willian de Souza Ferreira

Itajubá/MG

Março 2025



UNIVERSIDADE FEDERAL DE ITAJUBÁ
COORDENAÇÃO DE CURSO DE PÓS-GRADUAÇÃO EM MEIO
AMBIENTE E RECURSOS HÍDRICOS

ATA Nº 2

Às treze horas e trinta minutos do dia doze de março de dois mil vinte e cinco, no(a) <https://meet.google.com/kzc-pzxr-drw>, foram abertos os Trabalhos de Defesa Pública de Tese de Doutorado intitulada "Energias hídrica, eólica e solar no Brasil: Mudanças projetadas pelos modelos climáticos do CMIP6", do(a) candidato(a) GLAUBER WILLIAN DE SOUZA FERREIRA, como parte das exigências para obtenção do Título de Doutor(a) em Meio Ambiente e Recursos Hídricos, na Área de Concentração: Meio Ambiente e Recursos Hídricos. A Comissão Examinadora foi composta pelos(as) doutores(as): MICHELLE SIMOES REBOITA do(a) UNIFEI, 1º(a) Examinador(a) - Orientador(a) e Presidente da Sessão. BENEDITO CLAUDIO DA SILVA do(a) UNIFEI, 2º(a) Examinador(a); CARLOS HENRIQUE REBEIRO LIMA do(a) UNIFEI, 3º(a) Examinador(a); CARLOS HENRIQUE REBEIRO LIMA do(a) UNIFEI, 4º(a) Examinador(a); MARIA LEIDINICE DA SILVA do(a) The Abdus Salam International Centre for Theoretical Physics, Earth System Physics., 5º(a) Examinador(a); Conforme Art. 54 da Norma de Programas de Pós-Graduação da UNIFEI, instalados os trabalhos de Defesa Pública de Tese seguiram-se as seguintes fases: Apresentação dos demais membros da banca pelo(a) presidente; chamada do(a) candidato(a) e leitura do título do trabalho a ser defendido; exposição oral do conteúdo do trabalho pelo(a) candidato(a); e arguição do(a) candidato(a) por cada examinador(a). Feito isso, foi suspensa a Sessão de Defesa para início da Sessão de Julgamento. Durante a mesma, os examinadores atribuíram ao(a) candidato(a) os seguintes conceitos: 1º(a) Examinador(a) "A"; 2º(a) Examinador(a) "A"; 3º(a) Examinador(a) "A"; 4º(a) Examinador(a) "A"; 5º(a) Examinador(a) "A" sendo o(a) candidato(a) considerado(a) APROVADO(A). Voltando à Sessão de Defesa Pública de Tese, o(a) presidente convocou o(a) candidato(a) e proclamou o resultado final, apresentou seus agradecimentos e encerrou a sessão. Os trabalhos foram encerrados às dezessete horas e trinta minutos do dia doze de março de dois mil vinte e cinco e, para que tudo constasse, foi lavrada a presente ata, a qual foi lida, aprovada e assinada pelos membros da Comissão Examinadora.

Dr. CARLOS HENRIQUE RIBEIRO LIMA, UnB

Examinador Externo à Instituição

Dra. MARIA LEIDINICE DA SILVA

Examinadora Externa à Instituição

Dr. BENEDITO CLAUDIO DA SILVA, UNIFEI

Examinador Interno



UNIVERSIDADE FEDERAL DE ITAJUBÁ
COORDENAÇÃO DE CURSO DE PÓS-GRADUAÇÃO EM MEIO
AMBIENTE E RECURSOS HÍDRICOS

Dra. VANESSA SILVEIRA BARRETO CARVALHO, UNIFEI

Examinadora Interna

Dra. MICHELLE SIMOES REBOITA, UNIFEI

Presidente

GLAUBER WILLIAN DE SOUZA FERREIRA

Doutorando

UNIVERSIDADE FEDERAL DE ITAJUBÁ
PROGRAMA DE PÓS-GRADUAÇÃO EM MEIO AMBIENTE E RECURSOS
HÍDRICOS

Glauber Willian de Souza Ferreira

Hydro, wind, and solar energy in Brazil: Changes projected by CMIP6 climate models

Doctoral dissertation submitted to the Postgraduate Program in Environment and Water Resources in partial fulfillment of the requirements for the Doctor of Science in Environment and Water Resources degree.

Concentration Area: Environment and Water Resources

Advisor: Michelle Simões Reboita, Ph.D.

Examining Committee:

Prof. Dr. Michelle Simões Reboita (President)
Federal University of Itajubá, UNIFEI | Advisor

Prof. Dr. Benedito Cláudio da Silva
Federal University of Itajubá, UNIFEI

Prof. Dr. Vanessa Silveira Barreto Carvalho
Federal University of Itajubá, UNIFEI

Prof. Dr. Carlos Henrique Ribeiro Lima
University of Brasília, UnB

Dr. Maria Leidinice da Silva
International Centre for Theoretical Physics, ICTP

Itajubá/MG, 12 March, 2025

DEDICATION

“Dedicated to my Family.”

ACKNOWLEDGMENTS

I thank my Professor and Advisor, Michelle Reboita, for the Ph.D. opportunity, her patience and trust, and all the support she has given me since I was an undergraduate.

I thank Professors Benedito da Silva, Carlos Lima, Leidinice Silva, and Vanessa Carvalho for agreeing to participate in my work evaluation and for their valuable contributions.

I thank my parents and siblings for their love and support. I give special thanks to my Mother for her unconditional support.

I thank my colleague João Gabriel Ribeiro for his support in processing the data.

I thank Engie Brasil Energia for the opportunity to participate in the R&D project.

I thank the Brazilian Federal Agency for Support and Evaluation of Graduate Education (CAPES) for the scholarship provided.

I thank the Postgraduate Program in Environment and Water Resources (POSMARH) for the Ph.D. opportunity and apprenticeship.

I thank the Coupled Model Intercomparison Project (CMIP), the European Centre for Medium-Range Weather Forecasts (ECMWF), the Satellite Application Facility on Climate Monitoring (CM SAF) from the European Organization for the Exploitation of Meteorological Satellites (EUMETSAT), and the Climate Prediction Center for providing the data used in this study.

ABSTRACT

This study evaluated projected changes in key climate variables relevant to the energy sector in South America, with a focus on Brazil, using simulations from eight CMIP6 global climate models. The study analyzed precipitation, 100 m wind speed, wind power density, global horizontal irradiance, concentrated solar power (CSP), and photovoltaic potential (PVP). The Quantile Delta Mapping (QDM) method was applied for bias correction and statistical downscaling. The simulations indicate significant reductions in precipitation, increased duration and severity of droughts, and delays in the onset and demise of the South American monsoon, especially under the SSP5-8.5 scenario. A shortening of the rainy season was also observed over the South Atlantic Convergence Zone (SACZ) and the Brazilian Amazon. Regarding renewable energy, projections indicate a 25-50% increase in wind power density in Northeastern and Southern Brazil, Patagonia, northern Venezuela, Uruguay, Bolivia, and Paraguay. CSP potential is expected to increase by up to 6% in Northeastern Brazil and parts of Chile, while PVP is projected to rise by 1-4% in the Midwest, Southeast, and Amazon regions, with predominantly neutral or negative trends in Southern Brazil. The complementarity between sources (rain-solar and wind-solar) tends to strengthen in several areas, favoring hybrid energy systems. However, the growing intermittency of renewable sources and reduced hydropower storage capacity pose operational challenges. The results highlight the importance of integrated energy planning and infrastructure expansion in the context of climate change, with Brazil strategically positioned to lead the sustainable energy transition in the region.

Keywords: South America; Statistical Downscaling; Climate Change; Renewable Energies; Energetic Complementarity.

RESUMO

Este estudo avaliou projeções de mudanças em variáveis climáticas essenciais para o setor energético na América do Sul, com foco no Brasil, utilizando oito modelos climáticos do CMIP6. Foram analisadas precipitação, vento a 100 m, densidade de potência eólica, irradiância global horizontal, energia solar concentrada (CSP) e potencial fotovoltaico (PVP). Aplicou-se o método Quantile Delta Mapping (QDM) para correção de viés e downscaling estatístico. As simulações indicam redução significativa da precipitação, aumento da duração e severidade das secas e atrasos no início e término da monção sul-americana, especialmente sob o cenário SSP5-8.5. Também foi observada redução na duração da estação chuvosa na ZCAS e Amazônia. Em relação à energia renovável, projeta-se aumento de 25-50% na densidade eólica no Nordeste e Sul do Brasil, Patagônia, norte da Venezuela, Uruguai, Bolívia e Paraguai. O potencial solar CSP deve crescer até 6% no Nordeste do Brasil e partes do Chile, enquanto o PVP tende a aumentar 1-4% no Centro-Oeste, Sudeste e Amazônia. A complementariedade entre fontes (chuva-solar e vento-solar) tende a se fortalecer em várias regiões, favorecendo sistemas híbridos. No entanto, a intermitência e a menor capacidade de armazenamento hídrico impõem desafios operacionais. Os resultados reforçam a importância do planejamento energético integrado e da ampliação da infraestrutura frente às mudanças climáticas, com o Brasil posicionado estrategicamente para liderar a transição energética sustentável na região.

Palavras-chave: América do Sul; Downscaling Estatístico; Mudanças Climáticas; Energias Renováveis; Complementariedade Energética.

CONTENTS

1. GENERAL INTRODUCTION.....	10
2. MOTIVATION	12
3. AIMS.....	16
3.1 General Aim.....	16
3.2 Specific Aims	16
4. Assessment of precipitation and hydrological droughts in South America through statistically downscaled CMIP6 projections	18
5. South American monsoon lifecycle projected by statistical downscaling with CMIP6-GCMs.....	52
6. Assessment of the wind power density over South America simulated by CMIP6 models in the present and future climate	87
7. Assessment of the solar energy potential over South America estimated by CMIP6 models in the present and future climate	134
8. Assessing renewable resources complementarity in South America with statistically downscaled CMIP6 projections	169
9. GENERAL CONCLUSIONS	195
10. REFERENCES.....	200

1. GENERAL INTRODUCTION

Renewable energy plays an essential role in reducing greenhouse gas emissions, and it is expected to supply about 20-30% of global primary energy by 2040, with the potential to entirely replace the current energy system by 2050 (Gernaat et al., 2021). For South America, expanding the use of renewable energy is crucial, as countries in the region have set ambitious targets to reduce greenhouse gas emissions (Washburn and Pablo-Romero, 2019) and diversify clean energy resources (Icaza et al., 2022) in the coming years.

Abundant in renewable energy resources, Latin America currently has more than 319 GW of solar and wind energy production capacity (large-scale announced, in pre-construction or under construction) and could increase its production capacity by more than 460% by 2030 compared to the 69 GW (27.6 GW of solar and 41.5 GW of wind) that are currently in operation (Bauer et al., 2023). Although South America has a strong position in renewable energy compared to other regions (Icaza et al., 2022), recent trends indicate an increasing reliance on thermal energy sources (Arango-Aramburo et al., 2020). Additionally, there is a direct relationship between economic growth and the consumption of non-renewable energy, leading to higher greenhouse gas emissions in the region (Deng et al., 2020).

In this scenario, Brazil stands out, as the country currently has around 40 GW of installed solar photovoltaic capacity and could reach 68 GW in the next five years, which would place it as the fifth-largest solar producer in the world and the leader in solar production in Latin America (Brazilian Energy Balance, 2024; Cacciuttolo et al., 2024). However, the expansion of solar capacity in the country depends on several factors, such as the installation of solar farms, improvements to energy transmission and storage systems, the implementation of a management system that integrates solar energy into the Brazilian matrix, and incentives for new investments in the sector (Reuters, 2023).

Furthermore, approximately 46% of the Brazilian energy matrix comes from renewable sources, among which the hydraulic matrix predominates with 65.2%. Wind and solar sources represent 10.5% of the total produced (EPE, 2022). Currently, the hydraulic matrix is responsible for about 11% of primary energy and 65% of total electricity generated in Brazil (EPE, 2022).



However, reduced precipitation can substantially affect hydropower generation, and studies indicate that the impacts may be more severe on hydropower production in the North and Northeast regions (Schaeffer et al., 2015; Vasquez-Arroyo et al., 2020; Arias et al., 2021), where extreme events such as droughts, may reduce the volume of reservoirs and energy storage (Schaeffer et al., 2012). Additionally, the effects are not limited to supply but also affect demand. Changes in temperature and humidity can also lead to a greater need for cooling or heating environments, with greater impacts on the building sector (Schaeffer et al., 2012; Clarke et al., 2018). Given this, the high risk of water supply deficit to hydroelectric plants requires increasing investments in energy from other sources. The increased occurrence of extreme events can also put the energy production and transmission system at risk, with the impacts increasing on large infrastructures such as the National Interconnected System (SIN) (Vasquez-Arroyo et al. 2020).

Considering wind energy, studies show that its potential will not be considerably affected in Brazil, with climate projections pointing to an increase in wind capacity in the country in the coming decades, mainly in the Northeast and South regions (Lucena et al., 2010; Pereira et al., 2013; de Jong et al., 2019; Lima et al., 2020). Furthermore, projections estimate an increase in solar radiation and temperature in most of the country, which would favor the expansion of this energy matrix (Costa et al., 2020). Brazil's energy sector heavily relies on hydropower, making it particularly vulnerable to shifts in precipitation patterns driven by climate change. Given this dependency, evaluating the country's renewable energy matrix diversification is essential to ensuring long-term energy security and resilience. Within this framework, this doctoral dissertation aims to assess the potential impacts of climate change on the availability of hydro, solar, and wind resources across South America, with a primary focus on Brazil.

By analyzing projections from the latest generation of climate models (CMIP6), this research examines trends in precipitation, solar radiation, and wind availability, mapping the regions best suited for expanding renewable energy generation in the coming decades. Additionally, this study may support energy planning and climate adaptation strategies, contributing to a deeper understanding of how a changing climate may reshape the renewable energy landscape. Given the increasing urgency of transitioning to low-carbon energy sources, this research's findings are particularly relevant for policymakers, industry stakeholders, and researchers aiming to enhance Brazil's energy sustainability in the face of future climate challenges.

2. MOTIVATION

Anthropogenic activities are estimated to have caused a global increase of approximately 1.1 °C over pre-industrial levels (IPCC, 2021; Reboita and Ambrizzi, 2022). The increase in global average temperature is associated with changes in the entire climate system, including reduced snow and ice surfaces, sea level rise, increased frequency of heat extremes, intense precipitation events, drought periods, and rainfall deficits in many regions of the globe, configuring a risk situation for many ecosystems and human populations (IPCC, 2021). The effects concern Brazil, given that critical economic activities, such as energy generation and agriculture, depend highly on climate conditions.

Regarding South America, this continent is particularly vulnerable, as it concentrates on some of the most important biodiversity areas in the world, harboring many endemic species threatened by anthropogenic activities (Raven et al., 2020). Many regions of the continent are exposed to the risks of reduced water availability, increased flooding and overflows, decreased food production, and increased incidence of vector-borne diseases (Arias et al., 2021). Over the past four decades, several portions of South America have also experienced reduced rainfall volumes, indicating an expansion of dry subtropical zones and an increased frequency of drought events over these regions (Rivera and Arnould, 2020).

In South America, climate change's effects on droughts are evident in different sectors, such as Northeastern and Southeastern Brazil, Amazonia, and the continent's southeast. The semi-arid Northeast of Brazil is one of the historically most vulnerable regions to droughts (Marengo et al., 2018), with several events recorded since the 16th century (Marengo et al., 2016a, 2018, 2022) and numerous socio-economic impacts such as damage to agricultural production, livestock, loss of human life from hunger, malnutrition, disease, migrations to urban centers, and failures in regional and national economies (Marengo et al., 2016a). Southeastern Brazil (SEB) has also experienced some of the worst droughts in recent decades, such as in 2001 (Cavalcanti and Kousky, 2001), 2014/2015 (Seth et al., 2015; Nobre et al., 2016; Coelho et al., 2016; Abatan et al., 2022; Geirinhas et al., 2022), 2018 (Gozzo et al., 2019), and most recently, in 2020/2021 (Cuartas et al., 2022). Several drought events have also occurred in the Amazonia, accentuating forest fires, affecting the region's biota, and signaling the risk of a tipping point (Guimberteau et al., 2013; Duffy et al., 2015; Marengo et al., 2016b; Lima and AghaKouchak,

2017; Agudelo et al., 2019; Lovejoy and Nobre, 2019; Jimenez et al., 2021; Boulton et al., 2022). Additionally, in the last decade, other Brazilian areas have also experienced severe droughts, such as the 2019/2020 droughts in the Brazilian Pantanal and Midwest (Borges et al., 2018; Thielen et al., 2020; Marengo et al., 2021) and the 2012/2013 and 2019/2020 droughts in southern Brazil (SB) (Cunha et al., 2019; Fernandes et al., 2021).

On the other hand, most studies on the South American continent induce optimistic estimates of wind power in the coming decades (Pereira et al., 2013; Ruffato-Ferreira et al., 2017; Reboita et al., 2018; de Jong et al., 2019). Regarding offshore WPD, GCMs from the CMIP5 project for the end of the 21st century excellent conditions across the entire South Atlantic Ocean (Zheng et al., 2019). A possible cause for the higher projected wind speeds is the South Atlantic Subtropical Anticyclone (SASA) expansion and the longitudinal shift of its position to the west (Gilliland and Keim, 2018; Reboita et al., 2019), intensifying the pressure gradient and wind speeds along the Brazilian coast.

In this context of climate research, global climate models (GCMs) are a primary tool for investigating climate system elements (Avila-Diaz et al., 2023). A new generation of GCMs from CMIP has recently been available to the scientific community, comprising the sixth phase of the project's experiment (CMIP6). The CMIP6-GCMs present aspects of improvement over previous generations, such as higher spatial resolution and better parameterization schemes of the physical and biogeochemical processes of the climate system (Eyring et al., 2016). In addition, CMIP6 models employ the Scenario Model Intercomparison Project (ScenarioMIP), which provides climate projections based on the latest greenhouse gas emission and land use scenarios, the Shared Socio-economic Pathways (SSPs) (Riahi et al., 2017). SSPs characterize a more realistic socio-economic development by considering different social, economic, technological, and political scenarios (Carvalho et al., 2021).

Despite their crucial role in climate research, GCMs have limitations due to their coarse spatial resolution, which restricts their use in analyzing regional-scale processes and impacts. In this framework, dynamical and statistical downscaling techniques address these limitations of global models. Dynamical downscaling employs regional climate models (RCMs) that use initial and boundary conditions provided by GCMs, whilst statistical downscaling determines relationships between large-scale atmospheric circulation factors and local climate (Fowler et al., 2007). Dynamical downscaling is helpful for the analysis of local-scale climate phenomena, but such a procedure requires high computational costs (Ambrizzi et al., 2019). On the other hand,

statistical downscaling requires less computational effort and avoids the propagation of systematic errors arising from GCMs (Mutz et al., 2021).

Although both methods have advantages and weaknesses, a preference for studies in South America using dynamical downscaling has been observed in recent decades, mainly in the analysis of variables like precipitation and air temperature (da Rocha et al., 2009; Marengo et al., 2012; Chou et al., 2014; Reboita et al., 2014, 2016; Solman and Blázquez, 2019; Solman et al., 2021; Silva et al., 2023). However, there is a growing literature in recent years about statistical downscaling in the continent (Bettolli and Penalba, 2018; Mutz et al., 2021; Sulca et al., 2021; Solman et al., 2021; Olmo and Bettolli, 2022).

Statistical downscaling does not directly simulate the physical processes of the climate systems. It relies on establishing statistical relationships between large-scale climate variables (obtained from GCMs) and local-scale variables (obtained from in situ measurements). These relationships are derived from historical observations (perfect prognosis (PP) approach) or simulations (model output statistics (MOS) approach) and then applied to project future climate conditions (Maraun and Widmann, 2018). Traditionally, in climate research, the PP approach has been used, and it includes different methods (Maraun and Widmann, 2018), such as regression models (also called the transfer function model), weather type methods, and analog and resampling methods (Lee and Singh, 2019).

One of the statistical downscaling approaches that is less computationally expensive is the model based on transfer functions. Research with statistical downscaling of precipitation projections from CMIP6 to South America showed that the Quantile Delta Mapping (QDM) bias correction technique, developed by Cannon et al. (2015), performed well in correcting the systematic errors in the different quantiles of the probability distributions of the GCM raw simulations, evidencing its ability to reproduce seasonal variability and extreme properties (Ballarin et al., 2023).

With the QDM technique, it is possible to use data as reanalysis to interpolate the historical projections to the reference dataset's spatial resolution and, from transfer functions, apply the same correction to future predictions. The QDM method has proved advantageous since it preserves the model-projected relative changes and trends (i.e., if a model has a dry trend in a specific region, it will be kept after the spatial disaggregation and bias correction) (Cannon et al., 2015).

Until now, only Ballarin et al. (2023) applied the QDM approach to CMIP6-GCMs in South America. However, the present study introduces several distinctions from the former work. While Ballarin et al. (2023) focus solely on Brazil, this research extends the analysis to the entire South American continent, offering a broader perspective. Moreover, their study does not examine the projected impacts on various aspects analyzed here (renewable energy, droughts, changes in the rainy season etc.). Another distinction is the temporal scope since Ballarin et al. (2023) limit their projections to the last three decades, and this study presents long-term projections for the 21st century. These differences highlight this research's broader scope and relevance in assessing the future of renewable energy under a changing climate in South America.

Despite the growing urgency of renewable energy in South America, the region's literature on wind and solar energy is still relatively sparse, and few studies have used the latest generation of climate models. Notwithstanding, previous works relied on raw CMIP6 outputs (Almazroui et al., 2021; Arias et al., 2021; Ortega et al., 2021; Collazo et al., 2022; Dutta et al., 2022; Medeiros and Oliveira, 2022; Zuluaga et al., 2022; Ha et al., 2023). Additionally, research evaluating future changes in the South American monsoon lifecycle and the potential complementarities among renewable energy resources in Brazil is lacking. Thus, this research contributes by applying a novel approach to the national literature and seeks to bridge these gaps by providing perspectives that can support those interested in optimizing the future management of water resources and the expansion of wind and solar infrastructure in Brazil and, more broadly, across South America.

Given this background, this study aims to (a) apply the QDM bias correction technique and statistical downscaling to historical simulations and climate projections of precipitation, surface wind, and global horizontal irradiance from a CMIP6 multi-model ensemble; (b) use the bias-corrected data to generate intermediate-resolution (50 km) projections of precipitation, wind, and solar energy potential across South America, with a particular focus on Brazil; and (c) analyze the impacts of climate change on various aspects of renewable energy resources, including hydrological droughts, changes in the South American monsoon system's lifecycle, wind power density, concentrated solar power, photovoltaic solar energy, and the complementarities between these renewable resources.

3. AIMS

3.1 General Aim

The general objective of this study is to analyze projected changes in climate and renewable energy resources over South America, with a particular focus on Brazil, by applying statistical downscaling to historical simulations and future climate projections from the Coupled Model Intercomparison Project Phase 6 (CMIP6). The study investigates precipitation, wind speed at 100 meters, wind power density at 100 meters, global horizontal irradiance (GHI), concentrated solar power (CSP) output, photovoltaic (PV) potential, and the complementarity between these resources under the SSP2-4.5 and SSP5-8.5 scenarios, across four future timeframes (2020-2039, 2040-2059, 2060-2079, and 2080-2099), relative to the historical baseline (1995-2014).

3.2 Specific Aims

The specific objectives of this research are organized into three thematic axes, each associated with peer-reviewed scientific articles that comprise the core of this dissertation:

The specific objectives of this research include:

1) Assessment of hydrological droughts and the South American monsoon system

This objective aims to:

- Evaluate the frequency, duration, severity, and intensity of hydrological droughts using the SPI-12 index based on statistically downscaled projections;
- Investigate projected changes in the South American monsoon system lifecycle, particularly its onset, demise, and duration.

Associated articles:

- *Assessment of precipitation and hydrological droughts in South America through statistically downscaled CMIP6 projections (Climate, 2023)*
- *South American monsoon lifecycle projected by statistical downscaling with CMIP6-GCMs (Atmosphere, 2023)*

2) Evaluation of wind and solar energy potentials

This objective seeks to:

- Assess changes in wind speed and wind power density at 100 meters to estimate future wind energy potential;
- Analyze projections of GHI, CSP output, and PV potential to evaluate the solar energy resource base.

Associated articles:

- *Assessment of the wind power density over South America simulated by CMIP6 models in the present and future climate (Climate Dynamics, 2024)*
- *Assessment of the solar energy potential over South America estimated by CMIP6 models in the present and future climate (Journal of Environmental & Earth Sciences, 2024)*

3) Analysis of complementarity among renewable energy resources

This objective focuses on:

- Examining the spatiotemporal complementarity among key renewable resources (precipitation, wind speed, and solar irradiance) to enhance integrated energy strategies under climate change scenarios.

Associated article:

- *Assessing renewable resources complementarity in South America with statistically downscaled CMIP6 projections (manuscript in preparation)*

In addition to these goals, this research also developed a climate-energy atlas and a statistically downscaled dataset at 50 km spatial resolution, encompassing historical and future projections of all analyzed variables for South America. These outputs support energy planning, climate adaptation strategies, and scientific dissemination.

4. Assessment of precipitation and hydrological droughts in South America through statistically downscaled CMIP6 projections

23/02/2025, 18:39

E-mail de Universidade Federal de Itajubá - Permission to Include Published Article in Doctoral Dissertation



Glauber Willian de S. Ferreira <glauber_ferreira@unifei.edu.br>

Permission to Include Published Article in Doctoral Dissertation

Climate <climate@mdpi.com>

19 de novembro de 2024 às 23:14

Para: "Glauber Willian de S. Ferreira" <glauber_ferreira@unifei.edu.br>

Cc: climate@mdpi.com

Dear Ms. Ferreira,

Thank you for your email. *Climate* is an open access journal and the authors retain all copyrights.

For details information, please check on the following link (Benefits of Open Access to Authors and Readers):

https://www.mdpi.com/authors#Benefits_of_Open_Access_to_Authors_and_Readers

If you have any other questions, please feel free to contact me.

Climate Editorial Office
Building 2, Courtyard 4, Guanyinan North Street,
Tongzhou District, 101101 Beijing, China,
Tel.: +86 10 5730 8701
E-mail: climate@mdpi.com
<http://www.mdpi.com/journal/climate/>

Impact Factor (2023) of /Climate/: 3.0
CiteScore (2023) of /Climate/: 5.5
Editor's Choice Articles:
https://www.mdpi.com/journal/climate/editors_choice
Most Cited & Viewed: https://www.mdpi.com/journal/climate/most_cited

MDPI Climate Editorial Office
E-Mail: climate@mdpi.com
Website: <http://www.mdpi.com/journal/climate/>
Twitter@Climate_MDPI: https://twitter.com/climate_MDPI
LinkedIn: <https://www.linkedin.com/company/climate-mdpi/>
Subscribe to Climate at: <https://www.mdpi.com/journal/climate/toc-alert>

Awards, welcome to follow:
Climate 2025 Travel Award (Application deadline: 31 December 2024):
<https://www.mdpi.com/journal/climate/awards/2837>
Climate 2022 Best Paper Award winner interview:
<https://www.mdpi.com/journal/climate/awards/1709>
Climate 2023 Travel Award winner interview:
<https://www.mdpi.com/journal/climate/awards/1992>
Climate 2023 Outstanding Reviewer Award winner interview:
<https://www.mdpi.com/journal/climate/awards/2861>

Highly accessed articles, welcome to read:
The Climate Change Challenge: A Review of the Barriers and Solutions to Deliver a Paris Solution,
<http://www.mdpi.com/2225-1154/10/5/75>
Enhancing Climate Neutrality and Resilience through Coordinated Climate Action: Review of the Synergies between Mitigation and Adaptation Actions, <http://www.mdpi.com/2225-1154/11/5/105>
Comprehensive Review: Advancements in Rainfall-Runoff Modelling for Flood Mitigation,
<http://www.mdpi.com/2225-1154/10/10/147>
Adaptation of Agriculture to Climate Change: A Scoping Review, <http://www.mdpi.com/2225-1154/11/10/202>
The Impacts of Urbanisation and Climate Change on the Urban Thermal Environment in Africa,
<http://www.mdpi.com/2225-1154/10/11/164>

Open Special Issues, welcome to view and submit:
Impacts of Extreme Weather on Hydrological Process, Water Quality and Ecosystem in Agricultural and Forested Watersheds under the Changing Climate
https://www.mdpi.com/journal/climate/special_issues/ExtremeWeather_HydrologicalProcess
Climate, Climate Change and the Arctic: Environment, Infrastructure, Health and Well-Being
https://www.mdpi.com/journal/climate/special_issues/climate_Arctic_Health
The Importance of Long Climate Records (Second Edition)
https://www.mdpi.com/journal/climate/special_issues/6Q4Q92UI74

<https://mail.google.com/mail/u/2/?ik=b7e437194a&view=pt&search=all&permmsgid=msg-f:1816205847407346920&siml=msg-f:1816205847407...> 1/2

Article

Assessment of Precipitation and Hydrological Droughts in South America through Statistically Downscaled CMIP6 Projections

Glauber Willian de Souza Ferreira , Michelle Simões Reboita *, João Gabriel Martins Ribeiro and Christie André de Souza

Instituto de Recursos Naturais, Universidade Federal de Itajubá, Itajubá 37500-093, Brazil; glauber_ferreira@unifei.edu.br (G.W.d.S.F.); gabrielmr472@unifei.edu.br (J.G.M.R.); christie@unifei.edu.br (C.A.d.S.)

* Correspondence: reboita@unifei.edu.br

Abstract: Drought events are critical environmental threats that yield several socioeconomic impacts. Such effects are even more relevant for South America (SA) since different activities essential for the continent, such as agriculture and energy generation, depend highly on water resources. Thus, this study aimed to evaluate future changes in precipitation and hydrological drought occurrence in SA through climate projections from eight global climate models (GCMs) of CMIP6. To this end, statistical downscaling was applied to the projections obtained using the quantile delta mapping technique, and the method proved to be efficient in reducing systematic biases and preserving GCMs' trends. For the following decades, the results show considerable and statistically significant reductions in precipitation over most of SA, especially during the austral spring, with the most intense signal under the SSP5-8.5 forcing scenario. Furthermore, GCMs showed mixed signals about projections of the frequency and intensity of drought events. Still, they indicated agreement regarding the increased duration and severity of events over the continent and a substantial proportion of moderate and severe events over most of Brazil during the 21st century. These results can be helpful for better management of water resources by decision-makers and energy planners.

Keywords: statistical downscaling; CMIP6; precipitation; drought; climate change; South America



Citation: Ferreira, G.W.d.S.; Reboita, M.S.; Ribeiro, J.G.M.; de Souza, C.A. Assessment of Precipitation and Hydrological Droughts in South America through Statistically Downscaled CMIP6 Projections. *Climate* **2023**, *11*, 166. <https://doi.org/10.3390/cli11080166>

Academic Editor: Junqiang Yao

Received: 3 July 2023

Revised: 27 July 2023

Accepted: 31 July 2023

Published: 2 August 2023



Copyright: © 2023 by the authors. Licensee MDPI, Basel, Switzerland. This article is an open access article distributed under the terms and conditions of the Creative Commons Attribution (CC BY) license (<https://creativecommons.org/licenses/by/4.0/>).

1. Introduction

Climate change is undeniable, as is its attribution to anthropogenic greenhouse gas-emitting activities, which have unequivocally intensified global warming, evidenced by the 1.1 °C increase in global surface temperature from 2011 to 2020 relative to 1850–1900 [1]. Additionally, best estimates indicate that continued greenhouse gas emissions will cause a 1.5 °C increase in the near term (2021–2040) [1]. Moreover, even if the countries fully implement the commitments made in the Paris Agreement, global warming is expected to exceed 2 °C by the end of the century [2,3]. The progressive warming will intensify the global hydrological cycle so that compound heatwaves and droughts are projected to become more frequent, including concurrent events in multiple locations [1].

Droughts are a natural phenomenon characterized by a continuous persistence of precipitation deficit, which occurs in almost all climate zones, including those with high precipitation rates, such as Amazonia [4]. Prolonged periods of drought cause innumerable damages, such as losses in agriculture and livestock, contamination of waters, reduction of water availability for daily consumption and water energy generation, and environmental risks of fires [5,6]. Due to climate change and increasing temperatures, droughts are expected to increase in frequency and duration [7,8].

Studies with climate projections indicate an increased risk of extreme droughts in different parts of the world, depending on the seasons and drought indicators analyzed.

For example, considering North America, studies with climate projections of phases 5 and 6 of the Coupled Model Intercomparison Project (CMIP) show an increase in the duration and frequency of droughts in the southeast [9], central and northern [10–14] United States, and southwestern Canada [15]. Similarly, drought events are projected to intensify in parts of Asia [11–14,16,17], Europe [11,18], Oceania [11,13,14,18], Africa [11,14,19], and South America [11,13,14,18,20–25].

In South America (SA), climate change effects on droughts are evident in different sectors, such as northeastern and southeastern Brazil, Amazonia, and the continent's southeast. The semi-arid Northeast of Brazil is one of the historically most vulnerable regions to droughts [26], with several events recorded since the 16th century [26–28] and numerous socioeconomic impacts, such as damage to agricultural production and livestock, as well as loss of human life from hunger, malnutrition, disease, migrations to urban centers, and losses in regional and national economies [27]. Southeastern Brazil (SEB) has also experienced some of the worst droughts in recent decades, such as in 2001 [29], 2014/2015 [30–35], 2018 [6], and most recently, in 2020/2021 [36].

Several drought events have also occurred in Amazonia, accentuating forest fires, affecting the region's biota, and signaling the risk of a tipping point [37–43]. Additionally, in the last decade, other Brazilian regions have also experienced severe droughts, such as the 2019/2020 droughts in the Brazilian Pantanal and Midwest [44–46] and the 2012/2013 and 2019/2020 droughts in southern Brazil [47,48]. Another South American region affected by droughts is Southeastern South America (SESA), which covers northern Argentina, Paraguay, Uruguay, and southern Brazil. The 2008/2009 drought in the region was among the most severe in the last 50 years [49,50]. Additionally, several studies have shown an increasing trend of warm days/nights [51–54] and the occurrence of dry spells [54,55] in the region in the last decades.

Droughts are a complex and multiform phenomenon [35,36], and different quantitative indicators allow for their assessment [56]. The Standardized Precipitation Index (SPI), developed by McKee et al. [57], quantifies the rainfall deficit or excess on different time scales. SPI on time scales greater than six months is employed to identify and characterize hydrological droughts that cause reduced soil moisture levels, river flows, groundwater recharge, and reservoir levels [56,58,59]. The SPI index proves advantageous because, besides allowing for evaluating drought impacts on different hydrological cycle components (using different time scales), it requires only rainfall data as input variables in the index computation [58]. However, as SPI does not account for the temperature component, its analysis disregards evapotranspiration processes, which play an essential role in the hydrological cycle [56,58]. Despite its limitations, several studies have employed the SPI-12 index (SPI index on a 12-month time scale) due to its simplicity of implementation to identify hydrological droughts in SA [6,56,58,60–66].

In this context of climate research, global climate models (GCMs) are a primary tool for investigating climate system elements [67]. A new generation of GCMs from CMIP has recently been available to the scientific community, comprising the sixth phase (CMIP6) of the project's experiment. The CMIP6-GCMs present aspects of improvement over previous generations, such as higher spatial resolution and better parameterization schemes of the physical and biogeochemical processes of the climate system [68]. In addition, CMIP6 models employ the Scenario Model Intercomparison Project (ScenarioMIP), which provides climate projections based on the latest greenhouse gas emission and land use scenarios, the Shared Socioeconomic Pathways (SSPs) [69]. SSPs characterize a more realistic socioeconomic development by considering different social, economic, technological, and political scenarios [70].

Despite their crucial role in climate research, GCMs have limitations due to their coarse spatial resolution, which restricts their use in analyzing regional-scale processes and impacts. In this framework, dynamical and statistical downscaling techniques address these limitations of global models. Dynamical downscaling employs regional climate models (RCMs) that use initial and boundary conditions provided by GCMs, while statistical

downscaling determines relationships between large-scale atmospheric circulation factors and local climate [71]. Dynamical downscaling is helpful for the analysis of local-scale climate phenomena, but such a procedure requires high computational costs [72]. On the other hand, statistical downscaling requires less computational effort and avoids the propagation of systematic errors arising from GCMs [73].

Regarding SA, the literature focuses more on the dynamical approach of air temperature, precipitation, and wind [74–84]. However, recent studies have also applied the statistical method and demonstrated its competence in representing the spatial distribution and extreme temperature and precipitation events [73,82,85–90]. Research with statistical downscaling of precipitation projections from CMIP6 to SA showed that the quantile delta mapping (QDM) bias correction technique, developed by Cannon et al. [91], performed well in correcting the systematic errors in the different quantiles of the probability distributions of the GCM raw simulations, evidencing its ability to reproduce seasonal variability and extreme properties [90]. With the QDM technique, it is possible to use data as reanalysis to interpolate the historical projections to the reference dataset's spatial resolution and, from transfer functions, apply the same correction to future predictions. The QDM method has proved to be advantageous since it preserves the model-projected relative changes and trends (i.e., if a model has a dry trend in a specific region, it will be kept after the spatial disaggregation and bias correction) and corrects the systematic biases in the quantiles of the modeled data with respect to the observations [91].

Given the background, this study aims to: (a) apply the QDM bias correction technique and statistical downscaling to historical simulations and climate projections of precipitation from a CMIP6 multi-model ensemble; (b) employ the bias-corrected estimates to present a set of precipitation projections at intermediate resolution (50 km) in SA; and (c) employ the bias-corrected projections and the SPI-12 index to identify the four types of hydrological drought events (mild, moderate, severe, and extreme), and their aspects (frequency, duration, severity, intensity, and peak) in eight subdomains of SA. There is still a shortage of studies analyzing hydrological droughts in SA with post-processed projections from the CMIP6-GCMs, and this study intends to fill such a gap. In addition, this research can assist decision-makers and energy planners in better future management of water resources on the continent.

2. Materials and Methods

2.1. Study Area

The study area comprises the SA continent (Figure 1), located at latitudes 12° N–55° S. Its extensive latitudinal coverage provides climate heterogeneity of tropical, subtropical, and extratropical regions, as well as diverse geography that includes particular areas such as the Andes Mountains, the Atacama Desert, the Amazon rainforest, and the semi-arid Northeast of Brazil [92,93]. The South American monsoon system (SAMS) primarily influences the central SA, with two well-defined seasons marked by the rainy season from November to March and the dry season from May to September [92–94]. On the other hand, the subtropical western portion of the continent concentrates its rainfall in the austral winter months due to the passage of cold fronts and cutoff lows [92,93]. Still, the northern portion of SA does not have a well-defined dry season, being strongly influenced by the Intertropical Convergence Zone (ITCZ), with maximum rainfall in the austral autumn and early winter [95], and being one of the wettest places in the globe [96].

The rectangles illustrated in Figure 1 indicate the subdomains selected (Table 1) to analyze hydrological drought events on the continent. We considered subdomain 8 (Patagonia) because, in this region, the Andes have a lower height, while we did not perform analysis for the other parts of the Cordillera due to uncertainties in the reference data [97].

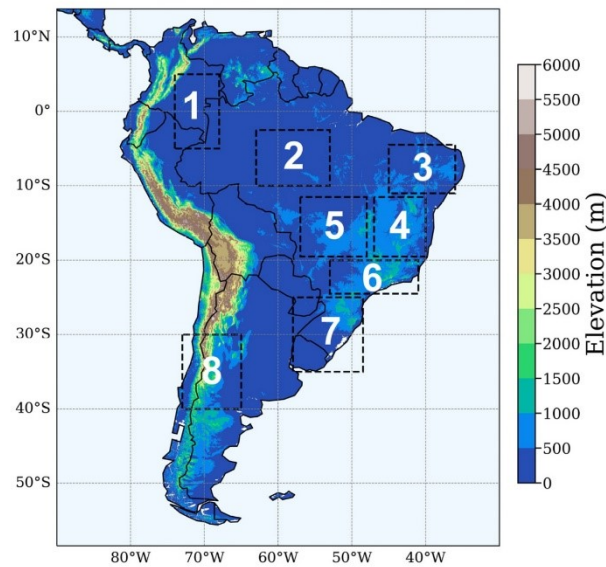


Figure 1. Illustration of the study area with elevation (m). Rectangles indicate subdomains selected for the analysis of drought events. Source: United States Geological Survey, Earth Resources Observation System (EROS) Center.

Table 1. Geographic coordinates of the subdomains selected for hydrological drought analysis.

Subdomain	Area
1	5° N–5° S 68° W–74° W
2	2.5° S–10° S 53° W–63° W
3	4.5° S–11° S 36° W–45° W
4	11.5° S–19.5° S 40° W–47° W
5	11.5° S–19.5° S 48° W–57° W
6	20° S–24.5° S 41° W–53° W
7	25° S–35° S 48.5° W–58° W
8	30° S–40° S 65° W–73° W

2.2. CMIP6-GCMs Selection

The study employed precipitation projections from eight CMIP6-GCMs, comprehending the historical period (1995–2014) and two greenhouse gas emission scenarios (SSP2-4.5 and SSP5-8.5) in the future period (2020–2099). The SSP2-4.5 scenario denotes a moderate emission scenario, while SSP5-8.5 considers a high greenhouse gas emission context, representing a period with little effort to mitigate climate change effects [69]. The GCMs dataset comprises precipitation projections every three hours provided on the Earth System Grid Federation (ESGF) platform—available online: <https://esgfnodl.llnl.gov/search/cmip6> (accessed on 26 January 2022).

At the early stage of this study (January 2022), we selected the models that best represented the South American climate in terms of precipitation and air temperature, which is a response to atmospheric circulation. To choose the GCMs, we used the methodology of Rupp et al. [98], whereby several metrics evaluate the best models based on regionally averaged properties and large-scale patterns. Thus, the identification of the best-performing models included the calculation of the following parameters with monthly data from 50 CMIP6-GCMs for different SA subdomains: (a) mean and standard deviation for each

year (1995–2014); (b) spatial correlation calculated for each season (DJF, MAM, JJA, SON) and year (1995–2014) with Pearson’s correlation coefficient; (c) mean amplitude, defined as the difference of the variables between January and July; (d) and a linear trend, calculated for complete time series (rather than by seasons) using the method of least squares and angular coefficients for the indication of a positive or negative trend.

Ranking the GCMs according to their performance is not trivial, as several statistical metrics and seasonal seasons are evaluated. Therefore, we compiled all the information by standardizing the metrics (giving equal weight/importance to each metric) to rank the GCMs in terms of performance according to the methodology proposed by Rupp et al. [98]. Figure 2 illustrates that the best models are on the left-hand side (values closest to zero). We could not necessarily select the best models shown in Figure 2 due to the absence of hourly/daily data and/or projections in the ESGF database. Thus, by concurrently analyzing the availability of high-frequency data and projections, the best models (indicated with red bars) were selected for this study (Table 2). Furthermore, three selected GCMs (EC-Earth3, IPSL-CM6A-LR, and MPI-ESM1-2-LR) were previously validated and performed well in representing the SA climate [99]. Although a good simulation of the historical period does not determine more accurate climate projections for the same model, it ensures more reliable future estimates since the poor ability to simulate historical climate is likely reflected in poorer future projections [100].

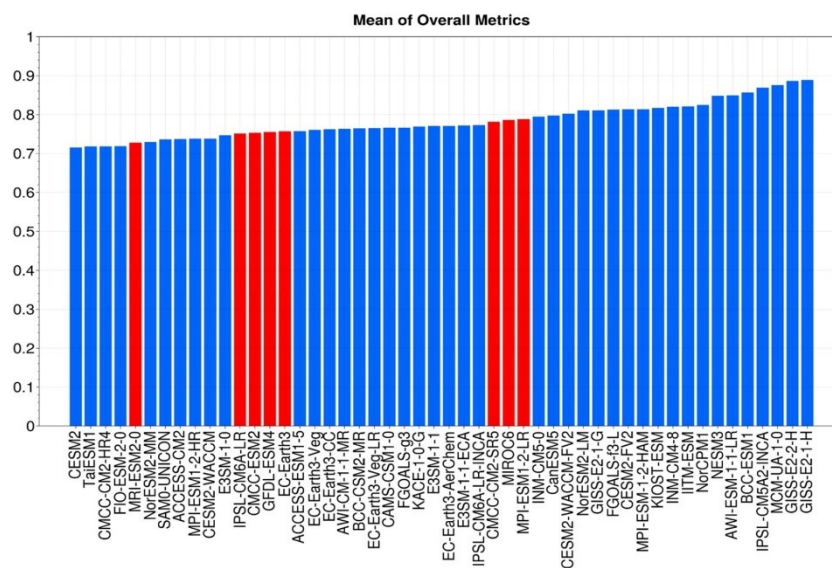


Figure 2. Ranked models after applying the methodology of Rupp et al. [98], obtained with monthly data from 50 CMIP6-GCMs for the historical period (1995–2014). Best performing models are located on the left-hand side of the X-axis, and red bars indicate the models selected for the study.

Last, it is valid to mention that the ensemble composition included two models (CMCC-CM2-SR5 and CMCC-ESM2) from the Fondazione Centro Euro-Mediterraneo sui Cambiamenti Climatici (CMCC). Given their equal origin, there may be a higher likelihood of shared biases or underlying assumptions, leading to correlated errors and limited diversity within the ensemble. In this context, the “institutional democracy” approach addresses these uncertainties by selecting one GCM from each modeling institute [101,102]. While this is an effective way to account for model dependence, it is worth noting that as

institutes progressively copy or collaboratively develop models or components, there is no guarantee that such an approach will continue to be efficient in future studies [103].

Table 2. Information on each CMIP6-GCM employed in the study.

Model	Resolution (°Lat × °Lon)	Institute	Reference
CMCC-CM2-SR5	1.25 × 0.94	Fondazione Centro Euro-Mediterraneo sui Cambiamenti Climatici	Lovato and Peano [104]
CMCC-ESM2	1.25 × 0.94	Fondazione Centro Euro-Mediterraneo sui Cambiamenti Climatici	Lovato et al. [105]
EC-Earth3	0.70 × 0.70	EC-Earth Consortium	Döscher et al. [106]
GFDL-ESM4	1.25 × 1.00	Geophysical Fluid Dynamics Laboratory	Krasting et al. [107]
IPSL-CM6A-LR	2.50 × 1.26	Institut Pierre Simon Laplace	Boucher et al. [108]
MIROC6	1.41 × 1.41	Japan Agency for Marine-Earth Science and Technology	Tatebe and Watanabe [109]
MPI-ESM1-2-LR	0.94 × 0.94	Max Planck Institute for Meteorology	Wieners et al. [110]
MRI-ESM2-0	1.13 × 1.13	Meteorological Research Institute	Yukimoto et al. [111]

2.3. Reference Dataset

The study used precipitation analysis from the Climate Prediction Center (CPC) gauge-based analysis of global daily precipitation [112] to validate the historical simulations of the CMIP6-GCMs. For this, daily data from 1995 to 2014 were used, with 0.5° horizontal resolution—available online: https://ftp.cpc.ncep.noaa.gov/precip/CPC_UN1_PRCP/GAUGE_GLB/RT/ (accessed on 25 January 2022). CPC data proved adept at representing average and seasonal precipitation patterns over most of SA [93] but presented uncertainties in regions of complex topography, such as the Andes Mountains [97].

We point out that the information in the CMIP6 tutorials does not clarify the period of daily precipitation accumulation. Precipitation data were obtained with a frequency of three hours, and the daily accumulation followed the recommendations of the World Meteorological Organization (WMO) [113] to avoid errors, such as comparing data with different periods for the daily accumulation—that is, the rainfall for a given day is accumulated from 1200 Z of the previous day to 1200 Z of the day in question. However, it is worth noting that the CMIP6 models provide the accumulations at 0130, 0430 Z until completing 24 h. Thus, the accumulation was performed from 1330 Z to 1030 Z the following day to be as close as possible to the WMO definition. Furthermore, CPC precipitation analysis also accounts for the daily rainfall accumulated in the 1200 to 1200 Z interval.

2.4. Bias Correction and Statistical Downscaling

One way to overcome the limitations imposed by the coarse resolution of GCMs is through statistical downscaling methods, which establish statistical relationships between model outputs and reference data [114]. Statistical downscaling techniques are classified into three types—transfer function or regression models, weather generators, and weather typing [114]—and this study used transfer functions. This method was chosen due to its simplicity of implementation and for preserving time series trends (for more details, see Cannon et al. [91]). This methodology is also known as Bias Correction Statistical Downscaling (BCSD).

This study used the BCSD method to downscale the simulations and projections of CMIP6-GCMs. Bias correction was performed by applying the QDM technique [91] to the historical simulations (1995–2014) and by applying the transfer functions to the future projections (2020–2099). According to Cannon et al. [91], the QDM technique preserves the model-projected trends and relative changes (e.g., if the GCM shows a dry trend in a given region, that trend will be maintained after bias correction) and corrects systematic biases in the quantiles of the modeled data relative to the reference one. Moreover, compared with the quantile mapping technique, the QDM technique has proved advantageous because it is less susceptible to problems such as inflating relative trends in extreme values [91].

Before bias correction, spatial disaggregation was applied to the CMIP6-GCM outputs, and the model data were downscaled to the 0.5° resolution as the CPC data with bilinear interpolation. Several studies show that bilinear interpolation provides consistent estimates by adjusting the spatially correlated behavior of the variable [90,115–122].

After spatial disaggregation, bias correction is applied using the QDM method. This method follows three steps [91]: First, the trend is removed from all projected individual quantiles. Next, the detrended quantiles are bias-corrected using the quantile mapping technique. Finally, the projected changes are superimposed on the bias-corrected outputs. Let o and p be the observed and projected data, whereas h and f are the historical and future periods, respectively. The definition of the non-exceedance probability of the observed ($x_{h,o}$) and projected ($x_{h,p}$) historical and future ($x_{f,p}$) data is accounted for as:

$$\begin{aligned} P_{f,p}(t) &= F(x_{f,p}(t)) \\ P_{h,p}(t) &= F(x_{h,p}(t)) \\ P_{h,o}(t) &= F(x_{h,o}(t)) \end{aligned} \quad (1)$$

where p and F denote the non-exceedance probability associated with a specific value in time and the cumulative distribution function (CDF), respectively. The change factor, which associates the historical simulation outputs with those of the future period, is calculated with Equation (2):

$$\Delta^M(t) = \frac{F_{f,p}^{-1}(P_{f,p}(t))}{F_{h,p}^{-1}(P_{f,p}(t))} = \frac{x_{f,p}(t)}{F_{h,p}^{-1}(P_{f,p}(t))}, \quad (2)$$

where F^{-1} denotes the inverse CDF and $\Delta^M(t)$ is the multiplicative factor of change between the simulated quantiles of the historical and future periods. Finally, the bias correction in the future projections is obtained by applying the multiplicative relative change $\Delta^M(t)$ to the historical values with the corrected bias, according to Equation (3):

$$\hat{x}_{f,p}(t) = \Delta^M(t) \cdot F_{h,o}^{-1}(P_{f,p}(t)), \quad (3)$$

The historical period (1995–2014) was used for the training set to adjust the future projections (2020–2099) using the QDM algorithm. This time window was chosen due to computational resources and to follow the same reference period used by the International Panel on Climate Change (IPCC). The Python-based package *xclim* [123] was used to perform the calculations.

2.5. Test of Statistical Significance for the Difference in Climatological Mean Values

To assess whether the differences in mean climatological values in the future period (2020–2099) of the CMIP6-GCMs are statistically significant compared with the historical period (1995–2014), we used the Student's *t*-test. This test assumes the null hypothesis (H_0) of no difference between the two datasets against the alternative hypothesis of a difference between the two ensembles. The test was computed according to Equation (4):

$$t = \frac{\bar{X}_f - \bar{X}_h}{\sqrt{\frac{s_f^2}{n} + \frac{s_h^2}{n}}}, \quad (4)$$

where s_f and s_h are the standard deviation values of the future and historical datasets, respectively, and n comprises the number of values in each set. The associated degree of freedom v is estimated as:

$$v = \frac{\left(\frac{s_f^2}{n} + \frac{s_h^2}{n}\right)^2}{\frac{s_f^4}{n^2(n-1)} + \frac{s_h^4}{n^2(n-1)}}, \quad (5)$$

The test was performed using a significance level α of 5%. Thus, when the probability value (p -value) found was less than 5%, the null hypothesis of no difference between the two sets was rejected in favor of the alternative hypothesis, indicating statistical evidence of the difference between the mean values of the two periods evaluated.

2.6. Standardized Precipitation Index (SPI)

The SPI index, developed by McKee et al. [57], quantifies the rainfall deficit or excess on different time scales, evaluating the intensity of dry and wet periods. The SPI-12 index uses a time scale of 12 months. Besides identifying long-term rainfall patterns, SPI-12 can also be associated with flows, reservoir levels, and groundwater anomalies, helping to evaluate hydrological droughts [56,58]. More detailed information about the SPI calculation can be found in Santos et al. [61] and Wilks [124].

As our results show that the SSP5-8.5 scenario presents the most significant changes, the SPI-12 analysis was performed only under this scenario. Each bias-corrected CMIP6-GCM calculated SPI-12, and the BSCD ensemble (the bias-corrected CMIP6 ensemble) index was obtained by averaging the indices estimated by the individual models.

Drought starts when the SPI falls below zero and ends when it becomes positive [57]. In this work, we used the thresholds defined by McKee et al. [57] (Table 3) to select and analyze all the drought events from mild to extreme categories. In addition, drought events were analyzed based on five characteristics: frequency (number of drought events in a period), duration (number of months between the first and last month of the event), severity (absolute sum of all SPI values during the event), intensity (ratio between severity and duration), and peak (largest absolute value of SPI recorded during the event).

Table 3. Drought events classification, adapted from McKee et al. [57].

SPI Values	Drought Category
0 to −0.99	Mild drought
−1.00 to −1.49	Moderate drought
−1.50 to −1.99	Severe drought
≤ −2.00	Extreme drought

3. Results and Discussion

3.1. Historical Simulations

The historical simulations (1995–2014) of precipitation obtained by the ensemble of eight CMIP6-GCMs before (raw ensemble) and after applying statistical downscaling (BSCD ensemble) are presented in Figure 3. Considering the austral summer (DJF), the raw ensemble tends to overestimate precipitation over most of Brazil and the west coast of SA (Figure 3(a5)). Contrarily, underestimates occur in northwest SA and north-central Argentina. In addition, the overestimation of rainfall over the Andes is notable. During summer, precipitation patterns exhibit a northwest-southeast orientation over the continent due to the action of the South Atlantic Convergence Zone (SACZ) [93]. On average, the raw ensemble represents the continental distribution of rainfall associated with the SACZ, but it amplifies and shifts the core of maximum precipitation to the southeast and northeast of SA.

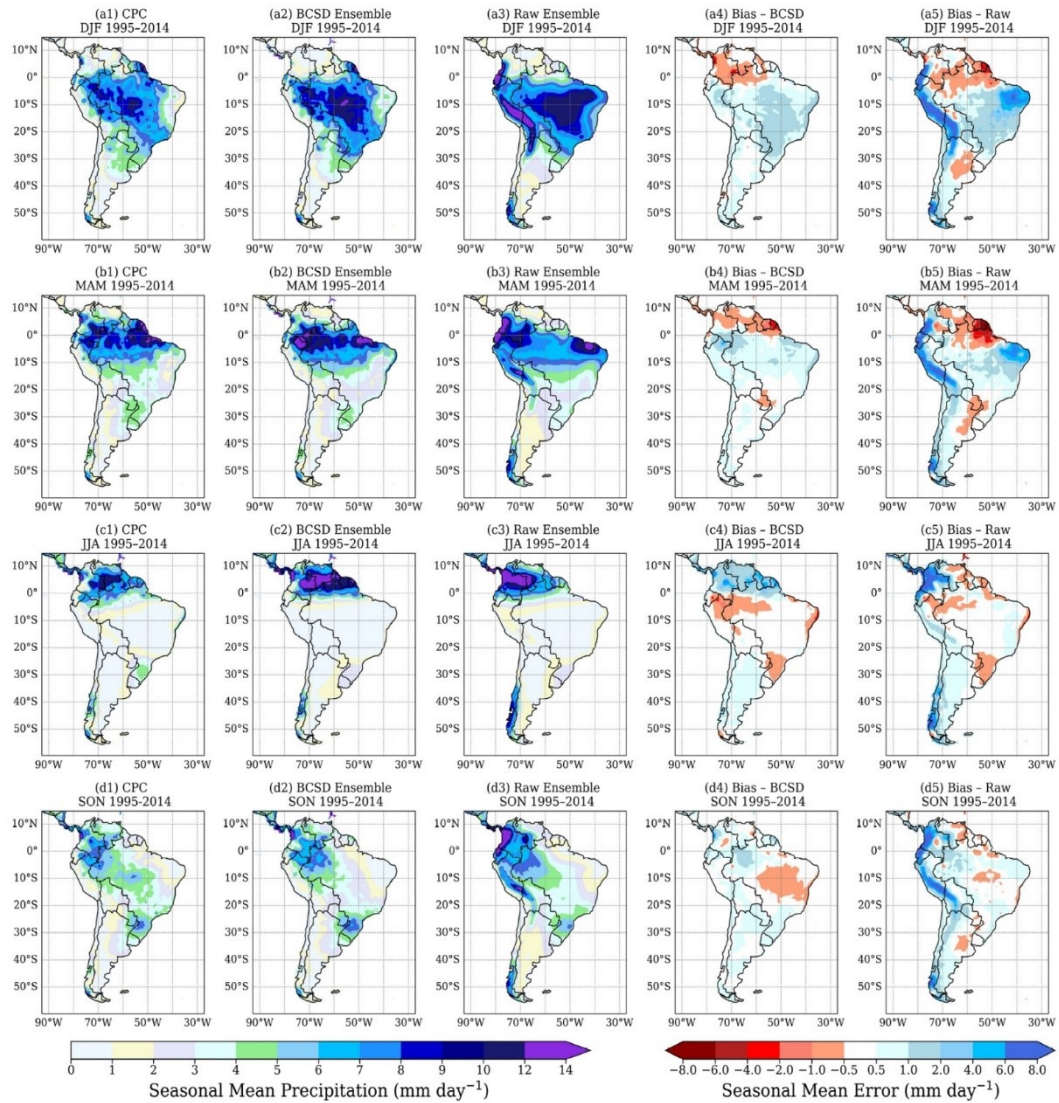


Figure 3. Seasonal climatology of precipitation (mm day^{-1}) in the historical period (1995–2014) obtained by CPC (first left column), BCSD ensemble (CMIP6 ensemble with BCSD) (second left column), raw ensemble (CMIP6 ensemble without BCSD) (middle column), and seasonal bias (mm day^{-1}) between the BCSD ensemble and CPC (second right column) and between the raw ensemble and CPC (first right column).

The underestimation of precipitation during summer over northwestern SA and northern Brazil is also seen in other studies with CMIP6 models [125–127], as well as with CMIP5 models [128], which are associated with a less satisfactory representation of the Intertropical Convergence Zone (ITCZ), arising from the models' oversensitivity to sea surface temperature (SST) and deficiency in simulating surface wind convergence.

Although the CMIP6 models show considerable improvement in reproducing rainfall magnitudes over SA relative to the CMIP5 models, the simulation of ITCZ position and intensity is still deficient, which partially justifies the negative rainfall biases over northern Brazil and northern SA [127]. The systematic underestimation of rainfall in the Amazon Basin is due to an insufficient representation of different processes, such as cumulus convection, biosphere–atmosphere interactions in the forest, soil moisture, and surface processes, as well as a low coverage of rainfall stations in the region, which influences the analysis of the magnitude and location of precipitation [129].

In addition, GCMs tend to produce overly intense precipitation over the Central Andes in Bolivia, Peru, Ecuador, and southwestern Colombia due to excessive modeled convection and lack of topographic representativeness. Validating the simulations in these areas includes many uncertainties due to the scarcity of rainfall stations in mountainous regions [125,130]. Historical simulations of the CMIP6 ensemble without bias correction indicate better performance in reproducing precipitation patterns in SA during winter and spring, reiterating previous results [127].

Considering the BCSD ensemble, one notices a significant reduction of biases across the continent, especially on the west coast of SA and northeastern Brazil. Despite a better representation of the intensity and location of rainfall maxima associated with the SACZ, the ensemble still overestimates precipitation at the center of the continental SACZ, which is mainly controlled by internal climate variability and has low or negligible predictability associated with SST variations [131,132].

Similarly, during austral autumn (Figure 3(b4)), there is a marked reduction in the ensemble systematic biases, and the errors concentrate in northern SA, portions of northern and northeastern Brazil, northeastern Peru, central Brazil, and western Chaco. Considering the rainfall biases north of 10° S obtained by the raw ensemble (Figure 3(b3)), BCSD adjusts the spatial distribution of rainfall, providing a simulated field analogous to the observed one, although with the persistence of larger overestimates in the far north of Peru and Brazil (Figure 3(b2)).

In the winter and spring seasons, the reduction in raw ensemble's systematic errors in most of SA is notable, mainly on the continent's west coast and portions of Colombia and Venezuela (Figure 3(c4,d4)). In winter, rainfall overestimates concentrate north of the equator, partially justified by the less satisfactory representation of the ITCZ by GCMs, while in spring, the positive precipitation bias in western Amazonia persists even after correction. In summary, we conclude that BCSD efficiently reduces the systematic errors of GCMs and ensures more reliable projections about future climate conditions. In general, the biases that persist after applying the correction occur in problematic sectors for global climate modeling, such as the tropical region and continental portion of the SACZ.

3.2. BCSD Ensemble Projections of Precipitation under the SSP2-4.5 and SSP5-8.5 Forcing Scenarios

Figures 4 and 5 present the precipitation climate projections obtained by the BCSD ensemble under the SSP2-4.5 and SSP5-8.5 forcing scenarios, respectively. To complement the seasonal analyses, Figure S1 in the Supplementary Material presents the mean annual projections of precipitation change relative to the historical period for both scenarios used. Under the SSP2-4.5 scenario, for summer and fall, BCSD ensemble projects increase by up to 10% over much of Brazil for the coming decades. From 2080, up to 20% growth is projected in Brazil's southeastern and northeastern sectors. In contrast, up to 20% reductions are projected in the extreme north of SA, with their sign diminished by the end of the 21st century.

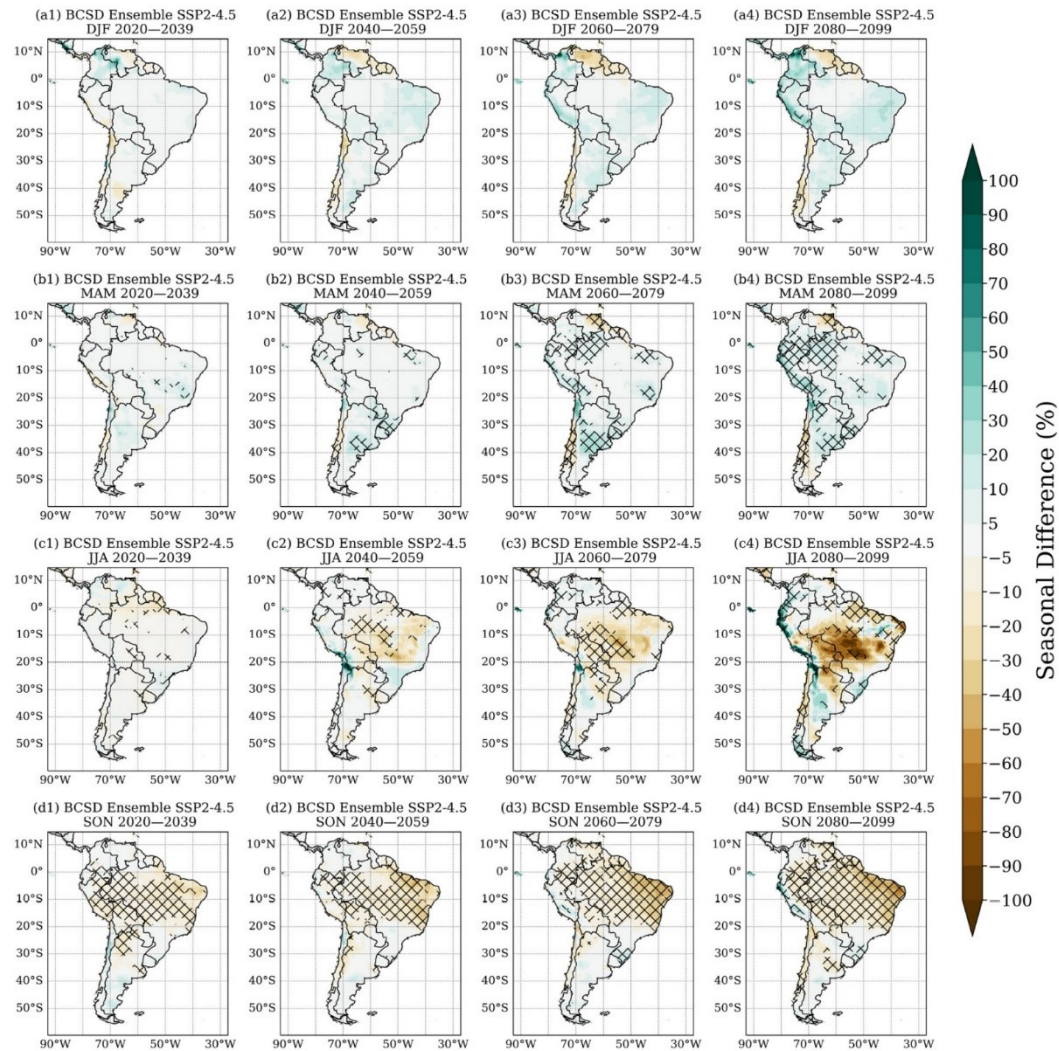


Figure 4. Seasonal differences of precipitation (%) between the future (2020–2039, 2040–2059, 2060–2079, 2080–2099) and historical period (1995–2014), projected by the BCSd ensemble under the SSP2-4.5 forcing scenario. Hatched areas indicate statistical significance at a 95% confidence level.

In the winter season (Figure 4(c1–c4)), the BCSd ensemble projects more expressive reductions starting in 2040, with regions of maximum decrease (up to 50%) beginning in 2080 in the central-western and northeastern Brazil sectors. In the spring (Figure 4(d1–d4)), the BCSd ensemble projects a significant reduction in rainfall, intensified after 2060, with reductions above 20% in large parts of central and northeastern Brazil. The results obtained here partially agree with those of other studies that used projections from the CMIP5 and CMIP6 models. Under the RCP4.5 forcing scenario, mean annual patterns from the ensemble of 26 CMIP5 models indicate decreases of up to 150 mm year⁻¹ in the far north

of SA, decreases in annual rainfall over much of central SA, a slight increase over isolated portions of Northeast Brazil, and larger increases over southern Brazil [133].

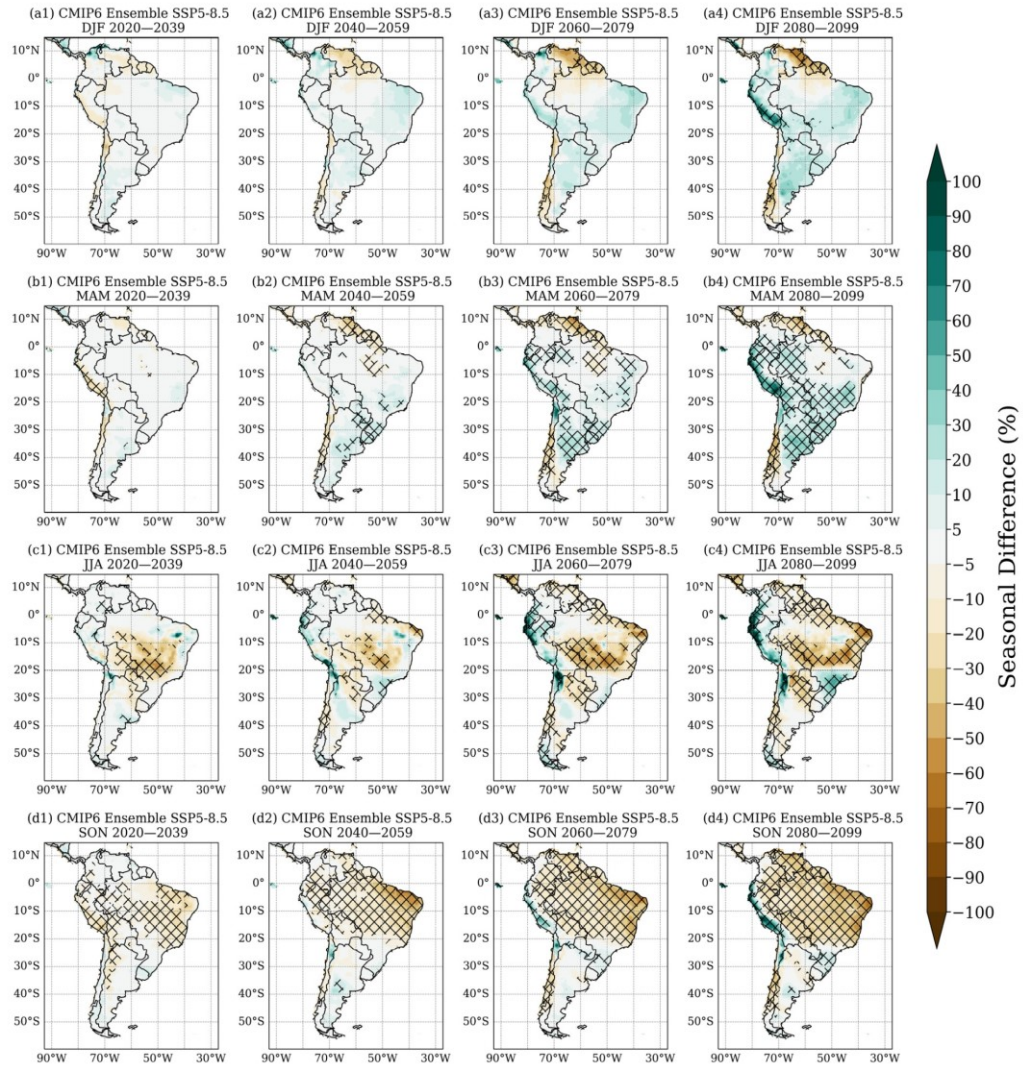


Figure 5. Seasonal differences of precipitation (%) between the future (2020–2039, 2040–2059, 2060–2079, 2080–2099) and historical period (1995–2014), projected by the BCSD ensemble under the SSP5-8.5 forcing scenario. Hatched areas indicate statistical significance at a 95% confidence level.

Similarly, the CMIP5 ensemble indicates increased rainfall over southeastern SA and reduced rainfall over Amazonia and northern SA during the summers of 2050–2080 [23]. In winter, increased precipitation is also seen over western SA, extending from Ecuador to Argentina [23], a pattern analogous to that found here. Additionally, an ensemble composed of 38 CMIP6-GMCs projects increased precipitation ($\sim 0.3 \text{ mm day}^{-1}$) over Brazil’s Northeast and South sectors during the summers of 2040–2059 and a reduction

of the same magnitude over nearly all of SA during the winter [125]. For the period 2080–2099, projections show even wetter (drier) conditions in southern Brazil (Amazonas and northern SA) during summer and intensified rainfall reduction across the continent during winter [125]. On the other hand, a study with the global HadGEM2-ES model nested with the Eta regional model under the RCP4.5 forcing scenario shows a projection of increased precipitation over most of the Amazon Basin, southern Brazil, and the northern portion of the coastal Northeast of Brazil, as well as decreased rainfall over much of the Midwest, Southeast, and central Northeast regions of Brazil [134]. We stress that the similarities and differences between the results of the studies are due to factors such as different models used, emission scenarios employed, reference periods chosen, and validation data.

Considering the SSP5-8.5 emission scenario (Figure 5), spatial patterns of projected seasonal change in precipitation are similar to those obtained for the SSP2-4.5 scenario but with the most intense sign of change. During summer (Figure 5(a1–a4)), an average increase of 10% is projected over most of Brazil and Argentina, and the growth intensifies after 2060, principally over portions of northeastern Brazil and central-southern Argentina. The changes in fall (Figure 5(b1–b4)) are similar to the SSP2-4.5 scenario but indicate more intense precipitation increases in the Bahia state (Brazil), southern Brazil, central-eastern Argentina, and the central Andes.

In winter (Figure 5(c1–c4)), the BCSD ensemble projects rainfall a decrease over much of central Brazil and Bolivia, extending into northern Argentina and southeastern, northeastern, and northern Brazil. From 2060 onwards, the BCSD ensemble shows up to 50% decreases in the Midwest and coastal Northeast areas. In contrast, a substantial rainfall increase for Brazil's southeast and southern coasts is observed from 2080 onward. In spring (Figure 5(d1–d4)), the projections indicate more drastic changes, with decreases of more than 10% over most of Brazil and northern SA, with more intense reductions (up to 50%) over the northern portion of the coastal Northeast of Brazil. During this season, projected increases in precipitation occur in isolated regions, such as the coasts of Peru and Ecuador and northern Chile.

The results agree with those of Ruffato-Ferreira et al. [134], in which there is a trend of increasing water scarcity, mainly in central Brazil, and a progressive increase in water availability in the southern and southeastern Atlantic basins, favoring southern Brazil. In addition, the São Francisco River Basin is the most vulnerable in the maximum emission scenario, accentuating water scarcity in the Northeast of Brazil. Similarly, CMIP5 projections indicate increases of about 100 mm year⁻¹ by the end of the 21st century in southern Brazil and parts of Peru, Ecuador, Colombia, and Venezuela. In comparison, areas between southern Chile and Argentina and the far north of SA may experience reductions of up to 150 mm year⁻¹ [133].

The higher severity of precipitation reductions in SA under the SSP5-8.5 scenario was also obtained by CMIP5 models nested with different regional climate models [23,24,135]. Among the possible causes for the dry conditions projected for Amazonia and northern SA is the weakening of the northeast trade winds at the end of the 21st century, inducing a decrease in moisture transport from the ocean to the continent [23,72]. Additionally, studies with CMIP6-GCMs under the SSP5-8.5 forcing scenario also provide projections of expressive precipitation reduction over much of the continent, mainly in the Midwest, Southeast, Northeast, and North of Brazil and northern SA, with decreases of up to 1.2 mm day⁻¹ in the most affected regions [125,127]. On the other hand, SESA and southern Brazil will likely experience higher rainfall volumes in the coming decades, exposing these regions to the progressive frequency of extreme daily precipitation events and an increase in the number of consecutive wet days [23].

Analyses of projected changes in rainfall with GCMs from CMIP3, CMIP5, and CMIP6 over Brazil show that the projected signal depends on the CMIP generation considered, except for southern Brazil, where an increase is seen in all cases [136]. While CMIP3 projects an increase in rainfall in northern Brazil (especially in the western portion), CMIP5 and CMIP6 models project a reduction. In the Northeast of Brazil, the projections are also

divergent among the CMIP generations, with CMIP5 indicating an increase in rainfall throughout the territory. At the same time, CMIP3 and CMIP6 project an increase (reduction) in rainfall in the region's northern (southern) sector. In the Midwest and Southeast regions, the sign depends on the family of CMIP used, with increased precipitation projected by CMIP5 and decreased rainfall estimated by CMIP3 and CMIP6. In summary, multi-model ensembles show that CMIP3 most accurately represents precipitation extremes in northeastern Brazil, while CMIP5 performs best for the Midwest, and CMIP6 provides the most accurate projections for the remaining Brazilian regions [136].

In this context of uncertainties, it is relevant to highlight some limitations of this study. An important aspect to consider is the need to analyze potential changes in bias and its propagation to future climates. Buser et al. [137] have demonstrated that different assumptions about these biases (considering time-dependent model biases, which can be either additive or multiplicative) can lead to substantially discrepant estimates of future conditions, particularly for the summer. Similarly, Blázquez and Solman [138] verified that models with higher warm biases and more clouds in both central Argentina and northeast Brazil might drive the wet and warm biases in the regions, especially during the summer. This way, the uncertainty in the intricate relationship between bias (which may not be stationary) and mean state poses significant challenges in accurately projecting future climate scenarios. A better comprehension of bias behavior can aid in a better interpretation of climate change signals.

Moreover, we did not investigate the spatial aspects of systematic errors. In this respect, Arisido et al. [139] evaluated systematic errors in coupled climate models by considering their spatial and temporal relationships and providing estimates of the associated uncertainties through posterior distributions. Their findings revealed a considerable warm bias in the Angola–Benguela front region, and the posterior analysis showed that both the estimated bias and its associated uncertainty changed over time.

Given the study constraints, we recommend caution for energy planning with the projections analyzed here. More robust evaluations should also consider the vegetation of different biomes since it plays a crucial role in the water balance and greater detail of the projected scenarios of land use and land cover changes. Furthermore, intrinsic to the process of climate modeling, the uncertainties and inaccuracies associated with different models limit a greater assertiveness and require pondering in decision-making based on the projections.

3.3. Temporal Series of the BCSD Ensemble SPI-12 Index under the SSP5-8.5 Forcing Scenario

Figure 6 shows the SPI-12 temporal series (2020–2099) and the annual precipitation anomalies (in percent) relative to 1995–2014 provided by the BCSD ensemble under the SSP5-8.5 emission scenario for eight SA subdomains. The SPI-12 index presented here is obtained by averaging the indices calculated for each projection. Thus, the numbers of hydrological drought events and classes reported here refer to the estimates obtained from the average of all SPI-12 values projected by each model individually. Therefore, the projections are based on the ensemble mean, biased by smoothing internal/naturally forced variability. Additionally, Figures S2 and S3 in the Supplementary Materials present the SPI-12 projections and the classification of hydrological drought events provided individually by each ensemble member. In R1 (northwestern Amazonia), 31 drought episodes were identified between 2020–2099, all belonging to the mild drought category. The longest episode occurs from 07/2086 to 09/2088, totaling 37 months, followed by the episode from 06/2065 to 05/2068 (36 months) with a severity of 10.02. In addition, other long-lasting drought episodes occur from 11/2044 to 08/2047 and from 08/2049 to 05/2052 (34 months each). In general, negative (positive) precipitation anomalies accompany lower (higher) SPI-12 values.

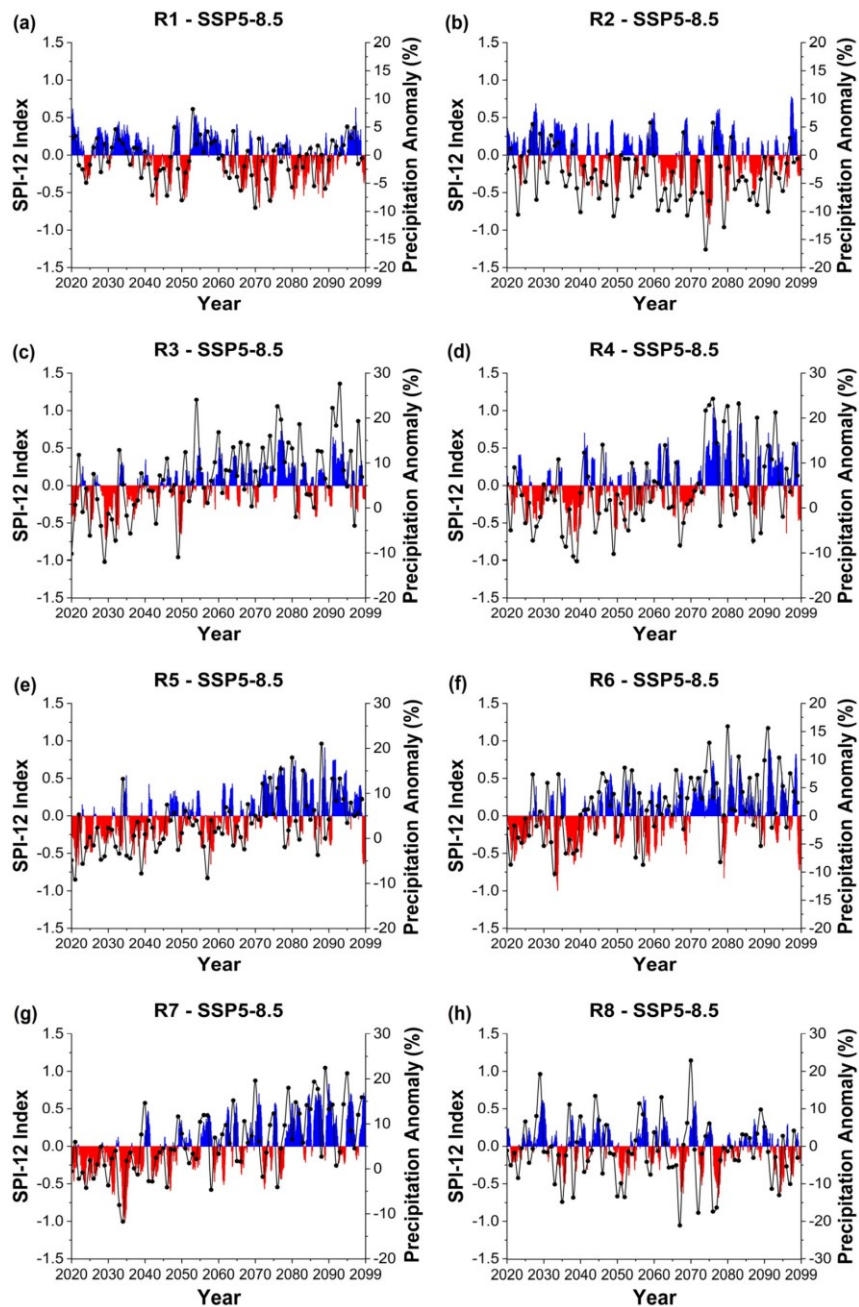


Figure 6. Temporal series (2020–2099) of the SPI-12 index and mean annual precipitation anomalies (black dotted line) relative to 1995–2014 (in percent) projected by the BCSO ensemble under the SSP5-8.5 scenario for eight SA subdomains ((a–h), Figure 1). Red (blue) bars indicate SPI-12 values below (above) zero.

For R2 (central Amazonia), 30 drought episodes were identified in the period 2020–2099, categorized as mild droughts, and 56% of the episodes (17 cases) have a duration of 10 months or longer. The longest episode occurs from 03/2061 to 11/2065 (57 months), with a severity of 13.89. Other longer episodes occur from 12/2085 to 02/2089 (39 months), from 04/2039 to 08/2041 (29 months), and from 10/2073 to 12/2075 (27 months), which also indicates the largest negative precipitation anomaly in the period ($\sim -17\%$).

Although different droughts have occurred in Amazonia during El Niño-Southern Oscillation (ENSO) events, SST anomalies in the tropical North Atlantic (TNA) also play an important role in the region's rainfall regime [4,37,40,140,141]. The anomalous warming in the TNA is associated with the northward displacement of the ITCZ, changes in the north-south divergent circulation, and weakening of the trade winds and moisture flux from the tropical Atlantic, inducing a reduction of rainfall in the southern, northern, and eastern sectors of Amazonia [4,37,141]. Furthermore, ENSO events are related to anomalies in the east-west Walker circulation, with convection over the central Pacific and subsidence over eastern and central Amazonia [4,140,141].

In general, drought events related to warm SST anomalies in the TNA show a north-south gradient with drier (wetter) conditions in southern (northern) Amazonia, while droughts linked to ENSO events show a southwest-northeast gradient with drier conditions in northeastern Amazonia [141]. However, overlapping effects of both teleconnection mechanisms also affect the region, such as the 2010 drought associated with successive ENSO episodes during the austral summer and the warmer TNA during the austral autumn and winter [37]. Similarly, the severe drought of 2015–2016 was associated with intense warm anomalies in the central Pacific and TNA, with marked effects in northeastern Amazonia [142].

Considering the occurrence of drought events in 2015–2100 relative to the 1850–2014 period under the SSP5-8.5 scenario, Wang et al. [14] found an increase in the frequency of droughts in northern SA during the 21st century, as well as more prolonged droughts and more than 50% increase in the extent of areas affected. On the other hand, the variability of drought-related statistical results provided by CMIP6 models is greater in the tropics than in other latitudinal zones, implying that GCMs need improvement in capturing drought-causing patterns in equatorial regions [7]. Furthermore, models from CMIP5 and CMIP6 indicate divergence in rainfall projections over the area, and models from CMIP6 show no improvement in simulating total precipitation and consecutive dry days relative to the previous generation of CMIP [143].

In R3 (northern sector of Northeast Brazil), 31 drought episodes have been identified in 2020–2099, all belonging to the mild drought category. About 61% of the episodes (19 events) present a duration equal to or longer than 10 months. The longest-lasting hydrological drought episode occurs from 11/2027 to 12/2032 (62 months), followed by the episodes from 01/2041 to 02/2044 (38 months) and 12/2034 to 12/2037 (37 months). In R4 (central sector of Northeast Brazil), 32 hydrological drought episodes have been counted in 2020–2099, all classified as mild droughts. About 72% of the episodes (23 cases) are 10 months or longer. Four longer-lasting episodes are obtained from 01/2035 to 12/2040 (72 months), from 11/2026 to 11/2030 (49 months), from 01/2067 to 12/2069 (36 months), and from 12/2085 to 02/2088 (27 months). Our results corroborate previous analyses since CMIP6 projections suggest an increase in the number of dry days in Northeast Brazil (mainly in DJF and MAM), with an estimated increase of up to 8.0 and 14.7% in the near (2016–2040) and far (2076–2100) future, respectively, under the SSP5-8.5 scenario [8].

Precipitation in the Northeast of Brazil is marked by interannual variability, and drought events are attributed to ENSO and the anomalously northern position of the ITCZ, resulting from the warmer TNA [12,37,64,141]. However, extratropical variability modes also influence rainfall distribution in the region, as analyses from 1980–2009 concluded that drought events in this period showed annular patterns in both hemispheres (South Annular Mode and North Annular Mode) well configured during DJF (pre-rainy season in the region), both in years with and without ENSO [144].

For R5 (Midwest region of Brazil), 31 drought episodes have been identified, all classified as mild droughts, with the most extended episode from 11/2026 to 02/2031 (52 months), followed by other long-lasting events from 02/2043 to 10/2046 (45 months), and from 10/20635 to 11/2038 (38 months). About 61% of the drought episodes (19 cases) are 10 months or longer. Marengo et al. [46] report no evident direct relationship between drought events in the region and SST anomalies in the Pacific and Atlantic Oceans. While the 2019–2020 drought was associated with anomalous warming in TNA, earlier events occurred with simultaneous warming of the northern tropical and equatorial Pacific and cooling of the TNA. Overall, the authors conclude that droughts in the region may be triggered by warmer SSTs in the North Atlantic and North Pacific (which promote the northward displacement of the ITCZ and reduce precipitation in southern Amazonia and the Midwest), which reduce moisture transport from Amazonia to the region. However, regional factors, such as water balance and soil moisture, influence the sector's interannual seasonality of droughts and floods. In this context, there is an increasing tendency in the water deficit in deforested regions due to the expansion of agriculture and cattle ranching, contributing to local warming and reduced precipitation [46].

In R6 (Southeast region of Brazil), 33 drought episodes have been counted in the period 2020–2099, all belonging to the mild drought category, with the longest-lasting episode from 04/2020 to 01/2026 (70 months), followed by episodes with 61 months (from 12/2035 to 12/2040) and 23 months (11/2032 to 09/2034). Approximately 60% of projected drought episodes are 10 months or longer. Analyses of SPI-1 and SPI-12 in the north and northwest areas of the Rio de Janeiro state for the 1967–2013 period indicated a higher occurrence of events in the moderately and extremely dry categories, as well as a higher frequency of droughts in the two regions of the state during ENSO cycles in both phases of the Pacific Decadal Oscillation [62]. Analyses of drought events in the Paraná River Basin showed that hydrological droughts in the 1981–2021 period were the most severe and intense [33].

Furthermore, studies show that the severe drought of 2014–2015 was associated with anomalous warming in the western tropical Pacific that initiated a wave train along the South Pacific, which in turn resulted in anomalous anticyclonic circulation in the Southwest Atlantic, expanding the west flank of the South Atlantic Subtropical Anticyclone (SASA) and restricting the entry of low-pressure systems into southeastern Brazil [30,32]. Additionally, analyses of summer droughts during 1961–2010 in the São Paulo state show a prevalence of anomalous subsidence of the Hadley cell's descending branch and reduced moisture convergence anomaly associated with upper-level convergence and lower-level divergence, inhibiting convective activity in the region [33].

In R7 (southern Brazil and Uruguay region), 29 drought episodes have been computed, all categorized as mild droughts, of which 62% (18 episodes) have a duration of 10 months or longer. The longest drought episode refers to the period from 01/2022 to 01/2028 (73 months), followed by cases of 41 months (12/2032 to 04/2036) and 39 months (08/2036 to 10/2039). Many of the droughts that have occurred in the region are linked to the cold phase of ENSO (La Niña), but other factors also contribute to the onset and intensification of droughts in the sector, such as the development of atmospheric blockings in the South Pacific, warmer SST anomalies in the TNA occurring concurrently with La Niña, as well as more regional and local aspects, such as reduced moisture transport to the region caused by deforestation in Amazonia [49,50,145,146]. Attribution study infers that the rainfall deficit occurring in the southern part of Brazil, Argentina, and Uruguay since 2019 is not only partially induced by the action of La Niña but also caused by higher temperatures that reduce water availability in the region, indicating that although the decrease in rainfall is associated with natural climate variability, the consequences of drought are becoming more severe due to increasing temperatures [146].

Finally, in R8 (western Patagonia), 40 drought episodes have identified in 2020–2099, all classified as mild droughts, of which 52.5% (21 cases) have a duration of 10 months or more. The longest-lasting episode occurs from 06/2050 to 07/2053 (38 months), followed by episodes of 32 months (01/2076 to 08/2078) and 28 months (09/2066 to 12/2068). This sector

has experienced intense droughts recently [147], substantially affecting socio-economic activities in the region.

We emphasize that explaining the physical mechanisms associated with drought events in different sectors of SA is not trivial, as each region responds differently to the various teleconnection mechanisms. Such a purpose is beyond the scope of this study, and related information can be found in the extensive literature available. For example, an overview of the impacts of teleconnection patterns on SA is discussed by Reboita et al. [141]. Additionally, the specificity of physical mechanisms associated with different drought events in sectors of SA is argued in Marengo et al. [22,26–28], Marengo and Espinoza [37], and Oliveira-Júnior et al. [62] (Northeast Brazil and Amazonia), and in Coelho et al. [32,35], Abatan et al. [33], and Freitas et al. [56,58] (Southeast Region and Paraná Basin).

The BCSD ensemble shows that all SA subdomains analyzed are prone to drought episodes during the 21st century. Although the ensemble projects predominantly mild droughts due to smoothing the most extreme projections, a considerable proportion of episodes last longer than 10 months. Additionally, the individual SPI-12 projections and the classification of hydrological drought events identified by each GCM demonstrate that all models project substantial proportions of moderate, severe, and extreme drought events (see Supplementary Materials). The significant occurrence of longer hydrological drought episodes corroborates analyses previously performed with CMIP6 models that indicate an increase in event duration during the 21st century under the SSP5-8.5 scenario in SA and a higher frequency of longer-lasting events [14].

3.4. Projections of Drought Parameters by the Bias-Corrected CMIP6-GCMs and BCSD Ensemble

Figures 7 and 8 show the drought parameters projected by the eight bias-corrected CMIP6-GCMs, as well as by CPC (for the historical period only) and BCSD ensemble under the SSP5-8.5 scenario. It is worth noting that the drought events and parameters reported here were obtained from the individual projections yielded by each CMIP6-GCM used. The Supplementary Materials present more information regarding the SPI-12 index and different hydrological drought classes projected by each CMIP6-GCM.

For R1, of the 301 episodes identified by all datasets (including all GCMs and the ensemble mean), 72% (218 cases) belong to the mild drought category, 16% (48 cases) correspond to the moderate drought class, 9% (28 cases) are of severe drought events, and 2% (7 cases) belong to the extreme drought category. Moreover, only three GCMs (CMCC-CM2-SR5, CMCC-ESM2, and MPI-ESM1-2-LR) indicate a slight increase in the average number of drought episodes in the 2020–2099 relative to the historical period, while the IPSL-CM6A-LR model and BCSD ensemble suggest a reduction of up to 27% and 23%, respectively.

On the other hand, seven of the nine datasets show an increase in the duration of drought episodes in 2020–2099 relative to 1996–2014. The IPSL-CM6A-LR and EC-Earth3 models indicate an increase of 47% and 32% in the duration (in months) of the events, respectively, while the BCSD ensemble provides an average increase of 25%. Similarly, most GCMs (and the BCSD ensemble) converge on increasing severity of drought episodes in the 21st century, with the IPSL-CM6A-LR model and the BCSD ensemble indicating increases of 51% and 40%, respectively. Regarding the intensity and peak parameters, GCMs show mixed signals, and the MRI-ESM2-0 and EC-Earth3 models show 12% and 18% increases in intensity and peak, respectively. In general, in this region, all GCMs overestimate the number of drought episodes over the historical period, and the GFDL-ESM4 and IPSL-CM6A-LR models show the largest range of parameter estimates for the 2020–2099 period.

has experienced intense droughts recently [147], substantially affecting socio-economic activities in the region.

We emphasize that explaining the physical mechanisms associated with drought events in different sectors of SA is not trivial, as each region responds differently to the various teleconnection mechanisms. Such a purpose is beyond the scope of this study, and related information can be found in the extensive literature available. For example, an overview of the impacts of teleconnection patterns on SA is discussed by Reboita et al. [141]. Additionally, the specificity of physical mechanisms associated with different drought events in sectors of SA is argued in Marengo et al. [22,26–28], Marengo and Espinoza [37], and Oliveira-Júnior et al. [62] (Northeast Brazil and Amazonia), and in Coelho et al. [32,35], Abatan et al. [33], and Freitas et al. [56,58] (Southeast Region and Paraná Basin).

The BCSD ensemble shows that all SA subdomains analyzed are prone to drought episodes during the 21st century. Although the ensemble projects predominantly mild droughts due to smoothing the most extreme projections, a considerable proportion of episodes last longer than 10 months. Additionally, the individual SPI-12 projections and the classification of hydrological drought events identified by each GCM demonstrate that all models project substantial proportions of moderate, severe, and extreme drought events (see Supplementary Materials). The significant occurrence of longer hydrological drought episodes corroborates analyses previously performed with CMIP6 models that indicate an increase in event duration during the 21st century under the SSP5-8.5 scenario in SA and a higher frequency of longer-lasting events [14].

3.4. Projections of Drought Parameters by the Bias-Corrected CMIP6-GCMs and BCSD Ensemble

Figures 7 and 8 show the drought parameters projected by the eight bias-corrected CMIP6-GCMs, as well as by CPC (for the historical period only) and BCSD ensemble under the SSP5-8.5 scenario. It is worth noting that the drought events and parameters reported here were obtained from the individual projections yielded by each CMIP6-GCM used. The Supplementary Materials present more information regarding the SPI-12 index and different hydrological drought classes projected by each CMIP6-GCM.

For R1, of the 301 episodes identified by all datasets (including all GCMs and the ensemble mean), 72% (218 cases) belong to the mild drought category, 16% (48 cases) correspond to the moderate drought class, 9% (28 cases) are of severe drought events, and 2% (7 cases) belong to the extreme drought category. Moreover, only three GCMs (CMCC-CM2-SR5, CMCC-ESM2, and MPI-ESM1-2-LR) indicate a slight increase in the average number of drought episodes in the 2020–2099 relative to the historical period, while the IPSL-CM6A-LR model and BCSD ensemble suggest a reduction of up to 27% and 23%, respectively.

On the other hand, seven of the nine datasets show an increase in the duration of drought episodes in 2020–2099 relative to 1996–2014. The IPSL-CM6A-LR and EC-Earth3 models indicate an increase of 47% and 32% in the duration (in months) of the events, respectively, while the BCSD ensemble provides an average increase of 25%. Similarly, most GCMs (and the BCSD ensemble) converge on increasing severity of drought episodes in the 21st century, with the IPSL-CM6A-LR model and the BCSD ensemble indicating increases of 51% and 40%, respectively. Regarding the intensity and peak parameters, GCMs show mixed signals, and the MRI-ESM2-0 and EC-Earth3 models show 12% and 18% increases in intensity and peak, respectively. In general, in this region, all GCMs overestimate the number of drought episodes over the historical period, and the GFDL-ESM4 and IPSL-CM6A-LR models show the largest range of parameter estimates for the 2020–2099 period.

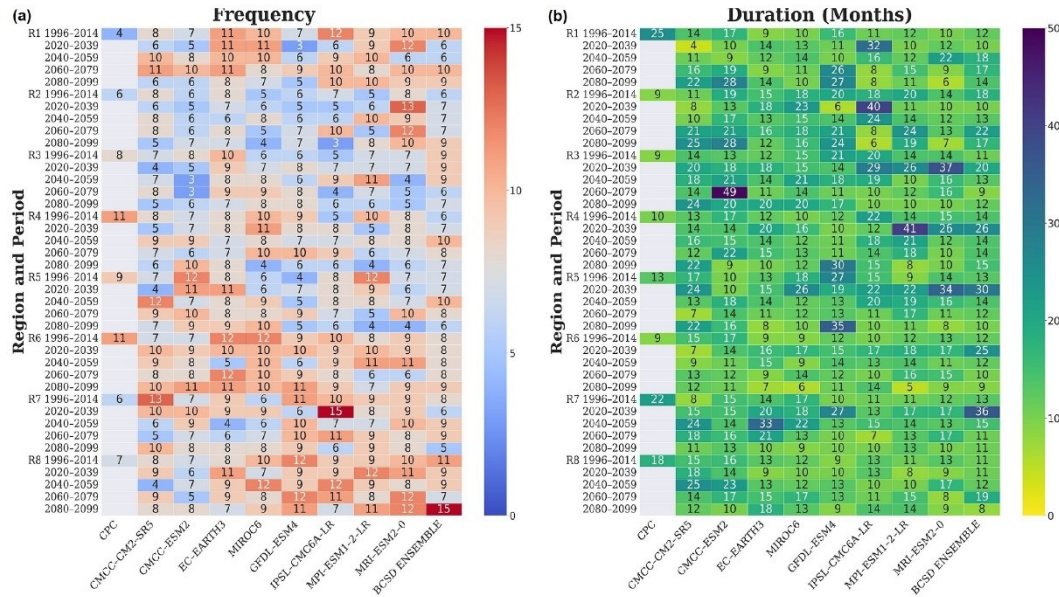
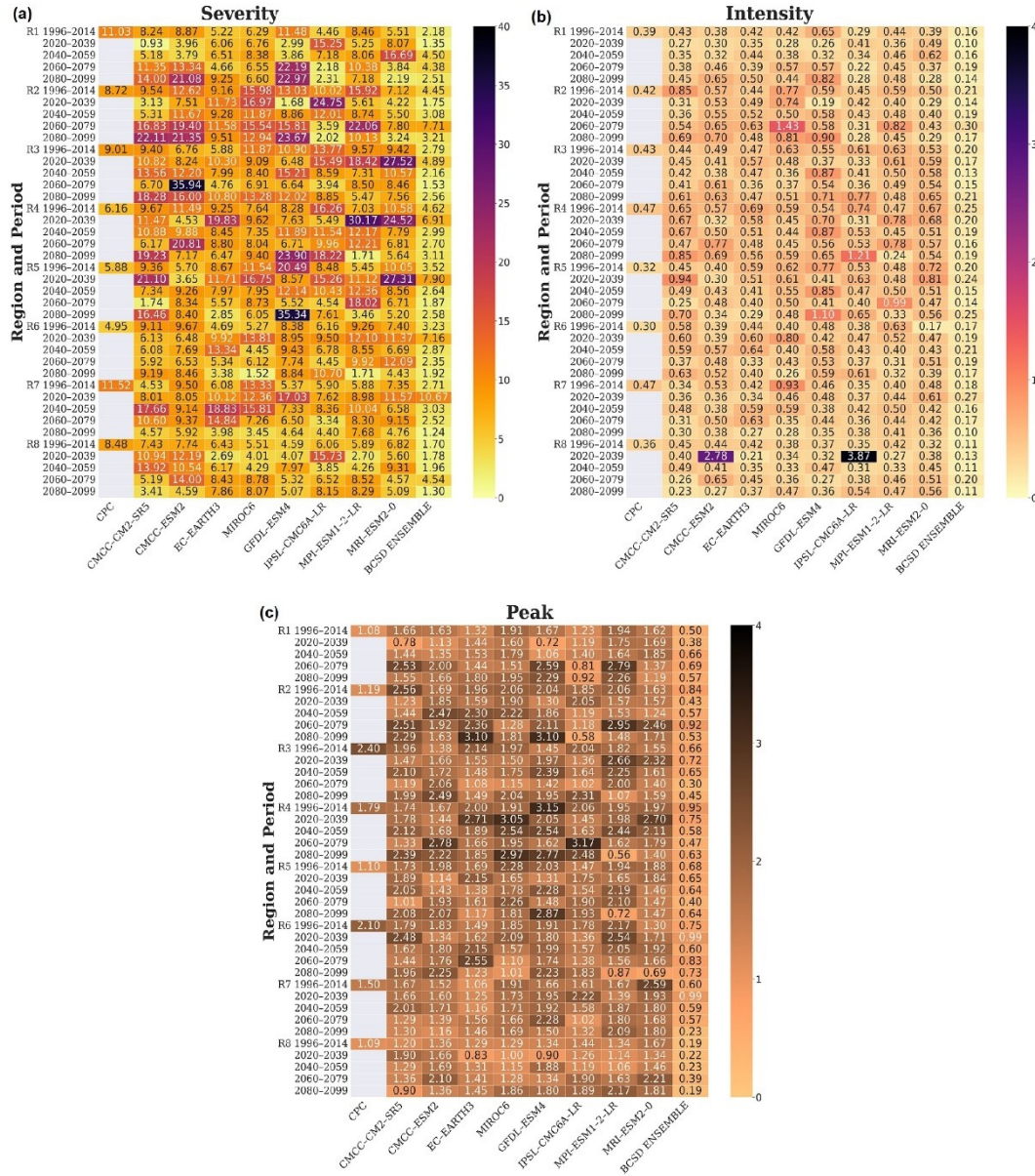


Figure 7. Heatmaps of drought frequency (a) and duration (b) projected by the bias-corrected CMIP6-GCMs and BCSd ensemble under the SSP5-8.5 scenario for eight subdomains of SA (R1–R8, Figure 1).

In R2, of the 252 episodes identified by all datasets, 65% (163 cases) correspond to the mild drought class, 17% (43 cases) to moderate drought events, 12% (30 cases) refer to severe drought events, and 6% (16 cases) are of extreme drought events. Additionally, about 70% of the datasets converge to a growing number of drought episodes in the coming decades relative to 1996–2014, with the MPI-ESM1-2-LR and MRI-ESM2-0 models indicating an average increase of up to 45% and 38%, respectively. In addition, half of the datasets show an increase in drought duration in the 21st century, with the CMCC-CM2-SR5 model providing an average increase of up to 50%. Similarly, this model projects an average increase of 24% in the severity of drought episodes. For the intensity and peak parameters, the GCMs show mixed signals, with the EC-Earth3 model providing an average increase of up to 19% in the magnitude of both parameters. In general, in this region, the GCMs perform better in representing drought episodes during the historical period, with the CMCC-ESM2 and GFDL-ESM4 models providing the same number of episodes obtained by CPC.

In R3, 245 drought episodes have been identified by the datasets, of which 64% (156 cases) correspond to mild drought episodes, 23% (56 cases) are moderate droughts, 9% (21 cases) are severe drought events, and 5% (12 cases) are extreme drought events. In this region, half of the datasets project an increase in the frequency of drought episodes in the 2020–2099 period (relative to 1996–2014), and half show a decrease. CMCC-ESM2 model indicates an average reduction of up to 47% in the number of episodes, but the MIROC6 model shows an average increase of up to 33%. Contrarily, only two GCMs (GFDL-ESM4 and IPSL-CM6A-LR) provide a reduction in episode duration, while all the others project increase during the following decades. MRI-ESM2-0 and CMCC-ESM2 yield average increases in the duration of drought episodes of up to 44% and 100%, respectively. The same models also provide the largest average increases in severity, corresponding to 44% and 168% (by MRI-ESM2-0 and CMCC-ESM2, respectively). As for the other regions, the intensity and peak projections show mixed signals, with the CMCC-ESM2 model

indicating a 44% increase in the average peak magnitude of episodes in 2020–2099, while the EC-Earth3 model shows a 34% reduction.



For R4, 267 drought episodes have been identified by all datasets, of which 58% (156 cases) are classified as mild droughts, 21% (57 cases) as moderate droughts, 11% (29 cases) as severe droughts, and 9% (25 cases) as extreme droughts. In this sector, GCMs show divergent projections about the frequency of drought episodes in 2020–2099. While the IPSL-CM6A-LR model projects an average increase of up to 50% in frequency, the MPI-ESM1-2-LR model estimates an average reduction of up to 43%. However, models converge about the increasing duration over the coming decades, with only three GCMs projecting reductions (CMCC-ESM2, IPSL-CM6A-LR, and MRI-ESM2-0) and the MPI-ESM1-2-LR model indicating an average increase of up to 61%. Similarly, GCMs are more homogenous concerning increasing severity, with the MPI-ESM1-2-LR model providing an average increase of up to 100%. While GCMs project mixed signals about changes in intensity, projections of peak changes are more concordant, with most models indicating an increase. In this case, the MIROC6 model projects an average increase of up to 37% in peak episodes over the coming decades.

In R5, all datasets total 277 drought episodes, of which 64% (176 cases) correspond to the mild drought class, 21% (58 cases) are moderate drought events, 11% (31 cases) are severe drought events, and 4% (12 cases) are extreme drought events. In this region, more than half of the datasets project an increasing frequency in drought episodes in 2020–2099, with the GFDL-ESM4 model indicating an average increase of up to 63%, while the MPI-ESM1-2-LR model projects an average reduction of up to 46%. Similarly, the same proportion of models projects an increase in episode duration over the coming decades, with the CMCC-ESM2 and MPI-ESM1-2-LR models providing average increases of up to 40% and 90%, respectively.

Regarding severity, only three GCMs project a reduction (EC-Earth3, MIROC6, and GFDL-ESM4), and the MPI-ESM1-2-LR model estimates an average increase of up to 106%. For the intensity and peak parameters, the signals provided are heterogeneous, with projections of change in intensity ranging from –32% (by EC-Earth3) to 34% (by CMCC-CM2-SR5) and amplitude of change in peak from –17% (by MRI-ESM2-0) to 21% (by IPSL-CM6A-LR).

For R6, of the 324 episodes identified by the datasets, 70% (227 cases) are classified as mild droughts, 16% (51 cases) as moderate droughts, 12% (38 cases) as severe droughts, and 2% (8 cases) as extreme droughts. In this sector, half of the ensembles project a reduction in the frequency of drought episodes (with the EC-Earth3 model providing an average reduction of up to 21%). Inversely, another half suggests an increase (with the CMCC-CM2-SR5 model projecting an average increase of up to 32%). Regarding episode duration in the 2020–2099 period, only two GCMs project a reduction (CMCC-CM2-SR5 and CMCC-ESM2), while the MIROC6 and EC-Earth3 models provide an average increase of 29% and 37%, respectively. Likewise, only three GCMs indicate a reduction in severity (CMCC-CM2-SR5, CMCC-ESM2, and MPI-ESM1-2-LR), while the IPSL-CM6A-LR and EC-Earth3 models project an average increase of 27% and 70%, respectively. Of the same, only the models CMCC-CM2-SR5 and MPI-ESM1-2-LR project a reduction in the intensity of drought episodes in 2020–2099, while the MRI-ESM2-0 model indicates an average increase of up to 158%. Regarding the peak of identified episodes, the outputs indicate mixed signals, with the EC-Earth3 model projecting an average increase of 26% and the MIROC6 model providing an average reduction of up to 22%.

In R7, a total of 293 drought episodes have been obtained, with 70% (206 cases) being mild droughts, 19% (56 cases) moderate droughts, 9% (27 cases) severe droughts, and 1% (4 cases) extreme droughts. Regarding the frequency, only two GCMs project an increase in the incidence (21% and 25% by the CMCC-ESM2 and MIROC6 models, respectively), while models such as EC-Earth3 and CMCC-CM2-SR5 indicate a reduction of 25% and 40%, respectively. Contrarily, only two GCMs project a reduction in episode duration (2% and 5% by CMCC-ESM2 and MIROC6 models, respectively), while EC-Earth3 and CMCC-CM2-SR5 models indicate a 49% and 101% increase, respectively. Alike, most models converge to a signal of increased severity of hydrological drought episodes in

the region in 2020–2099, with the GFDL-ESM4, EC-Earth3, and CMCC-CM2-SR5 models projecting average increases of 65%, 96%, and 125%, respectively. The datasets indicate mixed signals for intensity, with decreases and increases ranging from 4% to 55% and 6% to 13%, respectively. Similarly, projections of change in episode peaks are also more heterogeneous, with reductions and increases ranging from 0.10% to 30% and 7% to 28%, respectively.

Finally, in R8, all datasets give a total of 331 drought episodes in 2020–2099, of which 81% (268 cases) are classified as mild droughts, 13% (43 cases) as moderate droughts, 5% (17 cases) as severe droughts, and 1% (3 cases) as extreme droughts. Half of the outputs project a reduction in the duration of episodes in the sector, while another indicates an increase. As for the other regions, most GCMs converge on a signal of increasing duration of drought episodes, with the GFDL-ESM4 model projecting an average increase of up to 34%. Likewise, projections among the models are more concordant about the increasing severity, with the IPSL-CM6A-LR model providing an average increase of up to 41%. Additionally, most GCMs project an increase in peak episodes in 2020–2099 (only the EC-Earth3 model indicates an average reduction of up to 3%), with the BCSD ensemble providing an average increase of up to 32%.

In summary, GCMs project mixed signals about changes in drought events' frequency, intensity, and peak magnitudes during the coming decades in the SA subdomains. On the other hand, the projections are more homogeneous regarding the duration and severity of the episodes, with most models converging to increasing magnitudes of both parameters in all sectors evaluated. Concerning the different categories of droughts (mild, moderate, severe, and extreme), results show a larger occurrence of mild droughts. However, regions such as the northern and central Northeast, Midwest, and Southeast Brazil show a substantial proportion (above 20%) of moderate drought events, as well as a relevant occurrence (above 10%) of severe drought events in the Amazonia region, central Northeast, Midwest, and Southeast Brazil (see Supplementary Materials). Based on this, we highlight that although the BCSD ensemble provides predominantly mild drought episodes, individual analyses of the CMIP6-GCMs indicate expressive frequencies of moderate and severe events in all the evaluated subdomains.

4. Conclusions

In this study, we applied statistical downscaling to CMIP6 precipitation projections in SA using the CPC data as a reference to evaluate future changes in precipitation and the occurrence of hydrological droughts on the continent. To this end, we used the QDM technique developed by Cannon et al. [91], and the method proved effective in reducing systematic biases and preserving the trends of GCM projections. For the coming decades, the post-processed precipitation projections indicate reduced rainfall in sectors such as northern SA, North, Northeast, Midwest, and Southeast Brazil and increased precipitation in southern Brazil and SESA regions. Such changes are more prominent during the austral spring (SON), and their signal is more robust under the SSP5-8.5 scenario, corroborating the literature.

The SPI-12 index analysis shows considerable variability of projections among the GCMs about drought event parameters, such as frequency, intensity, and peak. On the other hand, concerning duration and severity, a more remarkable agreement is observed among the GCMs regarding the intensification of both aspects in practically all the subdomains analyzed. Considering the different categories of drought events, the results showed a substantial frequency of moderate and severe droughts in Brazil's Northeast, Midwest, and Southeast. In addition, the individual CMIP6-GCMs and the BCSD ensemble project a considerable proportion of events with a duration equal to or greater than 10 months in all evaluated South American sectors.

Given the results, it is valid to highlight some limitations of the study. First, we point out that although the SPI-12 analysis is easy to implement because it uses only precipitation information, it disregards crucial aspects of the droughts related to temperature and

evapotranspiration processes. In this context, analyses have indicated that the frequency and duration of droughts in SA are driven mainly by climate factors such as maximum and minimum temperatures, net surface radiation, and precipitation [148]. Thus, future studies employing statistical downscaling should address these aspects for assessing droughts on the continent during the 21st century.

In addition, we mention that although the statistical downscaling technique reduces model biases, considerable systematic errors persist and may propagate into future projections. The precipitation simulation by climate models poses several challenges due to the many processes involved, mostly parameterized, operating, and interacting at different temporal and spatial scales. Even though the refinement of the horizontal grid improves precipitation simulation, it does not deterministically guarantee better results. Added to these difficulties is the uncertainty associated with data sources for validation and the scarcity of precipitation observational networks across the continent. All these factors constrain the assertiveness of the estimates, and their uncertainties should be pointed out since the results are of interest to decision-makers.

Furthermore, although the study employed eight GCMs and the multi-model ensemble, it is recommended that future studies use a larger number of models and forcing scenarios to constrain the uncertainties associated with the projections. The projections presented here have an intermediate spatial resolution of 50 km, which limits the spatial detail of the analyses performed. In this sense, further research should consider climate projections with a finer spatial resolution to ensure greater accuracy of the results. However, the feasibility of such approaches demands high computational costs. Overall, despite the uncertainties associated with GCMs, identifying hydrological drought episodes, and the bias correction technique, the results presented here can provide valuable contributions to decision-makers and energy planners for better managing water resources on the South American continent for the coming decades.

Supplementary Materials: The following supporting information can be downloaded at: <https://www.mdpi.com/article/10.3390/cli11080166/s1>, Figure S1: Mean annual differences of precipitation (%) between the future (2020–2039, 2040–2059, 2060–2079, 2080–2099) and historical period (1995–2014), projected by the BCSD ensemble under the SSP2-4.5 (a–d) and SSP5-8.5 (e–h) forcing scenarios. Hatched areas indicate statistical significance at a 95% confidence level; Figure S2: Temporal series (2020–2099) of the SPI-12 index projected by the eight CMIP6-GCMs used in the study and the BCSD ensemble (solid black line) under the SSP5-8.5 scenario for eight SA subdomains; Figure S3: Classification of hydrological drought events identified by each CMIP-GCM used in the study and the BCSD ensemble for eight SA subdomains in 2020–2099 under the SSP5-8.5 scenario.

Author Contributions: Conceptualization, G.W.d.S.F. and M.S.R.; methodology, G.W.d.S.F. and M.S.R.; software, G.W.d.S.F., M.S.R., J.G.M.R. and C.A.d.S.; formal analysis, G.W.d.S.F. and M.S.R.; writing—original draft preparation, G.W.d.S.F. and M.S.R.; writing—review and editing, G.W.d.S.F. and M.S.R. All authors have read and agreed to the published version of the manuscript.

Funding: The authors thank the Coordination for the Improvement of Higher Education Personnel (CAPES, Finance Code 001), the National Council for Scientific and Technological Development (CNPq), and the R&D project from Engie Brazil Energy (R&D-00403-0054/2022) regulated by the Brazilian National Electric Energy Agency (ANEEL).

Institutional Review Board Statement: Not applicable.

Informed Consent Statement: Not applicable.

Data Availability Statement: All datasets used in this study are available on public online databases.

Acknowledgments: The authors thank the Coordination for the Improvement of Higher Education Personnel (CAPES), the Brazilian National Electric Energy Agency (ANEEL), the National Council for Scientific and Technological Development (CNPq), and ENGIE Brazil Energy for the financial support. The authors also thank the Coupled Model Intercomparison Project (CMIP) and Climate Prediction Center (NOAA-CPC) for providing the datasets used in this study.

Conflicts of Interest: The authors declare no conflict of interest. The funders had no role in the design of the study; in the collection, analyses, or interpretation of the data; in the writing of the manuscript; or in the decision to publish the results.

References

1. Intergovernmental Panel on Climate Change (IPCC). Summary for Policymakers. In *Climate Change 2023: Synthesis Report. A Report of the Intergovernmental Panel on Climate Change. Contribution of Working Groups I, II and III to the Sixth Assessment Report of the Intergovernmental Panel on Climate Change*; Core Writing Team, Lee, H., Romero, J., Eds.; IPCC: Geneva, Switzerland, 2023; p. 36. Available online: https://www.ipcc.ch/report/ar6/syr/downloads/report/IPCC_AR6_SYR_SPM.pdf (accessed on 2 May 2023).
2. United Nations Environment Programme (UNEP). Emissions Gap Report 2022: The Closing Window—Climate Crisis Calls for Rapid Transformation of Societies. *Nairobi*. 2022. Available online: <https://www.unep.org/emissions-gap-report-2022> (accessed on 2 May 2023).
3. Tavares, P.S.; Acosta, R.; Nobre, P.; Resende, N.C.; Chou, S.C.; Lyra, A.A. Water balance components and climate extremes over Brazil under 1.5 °C and 2.0 °C of global warming scenarios. *Reg. Environ. Chang.* **2023**, *23*, 40. [[CrossRef](#)] [[PubMed](#)]
4. Panisset, J.S.; Libonati, R.; Gouveia, C.M.P.; Machado-Silva, F.; França, D.A.; França, J.R.A.; Peres, L.F. Contrasting patterns of the extreme drought episodes of 2005, 2010 and 2015 in the Amazon Basin. *Int. J. Climatol.* **2018**, *38*, 1096–1104. [[CrossRef](#)]
5. Gozzo, L.F.; Palma, D.S.; Custodio, M.S.; Machado, J.P. Climatology and trend of severe drought events in the state of Sao Paulo, Brazil, during the 20th century. *Atmosphere* **2019**, *10*, 190. [[CrossRef](#)]
6. Gozzo, L.F.; Drumond, A.; Pampuch, L.A.; Ambrizzi, T.; Crespo, N.M.; Reboita, M.S.; Bier, A.A.; Carpenedo, C.B.; Bueno, P.G.; Pinheiro, H.R.; et al. Intraseasonal drivers of the 2018 drought over São Paulo, Brazil. *Front. Clim.* **2022**, *4*, 852824. [[CrossRef](#)]
7. Papalexioiu, S.M.; Rajulapati, C.R.; Andreadis, K.M.; Foufoula-Georgiou, E.; Clark, M.P.; Trenberth, K.E. Probabilistic Evaluation of drought in CMIP6 simulations. *Earth's Future* **2021**, *9*, e2021EF002150. [[CrossRef](#)]
8. Medeiros, F.J.; Oliveira, C.P. Assessment of dry and heavy rainfall days and their projected changes over Northeast Brazil in Coupled Model Intercomparison Project Phase 6 models. *Int. J. Climatol.* **2022**, *42*, 8665–8686. [[CrossRef](#)]
9. Keellings, D.; Engström, J. The future of drought in the southeastern U.S.: Projections from downscaled CMIP5 models. *Water* **2019**, *11*, 259. [[CrossRef](#)]
10. Swain, S.; Hayhoe, K. CMIP5 projected changes in spring and summer drought and wet conditions over North America. *Clim. Dyn.* **2015**, *44*, 2737–2750. [[CrossRef](#)]
11. Cook, B.I.; Mankin, J.S.; Marvel, K.; Williams, A.P.; Smerdon, J.E.; Anchukaitis, K.J. Twenty-first century drought projections in the CMIP6 forcing scenarios. *Earth's Future* **2020**, *8*, e2019EF001461. [[CrossRef](#)]
12. Wu, C.; Yeh, P.J.-F.; Chen, Y.-Y.; Lv, W.; Hu, B.X.; Huang, G. Future precipitation-driven meteorological drought changes in the CMIP5 multimodel ensembles under 1.5 °C and 2 °C global warming. *J. Hydrometeorol.* **2020**, *21*, 2177–2196. [[CrossRef](#)]
13. Wu, C.; Yeh, P.J.-F.; Chen, Y.-Y.; Lv, W.; Hu, B.X.; Huang, G. Copula-based risk evaluation of global meteorological drought in the 21st century based on CMIP5 multi-model ensemble projections. *J. Hydrol.* **2021**, *598*, 126265. [[CrossRef](#)]
14. Wang, T.; Tu, X.; Singh, V.P.; Chen, X.; Lin, K. Global data assessment and analysis of drought characteristics based on CMIP6. *J. Hydrol.* **2021**, *596*, 126091. [[CrossRef](#)]
15. Tam, B.Y.; Szeto, K.; Bonsal, B.; Flato, G.; Cannon, A.J.; Rong, R. CMIP5 drought projections in Canada based on the Standardized Precipitation Evapotranspiration Index. *Can. Water Resour. J.* **2019**, *44*, 90–107. [[CrossRef](#)]
16. Javadinejad, S.; Hannah, D.; Ostad-Ali-Askari, K.; Krause, S.; Zalewski, M.; Boogaard, F. The impact of future climate change and human activities on hydro-climatological drought, analysis and projections: Using CMIP5 climate model simulations. *Water Conserv. Sci. Eng.* **2019**, *4*, 71–88. [[CrossRef](#)]
17. Nguyen-Ngoc-Bich, P.; Phan-Van, T.; Ngo-Duc, T.; Vu-Minh, T.; Trinh-Tuan, L.; Tangang, F.T.; Juneng, L.; Cruz, F.; Santisirisonboon, J.; Narisma, G.; et al. Projected evolution of drought characteristics in Vietnam based on CORDEX-SEA downscaled CMIP5 data. *Int. J. Climatol.* **2021**, *41*, 5733–5751. [[CrossRef](#)]
18. Coppola, E.; Raffaele, F.; Giorgi, F.; Giuliani, G.; Xuejie, G.; Ciarlo, J.M.; Sines, T.R.; Torres-Alavez, J.A.; Das, S.; di Sante, F.; et al. Climate hazard indices projections based on CORDEX-CORE, CMIP5 and CMIP6 ensemble. *Clim. Dyn.* **2020**, *57*, 1293–1383. [[CrossRef](#)]
19. Bouramdane, A.-A. Assessment of CMIP6 multi-model projections worldwide: Which regions are getting warmer and are going through a drought in Africa and Morocco? What changes from CMIP5 to CMIP6? *Sustainability* **2023**, *15*, 690. [[CrossRef](#)]
20. Betts, R.A.; Alfieri, L.; Bradshaw, C.; Caesar, J.; Feyen, L.; Friedlingstein, P.; Gohar, L.; Koutroulis, A.; Lewis, K.; Morfopoulos, C.; et al. Changes in climate extremes, fresh water availability and vulnerability to food insecurity projected at 1.5 °C and 2 °C global warming with a higher-resolution global climate model. *Philos. Trans. R. Soc. A* **2018**, *376*, 20160452. [[CrossRef](#)] [[PubMed](#)]
21. Campozano, L.; Ballari, D.; Montenegro, M.; Avilés, A. Future meteorological droughts in Ecuador: Decreasing trends and associated spatio-temporal features derived from CMIP5 models. *Front. Earth Sci.* **2020**, *8*, 17. [[CrossRef](#)]
22. Marengo, J.A.; Cunha, A.P.M.A.; Nobre, C.A.; Ribeiro Neto, G.G.; Magalhaes, A.R.; Torres, R.R.; Sampaio, G.; Alexandre, F.; Alves, L.M.; Cuartas, L.A.; et al. Assessing drought in the drylands of northeast Brazil under regional warming exceeding 4 °C. *Nat. Hazards* **2020**, *103*, 2589–2611. [[CrossRef](#)]
23. Reboita, M.S.; Kuki, C.A.C.; Marrafon, V.H.; Souza, C.A.; Ferreira, G.W.S.; Teodoro, T.; Lima, J.W.M. South America climate change revealed through climate indices projected by GCMs and Eta-RCM ensembles. *Clim. Dyn.* **2021**, *58*, 459–485. [[CrossRef](#)]

24. Reboita, M.S.; da Rocha, R.P.; Souza, C.A.; Baldoni, T.C.; Silva, P.L.L.S.; Ferreira, G.W.S. Future projections of extreme precipitation climate indices over South America based on CORDEX-CORE multimodel ensemble. *Atmosphere* **2022**, *13*, 1463. [CrossRef]
25. Gouveia, C.D.; Torres, R.R.; Marengo, J.A.; Avila-Diaz, A. Uncertainties in projections of climate extremes indices in South America via Bayesian inference. *Int. J. Climatol.* **2022**, *42*, 7362–7382. [CrossRef]
26. Marengo, J.A.; Alves, L.M.; Alvala, R.C.S.; Cunha, A.P.; Brito, S.; Moraes, O.L.L. Climatic characteristics of the 2010–2016 drought in the semi-arid Northeast Brazil region. *An. Acad. Bras. Ciéncia* **2018**, *90*, 1973–1985. [CrossRef] [PubMed]
27. Marengo, J.A.; Torres, R.R.; Alves, L.M. Drought in Northeast Brazil: Past, present, and future. *Theor. Appl. Climatol.* **2016**, *129*, 1189–1200. [CrossRef]
28. Marengo, J.A.; Galdos, M.V.; Challinor, A.; Cunha, A.P.; Marin, F.R.; Vianna, M.S.; Alvala, R.C.S.; Alves, L.M.; Moraes, O.L.; Bender, F. Drought in Northeast Brazil: A review of agricultural and policy adaptation options for food security. *Clim. Res. Sustain.* **2022**, *1*, e17. [CrossRef]
29. Cavalcanti, I.F.A.; Kousky, V.E. Drought in Brazil during Summer and Fall 2001 and Associated Atmospheric Circulation Features. *Rev. Climatolise* **2001**, *2*, 1. Available online: <http://climanalise.ctpec.inpe.br/~rclimanl/revista/pdf/criseing.pdf> (accessed on 5 May 2023).
30. Seth, A.; Fernandes, K.; Camargo, S.J. Two summers of São Paulo drought: Origins in the western tropical Pacific. *Geophys. Res. Lett.* **2015**, *42*, 10816–10823. [CrossRef]
31. Nobre, C.A.; Marengo, J.A.; Seluchi, M.E.; Cuartas, A.; Alves, L.M. Some characteristics and impacts of the drought and water Crisis in southeastern Brazil during 2014 and 2015. *J. Water Resour. Prot.* **2016**, *8*, 252–262. [CrossRef]
32. Coelho, C.A.S.; Oliveira, C.P.; Ambrizzi, T.; Reboita, M.S.; Carpenedo, C.B.; Campos, J.L.P.S.; Tomaziello, A.C.N.; Pampuch, L.A.; Custódio, M.S.; Dutra, L.M.M.; et al. The 2014 southeast Brazil austral summer drought: Regional scale mechanisms and teleconnections. *Clim. Dyn.* **2016**, *46*, 3737–3752. [CrossRef]
33. Abatan, A.A.; Tett, S.F.B.; Dong, B.; Cunningham, C.; Rudorff, C.M.; Klingaman, N.P.; de Abreu, R.C. Drivers and physical processes of drought events over the state of São Paulo, Brazil. *Clim. Dyn.* **2022**, *58*, 3105–3119. [CrossRef]
34. Geirinhas, J.L.; Russo, A.C.; Libonati, R.; Miralles, D.G.; Sousa, P.M.; Wouters, H.; Trigo, R.M. The influence of soil dry-out on the record-breaking hot 2013/2014 summer in Southeast Brazil. *Sci. Rep.* **2022**, *12*, 5836. [CrossRef] [PubMed]
35. Coelho, C.A.S.; Cardoso, D.H.F.; Firpo, M.A.F. Precipitation diagnostics of an exceptionally dry event in São Paulo, Brazil. *Theor. Appl. Climatol.* **2016**, *125*, 769–784. [CrossRef]
36. Cuartas, L.A.; Cunha, A.P.M.A.; Alves, J.A.; Parra, L.M.P.; Deusdará-Leal, K.; Costa, L.C.O.; Molina, R.D.; Amore, D.; Broedel, E.; Seluchi, M.E.; et al. Recent hydrological droughts in Brazil and their impact on hydropower generation. *Water* **2022**, *14*, 601. [CrossRef]
37. Marengo, J.A.; Espinoza, J.C. Extreme seasonal droughts and floods in Amazonia: Causes, trends and impacts. *Int. J. Climatol.* **2016**, *36*, 1033–1050. [CrossRef]
38. Agudelo, J.; Arias, P.A.; Vieira, S.C.; Martínez, J.A. Influence of longer dry seasons in the Southern Amazon on patterns of water vapor transport over northern South America and the Caribbean. *Clim. Dyn.* **2019**, *52*, 2647–2665. [CrossRef]
39. Lovejoy, T.E.; Nobre, C. Amazon tipping point: Last chance for action. *Sci. Adv.* **2019**, *5*, eaba2949. Available online: <https://www.science.org/doi/10.1126/sciadv.aba2949> (accessed on 7 May 2023). [CrossRef]
40. Jimenez, J.C.; Marengo, J.A.; Alves, L.M.; Sulca, J.C.; Takahashi, K.; Ferrett, S.; Collins, M. The role of ENSO flavours and TNA on recent droughts over Amazon forests and the Northeast Brazil region. *Int. J. Climatol.* **2021**, *41*, 3761–3780. [CrossRef]
41. Guimberteau, M.; Ronchail, J.; Espinoza, J.C.; Lengaigne, M.; Sultan, B.; Polcher, J.; Drapeau, G.; Guyot, J.-L.; Ducharne, A.; Ciais, P. Future changes in precipitation and impacts on extreme streamflow over Amazonian sub-basins. *Environ. Res. Lett.* **2013**, *8*, 014035. Available online: <https://iopscience.iop.org/article/10.1088/1748-9326/8/1/014035> (accessed on 7 May 2023). [CrossRef]
42. Duffy, P.B.; Brando, P.; Asner, G.P.; Field, C.B. Projections of future meteorological drought and wet periods in the Amazon. *Proc. Natl. Acad. Sci. USA* **2015**, *112*, 43. [CrossRef]
43. Boulton, C.A.; Lenton, T.M.; Boers, N. Pronounced loss of Amazon rainforest resilience since the early 2000's. *Nat. Clim. Chang.* **2022**, *12*, 271–278. [CrossRef]
44. Borges, P.A.; Bernhofer, C.; Rodrigues, R. Extreme rainfall indices in Distrito Federal, Brazil: Trends and links with El Niño southern oscillation and Madden-Julian oscillation. *Int. J. Climatol.* **2018**, *38*, 4550–4567. [CrossRef]
45. Thielen, D.; Schuchmann, K.-L.; Ramoni-Perazzi, P.; Marquez, M.; Rojas, W.; Quintero, J.I.; Marques, M.I. Quo vadis Pantanal? Expected precipitation extremes and drought dynamics from changing sea surface temperature. *PLoS ONE* **2020**, *15*, e0227437. [CrossRef] [PubMed]
46. Marengo, J.A.; Cunha, A.P.; Cuartas, L.A.; Deusdará-Leal, K.R.; Broedel, E.; Seluchi, M.E.; Michelin, C.M.; Baião, C.F.P.; Ângulo, E.C.; Almeida, E.K.; et al. Extreme drought in the Brazilian Pantanal in 2019–2020: Characterization, causes, and impacts. *Front. Water* **2021**, *3*, 639204. [CrossRef]
47. Cunha, A.P.M.A.; Zeri, M.; Deusdará-Leal, K.; Costa, L.; Cuartas, L.A.; Marengo, J.A.; Tomasella, J.; Vieira, R.M.; Barbosa, A.A.; Cunningham, C.; et al. Extreme drought events over Brazil from 2011 to 2019. *Atmosphere* **2019**, *10*, 642. [CrossRef]
48. Fernandes, V.R.; Cunha, A.P.M.A.; Pineda, L.A.C.; Leal, K.R.D.; Costa, L.C.O.; Broedel, E.; França, D.A.; Alvalá, R.C.S.; Seluchi, M.E.; Marengo, J.A. Secas e os impactos na região sul do Brasil. *Rev. Bras. Climatol.* **2021**, *28*, 561–584. [CrossRef]

49. Müller, O.V.; Berbery, E.H.; Alcaraz-Segura, D.; Ek, M.B. Regional model simulations of the 2008 drought in southern South America using a consistent set of land surface properties. *J. Clim.* **2014**, *27*, 6754–6778. [CrossRef]
50. Sgroi, L.C.; Lovino, M.A.; Berbery, E.H.; Müller, G.V. Characteristics of droughts in Argentina's core crop region. *Hydrol. Earth Syst. Sci.* **2021**, *25*, 2475–2490. [CrossRef]
51. Lovino, M.A.; Müller, O.V.; Berbery, E.H.; Müller, G.V. How have daily climate extremes changed in the recent past over northeastern Argentina? *Glob. Planet. Chang.* **2018**, *168*, 78–97. [CrossRef]
52. Olmo, M.; Bettolli, M.L.; Rusticucci, M. Atmospheric circulation influence on temperature and precipitation individual and compound daily extreme events: Spatial variability and trends over southern South America. *Weather. Clim. Extremes* **2020**, *29*, 100267. [CrossRef]
53. Lovino, M.A.; Müller, G.V.; Pierrestegui, M.J.; Espinosa, E.; Rodríguez, L. Extreme precipitation events in the Austral Chaco region of Argentina. *Int. J. Climatol.* **2022**, *42*, 5985–6006. [CrossRef]
54. Collazo, S.; Barrucand, M.; Rusticucci, M. Evaluation of CMIP6 models in the representation of observed extreme temperature indices trends in South America. *Clim. Chang.* **2022**, *172*, 21. [CrossRef]
55. Balmaceda-Huarte, R.; Olmo, M.E.; Bettolli, M.L.; Poggi, M.M. Evaluation of multiple reanalyses in reproducing the spatio-temporal variability of temperature and precipitation indices over southern South America. *Int. J. Climatol.* **2021**, *41*, 5572–5595. [CrossRef]
56. Freitas, A.A.; Reboita, M.S.; Carvalho, V.S.B.; Drumond, A.; Ferraz, S.E.T.; Silva, B.C.; da Rocha, R.P. Atmospheric and oceanic patterns associated with extreme drought events over the Paraná Hydrographic Region, Brazil. *Climate* **2023**, *11*, 12. [CrossRef]
57. McKee, T.B.; Doesken, N.J.; Kleist, J. The relationship of drought frequency and duration to time scales. In Proceedings of the 8th Conference on Applied Climatology, Anaheim, CA, USA, 17–22 January 1993; pp. 179–183. Available online: <https://climate.colostate.edu/pdfs/relationshipofdroughtfrequency.pdf> (accessed on 10 May 2023).
58. Freitas, A.A.; Drumond, A.; Carvalho, V.S.B.; Reboita, M.S.; Silva, B.C.; Uvo, C.B. Drought assessment in São Francisco River Basin, Brazil: Characterization through SPI and associated anomalous climate patterns. *Atmosphere* **2022**, *13*, 41. [CrossRef]
59. World Meteorological Organization (WMO). *Standardized Precipitation Index User Guide*; WMO-No. 1090; WMO: Geneva, Switzerland, 2012.
60. Brito, S.S.B.; Cunha, A.P.M.; Cunningham, C.C.; Alvalá, R.C.; Marengo, J.A.; Carvalho, M.A. Frequency, duration and severity of drought in the Semiarid Northeast Brazil region. *Int. J. Climatol.* **2017**, *38*, 517–529. [CrossRef]
61. Santos, S.R.Q.; Braga, C.C.; Sansigolo, C.A.; Santos, A.P.P. Determinação de regiões homogêneas do índice de precipitação normalizada (SPI) na Amazônia Oriental. *Rev. Bras. Meteorol.* **2017**, *32*, 111–122. [CrossRef]
62. Oliveira-Júnior, J.F.; Gois, G.; Terassi, P.M.B.; Silva Junior, C.A.; Blanco, C.J.C.; Sobral, B.S.; Gasparini, K.A.C. Drought severity based on the SPI index and its relation to the ENSO and PDO climatic variability modes in the regions North and Northwest of the State of Rio de Janeiro-Brazil. *Atmos. Res.* **2018**, *212*, 91–105. [CrossRef]
63. Pereira, V.R.; Blain, G.C.; Avila, A.M.; Pires, R.C.; Pinto, H.S. Impacts of climate change on drought: Changes to drier conditions at the beginning of the crop growing season in southern Brazil. *Bragantia* **2018**, *77*, 201–211. [CrossRef]
64. Costa, M.D.S.; Oliveira-Júnior, J.F.D.; Santos, P.J.D.; Correia Filho, W.L.F.; Gois, G.D.; Blanco, C.J.C.; Teodoro, P.E.; Silva Junior, C.A.; Santiago, D.B.; Souza, E.O.; et al. Rainfall extremes and drought in Northeast Brazil and its relationship with El Niño–Southern Oscillation. *Int. J. Climatol.* **2020**, *41*, E2111–E2135. [CrossRef]
65. Silva, D.F.; Lima, M.J.S.; Souza Neto, P.F.; Gomes, H.B.; Silva, F.D.S.; Almeida, H.R.R.C.; Pereira, M.P.S.; Costa, R.L. Caracterização de eventos extremos e de suas causas climáticas com base no índice padronizado de precipitação para o leste do Nordeste. *Rev. Bras. Geogr. Fis.* **2020**, *13*, 449–464. [CrossRef]
66. Xavier, L.C.P.; Silva, S.M.O.D.; Carvalho, T.M.N.; Pontes Filho, J.D.; Souza Filho, F.D.A.D. Use of machine learning in evaluation of drought perception in irrigated agriculture: The case of an irrigated perimeter in Brazil. *Water* **2020**, *12*, 1546. [CrossRef]
67. Avila-Diaz, A.; Torres, R.R.; Zuluaga, C.F.; Cerón, W.L.; Oliveira, L.; Benezoli, V.; Rivera, I.A.; Marengo, J.A.; Wilson, A.B.; Medeiros, F. Current and future climate extremes over Latin America and Caribbean: Assessing Earth System Models from High Resolution Model Intercomparison Project (HighResMIP). *Earth Syst. Environ.* **2023**, *7*, 99–130. [CrossRef] [PubMed]
68. Eyring, V.; Bony, S.; Meehl, G.A.; Senior, C.A.; Stevens, B.; Stouffler, R.J.; Taylor, K.E. Overview of the global coupled model intercomparison project phase 6 (CMIP6) experimental design and organization. *Geosci. Model. Dev.* **2016**, *9*, 1937–1958. [CrossRef]
69. Riahi, K.; van Vuuren, D.P.; Kriegler, E.; Edmonds, J.; O'Neill, B.C.; Fujimori, S.; Bauer, N.; Calvin, K.; Dellink, R.; Fricko, O.; et al. The Shared Socio-economic Pathways and their energy, land use, and greenhouse gas emissions implications: A review. *Glob. Environ. Chang.* **2017**, *42*, 153–168. [CrossRef]
70. Carvalho, D.; Rocha, A.; Costoya, X.; de Castro, M.; Gómez-Gesteira, M. Wind energy resource over Europe under CMIP6 future climate projections: What changes from CMIP5 to CMIP6. *Renew. Sustain. Energy Rev.* **2021**, *151*, 111594. [CrossRef]
71. Fowler, H.J.; Blenkinsop, S.; Tebaldi, C. Linking climate change modelling to impacts studies: Recent advances in downscaling techniques for hydrological modelling. *Int. J. Climatol.* **2007**, *27*, 1547–1578. [CrossRef]
72. Ambrizzi, T.; Reboita, M.S.; da Rocha, R.P.; Llopart, M. The state of the art and fundamental aspects of regional climate modeling in South America. *Ann. N. Y. Acad. Sci.* **2019**, *1436*, 98–120. [CrossRef]
73. Mutz, S.G.; Scherrer, S.; Muceniece, I.; Ehlers, T.A. Twenty-first century regional temperature response in Chile based on empirical-statistical downscaling. *Clim. Dyn.* **2021**, *56*, 2881–2894. [CrossRef]

74. Da Rocha, R.P.; Morales, C.A.; Cuadra, S.V.; Ambrizzi, T. Precipitation diurnal cycle and summer climatology assessment over South America: An evaluation of Regional Climate Model version 3 simulations. *J. Geophys. Res. Atmos.* **2009**, *114*, D10. [[CrossRef](#)]
75. Marengo, J.A.; Chou, S.C.; Kay, G.; Alves, L.M.; Pesquero, J.F.; Soares, W.R.; Santos, D.C.; Lyra, A.A.; Sueiro, G.; Betts, R.; et al. Development of regional future climate change scenarios in South America using the Eta CPTEC/HadCM3 climate change projections: Climatology and regional analyses for the Amazon, São Francisco and the Paraná River basins. *Clim. Dyn.* **2012**, *38*, 1829–1848. [[CrossRef](#)]
76. Chou, S.C.; Lyra, A.; Mourão, C.; Dereczynski, C.; Pilotto, I.; Gomes, J.; Bustamante, J.; Tavares, P.; Silva, A.; Rodrigues, D.; et al. Evaluation of the Eta simulations nested in three global climate models. *Am. J. Clim. Chang.* **2014**, *3*, 438–454. [[CrossRef](#)]
77. Reboita, M.S.; da Rocha, R.P.; Dias, C.G.; Ynoue, R.Y. Climate projections for South America: RegCM3 driven by HadCM3 and ECHAM5. *Adv. Meteorol.* **2014**, *2014*, 376738. [[CrossRef](#)]
78. Reboita, M.S.; Dutra, L.M.M.; Dias, C.G. Diurnal cycle of precipitation simulated by RegCM4 over South America: Present and future scenarios. *Clim. Res.* **2016**, *70*, 39–55. [[CrossRef](#)]
79. Reboita, M.S.; Amaro, T.R.; de Souza, M.R. Winds: Intensity and power density simulated by RegCM4 over South America in present and future climate. *Clim. Dyn.* **2018**, *51*, 187–205. [[CrossRef](#)]
80. Solman, S.A.; Blázquez, J. Multiscale precipitation variability over South America: Analysis of the added value of CORDEX RCM simulations. *Clim. Dyn.* **2019**, *53*, 1547–1565. [[CrossRef](#)]
81. Dereczynski, C.; Chou, S.C.; Lyra, A.; Sondermann, M.; Regoto, P.; Tavares, P.; Chagas, D.; Gomes, J.L.; Rodrigues, D.C.; Skansi, M.M. Downscaling of climate extremes over South America—Part I: Model evaluation in the reference climate. *Weather Clim. Extremes* **2020**, *29*, 100273. [[CrossRef](#)]
82. Solman, S.A.; Bettolli, M.L.; Doyle, M.E.; Olmo, M.E.; Feijoo, M.; Martinez, D.; Blázquez, J.; Balmaceda-Huarte, R. Evaluation of multiple downscaling tools for simulating extreme precipitation events over southeastern South America: A case study approach. *Clim. Dyn.* **2021**, *57*, 1241–1264. [[CrossRef](#)]
83. Silva, N.P.; Crespo, N.M.; Kaufmann, C.L.G.; Lima, J.A.M.; Andrioni, M.; Camargo, R.; da Rocha, R.P. Adjustment of extreme wind speed in regional climate downscaling over southwestern South Atlantic. *Int. J. Climatol.* **2022**, *42*, 9994–10008. [[CrossRef](#)]
84. Silva, M.L.; Oliveira, C.P.; Silva, C.M.S.; Araújo, J.M. Dynamic downscaling of climate simulations and projected changes in tropical South America using RegCM4.7. *Int. J. Climatol.* **2023**, *43*, 3391–3415. [[CrossRef](#)]
85. Bettolli, M.L.; Penalba, O.C. Statistical downscaling of daily precipitation and temperatures in southern La Plata Basin. *Int. J. Climatol.* **2018**, *38*, 3705–3722. [[CrossRef](#)]
86. Sulca, J.; Vuille, M.; Timm, O.E.; Dong, B.; Zubieta, R. Empirical–statistical downscaling of austral summer precipitation over South America, with a focus on the Central Peruvian Andes and the Equatorial Amazon Basin. *J. Appl. Meteorol. Climatol.* **2021**, *60*, 65–85. [[CrossRef](#)]
87. Balmaceda-Huarte, R.; Bettolli, M.L. Assessing statistical downscaling in Argentina: Daily maximum and minimum temperatures. *Int. J. Climatol.* **2022**, *42*, 8423–8445. [[CrossRef](#)]
88. Olmo, M.E.; Bettolli, M.L. Statistical downscaling of daily precipitation over southeastern South America: Assessing the performance in extreme events. *Int. J. Climatol.* **2022**, *42*, 1283–1302. [[CrossRef](#)]
89. Olmo, M.E.; Balmaceda-Huarte, R.; Bettolli, M.L. Multi-model ensemble of statistically downscaled GCMs over southeastern South America: Historical evaluation and future projections of daily precipitation with focus on extremes. *Clim. Dyn.* **2022**, *59*, 3051–3068. [[CrossRef](#)]
90. Ballarin, A.S.; Sone, J.S.; Gesualdo, G.C.; Schwaback, D.; Reis, A.; Almagro, A.; Wendland, E.C. CLIMBra—Climate change dataset for Brazil. *Sci. Data* **2023**, *10*, 47. [[CrossRef](#)]
91. Cannon, A.J.; Sobie, S.R.; Murdock, T.Q. Bias correction of GCM precipitation by Quantile Mapping: How well do methods preserve changes in quantiles and extremes? *J. Clim.* **2015**, *28*, 6938–6959. [[CrossRef](#)]
92. Reboita, M.S.; Gan, M.A.; da Rocha, R.P.; Ambrizzi, T. Regimes de precipitação na América do Sul: Uma revisão bibliográfica. *Rev. Bras. Meteorol.* **2010**, *25*, 185–204. [[CrossRef](#)]
93. Ferreira, G.W.S.; Reboita, M.S. A new look into the South American precipitation patterns: Observation and forecast. *Atmosphere* **2022**, *13*, 873. [[CrossRef](#)]
94. Zhou, J.; Lau, K.M. Does a monsoon climate exist over South America? *J. Clim.* **1998**, *11*, 1020–1040. [[CrossRef](#)]
95. Hoyos, I.; Cañón-Barriga, J.; Arenas-Suárez, T.; Dominguez, F.; Rodriguez, B.A. Variability of regional atmospheric moisture over Northern South America: Patterns and underlying phenomena. *Clim. Dyn.* **2019**, *52*, 893–911. [[CrossRef](#)]
96. Mejia, J.F.; Yepes, J.; Henao, J.J.; Poveda, G.; Zuluaga, M.D.; Raymond, D.J.; Fuchs-Stone, Z. Towards a mechanistic understanding of precipitation over the far eastern tropical Pacific and western Colombia, one of the rainiest spots on Earth. *J. Geophys. Res. Atmos.* **2021**, *126*, e2020JD033415. [[CrossRef](#)]
97. Lagos-Zúñiga, M.A.; Balmaceda-Huarte, R.; Regoto, P.; Torrez, L.; Olmo, M.; Lyra, A.; Pareja-Quispe, D.; Bettolli, M.L. Extreme indices of temperature and precipitation in South America: Trends and intercomparison of regional climate models. *Clim. Dyn.* **2022**. (under review). [[CrossRef](#)]
98. Rupp, D.E.; Abatzoglou, J.T.; Hegewisch, K.C.; Mote, P.W. Evaluation of CMIP5 20th century climate simulations for the Pacific Northwest USA. *J. Geophys. Res. Atmos.* **2013**, *118*, 10884–10906. [[CrossRef](#)]
99. Dias, C.G.; Reboita, M.S. Assessment of CMIP6 simulations over tropical South America. *Rev. Bras. Geogr. Fis.* **2021**, *14*, 1282–1295. [[CrossRef](#)]

100. Zhang, M.Z.; Xu, Z.; Han, Y.; Guo, W. Evaluation of CMIP6 models toward dynamical downscaling over 14 CORDEX domains. *Clim. Dyn.* **2022**, *1*–15. [\[CrossRef\]](#)
101. Brands, S. A circulation-based performance atlas of the CMIP5 and 6 models for regional climate studies in the Northern Hemisphere mid-to-high latitudes. *Geosci. Model. Dev.* **2022**, *15*, 1375–1411. [\[CrossRef\]](#)
102. Kuma, P.; Bender, F.A.-M.; Jönsson, A.R. Climate model code genealogy and its relation to climate feedbacks and sensitivity. *J. Adv. Model. Earth Syst.* **2023**, *15*, e2022MS003588. [\[CrossRef\]](#)
103. Abramovitz, G.; Herger, N.; Gutmann, E.; Hammerling, D.; Knutti, R.; Leduc, M.; Lorenz, R.; Pincus, R.; Schmidt, G.A. ESD Reviews: Model dependence in multi-model climate ensembles: Weighting, sub-selection and out-of-sample testing. *Earth Syst. Dyn.* **2019**, *10*, 91–105. [\[CrossRef\]](#)
104. Lovato, T.; Peano, D. CMCC CMCC-CM2-SR5 model output prepared for CMIP6 CMIP historical. Version 20200616. *Earth Syst. Grid Fed.* **2020**, *14*, e2021MS002814. [\[CrossRef\]](#)
105. Lovato, T.; Peano, D.; Butenschön, M.; Matera, S.; Iovino, D.; Scoccimarro, E.; Fogli, P.G.; Cherchi, A.; Bellucci, A.; Gualdi, S.; et al. CMIP6 simulations with the CMCC Earth System Model (CMCC1077 ESM2). *J. Adv. Model. Earth Syst.* **2022**, *14*, e2021MS002814. [\[CrossRef\]](#)
106. Döscher, R.; Acosta, M.; Alessandri, A.; Anthoni, P.; Arneth, A.; Arsouze, T.; Bergman, T.; Bernardello, R.; Bousetta, S.; Caron, L.P.; et al. The EC-Earth3 Earth System Model for the Climate Model Intercomparison Project 6. *Geosci. Model. Dev.* **2022**, *15*, 2973–3020. [\[CrossRef\]](#)
107. Krasting, J.P.; John, J.G.; Blanton, C.; McHugh, C.; Nikonov, S.; Radhakrishnan, A.; Rand, K.; Zadeh, N.T.; Balaji, V.; Durachta, J.; et al. NOAA-GFDL GFDL-ESM4 Model Output Prepared for CMIP6 CMIP Historical, Version 20190726; Earth System Grid Federation: Washington, DC, USA, 2018. [\[CrossRef\]](#)
108. Boucher, O.; Denvil, S.; Levassasseur, G.; Cozic, A.; Caubel, A.; Foujols, M.A.; Meurdesoif, Y.; Cadule, P.; Devilliers, M.; Ghattas, J.; et al. IPSL IPSL-CM6A-LR Model Output Prepared for CMIP6 CMIP Historical, Version 20180803; Earth System Grid Federation: Washington, DC, USA, 2018. [\[CrossRef\]](#)
109. Tatebe, H.; Watanabe, M. MIROC MIROC6 Model Output Prepared for CMIP6 CMIP Historical, Version 20181212; Earth System Grid Federation: Washington, DC, USA, 2018. [\[CrossRef\]](#)
110. Wieners, K.H.; Giorgetta, M.; Jungclaus, J.; Reick, C.; Esch, M.; Bittner, M.; Legutke, S.; Schupfner, M.; Wachsmann, F.; Gayler, V.; et al. MPI-M MPI-ESM1.2-LR Model Output Prepared for CMIP6 CMIP Historical, Version 20190710; Earth System Grid Federation: Washington, DC, USA, 2019. [\[CrossRef\]](#)
111. Yukimoto, S.; Koshiro, T.; Kawai, H.; Oshima, N.; Yoshida, K.; Urakawa, S.; Tsujino, H.; Deushi, M.; Tanaka, T.; Hosaka, M.; et al. MRI MRI-ESM2.0 Model Output Prepared for CMIP6 CMIP Historical, Version 20190222; Earth System Grid Federation: Washington, DC, USA, 2019. [\[CrossRef\]](#)
112. Chen, M.; Shi, W.; Xie, P.; Silva, V.B.S.; Kousky, V.E.; Higgins, R.W.; Janowiak, J.E. Assessing objective techniques for gauge-based analyses of global daily precipitation. *J. Geophys. Res.* **2008**, *113*, D04110. [\[CrossRef\]](#)
113. Silva, V.C.B.; Kousky, V.E.; Shi, W.; Higgins, W. An improved gridded historical daily precipitation analysis for Brazil. *J. Hydrometeorol.* **2007**, *8*, 847–861. [\[CrossRef\]](#)
114. Lee, T.; Singh, V.P. *Statistical Downscaling for Hydrological and Environmental Applications*, 1st ed.; Taylor & Francis Group: Boca Raton, FL, USA, 2019.
115. Mukherjee, S.; Aadhar, S.; Stone, D.; Mishra, V. Increase in extreme precipitation events under anthropogenic warming in India. *Weather. Clim. Extremes* **2018**, *20*, 45–53. [\[CrossRef\]](#)
116. Lee, M.-H.; Lu, M.; Im, E.-S.; Bae, D.-H. Added value of dynamical downscaling for hydrological projections in the Chungju Basin, Korea. *Int. J. Climatol.* **2019**, *39*, 516–531. [\[CrossRef\]](#)
117. Mishra, V.; Bhatia, U.; Tiwari, A.D. Bias-corrected climate projections for South Asia from Coupled Model Intercomparison Project-6. *Sci. Data* **2020**, *7*, 338. [\[CrossRef\]](#)
118. Xu, Z.; Han, Y.; Tam, C.-Y.; Yang, Z.-L.; Fu, C. Bias-corrected CMIP6 global dataset for dynamical downscaling of the historical and future climate (1979–2100). *Sci. Data* **2021**, *8*, 293. [\[CrossRef\]](#)
119. Tang, G.; Clark, M.P.; Papalexiou, S.M. EM-Earth: The Ensemble Meteorological dataset for planet Earth. *Bull. Am. Meteorol. Soc.* **2022**, *103*, E996–E1018. [\[CrossRef\]](#)
120. Wu, H.; Lei, H.; Lu, W.; Liu, Z. Future changes in precipitation over the upper Yangtze River basin based on bias correction spatial downscaling of models from CMIP6. *Environ. Res. Commun.* **2022**, *4*, 045002. [\[CrossRef\]](#)
121. Admasu, L.M.; Grant, L.; Thiery, W. Exploring global climate model downscaling based on tile-level output. *J. Appl. Meteorol. Climatol.* **2023**, *62*, 171–190. [\[CrossRef\]](#)
122. Tram-Anh, Q.; Ngo-Duc, T.; Espagne, E.; Trinh-Tuan, L. A 10-km CMIP6 downscaled dataset of temperature and precipitation for historical and future Vietnam climate. *Sci. Data* **2023**, *10*, 257. [\[CrossRef\]](#) [\[PubMed\]](#)
123. Logan, T.; Aoun, A.; Bourgault, P.; Huard, D.; Lavoie, J.; Rondeau-Genesse, G.; Smith, J.T.; Alegre, R.; Barnes, C.; Biner, S.; et al. *Ouranosinc/xclim*, version 0.37.0; Zenodo: Geneva, Switzerland, 2022. [\[CrossRef\]](#)
124. Wilks, D.S. *Statistical Methods in the Atmospheric Sciences*, 4th ed.; Elsevier: Cambridge, MA, USA, 2019.
125. Almazroui, M.; Ashfaq, M.; Islam, M.N.; Kamil, S.; Abid, M.A.; O'Brien, E.; Ismail, M.; Reboita, M.S.; Sörensson, A.A.; Arias, P.A.; et al. Assessment of CMIP6 performance and projected temperature and precipitation changes over South America. *Earth Syst. Environ.* **2021**, *5*, 155–183. [\[CrossRef\]](#)

126. Arias, P.A.; Ortega, G.; Villegas, L.D.; Martínez, J. Colombian climatology in CMIP5/CMIP6 models: Persistent biases and improvements. *Rev. Fac. Ing.* **2021**, *100*, 75–96. [[CrossRef](#)]
127. Ortega, G.; Arias, P.A.; Villegas, J.C.; Marquet, P.A.; Nobre, P. Present-day and future climate over Central and South America according to CMIP5/CMIP6 models. *Int. J. Climatol.* **2021**, *41*, 6713–6735. [[CrossRef](#)]
128. Huang, F.; Xu, Z.; Guo, W. The linkage between CMIP5 climate models' abilities to simulate precipitation and vector winds. *Clim. Dyn.* **2020**, *54*, 4953–4970. [[CrossRef](#)]
129. Torres, R.R.; Marengo, J.A. Uncertainty assessments of climate change projections over South America. *Theor. Appl. Climatol.* **2013**, *112*, 253–272. [[CrossRef](#)]
130. Rivera, J.A.; Arnould, G. Evaluation of the ability of CMIP6 models to simulate precipitation over Southwestern South America: Climatic features and long-term trends (1901–2014). *Atmos. Res.* **2020**, *241*, 104953. [[CrossRef](#)]
131. Barreiro, M.; Chang, P.; Saravanan, R. Simulated precipitation response to SST forcing and potential predictability in the region of the South Atlantic Convergence Zone. *Clim. Dyn.* **2005**, *24*, 105–114. [[CrossRef](#)]
132. Bombardi, R.J.; Trenary, L.; Pegion, K.; Cash, B.; DelSole, T.; Kinter, J.L. Seasonal predictability of summer rainfall over South America. *J. Clim.* **2018**, *31*, 8181–8195. [[CrossRef](#)]
133. Torres, R.R.; Benassi, R.B.; Martins, F.B.; Lapola, D.M. Projected impacts of 1.5 and 2 °C global warming on temperature and precipitation patterns in South America. *Int. J. Climatol.* **2021**, *42*, 1597–1611. [[CrossRef](#)]
134. Ruffato-Ferreira, V.; Barreto, R.C.; Júnior, A.O.; Silva, W.L.; Viana, D.B.; Nascimento, J.A.S.; Freitas, M.A.V. A foundation for the strategic long-term planning of the renewable energy sector in Brazil: Hydroelectricity and wind energy in the face of climate change scenarios. *Renew. Sustain. Energy Rev.* **2017**, *72*, 1124–1137. [[CrossRef](#)]
135. De Jong, P.; Barreto, T.B.; Tanajura, C.A.S.; Oliveira-Esquerre, K.P.; Kiperstok, A.; Torres, E.A. The impact of regional climate change on hydroelectric resources in South America. *Renew. Energy* **2021**, *173*, 76–91. [[CrossRef](#)]
136. Medeiros, F.J.; Oliveira, C.P.; Avila-Diaz, A. Evaluation of extreme precipitation climate indices and their projected changes for Brazil: From CMIP3 to CMIP6. *Weather. Clim. Extrem.* **2022**, *38*, 100511. [[CrossRef](#)]
137. Buser, C.M.; Künsch, H.R.; Lüthi, D.; Wild, M.; Schär, C. Bayesian multi-model projection of climate: Bias assumptions and interannual variability. *Clim. Dyn.* **2009**, *33*, 849–868. [[CrossRef](#)]
138. Blázquez, J.; Solman, S.A. Temperature and precipitation biases in CORDEX RCM simulations over South America: Possible origin and impacts on the regional climate change signal. *Clim. Dyn.* **2023**, *61*, 2907–2920. [[CrossRef](#)]
139. Arisido, M.W.; Gaetan, C.; Zanchettin, D.; López-Parages, J.; Rubino, A. Spatio-temporal quantification of climate model errors in a Bayesian framework. *Stoch. Environ. Res. Risk Assess.* **2019**, *33*, 111–124. [[CrossRef](#)]
140. Cai, W.; McPhaden, M.J.; Grimm, A.M.; Rodrigues, R.R.; Taschetto, A.S.; Garreaud, R.D.; Dewitte, B.; Poveda, G.; Ham, Y.-G.; Santoso, A.; et al. Climate impacts of the El Niño-Southern Oscillation on South America. *Nat. Rev. Earth Environ.* **2020**, *1*, 215–231. [[CrossRef](#)]
141. Reboita, M.S.; Ambrizzi, T.; Crespo, N.M.; Dutra, L.M.M.; Ferreira, G.W.S.; Rehbein, A.; Drumond, A.; da Rocha, R.P.; Souza, C.A. Impacts of teleconnection patterns on South America climate. *Ann. N. Y. Acad. Sci.* **2021**, *1504*, 116–153. [[CrossRef](#)]
142. Jimenez, J.C.; Libonati, R.; Peres, L.F. Drought over Amazonia in 2005, 2010, and 2015: A cloud cover perspective. *Front. Earth Sci.* **2018**, *6*, 227. [[CrossRef](#)]
143. Li, J.; Huo, R.; Chen, H.; Zhao, Y.; Zhao, T. Comparative assessment and future prediction using CMIP6 and CMIP5 for annual precipitation and extreme precipitation simulation. *Front. Earth Sci.* **2021**, *9*, 687976. [[CrossRef](#)]
144. Cavalcanti, I.F.A. The influence of extratropical Atlantic Ocean region on wet and dry years in North-Northeastern Brazil. *Front. Earth Sci.* **2015**, *3*, 34. [[CrossRef](#)]
145. Ruiz-Vásquez, M.; Arias, P.A.; Martínez, J.A.; Espinoza, J.C. Effects of Amazon basin deforestation on regional atmospheric circulation and water vapor transport towards tropical South America. *Clim. Dyn.* **2020**, *54*, 4169–4189. [[CrossRef](#)]
146. Arias, P.A.; Rivera, J.A.; Sörensson, A.A.; Zachariah, M.; Barnes, C.; Philip, S.; Kew, S.; Vautard, R.; Koren, G.; Pinto, I.; et al. Vulnerability and High Temperatures Exacerbate Impacts of Ongoing drought in Central South America. *World Weather. Attribution* **2023**. Available online: <https://www.worldweatherattribution.org/wp-content/uploads/WWA-Argentina-Uruguay-drought-Scientific-Report.pdf> (accessed on 13 May 2023).
147. Rivera, J.A.; Otta, S.; Lauro, C.; Zazulie, N. A decade of hydrological drought in central-western Argentina. *Front. Water* **2021**, *3*, 640544. [[CrossRef](#)]
148. Xu, F.; Bento, V.A.; Qu, Y.; Wang, Q. Projections of global drought and their climate drivers using CMIP6 global climate models. *Water* **2023**, *15*, 2272. [[CrossRef](#)]

Disclaimer/Publisher's Note: The statements, opinions and data contained in all publications are solely those of the individual author(s) and contributor(s) and not of MDPI and/or the editor(s). MDPI and/or the editor(s) disclaim responsibility for any injury to people or property resulting from any ideas, methods, instructions or products referred to in the content.

SUPPLEMENTARY MATERIALS

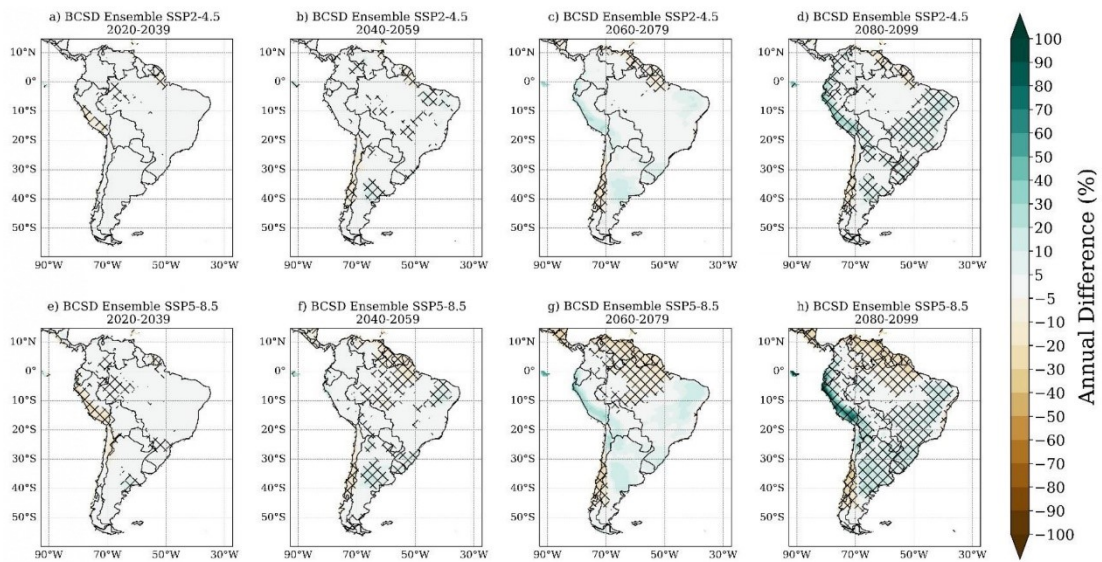


Figure S1. Mean annual differences of precipitation (%) between the future (2020-2039, 2040-2059, 2060-2079, 2080-2099) and historical period (1995-2014), projected by the BCSD ensemble under the SSP2-4.5 (a-d) and SSP5-8.5 (e-h) forcing scenarios. Hatched areas indicate statistical significance at a 95% confidence level.

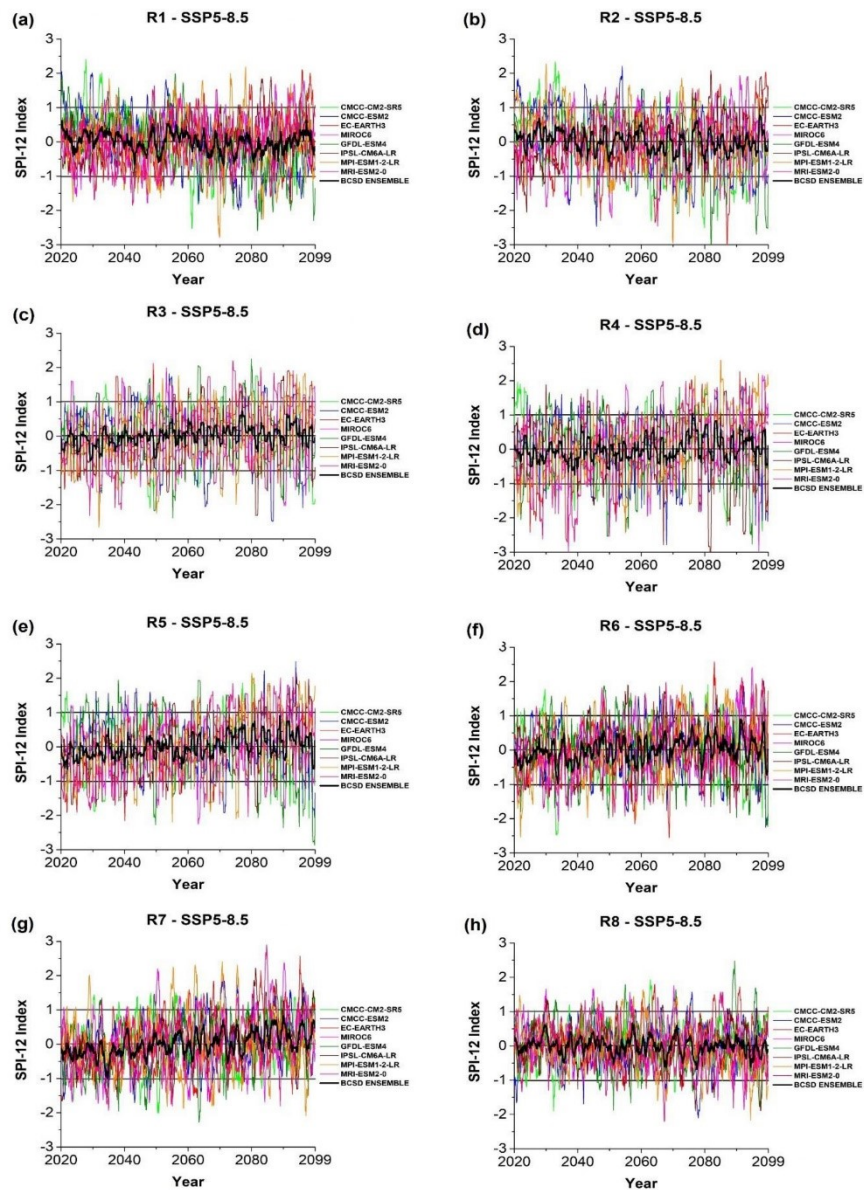


Figure S2. Temporal series (2020-2099) of the SPI-12 index projected by the eight CMIP6-GCMs used in the study and the BCSO ensemble (solid black line) under the SSP5-8.5 scenario for eight SA subdomains (a-h, Figure 1).

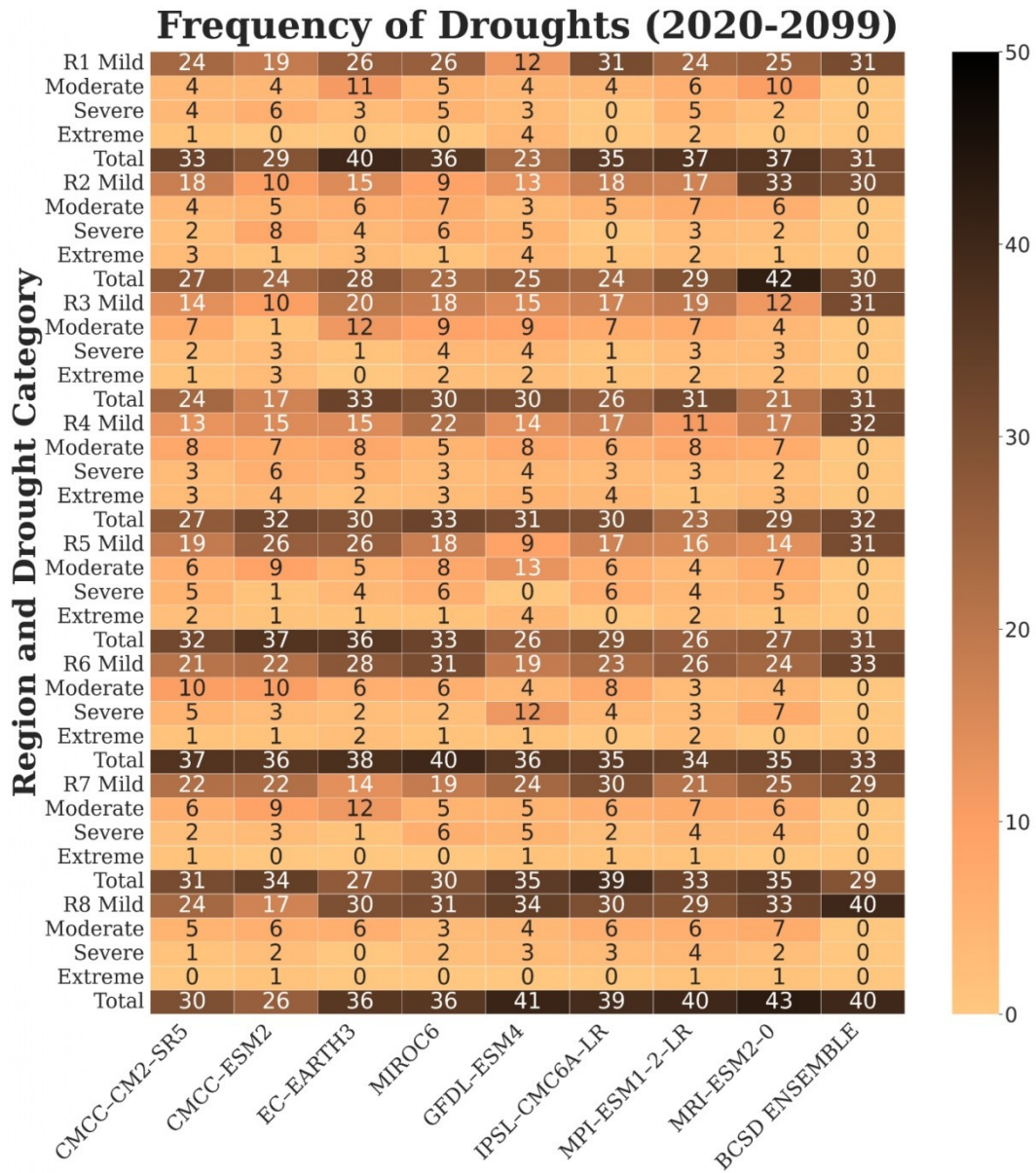


Figure S3. Classification of hydrological drought events identified by each CMIP-GCM used in the study and the BCSD ensemble in 2020-2099 under the SSP5-8.5 scenario for eight SA subdomains (R1-R8, Figure 1).

5. South American monsoon lifecycle projected by statistical downscaling with CMIP6-GCMs



atmosphere



Article

South American Monsoon Lifecycle Projected by Statistical Downscaling with CMIP6-GCMs

Michelle Simões Reboita ^{1,*}, Glauber Willian de Souza Ferreira ¹, João Gabriel Martins Ribeiro ¹, Rosmeri Porfírio da Rocha ² and Vadlamudi Brahmananda Rao ³

¹ Institute of Natural Resources, Federal University of Itajubá (UNIFEI), Itajubá 37500-903, Brazil

² Institute of Astronomy, Geophysics and Atmospheric Sciences, University of São Paulo (USP), São Paulo 05508-090, Brazil

³ Department of Meteorology and Oceanography, Andhra University, Visakhapatnam 530003, Andhra Pradesh, India

* Correspondence: reboita@unifei.edu.br

Abstract: This study analyzed the main features (onset, demise, and length) of the South American Monsoon System (SAMS) projected in different time slices (2020–2039, 2040–2059, 2060–2079, and 2080–2099) and climate scenarios (SSP2–4.5 and SSP5–8.5). Eight global climate models (GCMs) from the Coupled Model Intercomparison Project Phase 6 (CMIP6) that perform well in representing South America’s historical climate (1995–2014) were initially selected. Thus, the bias correction–statistical downscaling (BCSD) technique, using quantile delta mapping (QDM), was applied in each model to obtain higher-resolution projections than their original grid. The horizontal resolution adopted was 0.5° of latitude × longitude, the same as the Climate Prediction Center precipitation analysis used as a reference dataset in BCSD. The QDM technique improved the monsoon onset west of 60° W and the simulated demise and length in southwestern Amazonia. Raw and BCSD ensembles project an onset delay of approximately three pentads compared to the historical period over almost all regions and a demise delay of two pentads northward 20° S. Additionally, the BCSD ensemble projects a reduced length with statistical significance in most South Atlantic Convergence Zone regions and a delay of three pentads in the demise over the Brazilian Amazon from the second half of the 21st century.

Keywords: monsoon; precipitation; South America; statistical downscaling; climate scenarios



Citation: Reboita, M.S.; Ferreira, G.W.d.S.; Ribeiro, J.G.M.; da Rocha, R.P.; Rao, V.B. South American Monsoon Lifecycle Projected by Statistical Downscaling with CMIP6-GCMs. *Atmosphere* **2023**, *14*, 1380. <https://doi.org/10.3390/atmos14091380>

Academic Editor: Patrick Armand

Received: 7 August 2023

Revised: 29 August 2023

Accepted: 29 August 2023

Published: 31 August 2023



Copyright: © 2023 by the authors. Licensee MDPI, Basel, Switzerland. This article is an open access article distributed under the terms and conditions of the Creative Commons Attribution (CC BY) license (<https://creativecommons.org/licenses/by/4.0/>).

1. Introduction

The classical definition of a monsoon considers a region to have a monsoon climate when rainfall increases in association with a seasonal reversal in low-level wind direction [1]. Following this concept, South America (SA) does not have a monsoon climate. However, modern definitions of a monsoon consider a region to have this climate type based on the occurrence of a dry and a wet well-defined period in a year [2]. In this sense, SA is a region with a monsoon climate [3,4]. For instance, more than 50% of the total precipitation occurs in austral summer (DJF) in central and eastern Brazil, northern Argentina, and the central north of the Andes Mountains [5,6]. The onset of the South American rainy season is configured with the rapid shift of the area of intense convection between the northwestern extreme of the continent and latitudes south of the equator [7,8].

There are different approaches to studying the South American Monsoon System (SAMS), and one of them is in terms of the SAMS lifecycle [7,9–12]: onset, demise, length, and intensity (volume of precipitation). These studies, generally, use pentads of precipitation (mean or sum of five days) and have differences in methodology because some of them identify the SAMS lifecycle in each grid point of a dataset [12], while others consider Midwest Brazil (50°–60° W and 10°–20° S) as a hotspot region to study the monsoon [9]. In Midwest Brazil, the average SAMS lifecycle begins in 58–59 pentads, decaying by 18–21 pentads, and having a length of 33–34 pentads. Kousky [13] presents a table for the

pentads with the corresponding calendar dates. To complement information about the literature, the Supplementary Materials present comparative Tables S1–S4 of the SAMS lifecycle features obtained by different studies for various regions where the system operates.

The SAMS lifecycle can vary from one year to another. For instance, the rainy phase of the SAMS can have a short or long duration. Fu and Li [14] observed that the wetter land surface in southern Amazonia in the dry season could cause an abnormally lower convective inhibition energy (CINE), which promotes an earlier and more rapid increase in rainfall during the early phase of the transition. On the other hand, if the increase in surface evapotranspiration is significantly weakened during the dry season, for example, by a rise in runoff due to land use or a decrease in rainfall in previous seasons, the onset of the wet season would probably be delayed [14]. Similar results were obtained in the midwest and southeast of Brazil by Dias et al. [15]. These findings indicate an early or late SAMS onset, but they do not explain the causes of the precipitation and land-surface interaction variability, i.e., what are the drivers for a dryer or wetter dry season? Another group of researchers [16–22] has addressed this problem and studied the impact of the modes of atmospheric variability at different scales (interdecadal, decadal, interannual, and intraseasonal) on atmospheric circulation and their effects on SA. While the physical chain is simple—the changes in the atmospheric circulation caused by the atmospheric modes of variability affect the distribution of synoptic and mesoscale precipitation systems, which, in turn, affect the SAMS lifecycle (Mechoso et al. [23])—the predictability and the coupling effect of different teleconnection modes continue to present a challenge for researchers. For SA, most studies on teleconnection patterns and their impacts on monsoons focus on the rainfall intensity and spatial distribution rather than the implications for atmospheric systems that cause precipitation. Additionally, few studies analyze the effects of teleconnection patterns on the onset and demise of monsoons. Most studies address the SAMS lifecycle variability regarding land use and describe that in southern Amazonia, the wet seasons have become shorter due to deforestation [24–27].

In SA, land-use changes are mainly responsible for the historical cumulative CO₂ emissions [28]. The impact of global climate change and, on a regional scale, the effect of land use have been considered in the climate projections and indicated changes in the atmospheric circulation and, consequently, in precipitation in SA [29–31]. With the Couple Model Intercomparison Project Phase 3 (CMIP3) projections, Bombardi and Carvalho [10] evaluated the monsoon lifecycle in the twentieth century (1981–2000) and in the A1B scenario (2081–2100). The authors observed that most models represent the spatiotemporal variability of the annual precipitation cycle in central and eastern Brazil during the summer monsoon in the reference period. For the A1B scenario, the models do not indicate statistically significant changes in SAMS onset and demise dates. The most coherent feature projected was a reduction in precipitation over central-eastern Brazil. Jones and Carvalho [32] analyzed six global climate models (GCMs) of CMIP5 under the RCP8.5 scenario, and the models projected significant increases in seasonal amplitudes, early onsets (14 days or ~3 pentads), late demises (17 days or ~4 pentads), and durations of the SAMS. In terms of regional climate models (RCMs), Reboita et al. [11] projected the SAMS lifecycle using the RegCM3 nested in two GCMs (HadCM3 and ECHAM5) under the A1B scenario. Focusing on Midwest Brazil, for the period 2010–2040, a delay of one pentad was obtained at the beginning of the rainy season, while for the period 2070–2100, the authors obtained a reduction of ~2 pentads in the duration of the rainy season. Ashfaq et al. [12] evaluated the projections of global monsoons in an ensemble with RegCM4 nested in models from CMIP5 under the RCP2.6 and RCP8.5 scenarios. For SA, the RegCM4 ensemble simulated Amazonia's monsoon onset later in the reference period. However, the authors highlighted that the RegCM4 ensemble was within the uncertainties shown in Bombardi and Carvalho [10]. The projected changes are more intense in the RCP8.5 scenario. Even beyond SA, the authors found a delay in monsoon demise but less than the monsoon onset, which reflects a shrinking of the monsoon rainy seasons. In SA, under the RCP8.5 scenario, the onset is projected to be delayed in ~4 pentads and the demise in ~3 pentads. The authors

also explore the drivers of the changes in the monsoon lifecycle. They mention that every monsoon region receives a noticeable amount of pre-monsoon precipitation, which helps to warm up the upper troposphere and induce deep overturning through latent heat release in the atmosphere. In the future, the dry conditions will negatively affect the pre-monsoon precipitation, causing a delayed onset.

CMIP provides the projections with GCMs for developing studies for the International Panel on Climate Change (IPCC) assessment report. However, in regional and local studies of climate impacts, the GCMs' resolution is coarse, and downscaling techniques need to be applied to obtain high-resolution climate information [33–35]. There are two types of downscaling: dynamical and statistical [36,37]. In dynamical downscaling, RCMs are nested into GCM outputs, and RCMs simulate the physical processes of the climate system. This methodology requires substantial computing power and time. For this reason, this task is generally performed by international projects, such as the Coordinated Regional Climate Downscaling Experiment (CORDEX, <https://cordex.org/>, accessed on 26 January 2022) under the World Climate Research Project (WCRP)'s supervision, which makes the projections available on the same platform as CMIP projections (Earth System Grid Federation, ESGF).

Statistical downscaling does not directly simulate the physical processes of the climate systems. It relies on establishing statistical relationships between large-scale climate variables (obtained from GCMs) and local-scale variables (obtained from in situ measurements). These relationships are derived from historical observations (perfect prognosis—PP—approach) or simulations (model output statistics—MOS—approach) and then applied to project future climate conditions [36]. Traditionally, in climate research, the PP approach has been used, and it includes different methods [36], such as regression models (linear models, generalized linear models—GLM quantile regression), also called the transfer function model [37], weather type methods, and analog and resampling methods.

Statistical downscaling is less computationally demanding compared to dynamical downscaling. For this reason, many studies have used it. For SA, most of the studies focus on southeastern South America (SESA) [38–41]. Bettolli et al. [38] analyzed the capability of a set of projections using CORDEX dynamical downscaling and statistical downscaling based on regression models (analog and GLM) in simulating daily precipitation during the 2009–2010 austral warm season over SESA. The results revealed that no single model performs best in all aspects evaluated and that most models capture the extreme events selected, although with a considerable spread in accumulated values and the location of heavy precipitation. Balmaceda-Huarte and Bettolli [39] applied statistical downscaling to simulate daily and maximum temperatures in Argentina, considering three approaches: analog, GLM, and artificial neural networks. According to the authors, depending on the aspect analyzed, one specific model was more/less skillful. In addition, the authors highlighted that it is a challenge to capture the local variability of daily extreme temperatures in regions with complex topography (Argentinian Patagonia and the subtropical Andes). A similar study but for precipitation over SESA was carried out by Olmo and Bettolli [40], while Olmo et al. [41] applied the CMIP5 and CMIP6-GCM projections.

Although statistical downscaling is less costly than dynamical downscaling, robust computational resources are still needed, justifying its application in small domains. One of the statistical downscaling approaches that is less computationally expensive is the model based on transfer functions. This approach was applied by Ballarin et al. [42] using quantile delta mapping. The authors developed a Brazilian dataset for different hydrological variables for both historical (1980–2013) and future (2015–2100) scenarios, under the Shared Socioeconomic Pathways (SSPs) 2–4.5 and 5–8.5, at a $0.25^\circ \times 0.25^\circ$ spatial resolution. To our knowledge, this is the only study of CMIP6-GCMs statistical downscaling covering a large area in SA.

In January 2022, the execution of the project “Hydro, wind, and solar energy in Brazil: Changes projected by CMIP6 climate models” (R&D Project 00403-0054/2022) began in order to provide a regional view of the climate change in different renewable energy

sources in SA. Therefore, this study aims to assess the projected changes in the monsoon lifecycle in SA, which significantly affects hydroelectric power generation on the continent. Considering this project's scope, CMIP6-GCMs have been statistically downscaled in the whole of SA, yielding a new dataset with a 0.5° horizontal resolution. Thus, the main objective of this work is to describe the projected changes to the SAMS lifecycle (onset, demise, and length) using an ensemble composed of eight CMIP6-GCMs under the SSP2–4.5 and SSP5–8.5 scenarios and considering four time slices until 2099. Hereby, this study addresses uncertainties about SAMS lifecycle projections and the absence of works with CMIP6 projections for SA.

2. Materials and Methods

2.1. Study Area and Reference Dataset

The study area comprises the SA continent (Figure 1), located at latitudes 12° N– 55° S. Due to its large latitudinal extension, different climate regimes occur over the continent but with a predominance of monsoon [3,4,43] with the local convection and the South Atlantic Convergence Zone (SACZ) as the main drivers of precipitation. The subdomains shown in Figure 1 indicate the main areas of the monsoon climate and will be used in our analyses. R1 indicates Amazonia, R2 Midwest Brazil, R3 southeastern Brazil (the boundary between São Paulo and Minas Gerais states), R4 north of Southeast Brazil, and R5 north Argentina and Paraguay. SACZ occurs from the southern R1 to R3, crossing R2. Therefore, when mentioned in the text, the “SACZ region” refers to such areas.

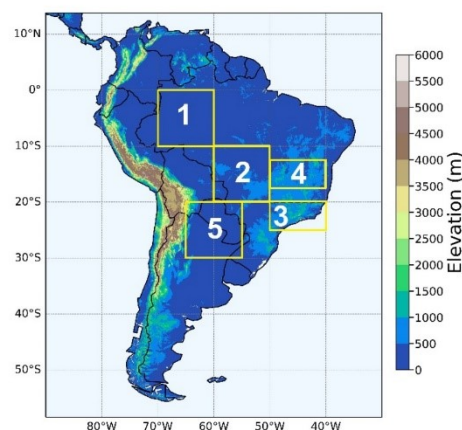


Figure 1. Study area with elevation (m) obtained from the United States Geological Survey–Earth Resources Observation System (EROS) Center. Yellow rectangles indicate subdomains selected for the extraction of time series. R1 covers the area 0° S– 10° S and 60° W– 70° W; R2, 10° S– 20° S and 50° W– 60° W; R3, 20° S– 25° S and 40° W– 50° W; R4, 12.5° S– 17.5° S and 40° W– 50° W; and R5, 20° S– 30° S and 55° W– 65° W.

The reference dataset is the precipitation analysis from the Climate Prediction Center Gauge-Based Analysis of Global Daily Precipitation (CPC) [44]. The CPC has a daily frequency and horizontal resolution of 0.5° (available at https://ftp.cpc.ncep.noaa.gov/precip/CPC_UNL_PRCP/GAUGE_GLB/RT/, accessed on 22 January 2022). It is developed through rain gauge observations and has been applied in several studies in SA [40,45–47]. In this study, the period from 1995 to 2014 is used.

2.2. CMIP6-GCMs

The projections of eight CMIP6-GCMs (Table 1) are used in this study. The models were selected in January 2022 under the R&D project 00403-0054/2022. As described in Ferreira et al. [48,49], the performance of 50 CMIP6-GCMs in representing the mean state of the SA climate was analyzed with the methodology of ranking analysis [50]. Monthly data (from 1995 to 2014) of air temperature at 2 m and precipitation of these models were used. Not all top-ranking models could be selected due to the absence of hourly/daily data and/or projections on the database of the ESGF platform (available at <https://esgfnode.llnl.gov/search/cmip6>, accessed on 20 January 2022). Thus, the selection followed the ranking and data availability on the ESGF platform.

Moreover, studies such as Dias and Reboita [51] have indicated that an ensemble of CMIP6-GCMs for the historical period composed of the models with better representation of the SA climate presents fewer biases with the reference datasets than an ensemble with around 50 GCMs. Therefore, the GCMs used in this study were selected based on the ranking method and data availability on the ESGF platform, but the validation previously carried out by Dias and Reboita [51] also corroborates the choice of some of the GCMs used, given their good performance in simulating the SA climate. We emphasize that if the model has a good representation of the historical climate, it can have a good representation in the future [52]. For this reason, we are using only eight models in the study, which helps to save computational resources. The main steps of the methodology are indicated in Figure 2.

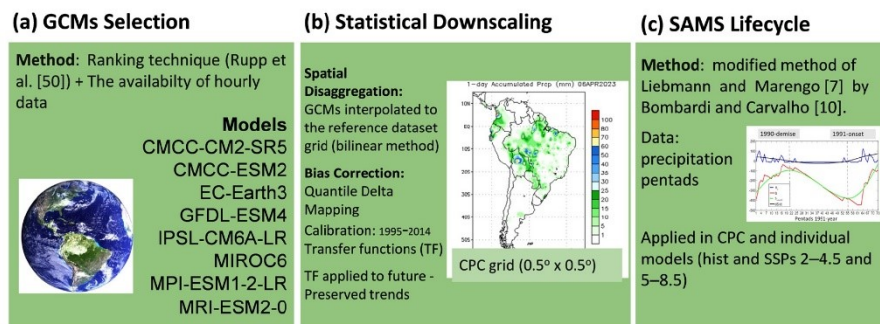


Figure 2. Main steps of the methodology: (a) CMIP6-GCMs selection [50], (b) statistical downscaling, and (c) defining the SAMS lifecycle [7,10].

After the eight CMIP6-GCMs (Table 1) were selected, precipitation projections every three hours were downloaded from ESGF and, posteriorly, were accumulated into daily data (the rainfall for a given day was accumulated from 1200 Z of the previous day to 1200 Z of the day in question). As CMIP6-GCMs present distinct horizontal resolutions (Table 1), the data were remapped into a regular $0.5^\circ \times 0.5^\circ$ grid using a bi-linear interpolation technique [42,53,54].

Table 1. Information on each CMIP6-GCM employed in the study.

Model	Resolution ($^\circ$ Lat \times $^\circ$ Lon)	Institute	Reference
CMCC-CM2-SR5	1.25 \times 0.94	Fondazione Centro Euro-Mediterraneo sui Cambiamenti Climatici	Lovato and Peano [55]
CMCC-ESM2	1.25 \times 0.94	Fondazione Centro Euro-Mediterraneo sui Cambiamenti Climatici	Lovato et al. [56]
EC-Earth3	0.70 \times 0.70	EC-Earth Consortium	Döscher et al. [57]
GFDL-ESM4	1.25 \times 1.00	Geophysical Fluid Dynamics Laboratory	Krasting et al. [58]

Table 1. Cont.

Model	Resolution (°Lat × °Lon)	Institute	Reference
IPSL-CM6A-LR	2.50 × 1.26	Institut Pierre Simon Laplace	Boucher et al. [59]
MIROC-6	1.41 × 1.41	Japan Agency for Marine-Earth Science and Technology	Tatebe and Watanabe [60]
MPI-ESM1-2-LR	0.94 × 0.94	Max Planck Institute for Meteorology	Wieners et al. [61]
MRI-ESM2-0	1.13 × 1.13	Meteorological Research Institute	Yukimoto et al. [62]

The historical period (1995–2014) follows the IPCC recommendation [12]. For the future, two greenhouse gas emission scenarios (SSP2–4.5 and SSP5–8.5) are evaluated in four time slices (2020–2039, 2040–2059, 2060–2079, and 2080–2099). SSPs are narratives describing different development paths of society [63]. The SSP2–4.5 scenario denotes a moderate emission scenario, in which the future trends in climate change stay relatively the same as they are currently, with moderate population growth, uneven development, slow progress towards sustainable development goals, environmental degradation, and persistent income inequality, resulting in a forcing pathway of 4.5 Wm^{-2} by 2100 [63,64]. SSP5–8.5 considers a high greenhouse gas emission context, representing a period with little effort to mitigate climate change effects, which leads to a forcing pathway of 8.5 Wm^{-2} in 2100. As in Ballarin et al. [42], we chose these two scenarios, moderate and extreme, because they represent a wide range of expected changes, covering other intermediate scenarios such as SSP3–7.0.

2.3. Statistical Downscaling

Our study aims to have projections with an intermediate horizontal resolution ($0.5^\circ \times 0.5^\circ$) and which are bias-corrected. As dynamical downscaling has time-dependent boundaries, a considerable quantity of data and computational power is necessary, becoming a working difficulty for small research laboratories. The best alternative is to use statistical downscaling. Thus, in this study, we use the PP approach with the transfer function method (quantile delta mapping, QDM). This method, also known as BCSD, was chosen for its simplicity of implementation and for preserving time-series trends [65]. This last feature is important because if the GCM shows, for instance, a dry trend in a given region, that trend will be maintained after bias correction. In addition, several studies in different global areas have used the method [42,66–69].

As the BCSD methodology is described in Ferreira et al. [48,49], here we provide only a summary. For obtaining a dataset with an intermediate horizontal resolution, initially, the daily precipitation from CMIP6-GCMs is spatially disaggregated, i.e., remapped to a grid of $0.5^\circ \times 0.5^\circ$, which is the same as that from the reference dataset (CPC), as mentioned in the previous section. The next step is to apply the QDM in the reference dataset and in each historical simulation to obtain the model representative of each grid point and to bias-correct the CMIP6-GCMs of the reference period. The last step is to apply the transfer functions in the future period. The Python-based package xclim [70] was used to perform the calculations.

The performance of bias correction applied to precipitation over SA in the reference period is presented in detail in Ferreira et al. [49]. Here, we only show a few comparisons of the GCMs with and without BCSD.

2.4. Determination of SAMS Lifecycle

The SAMS lifecycle is defined by the onset and demise dates of the rainy season using the Liebmann and Marengo [7] method adapted by Bombardi and Carvalho [10]. This method has also been used by Silva and Reboita [71], Reboita et al. [72], and Ashfaq et al. [12], for example. For the identification of the onset and demise dates, only precipitation in pen-

tads is required, and the method begins with the calculation of accumulated anomalies (S):

$$S_{\text{pentad}} = \sum_{n=\text{pentad}_1}^{\text{pentad}} (R_n - \bar{R})$$

where R_n is the precipitation of the n pentad (each year consists of 73 pentads, and when the year is bissextile, 29 February is included in the 12th pentad; a table with the pentads and corresponding dates is presented in Kousky [13]); \bar{R} is the climatological average of all the pentads under study. The first pentad in the summation (pentad_1) is chosen as the first pentad of the year (total precipitation from 1 January to 5 January), which, in turn, falls within the rainy season of the study region. After summing up the precipitation anomalies ($R_n - \bar{R}$) at each iteration, the resulting time series S is smoothed with a 3-point moving average applied 30 times. The next step involves calculating the first derivative of $S = dS/dt$ to identify the onset and demise of the rainy season for each year under study. This procedure is applied in CPC and each model for historical and future climates and each time slice.

The mentioned steps were implemented in a script in Python language by the authors of the present study. The algorithm performance was verified by comparing the monsoon’s onset, demise, and length obtained with the CPC (reference dataset) with the literature and considering each region shown in Figure 1. For brevity, here we only show R2 (Table 2), the most common area used to define the SAMS lifecycle, since it is the central core of the SA rainy season [9,73,74]. The tables for the other regions are presented in the Supplementary Materials. In general, the results obtained here reaffirm those of previous studies, particularly the works of Bombardi and Carvalho [10], Ashfaq et al. [12], Gan et al. [73], and Reboita et al. [75], indicating the good performance of the algorithm. Some slight variations between the results may be due to differences in the data, period, and methodology used for analysis. Not all mentioned studies in the tables were performed with the same methods applied in this work.

Table 2. Results of the computation of SAMS lifecycle parameters for R2 obtained here (shaded line) compared to previous works.

R2—Midwest Brazil—10° S–20° S 50° W–60° W			
Reference	Onset (Pentads)	Demise (Pentads)	Length (Pentads)
This study	57–59	20–23	34–36
Gan et al. [9]	51–63	22–25	33–44
Bombardi and Carvalho [10]	58–61	18–21	36–38
Ashfaq et al. [12]—GPCP	59	18–20	32–34
Ashfaq et al. [12]—RegCM4 ensemble	57–61	17–19	31–35
Gan et al. [73]	56–59	20–23	34–40
Bombardi et al. [74]	58	20	35
Reboita et al. [75]	57–59	20–22	32–34
Silva and Carvalho [76]	58–64	20–27	31–41
Raia and Cavalcanti [77]	60	18	31
Rodrigues et al. [78]	58	27	42

2.5. Analysis

All the analyses are performed considering the ensemble of the raw and BCSD projections. Initially, the performance of the raw and BCSD ensemble is evaluated through comparisons with the CPC analysis. Future projections under the SSP2–4.5 and SSP5–8.5 scenarios are described based on the spatial patterns during the different time slices (2020–2039, 2040–2059, 2060–2079, and 2080–2099). The average precipitation and onset, demise, and monsoon’s length are presented, as well as the difference of the time slices minus the

historical climate (1995–2014). Statistically significant differences at a 95% confidence level, computed with a *t*-test, are indicated in the figures. For a more detailed analysis, under the SSP2–4.5 and SSP5–8.5 scenarios, the changes projected for the monsoon’s lifecycle by the BCSD ensemble are evaluated in each region as shown in Figure 1. The statistical significance of the trends is calculated with the Mann–Kendall trend test [79,80], used to analyze trends in hydrological series [81,82]. In addition, Sen’s slope estimation test was also employed to detect the SAMS parameters’ linear trend in the selected subdomains.

3. Results and Discussion

3.1. BCSD Performance

Comparisons of the reference period evaluate the performance of the BCSD without and with the technique application and CPC for precipitation and the main features of the SAMS. In this section, we explore the spatial pattern of the variables without focusing specifically on the regions R1 to R5 (Figure 1), which will be described in more detail in Section 3.3. Figure 3 presents the historical simulations (1995–2014) of precipitation for the period from October to March (rainy season) obtained by the ensemble of eight CMIP6-GCMs without (middle column) and with (right column) applying the BCSD. The raw ensemble (Figure 3b,e) overestimates precipitation in most parts of Brazil and the western coast of SA, with great overestimations over the Andes. In contrast, underestimations occur in the Brazilian Amazon, northwest SA, central-north Argentina, Uruguay, and extreme southern Brazil. On average, the raw ensemble can represent the spatial distribution of the highest rainfall volumes associated with the SACZ, but it exhibits an unreal amplification and displacement of the system towards the southeast and northeast of Brazil.

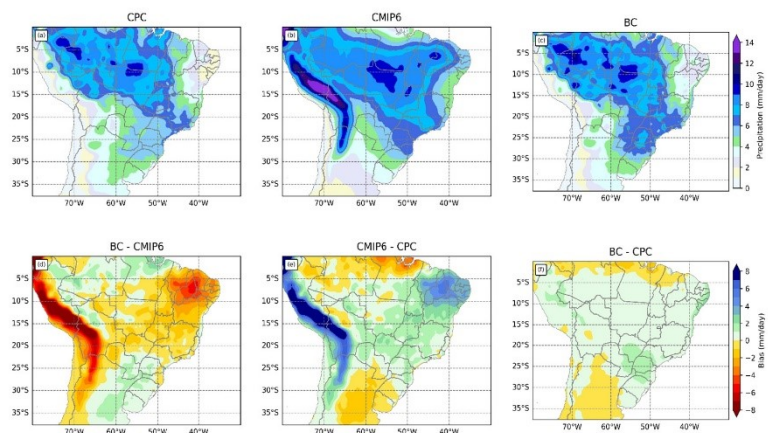


Figure 3. Seasonal climatology (from October to March) for the historical period (1995–2014) of precipitation (mm day^{-1} ; a–c) and bias (mm day^{-1} ; d–f), obtained by CPC (a) and simulated by the CMIP6 ensemble before (b,e) and after (c,f) the application of BCSD.

The underestimation of precipitation in northwest SA and northern Brazil corroborates the results of other studies using CMIP5 and CMIP6 models [83–87]. These systematic errors result from various factors, such as the models’ sensitivity to the sea surface temperature (SST) and their deficiency in simulating the Intertropical Convergence Zone (ITCZ) and surface wind convergence [83,87], limitations in cloud physics representation [88], and processes such as biosphere–atmosphere interactions and soil moisture [89], as well as uncertainties associated with the insufficient coverage of rain gauge networks for validating climate simulations [84,90].

The BCSD application notably reduces biases throughout the continent, especially on the western coast of SA and northeastern Brazil (Figure 3c,f). There is also a significant improvement in representing the intensity and location of precipitation maxima associated with SACZ despite a persistent overestimation of rainfall in the core of the continental SACZ. Figure 3d also indicates these features, showing the difference between the ensemble with and without BCSD application. In summary, the BCSD technique efficiently reduces systematic errors in the global models comprising the CMIP6-GCMs ensemble, thereby ensuring more reliable projections of future climate conditions. Additionally, the biases that persist after the application of correction are located in problematic sectors of global climate modeling, such as the tropical region and the continental portion of SACZ.

Figures 4–6 show the SAMS lifecycle: onset, demise, and length during the historical period. Regarding the SAMS onset, the raw ensemble (Figure 4b,e) approximately estimates the monsoon onset in the Brazilian Midwest from Pentads 60 (23–27 October) to 61 (28 October–1 November), indicating a delay of nearly two pentads compared to the onset in CPC (approximately in Pentad 58, 13–17 October). Considering the BCSD ensemble (Figure 4c,f), the onset of the rainy season in the Brazilian Midwest occurs around Pentad 61, indicating that the 2–3 pentad delay persists even after bias correction. For Southeast Brazil, the raw ensemble (Figure 4b,e) simulates the SAMS onset during Pentads 57–58 (8–12 October to 13–17 October), in agreement with the start obtained by CPC (Pentad 58). Similarly, the ensemble with BCSD (Figure 4c,f) indicates the onset of the rainy season around Pentads 57–58, analogous to the result from CPC. Regarding the sector encompassing Paraguay and northern Argentina, both the raw and BCSD ensembles provide the onset of the rainy season around Pentad 58, indicating an earlier start of the rainy season than obtained by the CPC, which is approximately around Pentad 61. In summary, the main gain with the BCSD ensemble is the enhancement of the onset results west of 60° W, which includes southern Amazonia. It is a good result since this region corresponds to the northern portion of the SACZ. In addition, BCSD also shows a slightly better performance over north Argentina.

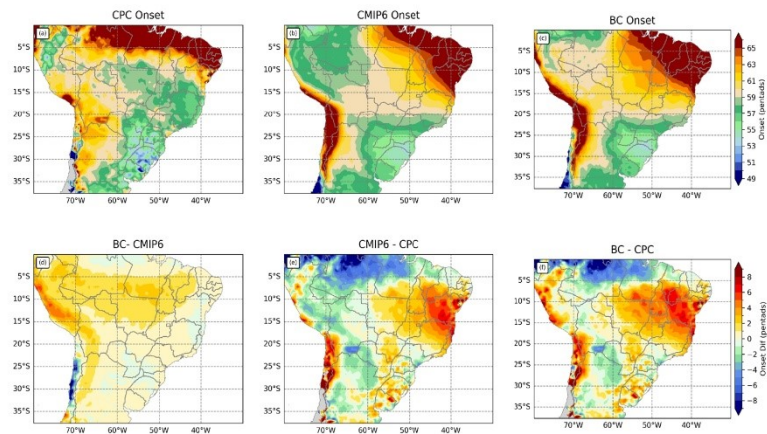


Figure 4. Seasonal climatology (from October to March) for the historical period (1995–2014) of the onset (in pentads) of the rainy season in SA (a–c) and bias (in pentads) (d–f), obtained by CPC (a) and simulated by the CMIP6 ensemble before (b,e) and after (c,f) the application of BCSD.

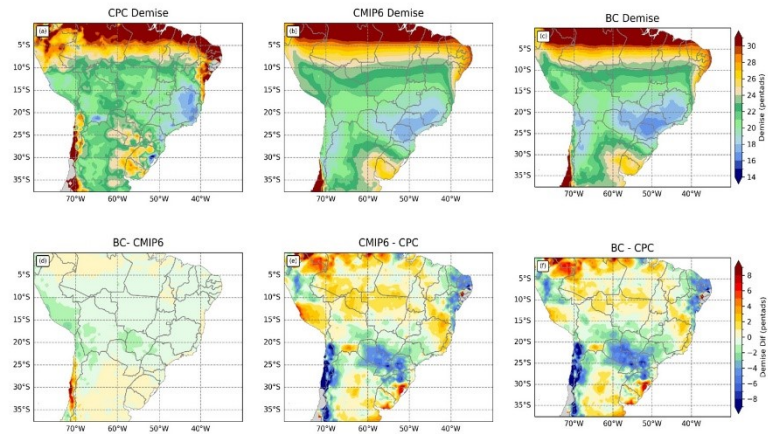


Figure 5. Seasonal climatology (from October to March) for the historical period (1995–2014) of the demise (in pentads) of the rainy season in SA (a–c) and bias (in pentads) (d–f), obtained by CPC (a) and simulated by the CMIP6 ensemble before (b,e) and after (c,f) the application of BCSD.

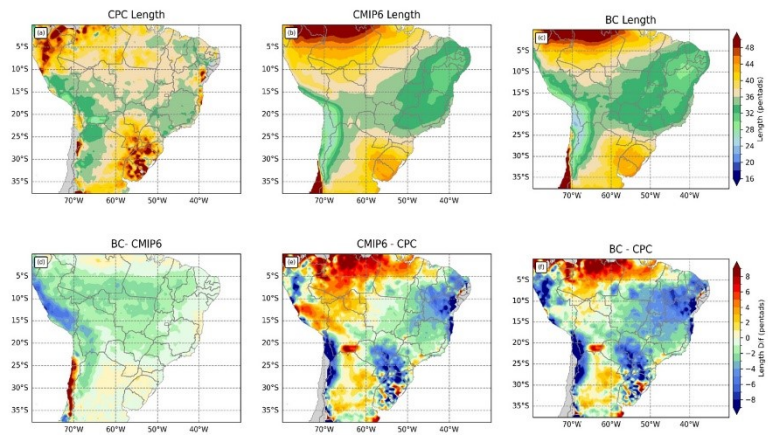


Figure 6. Seasonal climatology (from October to March) for the historical period (1995–2014) of the length (in pentads) of the rainy season in SA (a–c) and bias (in pentads) (d–f), obtained by CPC (a) and simulated by the CMIP6 ensemble before (b,e) and after (c,f) the application of BCSD.

Considering the demise of the rainy season (Figure 5), both the raw and BCSD ensembles indicate a delay in this parameter in Brazil’s southern Amazonia, Midwest, and north of Southeast Brazil. In contrast, the monsoon’s demise is anticipated in Paraguay and northern Argentina. Both ensembles show the rainy season’s demise around Pentads 21–22 (from 11–15 April to 16–20 April) in southern Amazonia and the Midwest, while the CPC indicates the demise during Pentad 20 (5–10 April). Similarly, a lag of approximately two pentads also occurs in the north of Southeast Brazil, with the simulations indicating the demise of the monsoon in Pentad 17 (22–26 March), while the CPC provides the end in Pentad 20 (Figure 5a–c). The most prominent difference between the raw and BCSD ensembles in these areas with a delay in the demise is that BCSD simulates a smaller area with the maximal values of delay (Figure 5e,f). Considering the demise anticipation by the ensembles over Paraguay and northern Argentina, the demise occurs in Pentad 19

(1–5 April), up to three pentads earlier than that provided by the CPC (Pentad 22). Generally, the BCSD ensemble improves the rainy season demise over southern Amazonia and Midwest Brazil. On the other hand, the BCSD ensemble does not decrease the bias over northern Argentina and Paraguay simulated in the raw ensemble.

The BCSD ensemble better represents the SAMS onset, demise, and length west of 60° W (Figure 6). Despite this, no significant changes exist between the BCSD and raw ensembles in the other continental regions. In the Brazilian Midwest, both ensembles indicate a SAMS duration of 35–36 pentads, while the CPC indicates 36–37 pentads. Similarly, in the southeastern region, both ensembles underestimate the duration of the monsoon, with a duration of ~32–33 pentads, up to two pentads shorter than that provided by the CPC (~34–35 pentads). Contrarily, in northern Argentina, the ensembles overestimate the duration of the rainy season by up to two pentads, indicating a duration of 40–41 pentads, while the CPC shows a duration of 38–39 pentads.

Overall, it is concluded that despite the modest changes brought about by BCSD in identifying the parameters of the rainy season's lifecycle, the technique improves the representation of the monsoon onset west of 60° W, as well as the representation of the demise and length in the southwestern Amazonia.

3.2. Climate Projections

Spatial Patterns

Figures 7 and 8 present the climate projections of precipitation from October to March for four time slices (2020–2039, 2040–2059, 2060–2079, and 2080–2099) and one historical period (1995–2014) obtained by the raw and BCSD ensembles, under the SSP2–4.5 and SSP5–8.5 scenarios, respectively. Under the SSP2–4.5 scenario (Figure 7), the raw ensemble projections maintain their unrealistic representation of the spatial distribution of the rainy season, extending its influence to the northern portion of Northeast Brazil. However, the BCSD ensemble corrects this deficiency and satisfactorily reproduces the rainfall spatial distribution. The projected changes in rainfall volumes in each time slice compared to the historical period show statistically significant increases in precipitation in sectors of the Midwest and the interior of the Northeast, particularly from 2040 onwards. From 2060 onwards, increases in rainfall are also projected in the South, Southeast, and a larger area of Northeast Brazil, as well as in Peru and northern Argentina. Similar results were obtained by studies using CMIP5 models under the RCP4.5 scenario [91,92] and a large ensemble of CMIP6 models under the SSP2–4.5 scenario [84]. Under the SSP5–8.5 scenario (Figure 8), the changes projected by both ensembles are similar to those provided by the SSP2–4.5 scenario, with the difference of having a more intense change signal and more significant rainfall reductions in the Brazilian North. The raw CMIP6 projections maintain their unrealistic representation of the rainy season, which is corrected by the statistically downscaled projections. The downscaled projections generally provide a stronger change signal than the raw projections. In both datasets, a more intense signal is observed towards the end of the 21st century, particularly under the SSP5–8.5 scenario.

The projections of changes found here corroborate the results of previous studies using models of different CMIP phases. The increase in rainfall in southeastern SA was also observed in studies using CMIP3, CMIP5 [93–96], and CMIP6 models [84,87,97]. Similarly, the reduction in precipitation in the Amazonia region agrees with the literature [11,84,87,91,92,94–97]. However, none of these CMIP studies focused on the SAMS lifecycle.

Figures 9–14 present the projections of the rainy season's onset, demise, and length under the SSP2–4.5 and SSP5–8.5 scenarios. Raw and BCSD ensembles, in both scenarios and in all time slices, project a delay in the onset of the rainy season, with a difference of approximately three pentads compared to the onset in the historical period in most of the study area (Figures 9 and 10), reaffirming the results obtained with the dynamical downscaling of CMIP5 models [12]. Over northern Argentina, the monsoon is projected to have an earlier onset. The difference between the ensembles is that the raw ensemble

shows an earlier onset over Midwest Brazil and Bolivia in the first three time slices, which BCSD does not project.

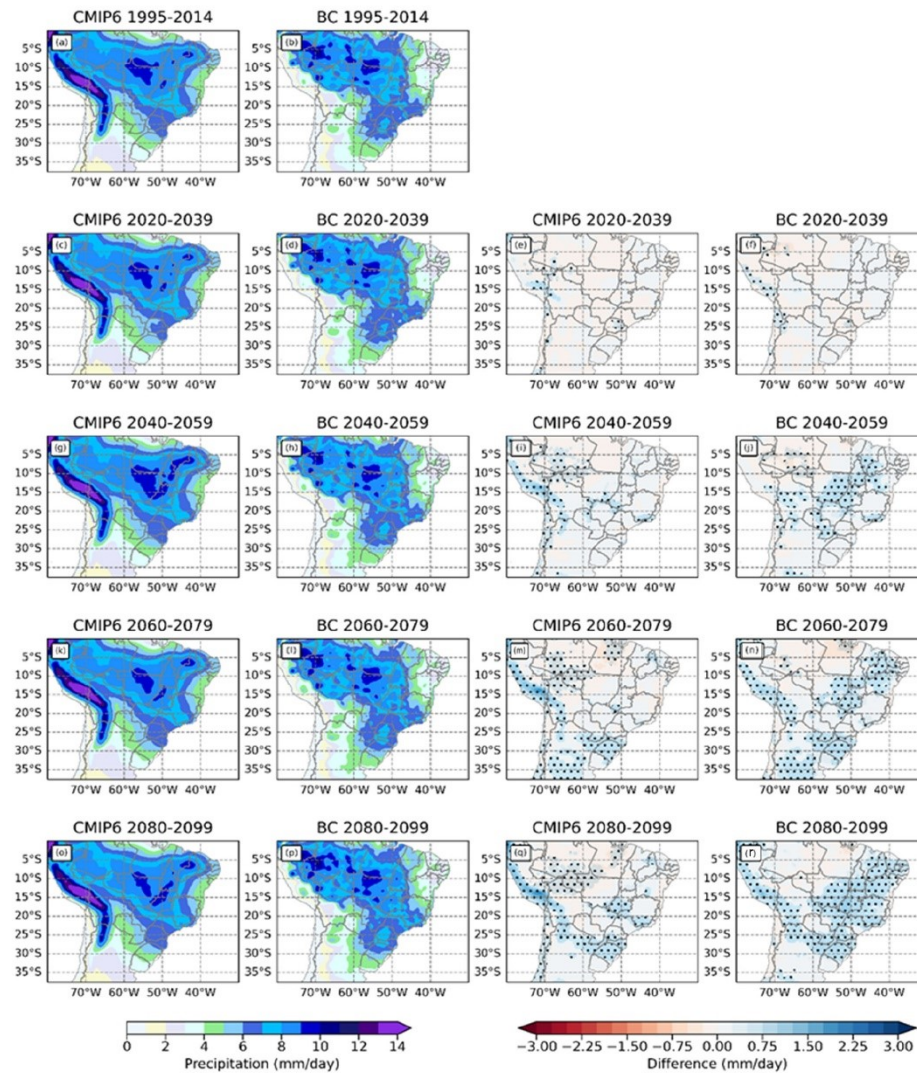


Figure 7. October–March precipitation (mm day^{-1}) during the historical period and the SSP2–4.5 scenario for different time slices 1995–2014, (a,b); 2020–2039, (c–f); 2040–2059, (g–j); 2060–2079, (k–n); 2080–2099, (o–r) and considering the raw and BCSD data (left side) and difference regarding the historical period (right side). From left to right: mean of the raw ensemble, mean of the BCSD ensemble, difference raw ensemble, and difference BCSD ensemble. The dots indicate statistical significance at 95% confidence in the difference fields based on the *t*-test.

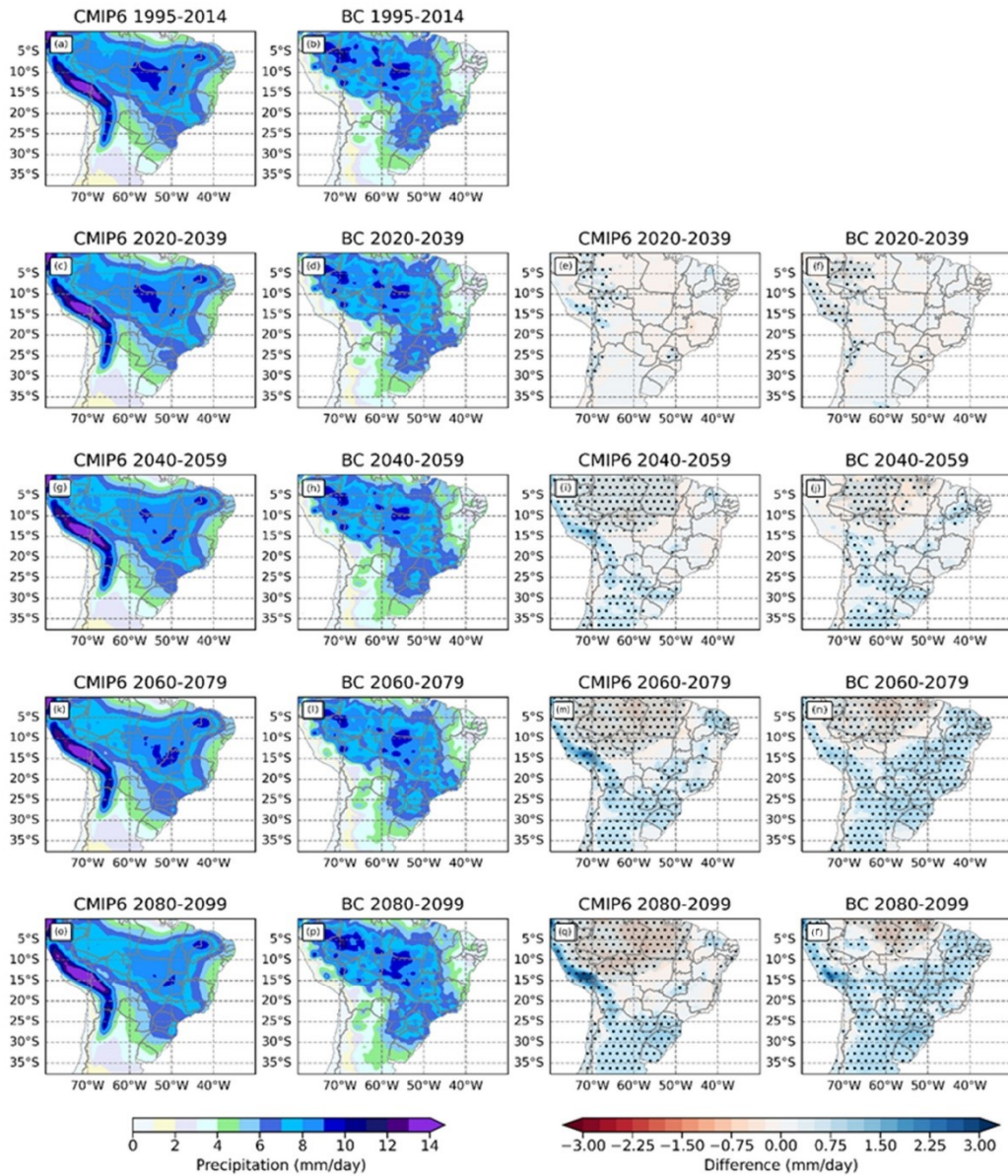


Figure 8. Similar to Figure 7, except for the SSP5-8.5 scenario. October–March precipitation (mm day^{-1}) during the historical period and the SSP2-4.5 scenario for different time slices 1995–2014, (a,b); 2020–2039, (c–f); 2040–2059, (g–j); 2060–2079, (k–n); 2080–2099, (o–r) and considering the raw and BCSD data (left side) and difference regarding the historical period (right side). From left to right: mean of the raw ensemble, mean of the BCSD ensemble, difference raw ensemble, and difference BCSD ensemble. The dots indicate statistical significance at 95% confidence in the difference fields based on the *t*-test.

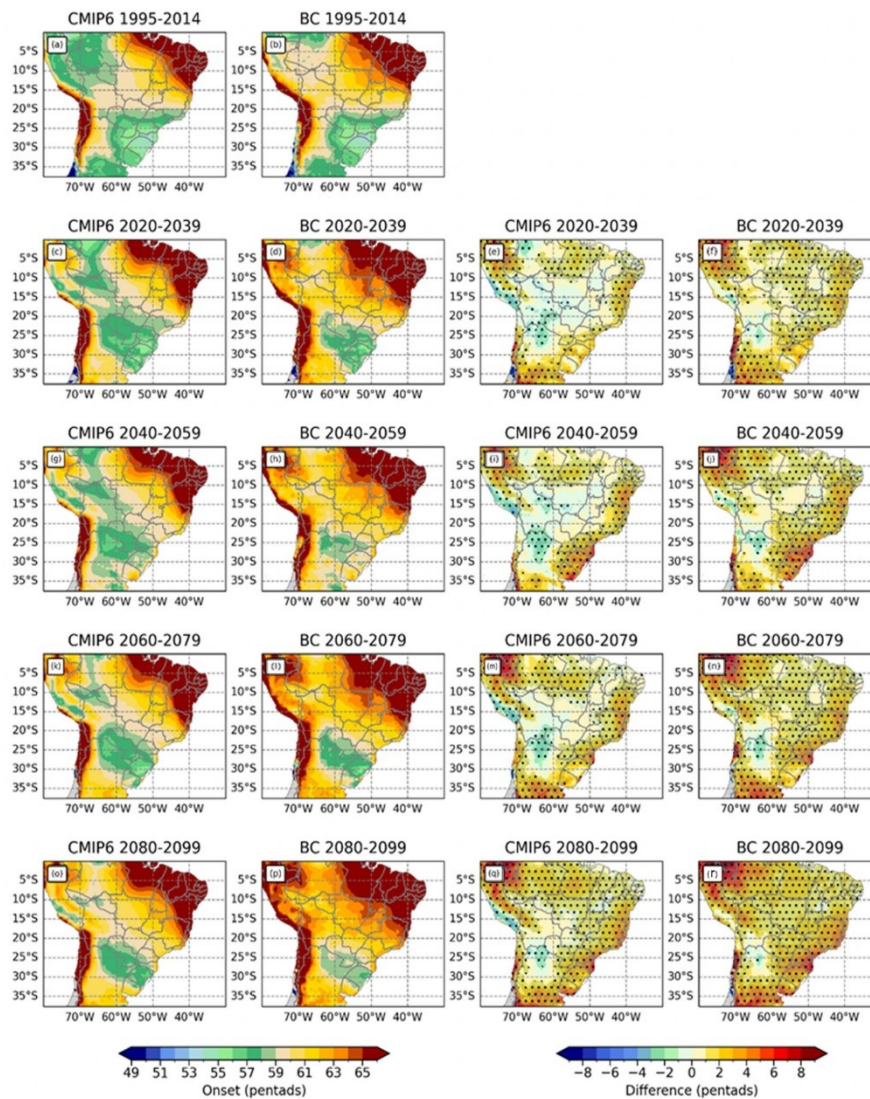


Figure 9. Similar to Figure 7, except for the monsoon onset (pentads) and SSP2–4.5 scenario. October–March precipitation (mm day^{-1}) during the historical period and the SSP2–4.5 scenario for different time slices 1995–2014, (a,b); 2020–2039, (c–f); 2040–2059, (g–j); 2060–2079, (k–n); 2080–2099, (o–r) and considering the raw and BCSD data (left side) and difference regarding the historical period (right side). From left to right: mean of the raw ensemble, mean of the BCSD ensemble, difference raw ensemble, and difference BCSD ensemble. The dots indicate statistical significance at 95% confidence in the difference fields based on the *t*-test.

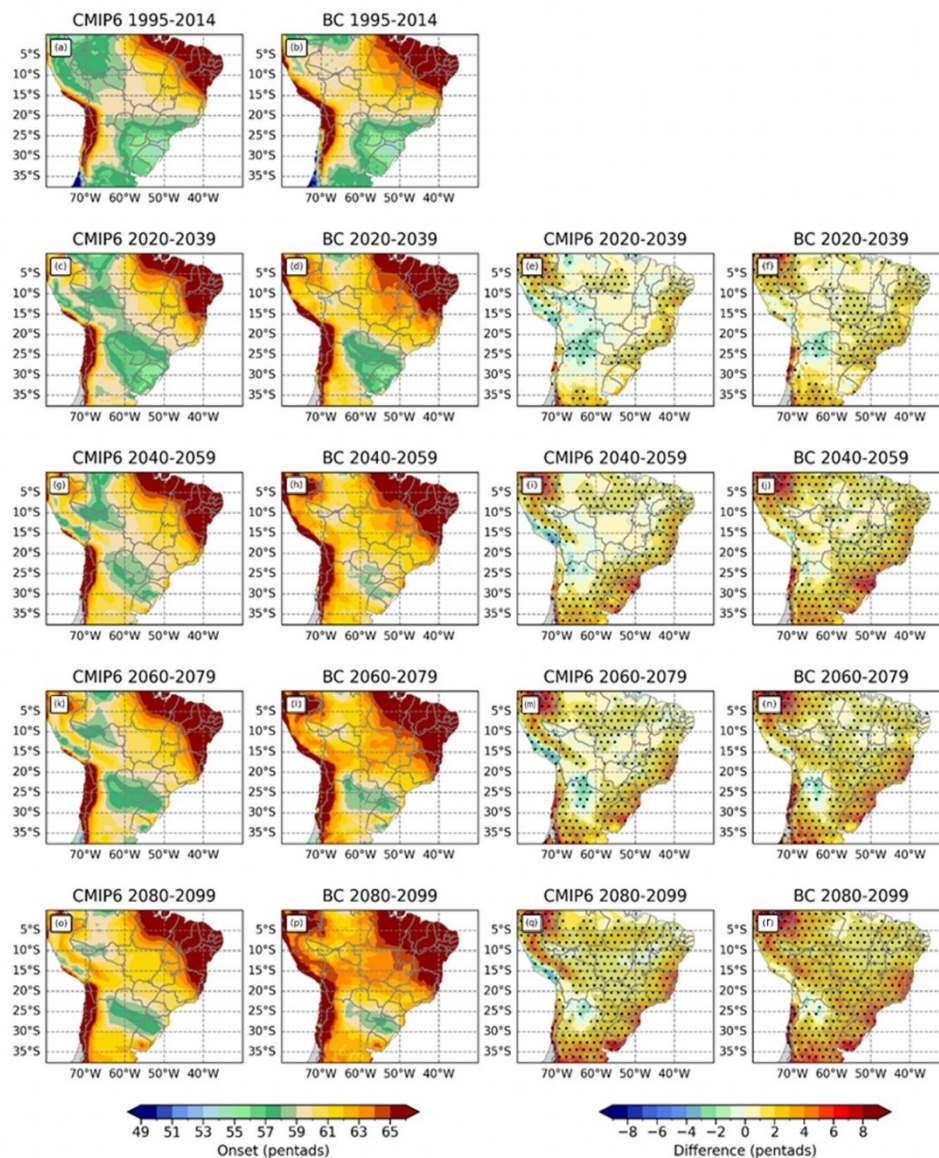


Figure 10. Similar to Figure 7, except for the monsoon onset (pentads) and SSP5–8.5 scenario. October–March precipitation (mm day^{-1}) during the historical period and the SSP2–4.5 scenario for different time slices (1995–2014, (a,b); 2020–2039, (c–f); 2040–2059, (g–j); 2060–2079, (k–n); 2080–2099, (o–r) and considering the raw and BCSD data (left side) and difference regarding the historical period (right side). From left to right: mean of the raw ensemble, mean of the BCSD ensemble, difference raw ensemble, and difference BCSD ensemble. The dots indicate statistical significance at 95% confidence in the difference fields based on the *t*-test.

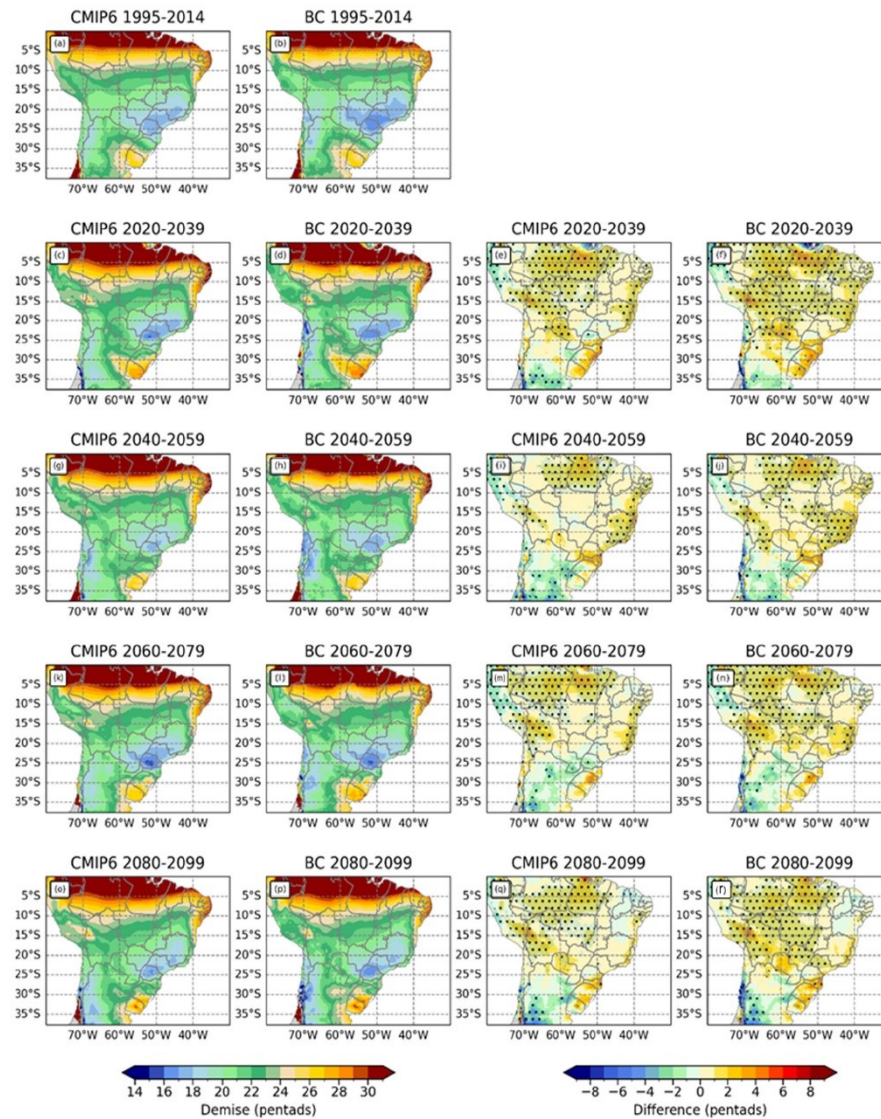


Figure 11. Similar to Figure 7, except for the monsoon demise (pentads) and SSP2-4.5 scenario. October–March precipitation (mm day^{-1}) during the historical period and the SSP2-4.5 scenario for different time slices (1995–2014, (a,b); 2020–2039, (c–f); 2040–2059, (g–j); 2060–2079, (k–n); 2080–2099, (o–r) and considering the raw and BCSD data (left side) and difference regarding the historical period (right side). From left to right: mean of the raw ensemble, mean of the BCSD ensemble, difference raw ensemble, and difference BCSD ensemble. The dots indicate statistical significance at 95% confidence in the difference fields based on the *t*-test.

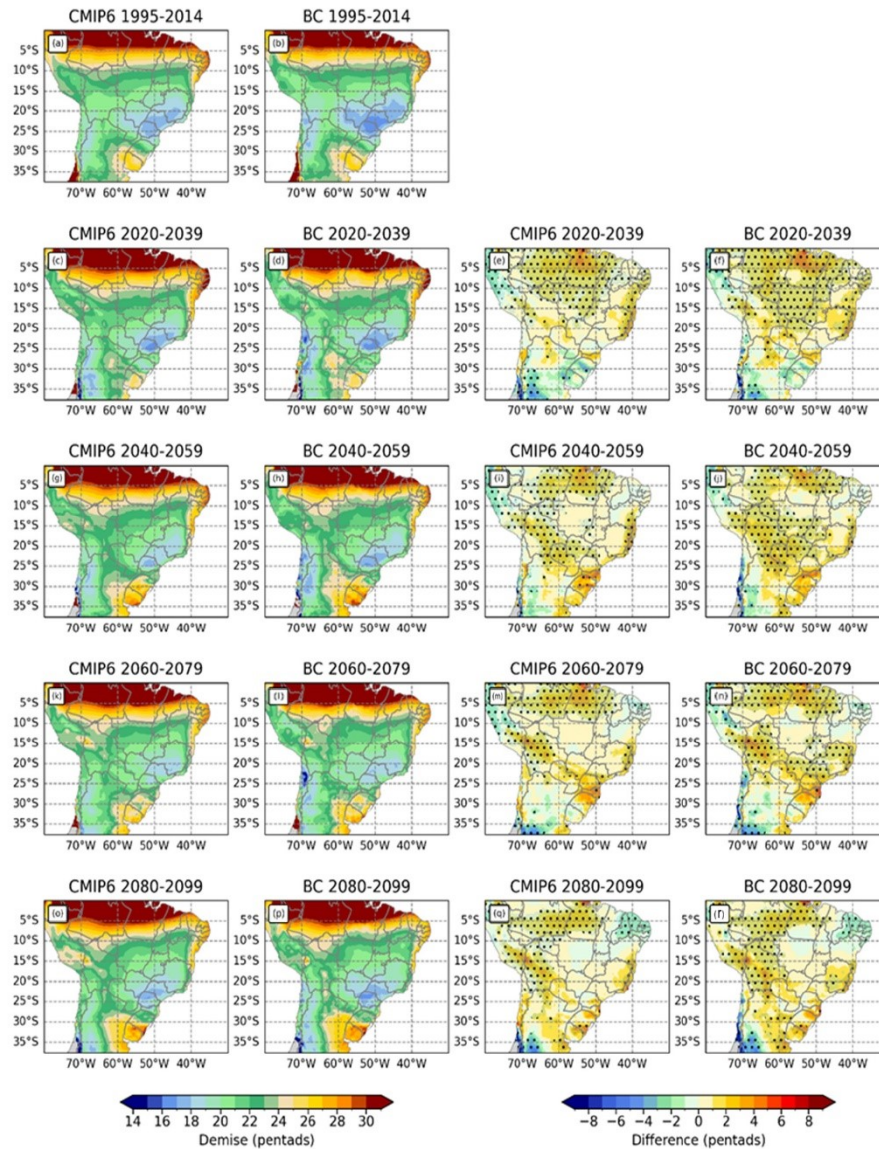


Figure 12. Similar to Figure 7, except for the monsoon demise (pentads) and SSP5–8.5 scenario. October–March precipitation (mm day^{-1}) during the historical period and the SSP2–4.5 scenario for different time slices (1995–2014, (a,b); 2020–2039, (c–f); 2040–2059, (g–j); 2060–2079, (k–n); 2080–2099, (o–r) and considering the raw and BCSD data (left side) and difference regarding the historical period (right side). From left to right: mean of the raw ensemble, mean of the BCSD ensemble, difference raw ensemble, and difference BCSD ensemble. The dots indicate statistical significance at 95% confidence in the difference fields based on the *t*-test.

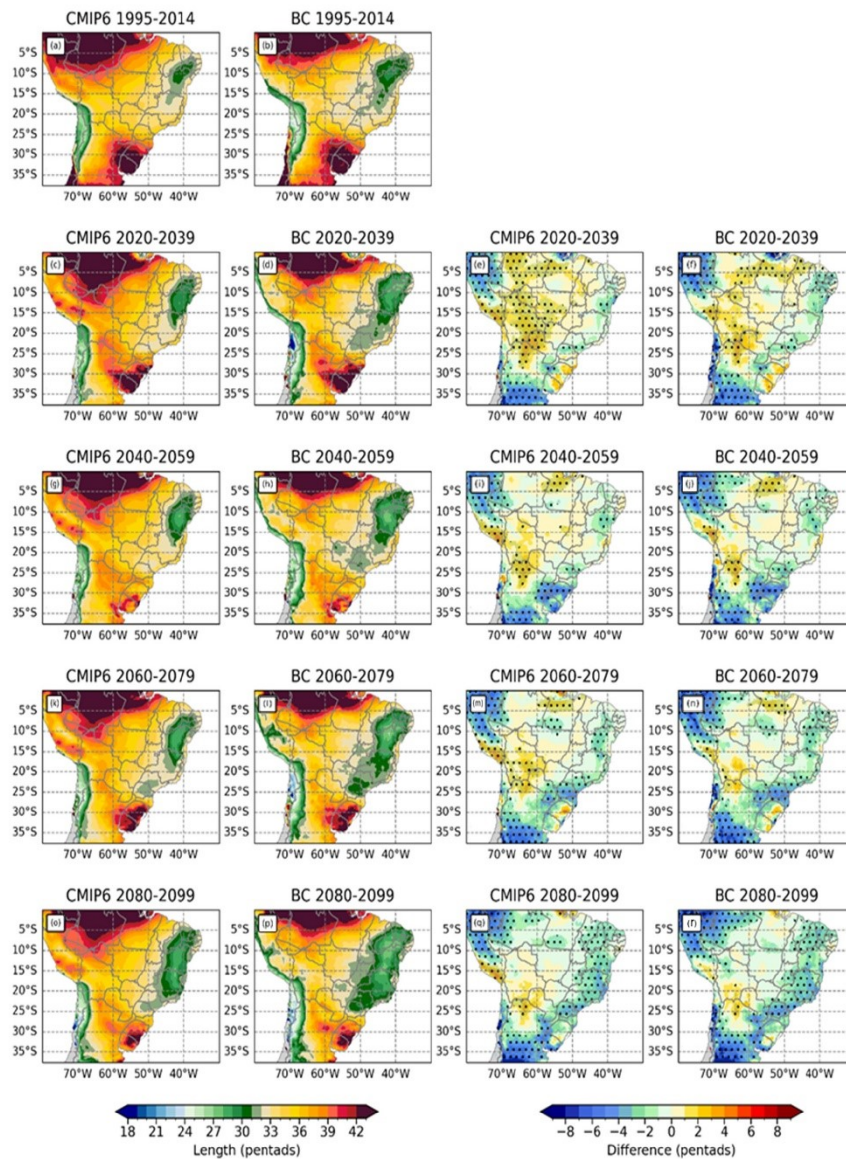


Figure 13. Similar to Figure 7, except for the monsoon length (pentads) and SSP2–4.5 scenario. October–March precipitation (mm day^{-1}) during the historical period and the SSP2–4.5 scenario for different time slices (1995–2014, (a,b); 2020–2039, (c–f); 2040–2059, (g–j); 2060–2079, (k–n); 2080–2099, (o–r) and considering the raw and BCSd data (left side) and difference regarding the historical period (right side). From left to right: mean of the raw ensemble, mean of the BCSd ensemble, difference raw ensemble, and difference BCSd ensemble. The dots indicate statistical significance at 95% confidence in the difference fields based on the t -test.

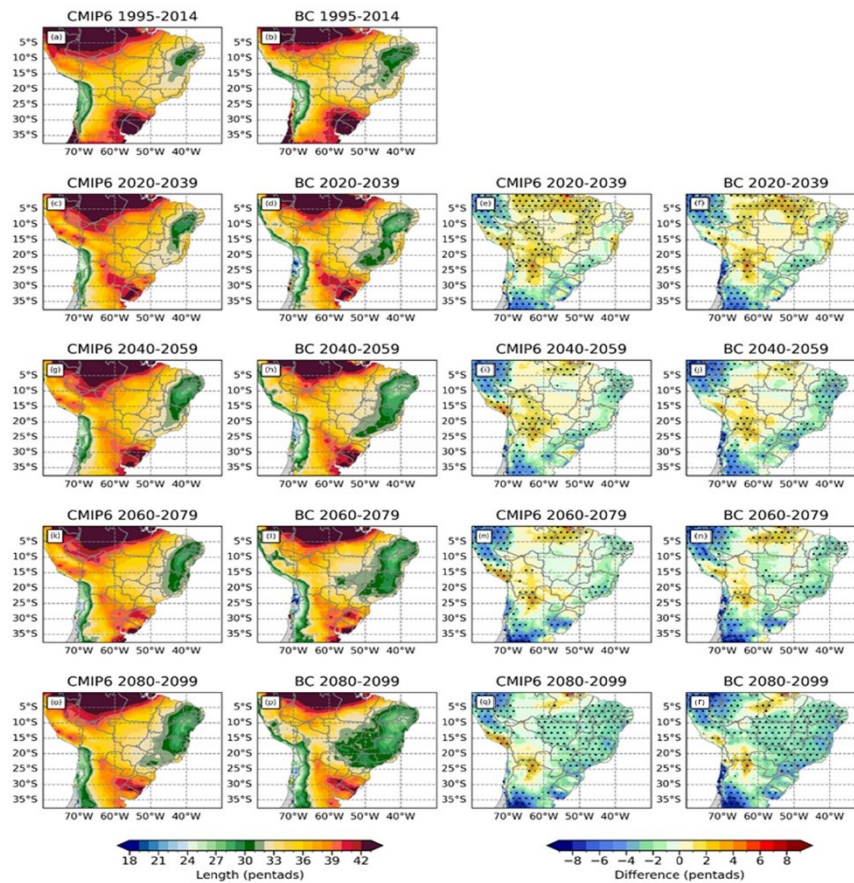


Figure 14. Similar to Figure 7, except for the monsoon length (pentads) and SSP5–8.5 scenario. October–March precipitation (mm day^{-1}) during the historical period and the SSP2–4.5 scenario for different time slices (1995–2014, (a,b); 2020–2039, (c–f); 2040–2059, (g–j); 2060–2079, (k–n); 2080–2099, (o–r) and considering the raw and BCSD data (left side) and difference regarding the historical period (right side). From left to right: mean of the raw ensemble, mean of the BCSD ensemble, difference raw ensemble, and difference BCSD ensemble. The dots indicate statistical significance at 95% confidence in the difference fields based on the *t*-test.

In both scenarios and ensembles, the demise of the rainy season (Figures 11 and 12) is projected to delay northward 20° S, with a difference of around two pentads compared to the historical period, but only reaching statistical significance over Amazonia and western SA. Over northern Argentina, while the trend to the end of the century is to delay the demise under SSP2.4–5 (Figure 11), it is to anticipate it under SSP5.8–5 (Figure 12). An interesting signal appears in Midwest Brazil in the BCSD ensemble: under SSP2.4–5, a significant area with late demise spread over the region toward the end of the century, while under SSP5–8.5, from 2020–2039 to 2040–2060 the area decreases with statistical significance and returns to increasing towards the end of the century. Still, the SSP5–8.5 scenario indicates a more intense change signal in the monsoon demise, with a delay of three pentads in

(1–5 April), up to three pentads earlier than that provided by the CPC (Pentad 22). Generally, the BCSD ensemble improves the rainy season demise over southern Amazonia and Midwest Brazil. On the other hand, the BCSD ensemble does not decrease the bias over northern Argentina and Paraguay simulated in the raw ensemble.

The BCSD ensemble better represents the SAMS onset, demise, and length west of 60° W (Figure 6). Despite this, no significant changes exist between the BCSD and raw ensembles in the other continental regions. In the Brazilian Midwest, both ensembles indicate a SAMS duration of 35–36 pentads, while the CPC indicates 36–37 pentads. Similarly, in the southeastern region, both ensembles underestimate the duration of the monsoon, with a duration of ~32–33 pentads, up to two pentads shorter than that provided by the CPC (~34–35 pentads). Contrarily, in northern Argentina, the ensembles overestimate the duration of the rainy season by up to two pentads, indicating a duration of 40–41 pentads, while the CPC shows a duration of 38–39 pentads.

Overall, it is concluded that despite the modest changes brought about by BCSD in identifying the parameters of the rainy season's lifecycle, the technique improves the representation of the monsoon onset west of 60° W, as well as the representation of the demise and length in the southwestern Amazonia.

3.2. Climate Projections

Spatial Patterns

Figures 7 and 8 present the climate projections of precipitation from October to March for four time slices (2020–2039, 2040–2059, 2060–2079, and 2080–2099) and one historical period (1995–2014) obtained by the raw and BCSD ensembles, under the SSP2–4.5 and SSP5–8.5 scenarios, respectively. Under the SSP2–4.5 scenario (Figure 7), the raw ensemble projections maintain their unrealistic representation of the spatial distribution of the rainy season, extending its influence to the northern portion of Northeast Brazil. However, the BCSD ensemble corrects this deficiency and satisfactorily reproduces the rainfall spatial distribution. The projected changes in rainfall volumes in each time slice compared to the historical period show statistically significant increases in precipitation in sectors of the Midwest and the interior of the Northeast, particularly from 2040 onwards. From 2060 onwards, increases in rainfall are also projected in the South, Southeast, and a larger area of Northeast Brazil, as well as in Peru and northern Argentina. Similar results were obtained by studies using CMIP5 models under the RCP-4.5 scenario [91,92] and a large ensemble of CMIP6 models under the SSP2–4.5 scenario [84]. Under the SSP5–8.5 scenario (Figure 8), the changes projected by both ensembles are similar to those provided by the SSP2–4.5 scenario, with the difference of having a more intense change signal and more significant rainfall reductions in the Brazilian North. The raw CMIP6 projections maintain their unrealistic representation of the rainy season, which is corrected by the statistically downscaled projections. The downscaled projections generally provide a stronger change signal than the raw projections. In both datasets, a more intense signal is observed towards the end of the 21st century, particularly under the SSP5–8.5 scenario.

The projections of changes found here corroborate the results of previous studies using models of different CMIP phases. The increase in rainfall in southeastern SA was also observed in studies using CMIP3, CMIP5 [93–96], and CMIP6 models [84,87,97]. Similarly, the reduction in precipitation in the Amazonia region agrees with the literature [11,84,87,91,92,94–97]. However, none of these CMIP studies focused on the SAMS lifecycle.

Figures 9–14 present the projections of the rainy season's onset, demise, and length under the SSP2–4.5 and SSP5–8.5 scenarios. Raw and BCSD ensembles, in both scenarios and in all time slices, project a delay in the onset of the rainy season, with a difference of approximately three pentads compared to the onset in the historical period in most of the study area (Figures 9 and 10), reaffirming the results obtained with the dynamical downscaling of CMIP5 models [12]. Over northern Argentina, the monsoon is projected to have an earlier onset. The difference between the ensembles is that the raw ensemble

shown, indicating whether the resulting trends are statistically significant (p -value < 0.05). In addition, Sen's slopes indicate whether the trends are positive (slope > 0) or negative (slope < 0).

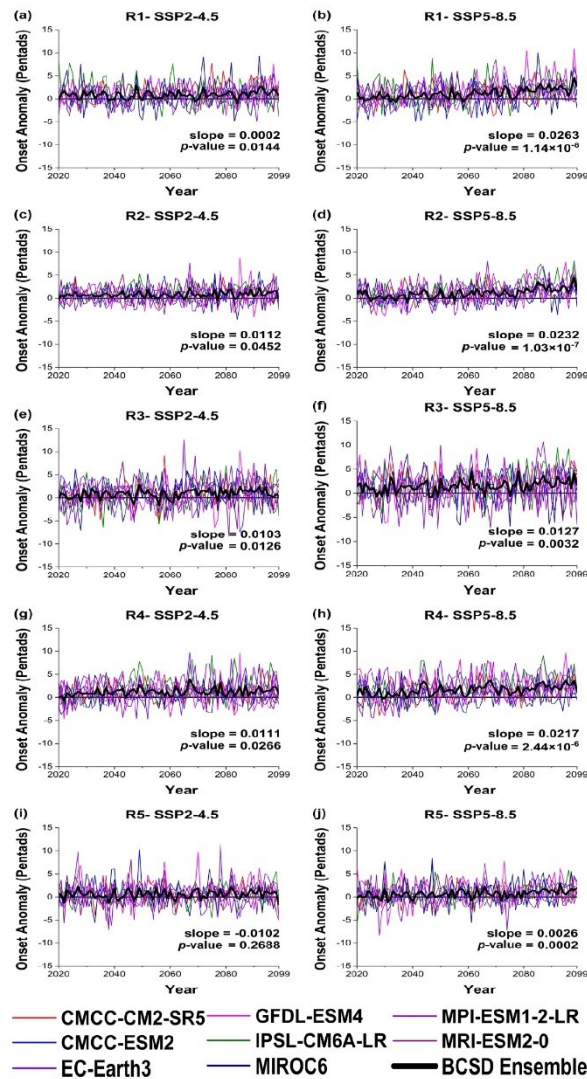


Figure 15. Time series of the monsoon's onset anomalies (in pentads) provided by the eight BCSD models and its ensemble (solid black line) for five SA subdomains (R1, (a,b); R2, (c,d); R3, (e,f); R4, (g,h); R5, (i,j) under the SSP2-4.5 (left column) and SSP5-8.5 (right column) scenarios. Anomalies refer to 2020–2099 in relation to 1995–2014. The p -value indicates the Mann–Kendall test result for the BCSD ensemble projections, and Sen's slopes indicate whether the trends are positive (slope > 0) or negative (slope < 0).

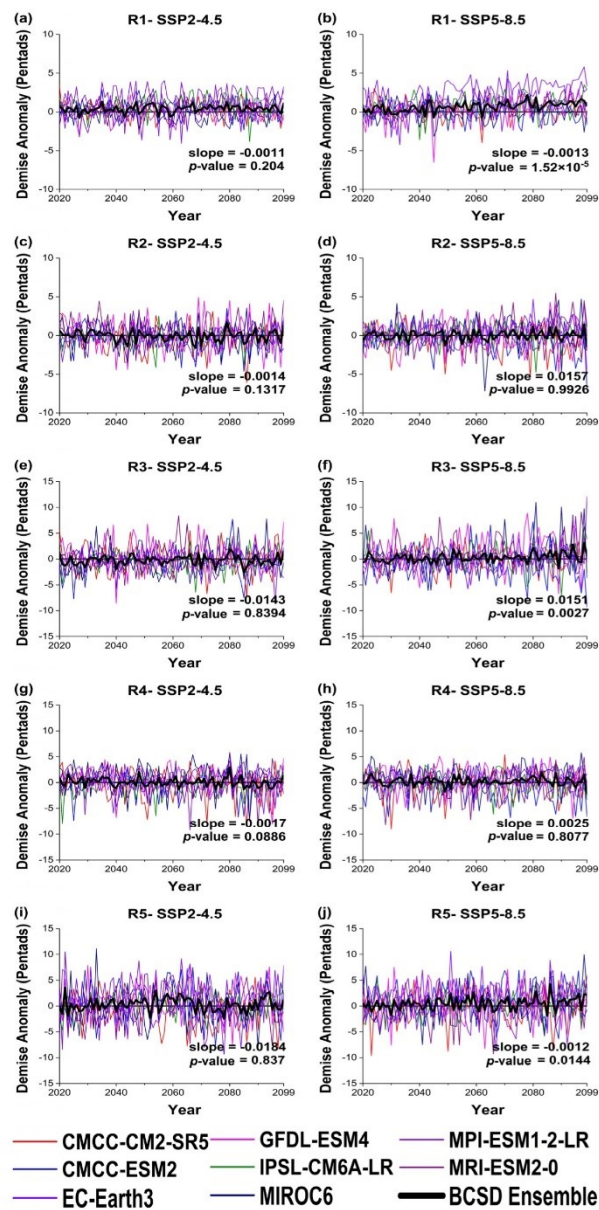


Figure 16. Similar to Figure 15, except for the monsoon’s demise (pentads). Time series of the monsoon’s onset anomalies (in pentads) provided by the eight BCSD models and its ensemble (solid black line) for five SA subdomains (R1, (a,b); R2, (c,d); R3, (e,f); R4, (g,h); R5, (i,j) under the SSP2–4.5 (left column) and SSP5–8.5 (right column) scenarios. Anomalies refer to 2020–2099 in relation to 1995–2014. The *p*-value indicates the Mann–Kendall test result for the BCSD ensemble projections, and Sen’s slopes indicate whether the trends are positive (slope > 0) or negative (slope < 0).

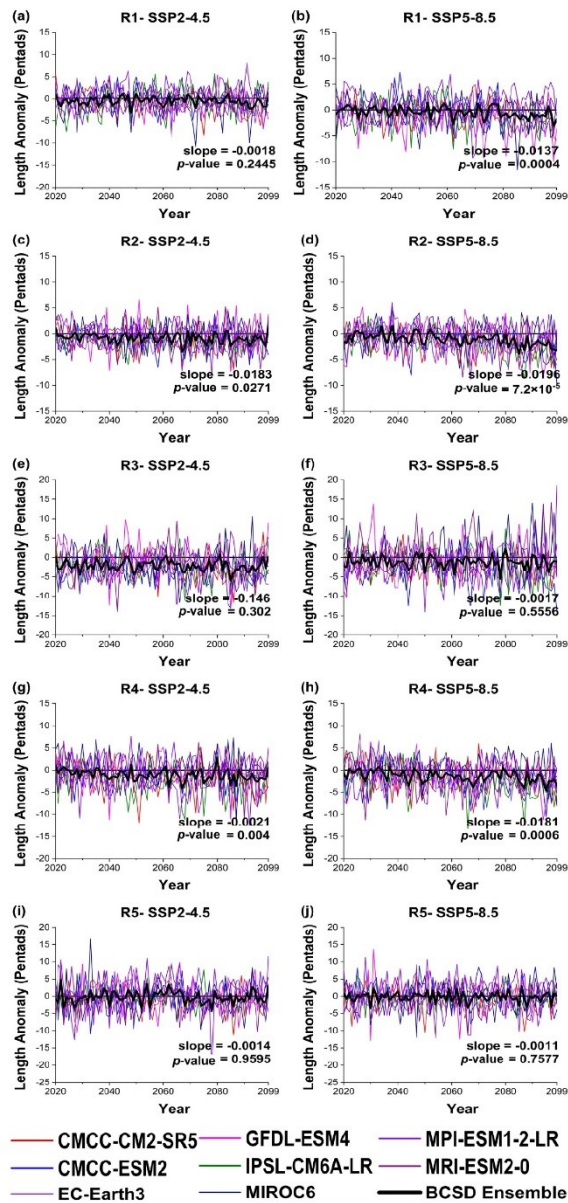


Figure 17. Similar to Figure 15, except for the monsoon’s length (pentads). Time series of the monsoon’s onset anomalies (in pentads) provided by the eight BCSD models and its ensemble (solid black line) for five SA subdomains (R1, (a,b); R2, (c,d); R3, (e,f); R4, (g,h); R5, (i,j) under the SSP2–4.5 (left column) and SSP5–8.5 (right column) scenarios. Anomalies refer to 2020–2099 in relation to 1995–2014. The *p*-value indicates the Mann–Kendall test result for the BCSD ensemble projections, and Sen’s slopes indicate whether the trends are positive (slope > 0) or negative (slope < 0).

For R1 (Amazonia), the ensemble projects an increase in the onset of the SAMS with statistical significance under both scenarios, which means a regional delay in the monsoon beginning. The ensemble generally shows changes from the SAMS onset ranging from -1 to 5 pentads. On the other hand, the individual models indicate considerable spread in the projections, with the CMCC-ESM2, GFDL-ESM4, and MIROC6 models providing monsoon onset shifts ranging from -5 to 11 pentads. Under the SSP2-4.5 scenario, the ensemble indicates the monsoon onset ranging from Pentads 58–62 (13–17 October to 2–6 November), which is partially similar to the ranges found in the reference periods of other studies [10,12,92]. Under the SSP5-8.5 scenario, the ensemble indicates a larger delay in the SAMS onset, which varies in Pentads 59–64 (18–22 October to 12–16 November), corroborating the results of previous studies [12,92].

Considering the projected changes in the SAMS demise in R1, only the SSP5-8.5 scenario results in a statistically significant increasing trend projected by the BCSD ensemble. While the ensemble projects the monsoon's demise changes ranging from -1 to 2 pentads, models such as EC-Earth3, GFDL-ESM4, and MPI-ESM1-2-LR provide anomalies ranging from -7 to 6 pentads. Despite this result suggesting an increase in the rainy season in R1, the analysis of the SAMS length shows that, under the SSP5-8.5 scenario, the ensemble projects a statistically significant decrease, with anomalies ranging from -3 to 1 pentad in relation to the historical period.

Moreover, the results found here agree with projections obtained by dynamical downscaling, which yielded a delay of one pentad at the monsoon's beginning and a reduction of up to two pentads in the duration for the period 2010–2040 [11]. Additionally, a study of the impacts of land use on the monsoon lifecycle in southern Amazonia indicated that deforestation has contributed to a delay of approximately 1 pentad at the beginning, an advance of 2 to 6 pentads at the demise, and a reduction of 2 to 8 pentads in the duration of the rainy season for the period 1998–2012 [104].

In R2 (Midwest Brazil), under both scenarios, the BCSD ensemble projects a statistically significant increase in the monsoon onset, which means a delay in the rainy season beginning over the region. In this sector, the ensemble presents onset anomalies ranging from -1 to 4 pentads, while other models, such as EC-Earth3 and GFDL-ESM4, project variations from -4 to 9 pentads. The BCSD ensemble projections of the rainy season demise in R2 do not result in statistically significant trends in both scenarios. On the other hand, the ensemble provides a statistically significant decreasing trend in the SAMS length in both scenarios, indicating a retraction in the rainy season over R2 during the 21st century. In this region, the ensemble projects anomalies of the monsoon's length ranging from -4 to 1 pentad, while models like CMCC-ESM2, EC-Earth3, and GFDL-ESM4 project anomalies from -10 to 6 pentads.

For R3 (Southeast Brazil), the ensemble projections result in statistically significant increasing trends in the monsoon onset for both scenarios, indicating that the rainy season's beginning tends to be delayed over the region during the 21st century. While the ensemble projects anomalies of SAMS onset ranging from -1 to 4 pentads, models such as EC-Earth3, MPI-ESM1-2-LR, and MRI-ESM2-0 estimate changes going from -7 to 11 pentads. Regarding the monsoon demise, the ensemble projects a statistically significant increasing trend only under the SSP5-8.5 scenario, with anomalies ranging from -2 to 3 pentads. For the monsoon's length projections, neither of the two scenarios results in a statistically significant trend, with the BCSD ensemble providing anomalies of -6 to 2 pentads about the reference period.

In R4 (northern sector of Southeast Brazil), the ensemble projects a statistically significant increase in the monsoon onset under both scenarios, reiterating the delay in the SAMS onset also found in other regions. In this sector, the ensemble shows onset anomalies ranging from 0 to 4 pentads, while models like GFDL-ESM4 and MPI-ESM1-2-LR provide changes from -4 to 10 pentads. The ensemble projections do not result in a statistically significant trend in either scenario regarding the monsoon demise. On the other hand,

under the two scenarios, the ensemble projects a statistically significant reduction in the rainy season's length, with anomalies ranging from -5 to 1 pentad.

Finally, in R5 (northern Argentina), the ensemble only projects a statistically significant increasing trend in the monsoon onset under the SSP5–8.5 scenario. In this region, the ensemble provides anomalies ranging from -1 to 3 pentads, while models such as GFDL-ESM4 and MPI-ESM1-2-LR project anomalies ranging from -8 to 8 pentads. Similarly, for the monsoon demise, the ensemble projects a statistically significant increasing trend only under the SSP5–8.5 scenario, with anomalies ranging from -2 to 4 pentads. On the other hand, neither scenario indicates a statistically significant trend in the monsoon's length, with the ensemble providing anomalies ranging from -4 to 3 pentads.

In general, the trend analysis shows that the BCSD ensemble projects a delay in the monsoon onset in practically all regions analyzed under the two scenarios employed (except in R5, where only the SSP5–8.5 scenario results in an increasing trend). Contrastingly, the ensemble projections for the SAMS demise provide statistically significant increasing trends only under the SSP5–8.5 scenario and for sectors R1, R3, and R5. Furthermore, the ensemble projections show a statistically significant decreasing trend in monsoon length in the regions R2 and R4 under both scenarios and in R1 only under the SSP5–8.5 scenario. Similarly, a study of deforestation effects in southern Amazonia showed that almost 90% of rainfall gauges in the transition zone between Amazonia and Midwest Brazil showed a decreasing monsoon length from 1971 to 2010, with a later onset and early demise [105].

Regarding the individual projections of the GCMs, there is considerable variability of estimates in all regions. In this context, the GFDL-ESM4 and EC-Earth3 models show significant variability in the SAMS lifecycle parameters in practically all sectors evaluated. In summary, these results suggest that, under both scenarios, the monsoon onset tends to be delayed, but its demise is almost unchanged. Additionally, most evaluated sectors tend to decrease the rainy season's length during the 21st century.

4. Conclusions

This study applied statistical downscaling to CMIP6 precipitation projections using the CPC data as a reference to evaluate future changes in the monsoon lifecycle and precipitation in SA. To this end, we used the QDM technique developed by Cannon et al. [65], and the method improved the representation of the monsoon onset west of 60°W , as well as the demise and length in southwestern Amazonia. Projections of precipitation showed an increase in rainfall in SESA and a reduction in the Amazonia region during the 21st century, in agreement with previous studies.

Raw and BCSD ensembles, in both scenarios and in all time slices, project a delay in the monsoon onset, with a difference of approximately three pentads compared to the onset in the historical period in most of the study area. Similarly, in both scenarios, the monsoon demise is projected to delay northward 20°S , with a difference of around two pentads compared to the historical period, although this exhibits statistical significance only over Amazonia and western SA. Furthermore, the SSP5–8.5 scenario indicates a more intense change signal in the monsoon demise, with a delay of three pentads in the Brazilian Amazon from the second half of the 21st century.

Additionally, the trend analysis shows that the BCSD ensemble projects a delay in the monsoon onset in practically all regions analyzed under the two scenarios assessed. Moreover, the ensemble projections show a statistically significant decreasing trend in the monsoon's length in most SACZ regions.

For future studies, we recommend using more forcing scenarios to minimize the uncertainties associated with the projections. Moreover, despite the statistical downscaling technique refining the grid of projections (yielding estimates with an intermediate spatial resolution of 50 km), further research should employ finer climate projections to ensure a greater accuracy. But, for this end, observed data in high resolution are needed. This remains a gap and the subject of much discussion by the scientific community (few monitoring stations, data quality, data availability etc.). Nonetheless, despite the uncertainties

associated with projections, our findings can provide helpful information to decision-makers and energy planners for the better management of water resources on the South American continent over the coming decades.

Supplementary Materials: The following supporting information can be downloaded at: <https://www.mdpi.com/article/10.3390/atmos14091380/s1>, Table S1: Results of the computation of SAMS lifecycle parameters for R1 obtained here (shaded line) compared to previous works; Table S2: Results of the computation of SAMS lifecycle parameters for R3 obtained here (shaded line) compared to previous works; Table S3: Results of the computation of SAMS lifecycle parameters for R4 obtained here (shaded line) compared to previous works; Table S4: Results of the computation of SAMS lifecycle parameters for R5 obtained here (shaded line) compared to previous works; Figure S1: Time series of the monsoon onset (in pentads) provided by eight CMIP6-GCMs and the BCSD ensemble for five SA subdomains under the SSP2–4.5 and SSP5–8.5 scenarios; Figure S2: Similar to Figure S1, except for the monsoon demise (in pentads); Figure S3: Similar to Figure S1, except for the monsoon’s length (in pentads).

Author Contributions: Conceptualization, M.S.R.; methodology, M.S.R.; software, M.S.R., G.W.d.S.F. and J.G.M.R.; formal analysis, M.S.R. and G.W.d.S.F.; writing—original draft preparation, M.S.R. and G.W.d.S.F.; writing—review and editing, M.S.R., G.W.d.S.F., J.G.M.R., R.P.d.R. and V.B.R. All authors have read and agreed to the published version of the manuscript.

Funding: The authors thank the Coordination for the Improvement of Higher Education Personnel (CAPES, Finance Code 001), the National Council for Scientific and Technological Development (CNPq), and the R&D project from Engie Brazil Energy (R&D-00403-0054/2022) regulated by the Brazilian National Electric Energy Agency (ANEEL).

Institutional Review Board Statement: Not applicable.

Informed Consent Statement: Not applicable.

Data Availability Statement: All datasets used in this study are available on public online databases. BCSD models can be provided upon request.

Acknowledgments: The authors thank the Coordination for the Improvement of Higher Education Personnel (CAPES), the Brazilian National Electric Energy Agency (ANEEL), the National Council for Scientific and Technological Development (CNPq), and Engie Brazil Energy for their financial support. The authors also thank the Coupled Model Intercomparison Project (CMIP) and Climate Prediction Center (NOAA–CPC) for providing the datasets used in this study.

Conflicts of Interest: The authors declare no conflict of interest. The funders had no role in the design of the study; in the collection, analyses, or interpretation of the data; in the writing of the manuscript; or in the decision to publish the results.

References

1. Ramage, C.S. *Monsoon Meteorology*, 1st ed.; Academic Press: New York, NY, USA, 1971.
2. Wang, B.; Liu, J.; Kim, H.-J.; Webster, P.J.; Yim, S.-Y. Recent change of the global monsoon precipitation (1979–2008). *Clim. Dyn.* **2012**, *39*, 1123–1135. [[CrossRef](#)]
3. Grimm, A.M.; Dominguez, F.; Cavalcanti, I.F.; Cavazos, T.; Gan, M.A.; Silva Dias, P.L.; Fu, R.; Castro, C.; Hu, H.; Barreiro, M. South and North American Monsoons: Characteristics, life cycle, variability, modeling, and prediction. In *The Multiscale Global Monsoon System*, 4th ed.; Chang, C.-P., Ha, K.-J., Johnson, R.H., Kim, D., Lau, G.N.C., Wang, B., Eds.; World Scientific: Singapore, 2020; pp. 49–66. [[CrossRef](#)]
4. Teodoro, T.A.; Reboita, M.S.; Llopart, M.; da Rocha, R.P.; Ashfaq, M. Climate change impacts on the South American Monsoon System and its surface-atmosphere processes through RegCM4 CORDEX-CORE projections. *Earth Syst. Environ.* **2021**, *5*, 825–847. [[CrossRef](#)]
5. Silva, V.B.; Kousky, V.E. The South American monsoon system: Climatology and variability. *Modern Climatol.* **2012**, *123*, 152. [[CrossRef](#)]
6. Carvalho, L.M.V.; Cavalcanti, I.F.A. The South American Monsoon System (SAMS). In *The Monsoons and Climate Change*, 1st ed.; Carvalho, L.M.V., Jones, C., Eds.; Springer: Sydney, Australia, 2016; pp. 121–148.
7. Liebmann, B.; Marengo, J.A. Interannual variability of the rainy season and rainfall in the Brazilian Amazon Basin. *J. Clim.* **2001**, *14*, 4308–4318. [[CrossRef](#)]

8. Vera, C.; Higgins, W.; Amador, J.; Ambrizzi, T.; Garreaud, R.; Gochis, D.; Gutzler, D.; Lettenmaier, D.; Marengo, J.A.; Mechoso, C.R.; et al. Toward a unified view of the American Monsoon Systems. *J. Clim.* **2006**, *19*, 4977–5000. [[CrossRef](#)]
9. Gan, M.A.; Kousky, V.; Ropelewski, C.F. The South America monsoon rainfall over West-Central Brazil. *J. Clim.* **2004**, *17*, 47–66. [[CrossRef](#)]
10. Bombardi, R.J.; Carvalho, L.M.V. IPCC global coupled model simulations of the South America monsoon system. *Clim. Dyn.* **2009**, *33*, 893–916. [[CrossRef](#)]
11. Reboita, M.S.; da Rocha, R.P.; Dias, C.G.; Ynoue, R.Y. Climate projections for South America: RegCM43 driven by HadCM3 and ECHAM5. *Adv. Meteorol.* **2014**, *2014*, 376738. [[CrossRef](#)]
12. Ashfaq, M.; Cavazos, T.; Reboita, M.S.; Torres-Alavez, J.A.; Im, E.-S.; Olusegun, C.F.; Alves, L.; Key, K.; Adeniyi, M.O.; Tall, M.; et al. Robust late twenty-first century shift in the regional monsoons in RegCM-CORDEX simulations. *Clim. Dyn.* **2021**, *57*, 1463–1488. [[CrossRef](#)]
13. Kousky, V.E. Pentad outgoing longwave radiation climatology for the South American sector. *Rev. Bras. Meteorol.* **1988**, *3*, 217–231.
14. Fu, R.; Li, W. The influence of the land surface on the transition from dry to wet season in Amazonia. *Theor. Appl. Climatol.* **2004**, *78*, 97–110. [[CrossRef](#)]
15. Dias, C.G.; Reboita, M.S.; da Rocha, R.P.; Cuadra, S.V. Validação dos Fluxos Turbulentos de Calor sobre a América do Sul Simulados pelo RegCM3. In *IV Simpósio Internacional de Climatologia*; SIC: João Pessoa, Brazil, 2011.
16. Carvalho, L.M.V.; Jones, C.; Liebmann, B. The South Atlantic Convergence Zone: Intensity, form, persistence, and relationships with intraseasonal to interannual activity and extreme rainfall. *J. Clim.* **2004**, *17*, 88–108. [[CrossRef](#)]
17. Gonzalez, P.L.M.; Vera, C.S. Summer precipitation variability over South America on long and short intraseasonal timescales. *Clim. Dyn.* **2014**, *43*, 1993–2007. [[CrossRef](#)]
18. Bombardi, R.J.; Carvalho, L.M.V.; Jones, C.; Reboita, M.S. Precipitation over eastern South America and the South Atlantic sea surface temperature during neutral ENSO periods. *Clim. Dyn.* **2014**, *42*, 1553–1568. [[CrossRef](#)]
19. Grimm, A.M. South American monsoon and its extremes. In *Tropical Extremes-Natural Variability and Trends*, 1st ed.; Venugopal, V., Sukhatme, J., Murtugudde, R., Roca, R., Eds.; Elsevier: Amsterdam, The Netherlands, 2019; pp. 51–93. [[CrossRef](#)]
20. Avila-Diaz, A.; Benezoli, V.; Justino, F.; Torres, R.R.; Wilson, A. Assessing current and future trends of climate extremes across Brazil based on reanalyses and earth system model projections. *Clim. Dyn.* **2020**, *55*, 1403–1426. [[CrossRef](#)]
21. Cai, W.; McPhaden, M.J.; Grimm, A.M.; Rodrigues, R.R.; Taschetto, A.S.; Garreaud, R.D.; Dewitte, B.; Poveda, G.; Ham, Y.G.; Santoso, A.; et al. Climate impacts of the El Niño-Southern Oscillation on South America. *Nat. Rev. Earth Environ.* **2020**, *1*, 215–231. [[CrossRef](#)]
22. Reboita, M.S.; Ambrizzi, T.; Crespo, N.M.; Dutra, L.M.M.; Ferreira, G.W.S.; Rehbein, A.; Drumond, A.; da Rocha, R.P.; Souza, C.A. Impacts of teleconnection patterns on South America climate. *Ann. N. Y. Acad. Sci.* **2021**, *1504*, 116–153. [[CrossRef](#)]
23. Mechoso, C.R.; Robertson, A.W.; Ropelewski, C.F.; Grimm, A.M. The American monsoon systems: An introduction. In *The Global Monsoon System: Research and Forecast*; Chap. 13. WMO ITD No. 1266 (TMRP Report No. 70); Chang, C.-P., Kuo, H.-C., Lau, N.-C., Johnson, R.H., Wang, B., Wheeler, M.C., Eds.; World Scientific: Singapore, 2005; pp. 197–206.
24. Fu, R.; Yin, L.; Li, W.; Arias, P.A.; Dickinson, R.E.; Huang, L.; Chakraborty, S.; Fernandes, K.; Liebmann, B.; Fisher, R.; et al. Increased dry-season length over southern Amazonia in recent decades and its implication for future climate projection. *Proc. Natl. Acad. Sci. USA* **2013**, *110*, 18110–18115. [[CrossRef](#)]
25. Arias, P.A.; Fu, R.; Vera, C.; Rojas, M. A correlated shortening of the North and South American monsoon seasons in the past few decades. *Clim. Dyn.* **2015**, *45*, 3183–3203. [[CrossRef](#)]
26. Sena, A.C.T.; Magnusdottir, G. Projected end-of-century changes in the South American Monsoon in the CESM large ensemble. *J. Clim.* **2020**, *33*, 7859–7874. [[CrossRef](#)]
27. Correa, I.; Arias, P.A.; Rojas, M. Evaluation of multiple indices of the South American monsoon. *Int. J. Climatol.* **2020**, *41*, 2801–2819. [[CrossRef](#)]
28. Dhakal, S.; Minx, J.C.; Toth, F.L.; Abdel-Aziz, A.; Meza, M.J.F.; Hubacek, K.; Jonckheere, I.G.C.; Kim, Y.-G.; Nemet, G.F.; Pachauri, S.; et al. Emissions Trends and Drivers. In *IPCC, 2022: Climate Change 2022: Mitigation of Climate Change. Contribution of Working Group III to the Sixth Assessment Report of the Intergovernmental Panel on Climate Change*; Shukla, P.R., Skea, J., Slade, R., Al Khourdajie, A., van Diemen, R., McCollum, D., Pathak, M., Some, S., Vyas, P., Fradera, R., et al., Eds.; Cambridge University Press: Cambridge, UK; New York, NY, USA, 2022. [[CrossRef](#)]
29. Llopart, M.; Reboita, M.S.; Coppola, E.; Giorgi, F.; da Rocha, R.P.; Souza, D.O. Land use change over the Amazon Forest and its impact on the local climate. *Water* **2018**, *10*, 149. [[CrossRef](#)]
30. Rizzo, R.; Garcia, A.S.; Vilela, V.M.F.N.; Ballester, M.V.R.; Neill, C.; Victoria, D.C.; da Rocha, H.R.; Coe, M.T. Land use changes in Southeastern Amazon and trends in rainfall and water yield of the Xingu River during 1976–2015. *Clim. Change* **2020**, *162*, 1419–1436. [[CrossRef](#)]
31. Marengo, J.A.; Jimenez, J.C.; Espinoza, J.C.; Cunha, A.P.; Aragão, L.E.O. Increased climate pressure on the agricultural frontier in the Eastern Amazonia-Cerrado transition zone. *Sci. Rep.* **2022**, *12*, 457. [[CrossRef](#)] [[PubMed](#)]
32. Jones, C.; Carvalho, L.M. Climate change in the South American monsoon system: Present climate and CMIP5 projections. *J. Clim.* **2013**, *26*, 6600–6678. [[CrossRef](#)]
33. Khalili, M.; Van Nguyen, V.T. A perfect prognosis approach for daily precipitation series in consideration of space-time correlation structure. *Stoch. Environ. Res. Risk Assess.* **2018**, *32*, 3333–3364. [[CrossRef](#)]

34. Di Virgilio, G.; Ji, F.; Tam, E.; Nishant, N.; Evans, J.P.; Thomas, C.; Riley, M.L.; Beyer, K.; Grose, M.R.; Narsey, S.; et al. Selecting CMIP6 GCMs for CORDEX dynamical downscaling: Model performance, independence, and climate change signals. *Earth's Future* **2022**, *10*, e2021EF002625. [[CrossRef](#)]
35. Rettie, F.M.; Gayler, S.; Weber, T.K.D.; Tesfaye, K.; Streck, T. High-resolution CMIP6 climate projections for Ethiopia using the gridded statistical downscaling method. *Sci. Data* **2023**, *10*, 442. [[CrossRef](#)]
36. Maraun, D.; Widmann, M. *Statistical Downscaling and Bias Correction for Climate Research*; Cambridge University Press: Cambridge, UK, 2018.
37. Lee, T.; Singh, V.P. *Statistical Downscaling for Hydrological and Environmental Applications*, 1st ed.; Taylor & Francis Group: Boca Raton, FL, USA, 2019.
38. Bettolli, M.L.; Solman, S.A.; da Rocha, R.P.; Llopart, M.; Gutierrez, J.M.; Fernández, J.; Olmo, M.E.; Lavin-Gullon, A.; Chou, S.C.; Rodrigues, D.C.; et al. The CORDEX Flagship Pilot Study in southeastern South America: A comparative study of statistical and dynamical downscaling models in simulating daily extreme precipitation events. *Clim. Dyn.* **2021**, *56*, 1589–1608. [[CrossRef](#)]
39. Balmaceda-Huarte, R.; Bettolli, M.L. Assessing statistical downscaling in Argentina: Daily maximum and minimum temperatures. *Int. J. Climatol.* **2022**, *42*, 8423–8445. [[CrossRef](#)]
40. Olmo, M.E.; Bettolli, M.L. Statistical downscaling of daily precipitation over southeastern South America: Assessing the performance in extreme events. *Int. J. Climatol.* **2022**, *42*, 1283–1302. [[CrossRef](#)]
41. Olmo, M.E.; Balmaceda-Huarte, R.; Bettolli, M.L. Multi-model ensemble of statistically downscaled GCMs over southeastern South America: Historical evaluation and future projections of daily precipitation with focus on extremes. *Clim. Dyn.* **2022**, *59*, 3051–3068. [[CrossRef](#)]
42. Ballarin, A.S.; Sone, J.S.; Gesualdo, G.C.; Schwaback, D.; Reis, A.; Almagro, A.; Wendland, E.C. CLIMBra—Climate change dataset for Brazil. *Sci. Data* **2023**, *10*, 47. [[CrossRef](#)] [[PubMed](#)]
43. Ferreira, G.W.S.; Reboita, M.S. A new look into the South American precipitation patterns: Observation and forecast. *Atmosphere* **2022**, *13*, 873. [[CrossRef](#)]
44. Chen, M.; Shi, W.; Xie, P.; Silva, V.B.S.; Kousky, V.E.; Higgins, R.W.; Janowiak, J.E. Assessing objective techniques for gauge-based analyses of global daily precipitation. *J. Geophys. Res.* **2008**, *113*, D04110. [[CrossRef](#)]
45. Balmaceda-Huarte, R.; Olmo, M.E.; Bettolli, M.L.; Poggi, M.M. Evaluation of multiple reanalyses in reproducing the spatio-temporal variability of temperature and precipitation indices over southern South America. *Int. J. Climatol.* **2021**, *41*, 5572–5595. [[CrossRef](#)]
46. Lagos-Zúñiga, M.A.; Balmaceda-Huarte, R.; Regoto, P.; Torrez, L.; Olmo, M.; Lyra, A.; Pareja-Quispe, D.; Bettolli, M.L. Extreme indices of temperature and precipitation in South America: Trends and intercomparison of regional climate models. *Clim. Dyn.* **2022**. *Under Review*. [[CrossRef](#)]
47. Martínez, D.M.; Solman, S.A. Synoptic patterns associated with extreme precipitation events over southeastern South America during spring and summer seasons. *Int. J. Climatol.* **2022**, *42*, 10387–10406. [[CrossRef](#)]
48. Ferreira, G.W.S.; Reboita, M.S.; Ribeiro, J.G.M.; Carvalho, V.S.B.; Santiago, M.E.V.; Silva, P.L.S.S.; Baldoni, T.C.; Souza, C.A. Assessment of the wind power density over South America simulated by CMIP6 models in the present and future climate. *Clim. Dyn.* **2023**. *Under Review*.
49. Ferreira, G.W.S.; Reboita, M.S.; Ribeiro, J.G.M.; Souza, C.A. Assessment of precipitation and hydrological droughts in South America through statistically downscaled CMIP6 projections. *Climate* **2023**, *11*, 166. [[CrossRef](#)]
50. Rupp, D.E.; Abatzoglou, J.T.; Hegewisch, K.C.; Mote, P.W. Evaluation of CMIP5 20th century climate simulations for the Pacific Northwest USA. *J. Geophys. Res. Atmos.* **2013**, *118*, 10884–10906. [[CrossRef](#)]
51. Dias, C.G.; Reboita, M.S. Assessment of CMIP6 simulations over tropical South America. *Rev. Bras. Geogr. Fis.* **2021**, *14*, 1282–1295. [[CrossRef](#)]
52. Zhang, M.Z.; Xu, Z.; Han, Y.; Guo, W. Evaluation of CMIP6 models toward dynamical downscaling over 14 CORDEX domains. *Clim. Dyn.* **2022**, 1–15. [[CrossRef](#)]
53. Admasu, L.M.; Grant, L.; Thiery, W. Exploring global climate model downscaling based on tile-level output. *J. Appl. Meteorol. Climatol.* **2023**, *62*, 171–190. [[CrossRef](#)]
54. Tram-Anh, Q.; Ngo-Duc, T.; Espagne, E.; Trinh-Tuan, L. A 10-km CMIP6 downscaled dataset of temperature and precipitation for historical and future Vietnam climate. *Sci. Data* **2023**, *10*, 257. [[CrossRef](#)]
55. Lovato, T.; Peano, D. CMCC CMCC-CM2-SR5 model output prepared for CMIP6 CMIP historical. Version 20200616. *Earth Syst. Grid Fed.* **2020**. [[CrossRef](#)]
56. Lovato, T.; Peano, D.; Butenschön, M.; Matera, S.; Iovino, D.; Scoccimarro, E.; Fogli, P.G.; Cherchi, A.; Bellucci, A.; Gualdi, S.; et al. CMIP6 simulations with the CMCC Earth System Model (CMCC1077 ESM2). *J. Adv. Model. Earth Syst.* **2022**, *14*, e2021MS002814. [[CrossRef](#)]
57. Döscher, R.; Acosta, M.; Alessandri, A.; Anthoni, P.; Arneth, A.; Arsouze, T.; Bergman, T.; Bernardello, R.; Bousetta, S.; Caron, L.P.; et al. The EC-Earth3 Earth System Model for the Climate Model Intercomparison Project 6. *Geosci. Model Dev.* **2022**, *15*, 2973–3020. [[CrossRef](#)]
58. Krasting, J.P.; John, J.G.; Blanton, C.; McHugh, C.; Nikonov, S.; Radhakrishnan, A.; Rand, K.; Zadeh, N.T.; Balaji, V.; Durachta, J.; et al. NOAA-GFDL GFDL-ESM4 model output prepared for CMIP6 CMIP historical. Version 20190726. *Earth Syst. Grid Fed.* **2018**. [[CrossRef](#)]

59. Boucher, O.; Denvil, S.; Levavasseur, G.; Cozic, A.; Caubel, A.; Foujols, M.A.; Meurdesoif, Y.; Cadule, P.; Devilliers, M.; Ghattas, J.; et al. IPSL IPSL-CM6A-LR model output prepared for CMIP6 CMIP historical. Version 20180803. *Earth Syst. Grid Fed.* **2018**. [[CrossRef](#)]
60. Tatebe, H.; Watanabe, M. MIROC MIROC6 model output prepared for CMIP6 CMIP historical. Version 20181212. *Earth Syst. Grid Fed.* **2018**. [[CrossRef](#)]
61. Wieners, K.H.; Giorgetta, M.; Jungclaus, J.; Reick, C.; Esch, M.; Bittner, M.; Legutke, S.; Schupfner, M.; Wachsmann, F.; Gayler, V.; et al. MPI-M MPI-ESM1.2-LR model output prepared for CMIP6 CMIP historical. Version 20190710. *Earth Syst. Grid Fed.* **2019**. [[CrossRef](#)]
62. Yukimoto, S.; Koshiro, T.; Kawai, H.; Oshima, N.; Yoshida, K.; Urakawa, S.; Tsujino, H.; Deushi, M.; Tanaka, T.; Hosaka, M.; et al. MRI MRI-ESM2.0 model output prepared for CMIP6 CMIP historical. Version 20190222. *Earth Syst. Grid Fed.* **2019**. [[CrossRef](#)]
63. Riahi, K.; van Vuuren, D.P.; Kriegler, E.; Edmonds, J.; O'Neill, B.C.; Fujimori, S.; Bauer, N.; Calvin, K.; Dellink, R.; Fricko, O.; et al. The Shared Socio-economic Pathways and their energy, land use, and greenhouse gas emissions implications: A review. *Glob. Environ. Change* **2017**, *42*, 153–168. [[CrossRef](#)]
64. Nguyen, P.A.; Abbott, M.; Nguyen, T.L.T. The development and cost of renewable energy 595 resources in Vietnam. *Util. Policy* **2019**, *57*, 59–66. [[CrossRef](#)]
65. Cannon, A.J.; Sobie, S.R.; Murdock, T.Q. Bias correction of GCM precipitation by Quantile Mapping: How well do methods preserve changes in quantiles and extremes? *J. Clim.* **2015**, *28*, 6938–6959. [[CrossRef](#)]
66. Ali, S.; Eum, H.-I.; Cho, J.; Dan, L.; Khan, F.; Dairaku, K.; Shrestha, M.L.; Hwang, S.; Nasim, W.; Khan, I.A.; et al. Assessment of climate extremes in future projections downscaled by multiple statistical downscaling methods over Pakistan. *Atmos. Res.* **2019**, *222*, 114–133. [[CrossRef](#)]
67. Xavier, A.C.F.; Martins, L.P.; Rudke, A.P.; Morais, M.V.B.; Martins, J.A.; Blain, G.C. Evaluation of Quantile Delta Mapping as a bias-correction method in maximum rainfall dataset from downscaled models in Sao Paulo state (Brazil). *Int. J. Climatol.* **2022**, *42*, 175–190. [[CrossRef](#)]
68. Ibebuchi, C.C.; Schönbein, D.; Adakudlu, M.; Xoplaki, E.; Paeth, H. Comparison of three techniques to adjust daily precipitation biases from regional climate models over Germany. *Water* **2022**, *14*, 600. [[CrossRef](#)]
69. Fan, L.-J.; Yan, Z.-W.; Chen, D.; Li, Z. Assessment of total and extreme precipitation over central Asia via statistical downscaling: Added value and multi-model ensemble projection. *Adv. Clim. Change Serv.* **2023**, *14*, 62–76. [[CrossRef](#)]
70. Logan, T.; Aoun, A.; Bourgault, P.; Huard, D.; Lavoie, J.; Rondeau-Genesse, G.; Smith, J.T.; Alegre, R.; Barnes, C.; Biner, S.; et al. Ouranosinc/xclim: v0.37.0 (v0.37.0). *Zenodo* **2022**. [[CrossRef](#)]
71. Silva, E.D.; Reboita, M.S. Estudo da Precipitação no Estado de Minas Gerais—MG. *Rev. Bras. Climatol.* **2013**, *13*, 120–136. [[CrossRef](#)]
72. Reboita, M.S.; da Rocha, R.P.; de Souza, M.R.; Llopart, M. Extratropical cyclones over the southwestern South Atlantic Ocean: HadGEM2-ES and RegCM4 projections. *Int. J. Climatol.* **2018**, *38*, 2866–2879. [[CrossRef](#)]
73. Gan, M.A.; Rao, V.B.; Moscati, M.C.L. South American monsoon indices. *Atmos. Sci. Lett.* **2006**, *6*, 219–233. [[CrossRef](#)]
74. Bombardi, R.J.; Kinter, J.L., III; Frauenweld, O.W. A global gridded dataset of the characteristics of the rainy and dry seasons. *Bull. Am. Meteorol. Soc.* **2019**, *100*, 1315–1328. [[CrossRef](#)]
75. Reboita, M.S.; Teodoro, T.A.; Ferreira, G.W.S.; Souza, C.A. Ciclo de vida do sistema de monção da América do Sul: Clima presente e futuro. *Rev. Bras. Geogr. Fis.* **2022**, *15*, 343–358. [[CrossRef](#)]
76. Silva, A.E.; Carvalho, L.M.V. Large-scale index for South America Monsoon (LISAM). *Atmos. Sci. Lett.* **2008**, *8*, 51–57. [[CrossRef](#)]
77. Raia, A.; Cavalcanti, I.F.A. The life cycle of the South American Monsoon System. *J. Clim.* **2008**, *21*, 6227–6246. [[CrossRef](#)]
78. Rodrigues, M.A.M.; Garcia, S.R.; Kayano, M.T.; Calheiros, A.J.P.; Andreoli, R.V. Onset and demise dates of the rainy season in the South American monsoon region: A cluster analysis result. *Int. J. Climatol.* **2022**, *42*, 1354–1368. [[CrossRef](#)]
79. Mann, H.B. Nonparametric tests against trend. *Econometrica* **1945**, *13*, 245–259. [[CrossRef](#)]
80. Kendall, M.G. Rank correlation methods. *Br. J. Psychol.* **1990**, *25*, 86–91. [[CrossRef](#)]
81. Hamed, K.H. Trend detection in hydrologic data: The Mann-Kendall trend test under the scaling hypothesis. *J. Hydrol.* **2008**, *349*, 350–363. [[CrossRef](#)]
82. Li, J.; Huo, R.; Chen, H.; Zhao, Y.; Zhao, T. Comparative assessment and future prediction using CMIP6 and CMIP5 for annual precipitation and extreme precipitation simulation. *Front. Earth Sci.* **2021**, *9*, 2021. [[CrossRef](#)]
83. Huang, F.; Xu, Z.; Guo, W. The linkage between CMIP5 climate models' abilities to simulate precipitation and vector winds. *Clim. Dyn.* **2020**, *54*, 4953–4970. [[CrossRef](#)]
84. Almazroui, M.; Ashfaq, M.; Islam, M.N.; Kamil, S.; Abid, M.A.; O'Brien, E.; Ismail, M.; Reboita, M.S.; Sörensson, A.A.; Arias, P.A.; et al. Assessment of CMIP6 performance and projected temperature and precipitation changes over South America. *Earth Syst. Environ.* **2021**, *5*, 155–183. [[CrossRef](#)]
85. Arias, P.A.; Ortega, G.; Villegas, L.D.; Martínez, J. Colombian climatology in CMIP5/CMIP6 models: Persistent biases and improvements. *Rev. Fac. Ing.* **2021**, *100*, 75–96. [[CrossRef](#)]
86. Firpo, M.A.F.; Guimarães, B.S.; Dantas, L.G.; Silva, M.G.B.; Alves, L.M.; Chadwick, R.; Llopart, M.P.; Oliveira, G.S. Assessment of CMIP6 models' performance in simulating present-day climate in Brazil. *Front. Clim.* **2022**, *4*, 2022. [[CrossRef](#)]
87. Ortega, G.; Arias, P.A.; Villegas, J.C.; Marquet, P.A.; Nobre, P. Present-day and future climate over Central and South America according to CMIP5/CMIP6 models. *Int. J. Climatol.* **2021**, *41*, 6713–6735. [[CrossRef](#)]

88. Khairoutdinov, M.; Randall, D.; DeMott, C. Simulations of the atmospheric general circulation using a cloud-resolving model as a superparameterization of physical processes. *J. Atmos. Sci.* **2005**, *62*, 2136–2154. [[CrossRef](#)]
89. Torres, R.R.; Marengo, J.A. Uncertainty assessments of climate change projections over South America. *Theor. Appl. Climatol.* **2013**, *112*, 253–272. [[CrossRef](#)]
90. Rivera, J.A.; Arnould, G. Evaluation of the ability of CMIP6 models to simulate precipitation over Southwestern South America: Climatic features and long-term trends (1901–2014). *Atmos. Res.* **2020**, *241*, 104953. [[CrossRef](#)]
91. Reboita, M.S.; Kuki, C.A.C.; Marrafon, V.H.; Souza, C.A.; Ferreira, G.W.S.; Teodoro, T.; Lima, J.W.M. South America climate change revealed through climate indices projected by GCMs and Eta-RCM ensembles. *Clim. Dyn.* **2021**, *58*, 459–485. [[CrossRef](#)]
92. Reboita, M.S.; da Rocha, R.P.; Souza, C.A.; Baldoni, T.C.; Silva, P.L.L.S.; Ferreira, G.W.S. Future projections of extreme precipitation climate indices over South America based on CORDEX-CORE multimodel ensemble. *Atmosphere* **2022**, *13*, 1463. [[CrossRef](#)]
93. Ruffato-Ferreira, V.; Barreto, R.C.; Júnior, A.O.; Silva, W.L.; Viana, D.B.; Nascimento, J.A.S.; Freitas, M.A.V. A foundation for the strategic long-term planning of the renewable energy sector in Brazil: Hydroelectricity and wind energy in the face of climate change scenarios. *Renew. Sustain. Energy Rev.* **2017**, *72*, 1124–1137. [[CrossRef](#)]
94. De Jong, P.; Barreto, T.B.; Tanajura, C.A.S.; Oliveira-Esquerre, K.P.; Kiperstok, A.; Torres, E.A. The impact of regional climate change on hydroelectric resources in South America. *Renew. Energy* **2021**, *173*, 76–91. [[CrossRef](#)]
95. Torres, R.R.; Benassi, R.B.; Martins, F.B.; Lapola, D.M. Projected impacts of 1.5 and 2 °C global warming on temperature and precipitation patterns in South America. *Int. J. Climatol.* **2021**, *42*, 1597–1611. [[CrossRef](#)]
96. Tavares, P.S.; Acosta, R.; Nobre, P.; Resende, N.C.; Chou, S.C.; Lyra, A.A. Water balance components and climate extremes over Brazil under 1.5 °C and 2.0 °C of global warming scenarios. *Reg. Environ. Change* **2023**, *23*, 40. [[CrossRef](#)] [[PubMed](#)]
97. Medeiros, F.J.; Oliveira, C.P.; Avila-Diaz, A. Evaluation of extreme precipitation climate indices and their projected changes for Brazil: From CMIP3 to CMIP6. *Weather Clim. Extrem.* **2022**, *38*, 100511. [[CrossRef](#)]
98. Schroth, G.; Läderach, P.; Martinez-Valle, A.I.; Bunn, C.; Jassogne, L. Vulnerability to climate change of cocoa in West Africa: Patterns, opportunities and limits to adaptation. *Sci. Total Environ.* **2016**, *556*, 231–241. [[CrossRef](#)]
99. Dhiman, R.C.; Pahwa, S.; Dhillon, G.P.S.; Dash, A.P. Climate change and threat of vector-borne diseases in India: Are we prepared? *Parasitol. Res.* **2010**, *106*, 763–773. [[CrossRef](#)]
100. Papalexiou, S.M.; Rajulapati, C.R.; Andreadis, K.M.; Fofoula-Georgiou, E.; Clark, M.P.; Trenberth, K.E. Probabilistic Evaluation of drought in CMIP6 simulations. *Earth's Future* **2021**, *9*, e2021EF002150. [[CrossRef](#)]
101. Wang, T.; Tu, X.; Singh, V.P.; Chen, X.; Lin, K. Global data assessment and analysis of drought characteristics based on CMIP6. *J. Hydrol.* **2021**, *596*, 126091. [[CrossRef](#)]
102. Lima, A.O.; Lyra, G.B.; Abreu, M.C.; Oliveira-Júnior, J.F.; Zeri, M.; Cunha-Zeri, G. Extreme rainfall events over Rio de Janeiro state, Brazil: Characterization using probability distribution functions and clustering analysis. *Atmos. Res.* **2021**, *247*, 105221. [[CrossRef](#)]
103. Aguiar, L.F.; Cataldi, M. Social and environmental vulnerability in southeast Brazil associated with the South Atlantic Convergence Zone. *Nat. Hazards* **2021**, *109*, 2423–2437. [[CrossRef](#)]
104. Leite-Filho, A.T.; Costa, M.H.; Fu, R. The southern Amazon rainy season: The role of deforestation and its interactions with large-scale mechanisms. *Int. J. Climatol.* **2019**, *40*, 2328–2341. [[CrossRef](#)]
105. Debortoli, N.S.; Dubreil, V.; Funatsu, B.; Delahaye, E.; de Oliveira, C.H.; Rodrigues-Filho, S.; Saito, C.H.; Fetter, R. Rainfall patterns in the Southern Amazon: A chronological perspective (1971–2010). *Clim. Change* **2015**, *132*, 251–264. [[CrossRef](#)]

Disclaimer/Publisher's Note: The statements, opinions and data contained in all publications are solely those of the individual author(s) and contributor(s) and not of MDPI and/or the editor(s). MDPI and/or the editor(s) disclaim responsibility for any injury to people or property resulting from any ideas, methods, instructions or products referred to in the content.

SUPPLEMENTARY MATERIALS

Tabel S1. Results of the computation of SAMS lifecycle parameters for R1 obtained here (shaded line) compared to previous works.

R1 – Amazonia - 0°-10°S 60°W-70°W			
Reference	Onset (pentads)	Demise (pentads)	Length (pentads)
This study	60-65	23-30	38-42
Bombardi and Carvalho [10]	60-63	22-26	34-38
Ashfaq et al. [12] - GPCP	59-65	25-31	39-45
Ashfaq et al. [12] – RegCM4 ensemble	56-64	21-30	30-47
Bombardi et al. [74]	62	30	41
Reboita et al. [75]	60-64	22-30	34-42
Rodrigues et al. [78]	56	30	47

Tabel S2. Results of the computation of SAMS lifecycle parameters for R3 obtained here (shaded line) compared to previous works.

R3 – Southeast Brazil - 20°S-25°S 40°W-50°W			
Reference	Onset (pentads)	Demise (pentads)	Length (pentads)
This study	58-60	19-20	36-38
Bombardi and Carvalho [10]	58-61	18-21	30-34
Ashfaq et al. [12] - GPCP	58-61	17-18	29-33
Ashfaq et al. [12] – RegCM4 ensemble	58-61	15-18	27-33
Silva and Reboita [71]	57-59	16-20	32-34
Bombardi et al. [74]	58	19	34
Reboita et al. [75]	58-60	16-19	30-34
Silva and Carvalho [76]	58-64	20-27	31-41
Raia and Cavalcanti [77]	50-69	10-28	18-40
Rodrigues et al. [78]	60	20	34

Table S3. Results of the computation of SAMS lifecycle parameters for R4 obtained here (shaded line) compared to previous works.

R4 – North of Southeast Brazil 12.5°S-17.5°S 40°W-50°W			
Reference	Onset (pentads)	Demise (pentads)	Length (pentads)
This study	56-57	16-19	34-36
Bombardi and Carvalho [10]	58-61	18-21	34
Ashfaq et al. [12] - GPCP	59-60	18-19	31-33
Ashfaq et al. [12] – RegCM4 ensemble	63-65	17-19	25-29
Silva and Reboita [71]	58-59	15-18	31-33
Bombardi et al. [74]	58	19	34
Reboita et al. [75]	58-60	15-21	34-36
Silva and Carvalho [76]	58-64	20-27	31-41
Raia and Cavalcanti [77]	50-69	10-28	18-40
Rodrigues et al. [78]	58-65	20-27	28-42

Table S4. Results of the computation of SAMS lifecycle parameters for R5 obtained here (shaded line) compared to previous works.

R5 – Northern Argentina - 20°-30°S 55°W-65°W			
Reference	Onset (pentads)	Demise (pentads)	Length (pentads)
This study	55-63	21-24	34-44
Bombardi and Carvalho [10]	58-61	17-21	34-38
Ashfaq et al. [12] - GPCP	57-62	19-22	30-38
Ashfaq et al. [12] – RegCM4 ensemble	58-60	12-20	25-35
Bombardi et al. [74]	60	26	39
Reboita et al. [75]	55-62	20-26	32-44

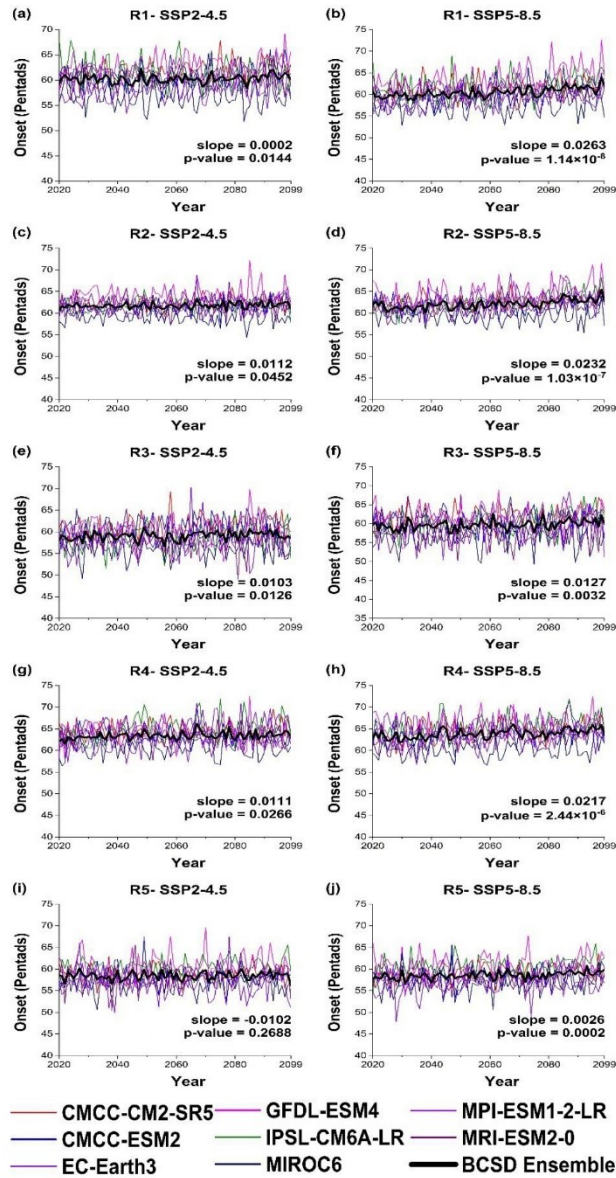


Figure S1. Time series of the monsoon onset (in pentads) provided by eight CMIP6-GCMs and the BCSD ensemble for five SA subdomains under the SSP2-4.5 and SSP5-8.5 scenarios. The p-value indicates the Mann-Kendall test result for the BCSD ensemble projections, and the Sen's slopes indicate whether the trends are positive (slope > 0) or negative (slope < 0).

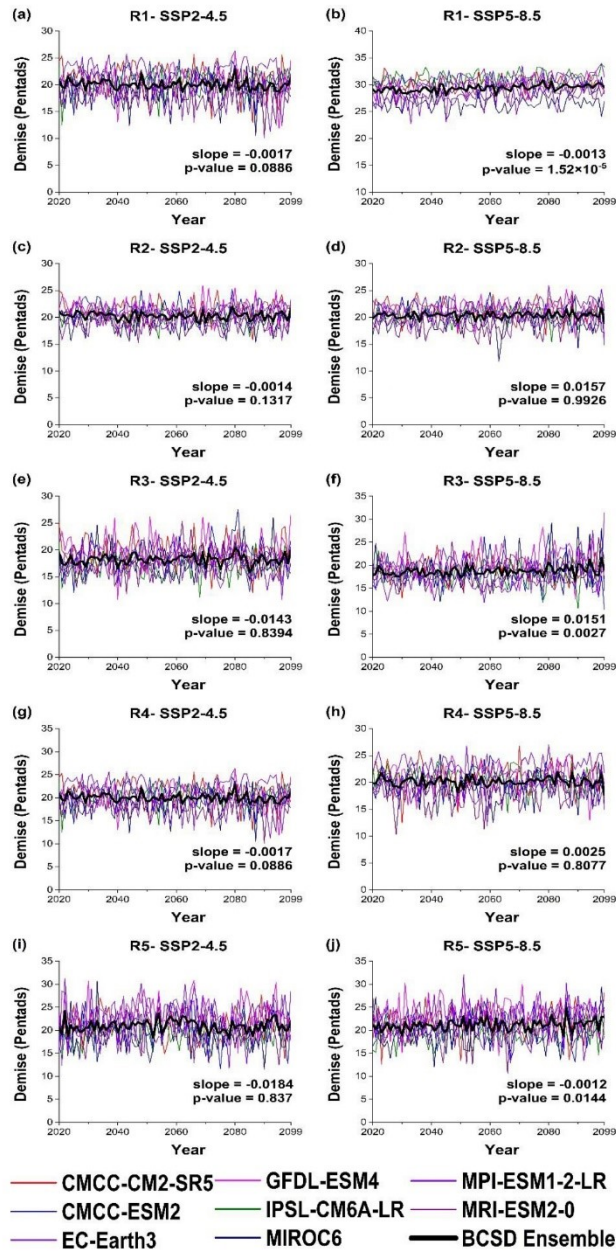


Figure S2. Similar to Figure S1, except for the monsoon demise (in pentads).

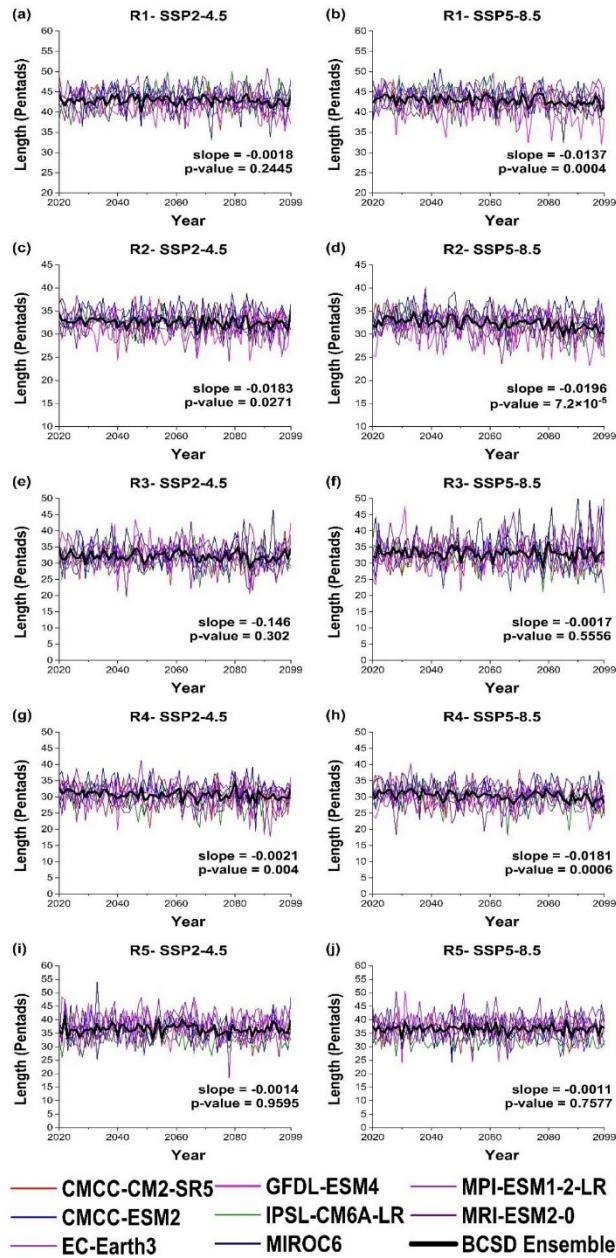


Figure S3. Similar to Figure S1, except for the monsoon's length (in pentads).



6. Assessment of the wind power density over South America simulated by CMIP6 models in the present and future climate

25/02/2025, 16:41

Rightslink® by Copyright Clearance Center



SPRINGER NATURE

Assessment of the wind power density over South America simulated by CMIP6 models in the present and future climate

Author: Glauber Willian de Souza Ferreira et al
 Publication: Climate Dynamics
 Publisher: Springer Nature
 Date: Oct 31, 2023

Copyright © 2023. The Author(s), under exclusive licence to Springer-Verlag GmbH Germany, part of Springer Nature

Order Completed

Thank you for your order.

This Agreement between Glauber Willian de Souza Ferreira / Federal University of Itajubá ("You") and Springer Nature ("Springer Nature") consists of your license details and the terms and conditions provided by Springer Nature and Copyright Clearance Center.

Your confirmation email will contain your order number for future reference.

License Number 5976060558043

[Printable Details](#)

License date Feb 25, 2025

☑ Licensed Content

Licensed Content Publisher	Springer Nature
Licensed Content Publication	Climate Dynamics
Licensed Content Title	Assessment of the wind power density over South America simulated by CMIP6 models in the present and future climate
Licensed Content Author	Glauber Willian de Souza Ferreira et al
Licensed Content Date	Oct 31, 2023

📁 Order Details

Type of Use	Thesis/Dissertation academic/university or research institute
Requestor Type	academic/university or research institute
Format	electronic
Portion	full article/chapter
Will you be translating?	no
Circulation/distribution	1 - 29
Author of this Springer Nature content	yes

📁 About Your Work

Title of new work	Hydro, wind and solar energy in Brazil: Changes projected by CMIP6 climate models
Institution name	Federal University of Itajubá
Expected presentation date	Mar 2025

📁 Additional Data

The Requesting Person / Organization to Appear on the License	Glauber Willian de Souza Ferreira / Federal University of Itajubá
---	---

https://s100.copyright.com/AppDispatchServlet

1/2



Assessment of the wind power density over South America simulated by CMIP6 models in the present and future climate

Glauber Willian de Souza Ferreira¹ · M. S. Reboita¹ · J. G. M. Ribeiro¹ · V. S. B. Carvalho¹ · M. E. V. Santiago² · P. L. L. S. Silva¹ · T. C. Baldoni¹ · C. A. de Souza¹

Received: 27 May 2023 / Accepted: 8 October 2023
© The Author(s), under exclusive licence to Springer-Verlag GmbH Germany, part of Springer Nature 2023

Abstract

Expanding the South American renewable energy matrix to ensure more sustainable socio-economic development, mitigate the climate change effects, and meet the targets set in the Paris Agreement is crucial. Hence, this study sought to estimate South America's wind speed and wind power density alterations projected by eight global climate models (GCMs) from the Coupled Model Intercomparison Project—Phase 6 (CMIP6). To this end, we applied statistical downscaling and bias correction to the GCMs outputs through the Quantile Delta Mapping method and assessed the projected changes in wind power in future climate under the Shared Socioeconomic Pathways (SSPs) SSP2-4.5 and SSP5-8.5 emission scenarios. ERA5 reanalysis data from 1995 to 2014 validated the models' historical simulations. The CMIP6 multi-model ensemble indicated an approximate 25–50% increase in wind power density in sectors such as Northeast and South Brazil and growing wind power in regions such as Argentine Patagonia, northern Venezuela, and portions of Uruguay, Bolivia, and Paraguay. Estimates of the wind power growth for the twenty-first century in those regions reiterated their potential performance in the historical period. For the SSP5-8.5 emission scenario, the ensemble projections indicated even more favorable wind power conditions in the sectors mentioned. However, individual projections of wind intensity anomalies obtained by each ensemble member showed a large spread among the GCMs, evidencing the uncertainties associated with the prospects of change in wind power on the continent. Furthermore, this study has presented a first analysis of CMIP6 projections for South American wind power generation, providing relevant information to the energy sector decision-makers.

Keywords Wind power · CMIP6 · Climate change · Statistical downscaling · South America

1 Introduction

One of the world's main challenges is meeting the growing energy demand with sustainable measures to preserve the environment and mitigate the effects of climate change. Anthropogenic activities, especially those associated with the emission of greenhouse gases (GHG), have caused the global average temperature to rise since the Industrial Revolution, leading to uncertain future climate conditions and making it urgent to increase the use of clean, renewable energy sources

for power generation (IPCC 2021). Renewable energy plays an essential role in reducing GHG emissions, and it may supply about 20–30% of global primary energy by 2040, being able to entirely replace the current energy system by 2050 (Gernaat et al. 2021). For South America (SA), the renewable energy usage expansion is crucial, as countries on the continent have proposed ambitious GHG emission reduction targets (Washburn and Pablo-Romero 2019) and diversification of clean energy sources (Icaza et al. 2022) for the coming years. Although SA has a favorable prominence in using renewable energy compared to the rest of the world (Icaza et al. 2022), recent years have shown progressive employment of thermal sources (Arango-Aramburo et al. 2020). Furthermore, there is a direct relationship between the increase in the South American gross domestic product (GDP) and the consumption of non-renewable energy and GHG emissions (Deng et al. 2020).

✉ Glauber Willian de Souza Ferreira
glauber_ferreira@unifei.edu.br

¹ Instituto de Recursos Naturais, Universidade Federal de Itajubá. Avenida BPS, 1303, Prédio M3, 37500-903 Itajubá, Minas Gerais, Brasil

² Instituto de Ciências Puras e Aplicadas, Universidade Federal de Itajubá, Itajubá, MG, Brasil

Among the current renewable energy sources available, wind energy is a feasible option due to its technological advancement and reduced cost (Wiser et al. 2021), representing a current global installed capacity of 837 GW (GWEC 2022), with an estimated installation of more than 6,000 GW by 2050 (IRENA 2019). Regarding SA, Brazil is the third main market in the world for new wind power installations, presenting an expansion of 20 GW of installed capacity in 2021, about 70% of all wind power in Latin America (GWEC 2022). In addition, countries like Argentina, Chile, Colombia, Ecuador, Peru, Venezuela, and Uruguay have relevant wind capacity. Still, several factors, such as the volatile economy, dependence on hydropower, lack of unified and ratified planning with long-term targets, as well as the absence of better management of decision-makers and federal incentives, hinder foreign investment and limit the full exploitation of the continent's wind power (Mattar et al. 2021; GWEC 2022; Icaza et al. 2022).

Wind turbines are generally installed at 100 m above the surface to generate wind energy, designed to avoid the constraining effect of surface roughness on wind speed (Reboita et al. 2021). The wind power density (WPD) measures the energy associated with wind speed at a given location, characterizing the wind power available per square meter of area swept by a turbine (Manwell et al. 2010; Reboita et al. 2021). WPD varies with the cube of wind speed, so even small reductions in wind speed can substantially decline WPD and negatively impact wind farms' energy production and incomes (Zhang and Li 2021). Despite that, wind power plants contemplate onshore and offshore parks, with onshore farms comprising the wind turbines installed over the land. Wind turbines over the sea, in areas far from the coast, and within deeper waters compose the offshore parks. Under current global policies to expand the renewable energy matrix, the annual global onshore market is estimated to grow to 6.1% by 2026, whilst the offshore market may see an increase of up to 8.3% over the same period (GWEC 2022). Offshore wind farms have an average construction period of 2–3 years and a useful operational life of 20–30 years; nonetheless, uncertainties regarding future climate conditions challenge long-term energy production (Zhang and Li 2021).

The wind power of a region can be assessed from observations (Alkhalidi et al. 2019; Arslan et al. 2020), reanalysis products (Tavares et al. 2020; Braga et al. 2021; de Oliveira Filho et al. 2022), and climate models (Reboita et al. 2018, 2021; Carvalho et al. 2021; Martinez and Iglesias 2021, 2022; Sawadogo et al. 2021; Hahmann et al. 2022; Ndiaye et al. 2022; Anandh et al. 2022). Global climate models (GCMs) provide essential information about future climate prospects and their impacts on winds. Recently, the sixth phase of the Coupled Model Intercomparison Project (CMIP6) launched by the World Climate Research

Programme's (WCRP) Working Group on Coupled Modeling (WGCM) has made available a prominent number of GCMs that represent state-of-the-art multi-model datasets, constituting a vital tool for better quality climate projections (Eyring et al. 2016). Such models have a set of historical simulations based on observations from 1850 to 2014, which help to analyze the ability to simulate climate variability and causes of forced climate change (Zhang and Li 2021). Moreover, in CMIP6, the Scenario Model Intercomparison Project (ScenarioMIP) plays a critical role in providing climate projections based on the latest scenarios of future GHG emissions and land use, the Shared Socioeconomic Pathways (SSPs) (Riahi et al. 2017). SSPs combine technological and social development with the future climate radiative forcing, characterizing society's more realistic future development by considering present and future social, economic, and political scenarios (Carvalho et al. 2021).

Studies using CMIP5 models estimate an increase in wind resources in the tropics and southern hemisphere (Karnauskas et al. 2018), especially in SA (Reboita et al. 2018) and sectors of Africa (Akinsanola et al. 2021; Sawadogo et al. 2021). On the other hand, a decrease is projected in the mid-latitudes of the northern hemisphere (Karnauskas et al. 2018), including large parts of Europe (Carvalho et al. 2021; Martinez and Iglesias 2021), North America (Kulkarni and Huang 2014; Chen 2020), and Asia (Kulkarni et al. 2018; Zhang and Li 2021; Anandh et al. 2022). Conversely, southerly latitudes in China and India are also projected to increase wind speed, especially during the winter months and the boreal monsoon (Zhang and Li 2021; Anandh et al. 2022). Karnauskas et al. (2018) concluded that a reduction in baroclinicity induces a decrease in wind resources in the boreal mid-latitudes due to the polar amplification of the climate change-induced temperature increase, causing changes in the direction and weakening of storm tracks. Contrastingly, over some equatorial and southern hemisphere regions, the more significant land surface warming than the ocean surface induces an increase in wind resources (Karnauskas et al. 2018). Findings from some studies assessing future WPD in different areas of the globe are presented in Table 1, which is not intended to be exhaustive but to highlight estimates from recent works focusing on CMIP projections. Jung and Schindler (2022a) present a more comprehensive overview of the current literature on wind power in SA (and other regions of the globe) obtained with climate models.

Most studies on the South American continent induce optimistic estimates of wind power generation in the coming decades (Pereira et al. 2013; Ruffato-Ferreira et al. 2017; Reboita et al. 2018; de Jong et al. 2019). Regarding offshore WPD, GCMs from the CMIP5 project for the end of the twenty-first century excellent power generation conditions across the entire South Atlantic Ocean (Zheng et al. 2019).

Assessment of the wind power density over South America simulated by CMIP6 models in the present...

Table 1 A brief review of global wind speed and WPD projections from CMIP5 and CMIP6 for the twenty-first century

Region	CMIP	Emission Scenarios	Results	References
Europe	CMIP6	SSP2-4.5/SSP5-8.5	Decrease about 10–20% in WPD over the British Isles, Poland, western Ukraine, and northern Norway. Increase of 15–30% over eastern Ukraine and Turkey	Carvalho et al. (2021)
			Decrease up to 35% in WPD over the northern continent and the Central Mediterranean. Increase of similar magnitude in West Finland	Martinez and Iglesias (2021)
		SSP5-8.5	Wind speed decreases in summer, extending from the British Isles to the Baltic Sea. Increase in winter in the Southern Baltic Sea	Hahmann et al. (2022)
		SSP1-2.6/SSP2-4.5/SSP5-8.5	Decrease below 20% in WPD over the south of the Northwest Passage. Increase in the region north of 72° N	Qian and Zang (2021)
Asia	CMIP5	RCP-4.5/RCP-8.5	Increase up to 29% in the annual average WPD across the Indian peninsular region from 2006 to 2032	Kulkarni et al. (2018)
	CMIP5	RCP-2.6/RCP-8.5	Increase above 20% and 40% in WPD over the Pakistan provinces of Balochistan and Sindh, respectively (under RCP-8.5)	Reboita et al. (2021)
	CMIP6	SSP2-4.5/SSP5-8.5	Decrease up to 10% in WPD over East China and increase over the South China Sea	Zhang and Li (2021)
	CMIP5/CMIP6	RCP-4.5/RCP-8.5 SSP2-4.5/SSP5-8.5	Decreasing (increasing) seasonal and annual wind speed over North India (South India)	Anandh et al. (2022)
Africa	CMIP6	SSP5-8.5	Increase up to 70% in WPD over the Guinea coast over West Africa. Decrease in the Sahel subregion	Akinsanola et al. (2021)
	CMIP5	RCP-2.6/RCP-8.5	Increase up to 20% in WPD over the continent	Sawadogo et al. (2021)
North America	CMIP5	RCP-4.5/RCP8.5	Decrease in WPD over the western USA and East Coast. Increase in WPD over the central USA. Increase up to 20% (10%) in the Southern Plains (Northern Plains and the Midwest)	Chen (2020)
	CMIP6	SSP5-8.5	Decrease of 15% in WPD in the United States and Canada. Increase up to 30% in southern Mexico	Martinez and Iglesias (2022)
South America	CMIP5	RCP-8.5	Increase in WPD over the northern continent, east-central Brazil, and above 50° S. Decrease in northern Patagonia and western Amazon	Reboita et al. (2018)
		RCP-4.5	Increase in WPD across most of Brazil, with significant growth in Northeastern Brazil and an increase above 40% at some wind farm locations	de Jong et al. (2019)
		RCP-4.5/RCP-8.5	Increase in offshore WPD across the entire South Atlantic Ocean	Zheng et al. (2019)

A possible cause for the higher projected wind speeds is the South Atlantic Subtropical Anticyclone (SASA) expansion and the longitudinal shift of its position to the west

(Gilliland and Keim 2018; Reboita et al. 2019), intensifying the pressure gradient and wind speeds along the Brazilian coast.

GCMs provide valuable information about many climate system elements, but their raw outputs are inappropriate for studies of mesoscale processes or regional-scale impacts of climate change due to coarse resolution. Downscaling techniques can address these limitations, comprising two approaches: dynamical and statistical downscaling. Dynamical downscaling involves regional climate models (RCMs) that use initial and boundary conditions provided by GCMs, whilst statistical downscaling establishes relationships between large-scale global circulation factors and local climate (Fowler et al. 2007). Although dynamical downscaling is useful for representing local-scale climate phenomena, such an approach requires high computational cost (Ambrizzi et al. 2019), besides being prone to the propagation of systematic biases originating from GCMs or relating to parameterization schemes (Kotlarski et al. 2014; Casanueva et al. 2016). On the other hand, statistical downscaling requires a long series of local data but demands less computational effort, avoids the propagation of systematic errors from the GCMs, and implicitly considers local factors such as topography and microclimate (Mutz et al. 2021).

Although both methods have advantages and weaknesses, a preference for studies in SA using dynamical downscaling has been observed in recent decades, mainly in the analysis of variables like precipitation and air temperature (da Rocha et al. 2009; Marengo et al. 2012; Chou et al. 2014; Reboita et al. 2014, 2016; Solman and Blázquez 2019; Solman et al. 2021; Silva et al. 2023). However, there is a growing literature in recent years about statistical downscaling in SA (Bettolli and Penalba 2018; Mutz et al. 2021; Sulca et al. 2021; Solman et al. 2021; Olmo and Bettolli 2022), evidencing its ability to represent spatial distributions and extreme events. Nevertheless, there is still a scarcity of studies that apply statistical downscaling to winds in SA (Gonçalves et al. 2010), preferably analyzed under the dynamical approach (Reboita et al. 2018; Silva et al. 2022). Recently, Ballarin et al. (2023) applied the Quantile Delta Mapping (QDM) bias correction process developed by Cannon et al. (2015) to statistically downscale CMIP6 surface wind simulations and obtained a significant improvement of the estimates, reducing the models' systematic bias in both the long-term mean and extreme values, and indicating its potential use for studies of climate change impacts.

Hence, this study aims to: (a) apply the QDM bias correction and statistical downscaling to historical simulations and climate projections of surface wind from a CMIP6 multi-model ensemble and; (b) employ the bias-corrected estimates for the evaluation of wind power generation potential in SA under different GHG emission scenarios. Overall, the South American literature on wind studies is still relatively sparse, and there is a lack of work assessing the possible impacts of climate change projected by CMIP6 models on wind power generation over the continent. Therefore, we

intend to fill this gap, analyzing the effects of the projected changes on SA wind power and mapping the regions with the best aptitude for the maintenance or installation of wind farms in the coming decades. Consequently, this study may be helpful for policymakers, energy planners, and stakeholders involved in developing and expanding wind energy infrastructure in SA.

2 Material and methods

2.1 Study area

The study area encompasses the SA continent (Fig. 1), located at 12° N–55° S latitudes and characterized by a vast meridional extent and complex topography. Besides its considerable latitudinal range (yielding a climate heterogeneity of tropical, subtropical, and extratropical regions), SA presents diverse geography, including particular areas such as the Andes Mountains, the Atacama Desert, the Amazon rainforest, and the semiarid Northeast of Brazil. These features propitiate the continent's occurrence of different atmospheric systems and climate contrasts (Reboita et al. 2010; Ferreira and Reboita 2022). Central SA (especially Brazil) is broadly influenced by the South American Monsoon System (SAMS), with two well-defined seasons marked by the rainy period from November to March and the dry season from May to September, as well as the presence of different circulation systems at high and low levels

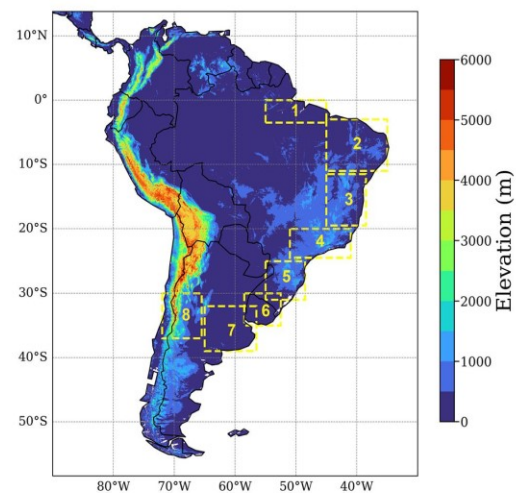


Fig. 1 Illustration of the study area with elevation (m). Rectangles indicate subdomains selected for individual analysis of GCMs from CMIP6. Source: United States Geological Survey–Earth Resources Observation System (EROS) Center

of the atmosphere during these periods (Zhou and Lau 1998; Pascale et al. 2019; Wang et al. 2020; Reboita et al. 2022). In contrast, in subtropical Chile, precipitation occurs predominantly during the austral winter, associated with the frequent passage of cold fronts and cut-off lows (Garreaud 2009). Furthermore, SA is surrounded by two oceans, with its eastern coast extending into the South Atlantic Ocean and experiencing trade winds and monsoon action. The western portion is strongly influenced by the South Pacific Subtropical Anticyclone (SPSA) and westerly disturbances (Reboita et al. 2010; Ferreira and Reboita 2022).

2.2 CMIP6-GCMs selection

This study used simulations of the zonal and meridional wind components at 10 m height from eight CMIP6-GCMs, comprising the historical period (1995–2014) and two GHG emission scenarios (SSP2-4.5 and SSP5-8.5) in the future period (2020–2099). While the SSP2-4.5 corresponds to a moderate emission scenario, the SSP5-8.5 represents a pathway with high GHG emissions, reflecting a future with limited climate change mitigation efforts. The GCMs data comprised simulations obtained every three hours provided on the Earth System Grid Federation (ESGF) platform (available at <https://esgfnode.llnl.gov/search/cmip6/>). Currently, over 100 models are available by CMIP6, each with biases and uncertainties (Eyring et al. 2016). While a good simulation of the historical period cannot guarantee accurate future projections for the same model, the low ability to simulate historical climate likely reflects poor future simulations. Thus, a fair simulation of past climate guarantees greater confidence in future climate projections (Zhang et al. 2022).

At the early stage of this study (January 2022), we selected the best models for representing the SA climate in terms of precipitation and air temperature, which are a response to atmospheric circulation. The GCMs selection followed the methodology of Rupp et al. (2013), whereby several metrics evaluate the best models considering both the properties of regionally averaged time series and large-scale patterns. Thus, the identification of the best-performing GCMs included the calculation of the following metrics of 50 models with monthly data for different subdomains of the continent (figure not shown): (a) mean and standard deviation: areal seasonal mean and standard deviation for each year (from 1995 to 2014); (b) spatial correlation: a way to assess the similarity of the spatial patterns of a variable in the observation and model datasets (Cohen 1998), which was calculated for each season (DJF, MAM, JJA, SON) and year (from 1995 to 2014) with the Pearson's coefficient equation; (c) mean amplitude: defined as the difference between July and January wind

speed; (d) linear trend: for the time series of the complete period (not by seasons), the linear trend was calculated using the least squares method and the angular coefficients that are an indication of a positive or negative trend.

Ranking GCMs according to performance is not straightforward since several statistical metrics and seasons are analyzed. One way to compile all the information is by standardizing all metrics (by signing equal weight/importance to each metric) to rank the models in terms of their performance, following the methodology proposed by Rupp et al. (2013). For each model i and metric j , the bias $E_{i,j}$ is calculated:

$$E_{i,j} = |x_{\text{obs},j} - x_{i,j}| \quad (1)$$

where $E_{i,j}$ is the absolute error (absolute bias value), and $x_{\text{obs},j}$ and $x_{i,j}$ are the observed and simulated metrics, respectively. The next step was to calculate the relative error $E_{i,j}^*$ (which can be interpreted as a standardized time series) by Eq. 2:

$$E_{i,j}^* = \frac{E_{i,j} - \min(E_{i,j})}{\max(E_{i,j}) - \min(E_{i,j})} \quad (2)$$

where $\max(E_{i,j})$ and $\min(E_{i,j})$ are the functions used to select a time series's maximum and minimum values, respectively. If the metric is a correlation, each function $\max(E_{i,j})$ or $\min(E_{i,j})$ is reversed. In this metric, since the absolute error $E_{i,j}$ is divided by the amplitude of the error, $E_{i,j}^* = 0$ indicates that the model has perfect performance and $E_{i,j}^* = 1$ denotes poor performance. According to Rupp et al. (2013), the relative error is then summed over all statistical metrics m of a model, which provides the total relative error $E_{i,\text{tot}}^*$:

$$E_{i,\text{tot}}^* = \sum_{j=1}^m E_{i,j}^* \quad (3)$$

The final step was to rank the models according to their respective relative error on a scale from 0 to 1, where each $E_{i,j}^*$ is divided by the maximum value of $E_{i,j}^*$. With the definition of the subdomain in SA, the statistics were computed, and the ranking method was applied. Figure 2 illustrates that the best models are on the left side (values closer to zero). We stress that the best models shown in Fig. 2 could not always be selected due to a lack of available hourly/daily data and/or projections in the ESGF databases. Thus, by jointly analyzing the availability of high-frequency data and projections, the models indicated with a red arrow were selected for this study (Fig. 2, Table 2). Furthermore, three selected GCMs (EC-Earth3, IPSL-CM6A-LR, and MPI-ESM1-2-LR) also performed best in reproducing the SA climate (Dias and Reboita 2021).

its choice are that there are functions that preserve the time series trends (see Cannon et al. 2015), and its application is not complicated. This methodology is also called Bias Correction-Statistical Downscaling (BCSD).

This study applied the statistical downscaling method by bias correction to downscale the CMIP6-GCMs. For bias correction, we employed the QDM technique (Cannon et al. 2015) to historical simulations (1995–2014), and the transfer functions were applied in future projections (2015–2099). Cannon et al. (2015) report that the QDM technique preserves the model-projected relative changes and trends (i.e., if a model has a dry trend in a specific region, it will be kept after BCSD) and corrects the systematic biases in the quantiles of the modeled data with respect to the observations.

Before bias correction, spatial disaggregation was applied to the CMIP6-GCMs. All CMIP6 models and ERA5 data were interpolated to $0.5^\circ \times 0.5^\circ$ resolution using bilinear interpolation. Bilinear interpolation was chosen since several studies show that this method adjusts the smooth and spatially correlated behavior of the variable, generating consistent fields (Mukherjee et al. 2018; Lee et al. 2019; Mishra et al. 2020; Xu et al. 2021; Tang et al. 2022; Wu et al. 2022; Admasu et al. 2023; Ballarin et al. 2023; Tram-Anh et al. 2023).

After spatial disaggregation, we applied bias correction through the QDM method. The QDM process follows three steps (Cannon et al. 2015). First, the trend is removed from all projected individual quantiles. Next, the detrended quantiles are bias-corrected with the quantile mapping technique. Finally, the projected changes are superimposed on the bias-corrected outputs. Let o and p be the observed and projected data, and h and f are the historical and future periods, respectively. The definition of the non-exceedance probability of the observed ($x_{h,o}$) and projected ($x_{h,p}$) historical and future ($x_{f,p}$) data is accounted for as:

$$P_{f,p}(t) = F(x_{f,p}(t))P_{h,p}(t) = F(x_{h,p}(t))P_{h,o}(t) = F(x_{h,o}(t)) \quad (4)$$

where p and F denote the non-exceedance probability associated with a specific value in time and the cumulative distribution function (CDF), respectively. The change factor, which associates the historical simulation outputs with those of the future period, was calculated with Eq. 5:

$$\Delta^A(t) = F_{f,p}^{-1}(P_{f,p}(t)) - F_{h,p}^{-1}(P_{f,p}(t)) = x_{f,p}(t) - F_{h,p}^{-1}(P_{f,p}(t)) \quad (5)$$

where F^{-1} denotes the inverse CDF and $\Delta^A(t)$ is the additive factor of change between the simulated quantiles of the historical and future periods. Finally, the bias correction in the future projections was obtained by applying the additive relative change $\Delta^A(t)$ to the historical values with the corrected bias, according to Eq. 6:

$$\hat{x}_{f,p}(t) = \Delta^A(t) + F_{h,o}^{-1}(P_{f,p}(t)) \quad (6)$$

The historical period (1995–2014) was used for the training set to adjust the future projections (2015–2099) with the QDM algorithm. This time window was chosen due to computational resources and to follow the same reference period used by the International Panel on Climate Change (IPCC 2021). The Python-based package xclim (Logan et al. 2022) was used to perform the calculations. According to Cannon et al. (2015), the QDM technique, compared to the quantile mapping technique, proved to have advantages because it is less susceptible to problems such as inflating relative trends in extreme values.

2.5 Wind power density (WPD)

After bias-correcting the simulations, vertical extrapolation of the wind intensity to 100 m was performed since most wind turbines are installed at this height to reduce friction effects in wind intensity (Custódio 2009). Since the methods used by ERA5 and the various CMIP6 models to interpolate the wind at 100 m are different and not always reported, we chose to obtain the wind component data every three hours and calculate the wind intensity per hour, and then the daily average, to maintain consistency between the procedures employed. Equation 7 (Nybø et al. 2020; Reboita et al. 2021) was used to calculate the wind extrapolation:

$$W_H = W_{10} \left(\frac{Z_H}{Z_{10m}} \right)^{\frac{1}{7}} \quad (7)$$

where W_H is the wind speed ($m\ s^{-1}$) at the desired height (Z_H , 100 m), and W_{10} is the wind speed ($m\ s^{-1}$) at the reference height of 10 m.

For investors in wind energy, the variable of interest is the WPD ($W\ m^{-2}$) computed according to Eq. 8:

$$WPD = \frac{1}{2} \rho v^3 \quad (8)$$

where ρ is the air density ($kg\ m^{-3}$), and v is the wind speed ($m\ s^{-1}$). Some studies (Silva et al. 2016; Reboita et al. 2018, 2021; Emeksiz and Cetin 2019; de Oliveira Filho et al. 2022) assume a constant value for air density, but here we estimate this variable with Eq. 9 (Custódio 2009):

$$\rho \cong \frac{353.4 \left(1 - \frac{z}{45271} \right)^{5.2624}}{T} \quad (9)$$

where ρ is the air density ($kg\ m^{-3}$), z is the height (meters) in analysis, and T is the air temperature (K).

Weather stations, reanalysis, and climate models do not provide air temperature at the height of 100 m. Hence, this variable was estimated by considering the atmosphere's

saturated adiabatic vertical rate, by which air temperature decreases by approximately 0.6 °C every 100 m (Wallace and Hobbs 2006):

$$T = T_{2m} - \Gamma_{sat} \quad (10)$$

where T is the air temperature (K) required for the air density calculation, T_{2m} is the air temperature (K) at 2 m obtained by ERA5, and Γ_{sat} is the atmosphere's saturated adiabatic vertical rate (0.6/100 m). Thus, for the height of 100 m, we employ the value of $\Gamma_{sat} = 0.6$.

Seasonal averages of wind intensity and WPD were calculated for the 100 m height, considering the historical (1995–2014) and future periods (2020–2039, 2040–2059, 2060–2079, 2080–2099) under the SSP2-4.5 and SSP5-8.5 emission scenarios. All calculations were performed individually for each model and the ensemble of CMIP6-GCMs. However, for brevity, only the seasonal ensemble results are presented here.

2.6 100 m WPD anomalies and trends time series

In a multi-model ensemble context, we present the change projections in WPD at 100 m estimated by each CMIP6-GCM. Thus, we calculated the 100 m WPD anomalies and trends relative to the 1995–2014 period for eight key regions (Fig. 1) that concentrate wind farms and wind hotspots in SA (Viviescas et al. 2019): northern Brazil (R1; 45° W–55° W, 0–3.5° S), northeastern Brazil (R2; 35° W–45° W, 3° S–11° S), coastal Bahia state (R3; 38.5° W–45° W, 11.5° S–19.5° S), Southeast Brazil (R4; 41° W–51° W, 20° S–24.5° S), South Brazil (R5; 48.5° W–55° W, 25° S–31° S), Uruguay and south of Rio Grande do Sul state, in Brazil (R6; 52.5° W–58.5° W, 30° S–35° S), central-eastern Argentina (R7; 56.5° W–65° W, 32° S–39° S), and south-central Chile and central-western Argentina (R8; 65.5° W–72° W, 30° S–37° S). This analysis allows an assessment of the spread of temporal evolution among the different CMIP6 models used.

2.7 Significance test for the difference in climatological mean values and Mann–Kendal trend test

Student's t-test was employed to assess whether the differences in the climatological mean values of wind speed and WPD at 100 m for the future period (2020–2099) from the CMIP6 ensemble were statistically significant relative to the historical period (1995–2014). This test assumes the null hypothesis (H_0) of no difference between the two datasets against the alternative hypothesis of a difference between the two ensembles. The test was computed according to Eq. 11:

$$t = \frac{\bar{X}_f - \bar{X}_h}{\sqrt{\frac{s_f^2}{n} + \frac{s_h^2}{n}}} \quad (11)$$

where s_f and s_h are the standard deviation values of the future and historical datasets, respectively, and n comprises the number of values in each set. The associated degree of freedom v was estimated as:

$$v = \frac{\left(\frac{s_f^2}{n} + \frac{s_h^2}{n}\right)^2}{\frac{s_f^4}{n^2(n-1)} + \frac{s_h^4}{n^2(n-1)}} \quad (12)$$

The test was performed using a significance level α of 5%. Thus, when the probability value (p-value) found was less than 5%, the null hypothesis of no difference between the two sets was rejected in favor of the alternative hypothesis, indicating statistical evidence of the difference between the mean values of the two periods evaluated.

Additionally, we analyzed the 100 m WPD trend time series obtained by the eight CMIP6-GCMs and the multi-model ensemble for eight subdomains of SA (Fig. 1) to present the climate change signal on WPD in different sectors of the continent. This procedure was done using the Mann–Kendall trend test (Mann 1945), which is widely used to analyze trends in hydrological series (Hamed 2008; Li et al. 2021). In this method, when the normalized standard Z-statistic exceeds the critical thresholds (–2.32, 2.32), the hydrological series has a significant rate of change with a 99% confidence level. The standard normalized Z-statistic is calculated according to Eq. 13:

$$Z = \begin{cases} \frac{(S-1)}{\sqrt{\text{Var}(S)}}, & S > 0 \\ 0, & S = 0 \\ \frac{(S+1)}{\sqrt{\text{Var}(S)}}, & S < 0 \end{cases} \quad (13)$$

where S is the statistic

$$S = \sum_{i=1}^{n-1} \sum_{j=i+1}^n \text{sgn}[x(j) - x(i)] \quad (14)$$

where n represents the length of the series, i, j represent the variable numbers, and sgn is calculated as:

$$\text{sgn}[x(j) - x(i)] = \begin{cases} 1, & x(i) > x(j) \\ 0, & x(i) = x(j) \\ -1, & x(i) < x(j) \end{cases} \quad (15)$$

In addition, Sen's slope estimation test was employed to detect the linear trend of WPD in the selected subdomains. The trend is given by Eq. 16:

Assessment of the wind power density over South America simulated by CMIP6 models in the present...

$$\beta = M\left(\frac{x_i - x_j}{i - j}\right), \forall j < i \quad (16)$$

where β is the magnitude of the trend of the data series, and M represents the median of the data series.

2.8 Classification of wind power density

Furthermore, we rated the wind energy potential in SA considering the thresholds presented in Table 3, which are adapted from the methodology proposed by Elliott et al. (1991) for calculating WPD using wind speed at 100 m. Hence, it is possible to map the regions suitable for wind power generation, corresponding to the “moderate” category or above (Reboita et al. 2021).

3 Results and discussion

3.1 Wind speed at 10 m

Figure 3 shows the seasonal climatology of the wind speed (m s^{-1}) at 10 m for the historical period (1995–2014) over SA and adjacent oceans, obtained by ERA5 (left column) and the CMIP6 ensemble with (middle column) and without (right column) the application of bias correction.

To complement the analyses, Figure S2 of the Supplementary Material shows the comparison of wind speed at 10 m obtained by ERA5 and BCSD ensemble with surface wind measurements taken at two weather stations (located at Sombrio and Petrolina), made available by the National Environmental Data Organization System (SONDA) network, belonging to the National Institute for Space Research (INPE). In addition, Figure S3 compares the extrapolated wind estimates at 25 and 50 m obtained by Eq. 7 with measurements from anemometer towers installed at these heights at two stations in the SONDA network (located at Petrolina and São João do Cariri). Biases persist even after correction. Still, both datasets (ERA5 and BCSD ensemble) satisfactorily simulate the seasonal cycles of wind speed and the

general behavior of the observational time series at the two stations analyzed. We would point out that, although observational data is available for different locations in SA, many of these datasets are composed of relatively short series, in addition to the absence of measurements or the poor quality of the observed series. Given this, reanalysis could be an alternative for studies evaluating large regions or where data is difficult to obtain.

The ensemble without bias correction indicates that GCMs underestimate the wind intensity in regions like northeastern Brazil and Argentine Patagonia during the entire year, with more expressive underestimations during the austral winter (Fig. 3 a3) and spring (Fig. 3 d3). The underestimation of wind intensity over northeastern Brazil was also identified in CMIP5 models (GFDL-ESM2M, HadGEM2-ES, and MPI-ESM-MR) nested to RegCM4, which showed a negative deviation of up to 2 m s^{-1} in the region for all seasons (Reboita et al. 2018).

Underestimates from the CMIP6 models also occur in the central portion of SA south of 10°S during austral autumn and winter (Fig. 3 b5, c5) and over Uruguay during spring (Fig. 3 d5). On the other hand, the CMIP6 ensemble adequately simulates the wind speed seasonal variability in the Amazonia region and the higher magnitudes in sectors such as northern Venezuela, Suriname, Guyanas, and extreme northern Brazil. Moreover, even without bias correction, the CMIP6 ensemble reproduces the two high wind speed offshore cores in the South Atlantic (in Rio de Janeiro state and along the coast of Santa Catarina and Rio Grande do Sul states, Brazil) during spring previously found by Tavares et al. (2020).

Regarding the low-level jets (LLJ) east of the Andes Mountains’ influence on the surface winds (10 m), the CMIP6 ensemble simulates the highest wind intensity (up to 4 m s^{-1}) over southeastern and southern Brazil in austral summer (Fig. 3 a3). However, it overestimates (underestimates) the variable over the region east of the Atacama Desert (eastern Colombia) throughout the year. CMIP5 models also overestimate wind speed over the mountainous terrain of the Andes, showing a strong positive bias in the region (of the order of 5 m s^{-1}), which is due to their horizontal resolution that constrains the ability to resolve the complex topography (Kumar et al. 2015). In addition, several CMIP5-GCMs (whose families encompass the models analyzed here) underestimate the warm and moist northerly flow originating from the tropical continent toward southeastern SA, causing the underestimation of the South Atlantic Convergence Zone (SACZ)-associated rainfall in the region (Barros and Doyle 2018). This deficiency is also evident in the CMIP6 ensemble underestimating winds over Bolivia and Paraguay throughout the year.

CMIP6 ensemble captures the intensity magnitude associated with wind convergence in the equatorial sector of

Table 3 Classes of WPD at 10 and 100 m adapted from Elliott et al. (1991) and Reboita et al. (2021)

Classes	10 m		100 m	
	v	WPD	v	WPD
Poor	0–4.4	0–52.2	0–6.2	0–146.9
Marginal	4.4–5.1	52.2–81.3	6.2–7.2	146.9–228.7
Moderate	5.1–5.6	81.3–107.6	7.2–7.9	228.7–302.8
Good	5.6–6.0	107.6–132.3	7.9–8.5	302.8–372.5
Excellent-1	6.0–6.4	132.3–160.6	8.5–9.0	372.5–452.0
Excellent-2	6.4–7.0	160.6–210.1	9.0–9.9	> 452.0

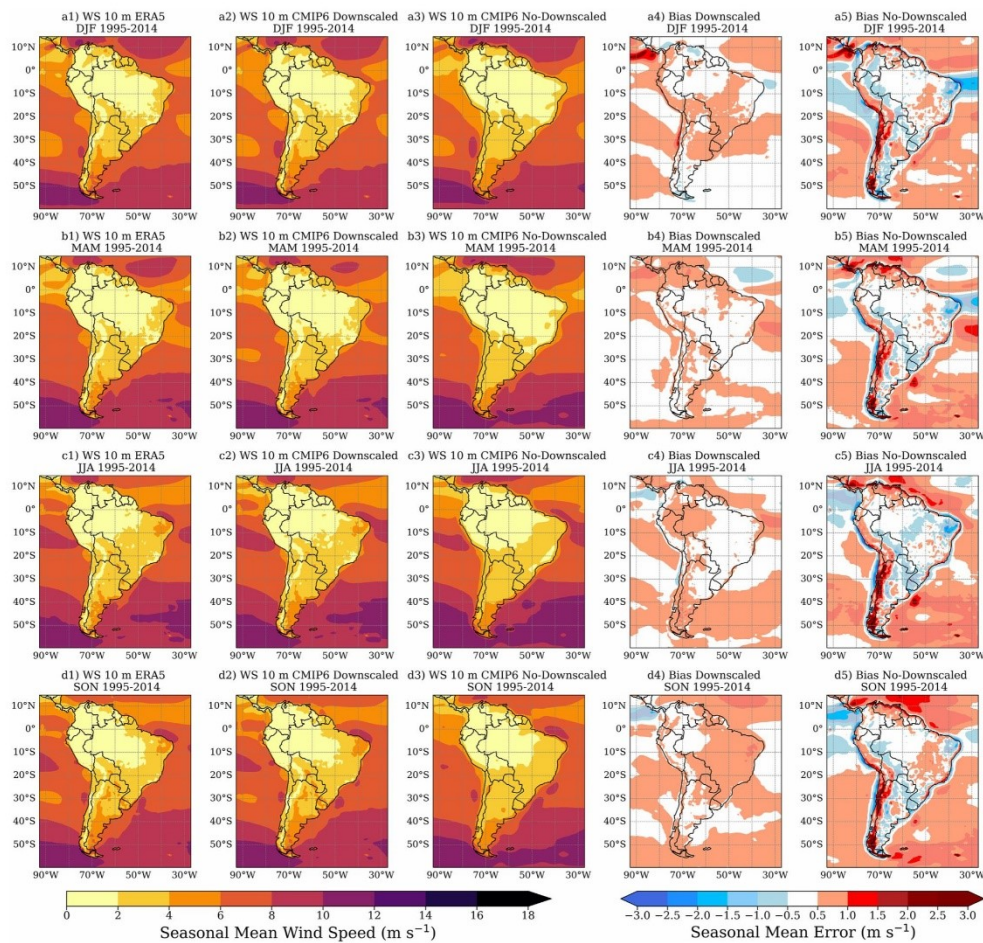


Fig. 3 Seasonal mean wind speed (m s^{-1}) at 10 m for the historical period (1995–2014) obtained by ERA5 (left column) and the CMIP6 ensemble with (middle column) and without (right column) the application of BCSD

the southern Atlantic Ocean. However, it underestimates the intensity off the coast of northeastern Brazil during austral summer (Fig. 3 a5). CMIP5-GCMs also indicated a large spread among the models in simulating the climatological mean wind vector, especially along the Intertropical Convergence Zone (ITCZ) and the equatorial Atlantic (Huang et al. 2020). Some factors that cause the spread are partially related to the different sea surface temperature (SST) generated by the models since differences in the SST warming patterns in the coupled models contribute

substantially to the spread of tropical rainfall and atmospheric circulation among the GCMs.

Furthermore, the ensemble overestimates the wind intensity at the center of the SASA during austral autumn (Fig. 3 b4, b5) and winter (Fig. 3 c4, c5). Still, such a deviation does not yield higher velocity values over northeastern Brazil. Regarding the western portion of SA, the ensemble simulates the SPSA action and its influence on the continent's west coast. In addition, it captures the higher intensity core on the south-central Chile coast, corroborating results from

the CMIP3 models (Garreaud and Falvey 2009). Since small changes in wind intensity cause considerable changes in wind power density, statistical downscaling with the QDM bias correction technique is applied to the wind speed at 10 m simulated by each CMIP6-GCM before the wind extrapolation calculation at 100 m. Figure 3 (second left column) shows that the methodology can reduce model biases in the historical period, which results in fields symmetric to those of ERA5 and allows for more reliable estimates about applying the wind speed from CMIP6 projections for the twenty-first century.

3.2 Wind speed and wind power density at 100 m

Figure 4 presents the seasonal mean wind power density (WPD) for the historical period (1995–2014) obtained with the ERA5 reanalysis and the CMIP6 ensemble mean after statistical downscaling. ERA5 indicates a seasonal variability with higher WPD values throughout the year in regions such as south-central Argentina, northern Venezuela, and Uruguay. At the same time, northeastern and southern Brazil show higher magnitudes during the austral spring and summer, recording values of up to 300 W m^{-2} .

Offshore WPD analyses on the coasts of Southeastern and Southern Brazil with different reanalysis products (ERA5, CFSv2, and MERRA2) indicated mean values of $400\text{--}475 \text{ W m}^{-2}$ for the Southeast and $425\text{--}550 \text{ W m}^{-2}$ for the South (Tavares et al. 2020), which are appropriately simulated by the CMIP6 ensemble, mainly in austral spring and summer. The ensemble also shows suitable conditions for wind power generation in much of Northeast Brazil during austral winter and spring, as well as high offshore potential on the northern coast of the Northeast, which corroborates previous analyses performed with regional climate model (Oliveira and Costa 2011).

WPD seasonal variability is associated with the wind's seasonality influenced by different phenomena, such as the confluence of the trade winds in the equatorial sector and the SASA spatial variability, and the CMIP6 ensemble can simulate the WPD seasonal variability during the historical period. However, it presents evident overestimations in northeastern, central-western, and southeastern Brazil throughout the year, even after applying the bias correction, with larger deviations in austral spring and summer. Considering the continental sector, generally, the mean deviations are between -0.5 and 1 W m^{-2} , with systematic overestimations over the west coast of SA and central-eastern Argentina throughout the year. Regarding the oceanic sectors, the CMIP6 ensemble overestimates WPD in the South Atlantic and South Pacific practically all year long (with more intense overestimates south of 40° S during winter), except over Equatorial Atlantic during austral fall and winter.

In the Brazilian southeast coast region, ERA5 and CMIP6 ensemble indicate WPD values above 400 W m^{-2} throughout the year, with an underestimation of up to 80 W m^{-2} by the ensemble during austral autumn and winter (Fig. 4 b3, c3). This region is a relevant area of interest for the installation of offshore wind farms, and analyses from 1979 to 2020 indicate that there has been a reduction (increase) in the frequency of low (high) intensity winds ($\geq 7.5 \text{ m s}^{-1}$) (Coriolano et al. 2022), which is mainly related to the intensification and expansion of the SASA in recent decades (Reboita et al. 2019). Except for the coastal regions of São Paulo and the southern coast of Rio de Janeiro, in Brazil, a consistent WPD increase of up to $1.89 \text{ W m}^{-2} \text{ year}^{-1}$ was observed over the last 40 years, which corresponded to the rise of up to 11.2% in the median WPD (Coriolano et al. 2022). In addition, it is estimated that there is a large area with offshore wind power in Southern Brazil in water depths of 50 m, as well as an area with an estimated technical potential of 344 GW near the state of Rio de Janeiro, located in water depths of 100 to 1500 m (Tavares et al. 2020).

Figure 5 presents the differences related to the historical period of extrapolated wind intensity at 100 m projected by the CMIP6 ensemble for the twenty-first century, considering the SSP2-4.5 scenario. For the period 2020–2039, slight differences are noted, with an increase of approximately 0.5 m s^{-1} in most of SA. Projections from the Eta regional model nested with the HadGEM2 GCM under the RCP-4.5 scenario showed similar estimates, indicating an average increase of 1 m s^{-1} in wind intensity over most of SA and higher speeds located in the North, Northeast, and South of Brazil, with more expressive increases in the austral spring (Ruffato-Ferreira et al. 2017). Similarities between the two studies include an increase in wind intensity on the coast of Southern Brazil, a fact most notable during the spring of the century's end, indicating an average increase of up to 1 m s^{-1} in the region. In addition, the decreasing wind intensity in northern Argentina is obtained in both analyses. Additionally, the results presented here corroborate other projections from CMIP5, which indicated a decreasing wind speed in Argentine Patagonia over the current century (Reboita et al. 2018).

Figure 6 illustrates the projected change in the percentage of WPD at 100 m over the coming decades relative to the historical period. Over most SA throughout the year, there is an increase of up to 15%. In contrast, northern and central Chile suggest a decreasing WPD over the entire year. Towards the end of the twenty-first century, regions like Venezuela, north of Brazil, coastal and central portions of northeastern Brazil, and parts of Paraguay concentrate the largest WPD increases.

Under the SSP5-8.5 scenario, the CMIP6 ensemble projects a mean increase of 0.5 m s^{-1} over much of SA (Fig. 7), similar to the SSP2-4.5 scenario projections. The

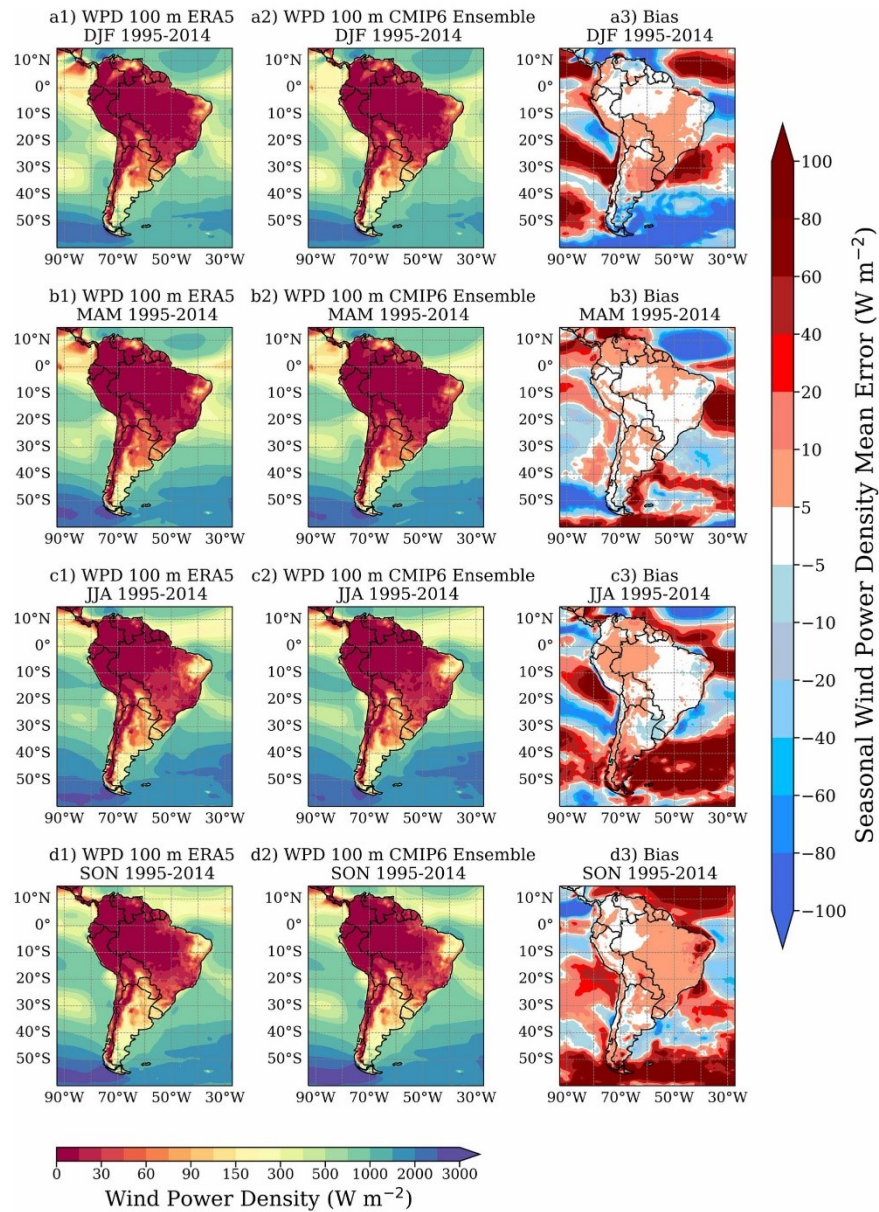


Fig. 4 Seasonal mean wind power density (W m^{-2}) at 100 m for the historical period (1995–2014) obtained by the ERA5 reanalysis (left column), the CMIP6 ensemble after BCS (middle column), and the seasonal differences between the CMIP6 ensemble (after BCS) and ERA5 (right column)

Assessment of the wind power density over South America simulated by CMIP6 models in the present...

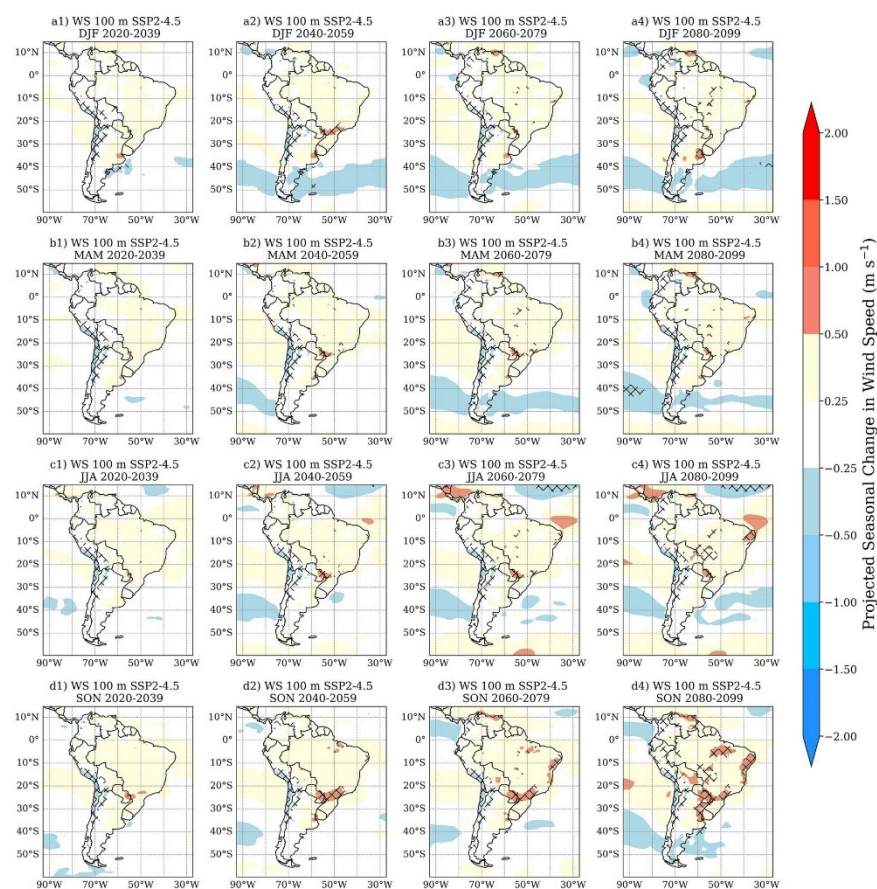


Fig. 5 Seasonal differences in wind speed (m s^{-1}) at 100 m between the future (2020–2039, 2040–2059, 2060–2079, and 2080–2099) and historical period (1995–2014), projected by the CMIP6 ensemble

under the SSP2-4.5 scenario. Hatched areas indicate 95% statistical significance, based on Student's t-test

Brazilian northeastern, southeastern, and southern coasts show an increase of up to 1 m s^{-1} , with more significant gains during the austral spring. Furthermore, in the center-south of the subtropical anticyclones, wind intensity is reduced in a band that extends from the Pacific to the Atlantic, crossing Patagonia and extreme southern Argentina throughout the year and with a more significant decrease during austral summer. Reboita et al. 2018 obtained a similar profile, attributing it to the displacement of storm tracks from 40 to 50° S to higher latitudes, related to the horizontal temperature gradient at the poles estimated in climate change scenarios. On the other hand, northern SA shows an increase of up to 1.5 m s^{-1} ,

especially in the austral spring, corroborating previous findings (Reboita et al. 2018).

In general, the projections of wind intensity change obtained here resemble those obtained by dynamical downscaling with GCMs from CMIP5 under the RCP-8.5 scenario (Ruffato-Ferreira et al. 2017). Similarities include an average increase of approximately 1 m s^{-1} in sectors such as southern, central, southeastern, and northern Brazil. However, the larger gains of up to 2 m s^{-1} found by Ruffato-Ferreira et al. (2017) for sectors such as the interior and north of Northeast Brazil are not reproduced here. Instead, these regions indicate more modest change values in the -0.5 to 1 m s^{-1} range. Dynamical downscaling of the regional model Eta

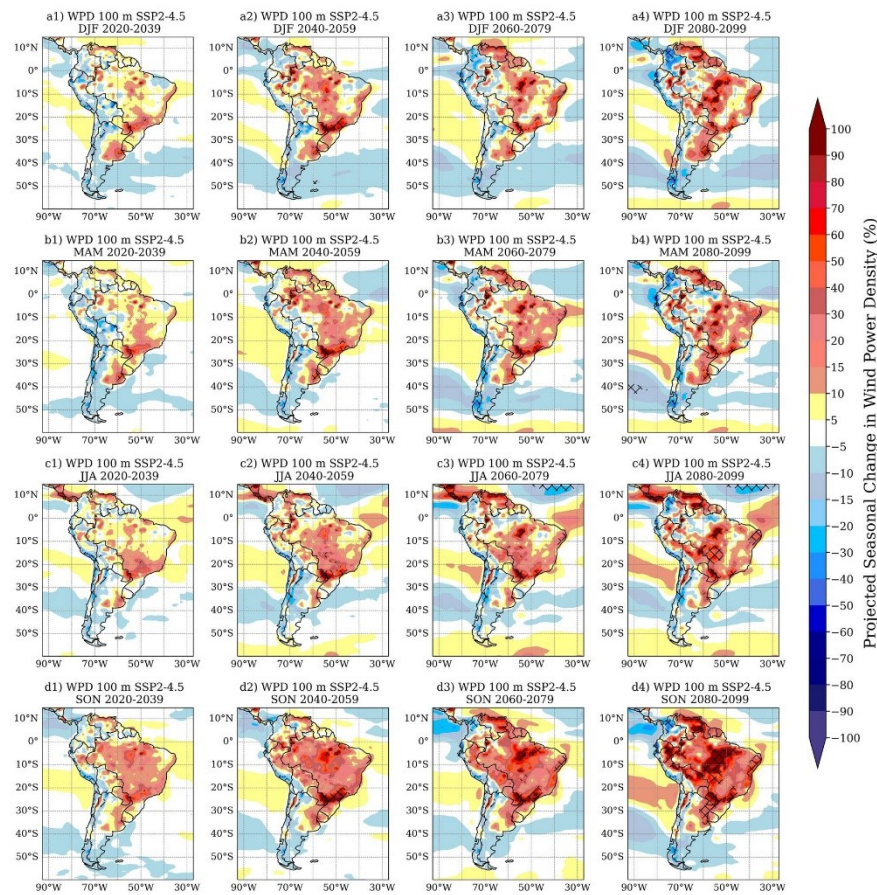


Fig. 6 Seasonal differences (%) in wind power density ($W\ m^{-2}$) at 100 m between the future (2020–2039, 2040–2059, 2060–2079, and 2080–2099) and historical period (1995–2014), projected by the

CMIP6 ensemble under the SSP2-4.5 scenario. Hatched areas indicate 95% statistical significance, based on Student's t-test

with GCMs from CMIP5 (HADGEM2-ES, CANESM2, and MIROC5) suggests a mean increase of up to 9.4% in wind intensity over most of northeastern Brazil by 2080 (de Jong et al. 2019), which is relatively similar to the more modest increases found here. In this context, it is emphasized that climate projections should be interpreted as indicators, given that the different models employed involve uncertainties.

Regarding the western coast of SA, an average increase of $1\ m\ s^{-1}$ is generally observed in the SPSA region, a pattern also detected by the CMIP3 climate projections under the A2 and B2 IPCC scenarios (Garreaud and Falvey 2009). The strengthening of winds on the west coast of subtropical SA (north-central and southern Chile) is associated with

an increasing surface pressure at mid-southern latitudes, intensifying the meridional pressure gradient (Garreaud and Falvey 2009). In addition, other studies identified an intensification of subtropical anticyclones in the Southern Hemisphere (Seth et al. 2010; Reboita et al. 2018).

Figure 8 presents the projected changes of WPD relative to the historical period, considering the SSP5-8.5 scenario. Northern and southeastern Brazil show an average increase of up to 100% towards the end of the twenty-first century. Reboita et al. (2018) also found an expressive rise in WPD in northern Brazil during the last decades of the twenty-first century, using the RCP8.5 scenario and the regional model RegCM4 nested with GCMs from CMIP5.

Assessment of the wind power density over South America simulated by CMIP6 models in the present...

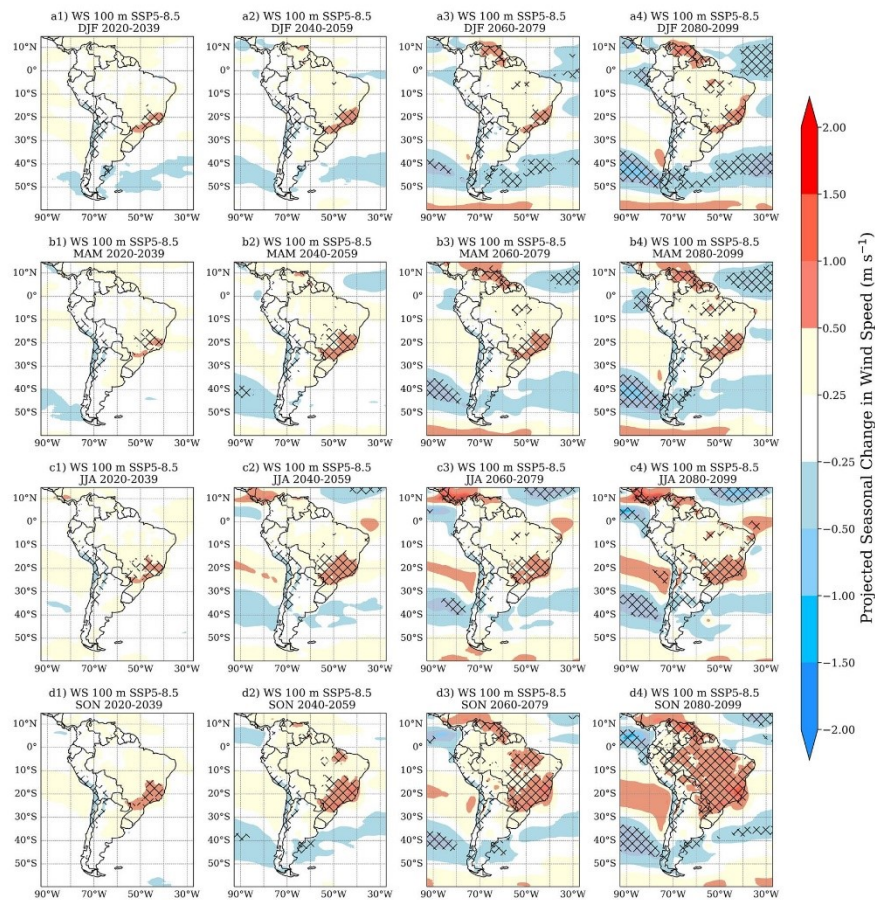


Fig. 7 Similar to Fig. 5, except for the SSP5-8.5 scenario

Although the increments found here are minor, both studies estimate a WPD increase over southeastern and north-central Brazilian regions, particularly from 2060 onwards.

WPD change estimates in Northeast Brazil present mixed associations with the results of Pereira et al. (2013) using the Eta-HadCM3 model. Although both studies show a potential wind increase in the interior (states of Bahia, Sergipe, and Alagoas) and east coast practically the entire year, results here indicate moderate changes and even slight reductions in the northern coast during the austral summer. Furthermore, Pereira et al. (2013) found an expressive decrease of offshore WPD on the Bahia coast, while our results show an average change of approximately – 10 to 15% throughout the year. On the other hand,

the average increase of around 15% in southern Brazil is identified in both studies.

Sectors such as south-central Chile and central Argentina indicate reduced WPD, with more noticeable decreases during austral autumn and winter, reiterating previous results (Reboita et al. 2018). Furthermore, several other CMIP5-GCMs have also provided projections of reduced WPD in the region under the RCP-2.6 and RCP-8.5 scenarios during almost the entire year, associated with a decrease in wind intensity also identified by GCMs (Kumar et al. 2015) and dynamical downscaling (Ruffato-Ferreira et al. 2017). On the other hand, a marked increase in WPD is observed in northern SA countries such as Venezuela, Guyanas, and Suriname, which corroborates projections of increased wind

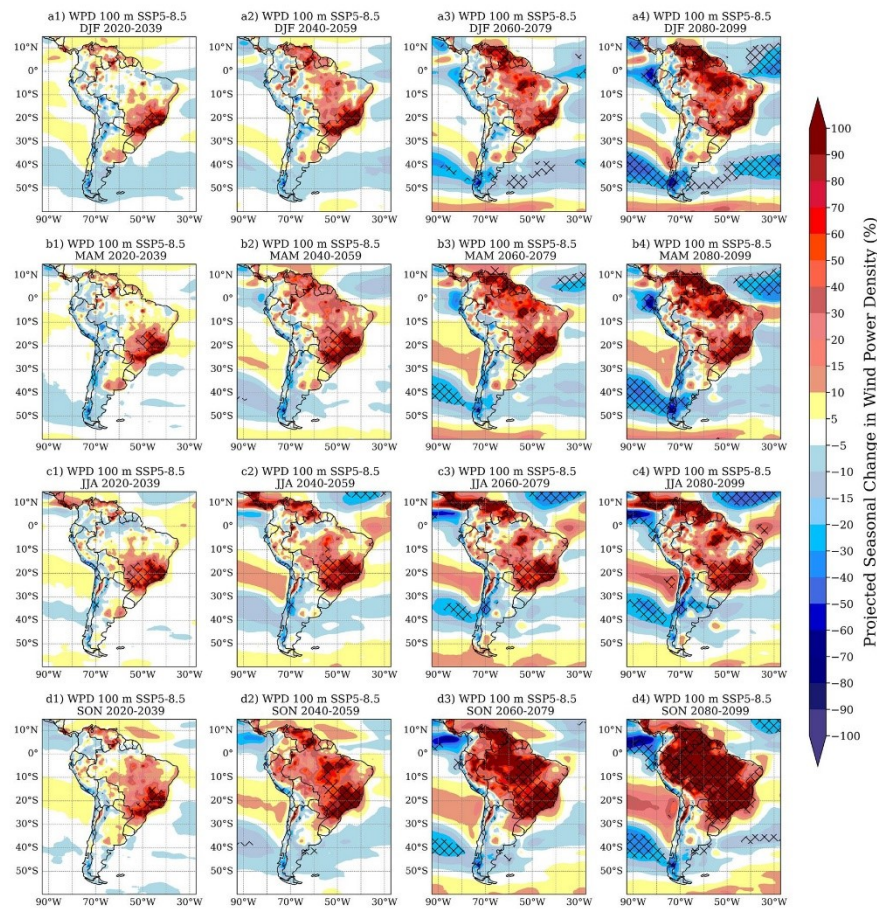


Fig. 8 Similar to Fig. 6, except for the SSP5-8.5 scenario

power in the region obtained by CMIP5 models (Donk et al. 2019).

Overall, the results suggest that the most promising regions for wind power generation in future climate include Brazil's northern, southern, and southeastern portions and the south-center of northeastern Brazil, endorsing previous studies (Ruffato-Ferreira et al. 2017; Reboita et al. 2018; de Jong et al. 2019; Donk et al. 2019; Gomes et al. 2019; Tavares et al. 2020). Similarly, Argentine Patagonia shows reduced wind sources, as found in other works (Kumar et al. 2015; Reboita et al. 2018). Moreover, WPD increases projected for northern SA, northeastern, southeastern, and southern Brazil corroborate analogous estimates (Pereira et al. 2013; Reboita et al. 2018). However, spatial and

temporal differences in wind intensity and WPD estimates occur among the different studies. They are likely due to factors such as the different models and scenarios used, the period analyzed, and data for validation. Hence, we emphasize that the uncertainties associated with climate projections require caution in interpreting such analyses so that they should be considered estimators and not as irrefutable truths about future climate conditions.

On the whole, the results indicate suitable conditions for wind power generation in most of the continent in the context of progressive warming in the twenty-first century, with more favoring patterns in the South, Southeast, North, and Northeast of Brazil and northern countries of SA. However, the ensemble projections also suggest that

sectors traditionally potential for wind power generation, such as Northeast Brazil, may experience slight reductions in energy production. Additionally, high wind generation estimates in areas such as the Andes and tropical SA should be cautiously analyzed. GCMs tend to overestimate wind intensity in regions of complex topography (Kumar et al. 2015) and exhibit a considerable spread in the climatological simulation of precipitation and winds in the equatorial region (Huang et al. 2020).

Furthermore, it is valid to point out the current study's limitations. First, we highlight that the results here refer to changes in the average wind regime but do not consider the changes caused by climate change on the wind speed distribution, whose non-stationary conditions may misrepresent future wind resources (Jung and Schindler 2019). Moreover, assessing the evolution of extreme wind speed is critical for wind analysis, given that extreme events structurally affect wind turbines, potentially causing damage under excessive speeds (Pryor and Barthelmie 2021). Estimates of GCMs from CMIP5 suggest an enhancement of extreme winds in SA during the twenty-first century, mainly over the tropics and extratropics (Kumar et al. 2015). Besides, wind power generation is not linearly proportional to wind intensity since once the wind speed exceeds the wind turbine speed (approximately $13\text{--}14\text{ m s}^{-1}$), there is no additional wind power generation beyond the typical turbine capacity (de Jong et al. 2019).

In addition, the current results describe the possible changes from a purely atmospheric point of view, not considering technological aspects such as the capacity factor related to the wind turbine and the development of turbines (Jung and Schindler 2022b). Here, we do not account for technological advancements and evolving energy policies that may influence the deployment and utilization of wind power resources. Future research should address these limitations and consider additional scenarios to provide a more comprehensive assessment of wind power in SA.

Moreover, the current study presents a simplified investigation of wind power evolution, as the lack of detail in the land use change projections employed by the GCMs restricts a more accurate future perspective. This issue is particularly relevant given that some regions presented here as prone to wind energy production also correspond to climate change hotspots under different CMIP3 and CMIP5 emission scenarios (Torres and Marengo 2014). In light of this problem, regional models are essential to describe such changes, and progressive use of multiple RCMs driven by GCMs from CMIP6 is expected.

Still, on the subject of GCMs, we would point out that they involve uncertainties since many physical processes in the sub-grid are parameterized in the numerical models. Many of these processes are fundamental for a satisfactory wind simulation, such as the effect of the planetary boundary

layer (PBL) scheme, which plays an essential role in modulating mass, energy, and moisture flows between the surface and the atmosphere, which in turn influences the simulation of temperature and winds at low levels (Falasca et al., 2021; Yu et al. 2022). In addition, a satisfactory wind simulation by numerical models also includes the choice of cloud microphysics and radiation parameterization since these factors affect the dynamic and thermodynamic processes of the atmosphere, influencing the vertical distribution patterns of heat and wind at low levels (Santos-Alamillos et al. 2013; Yu et al. 2022). In this context, we stress the need for studies that systematically evaluate the performance of parameterization combinations to investigate the sensitivity of parameterizations to wind simulation in SA. Despite the bias correction technique applied to the wind intensity modeled by the CMIP6 ensemble, the projections from the different models are still subject to biases, which should be considered when analyzing the results. In this sense, a more extensive base of observed data can reduce uncertainties about validating the simulations.

Finally, we emphasize that the validation of simulations and projections should employ the most accurate database since the validation data can be biased. For example, although ERA5 performs satisfactorily (Tavares et al. 2020), the reanalysis underestimates wind in regions with complex topography (Jourdi er 2020), which may induce erroneous wind power estimates. Reanalysis products also involve uncertainties since these data are obtained by assimilating information from different sources such as numerical models, surface data, airplanes, ships, satellites, radars, and radiosondes. In this context, Braga et al. (2021) concluded that the ERA5-Land reanalysis data correctly reproduces the seasonal and hourly cycles of wind speed over regions of the Rio de Janeiro state (Brazil) but tends to overestimate the variable, which consequently affects the estimated wind potential. Similarly, de Oliveira-Filho et al. (2022) found that the Global Forecast System (GFS) reanalysis satisfactorily simulates the spatial distribution of winds in the state of Minas Gerais (Brazil) but overestimates wind intensity in almost the entire region. Here, we can see that the ERA5 reanalysis is subject to biases but is adept at representing the temporal variability of surface wind data (Figure S2). Although reanalysis biases influence wind potential estimates, such products can be an alternative for regions where obtaining consistent and reliable data is difficult. However, we recommend caution when analyzing wind potential to consider the uncertainties inherent in the mapping process.

3.3 100m WPD anomaly and trends time series

Figures 9, 10, 11 and 12 show the 100 m WPD anomalies (in percentage) over the eight subdomains for each CMIP6-GCM under the SSP5-8.5 scenario. The data represent

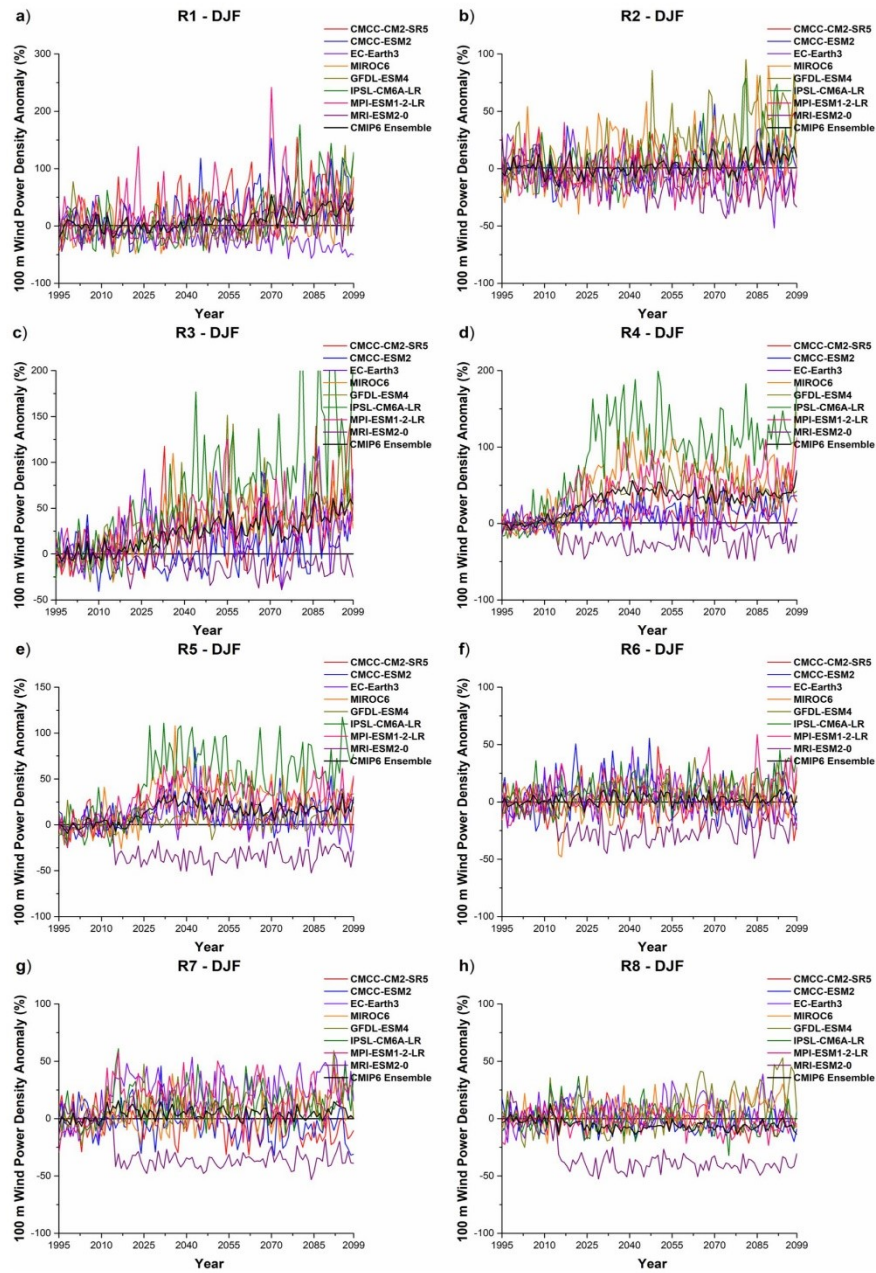


Fig. 9 Time series (1995–2099) of 100 m WPD anomalies (%) in the months of DJF for eight subdomains of SA (R1–R8), obtained after BCSD under the SSP5-8.5 scenario

Assessment of the wind power density over South America simulated by CMIP6 models in the present...

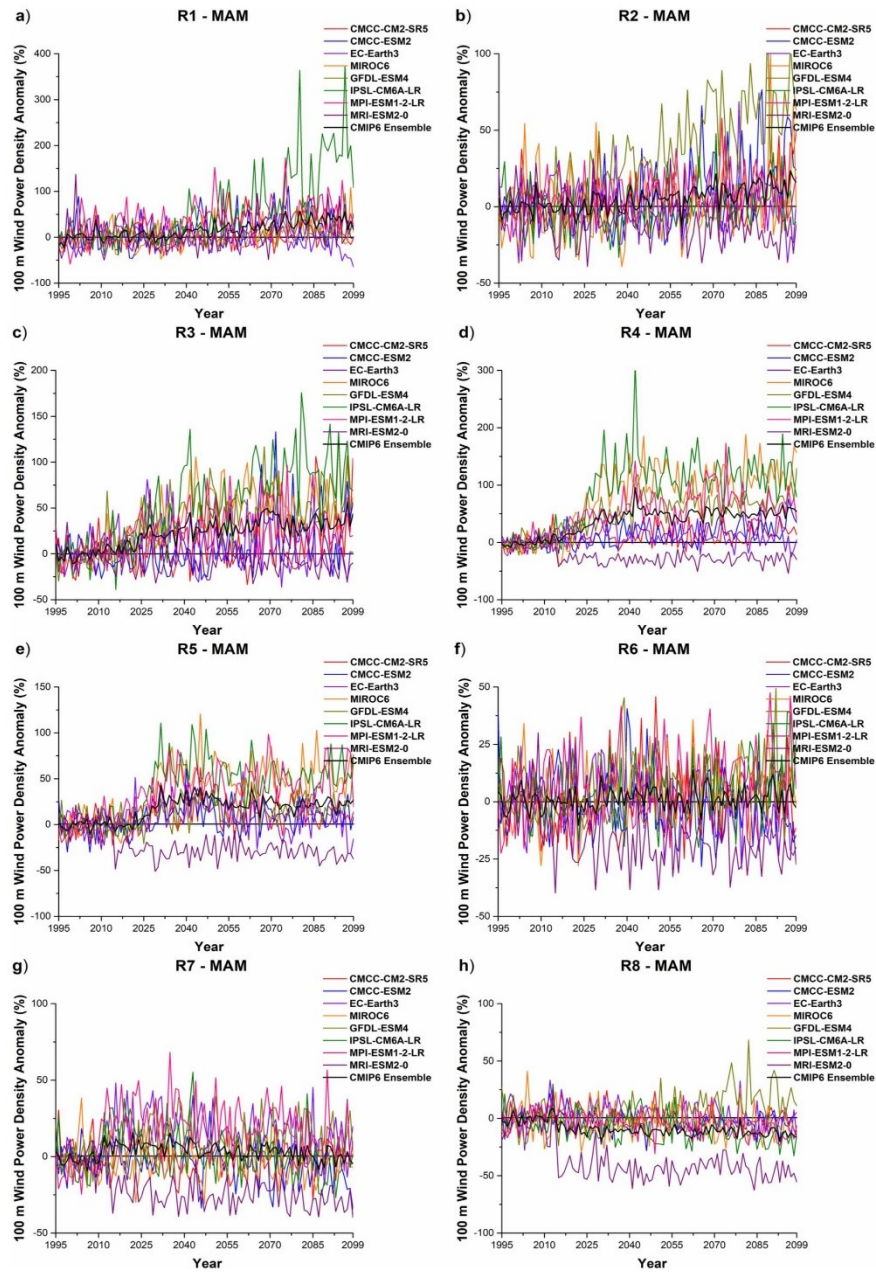


Fig. 10 Similar to Fig. 9, except for the months of MAM

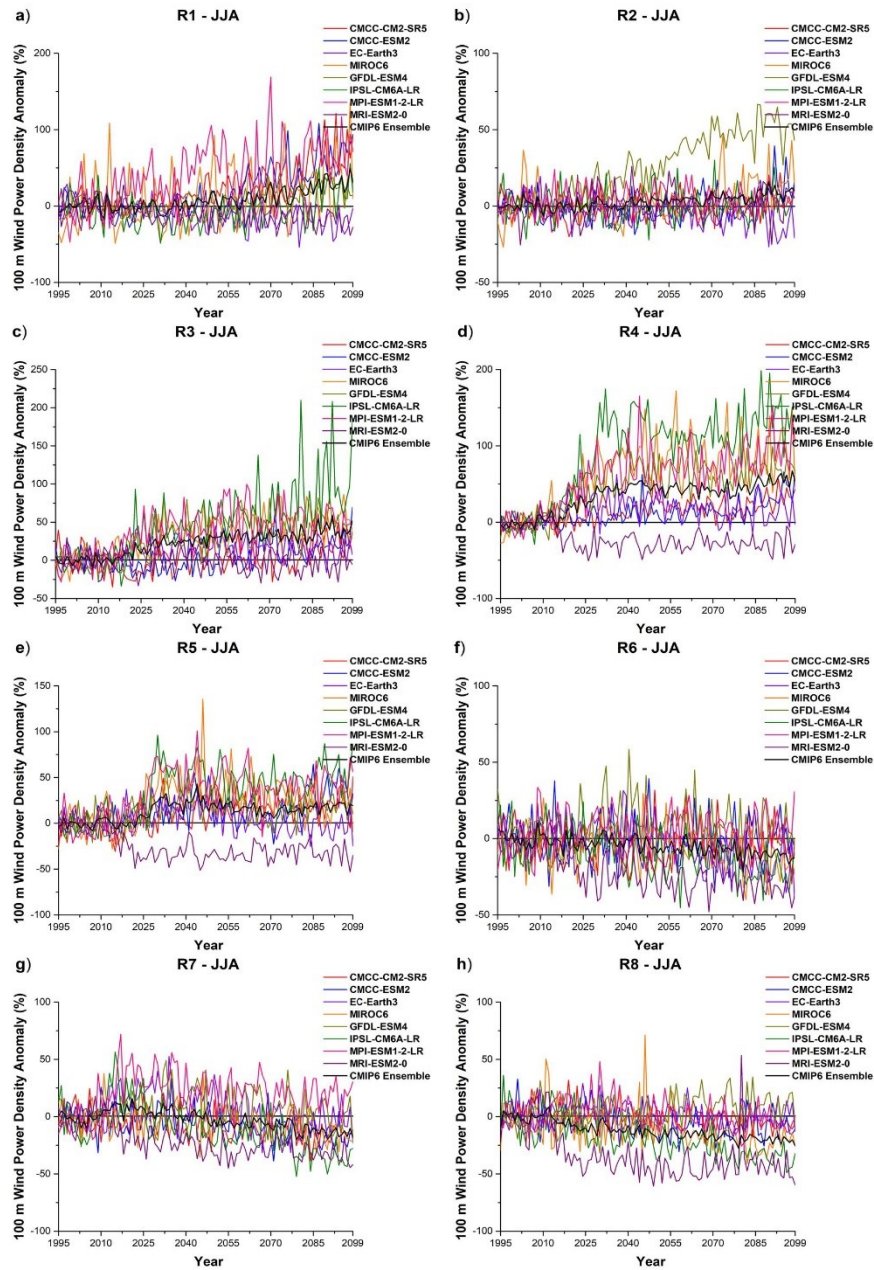


Fig. 11 Similar to Fig. 9, except for the months of JJA

Assessment of the wind power density over South America simulated by CMIP6 models in the present...

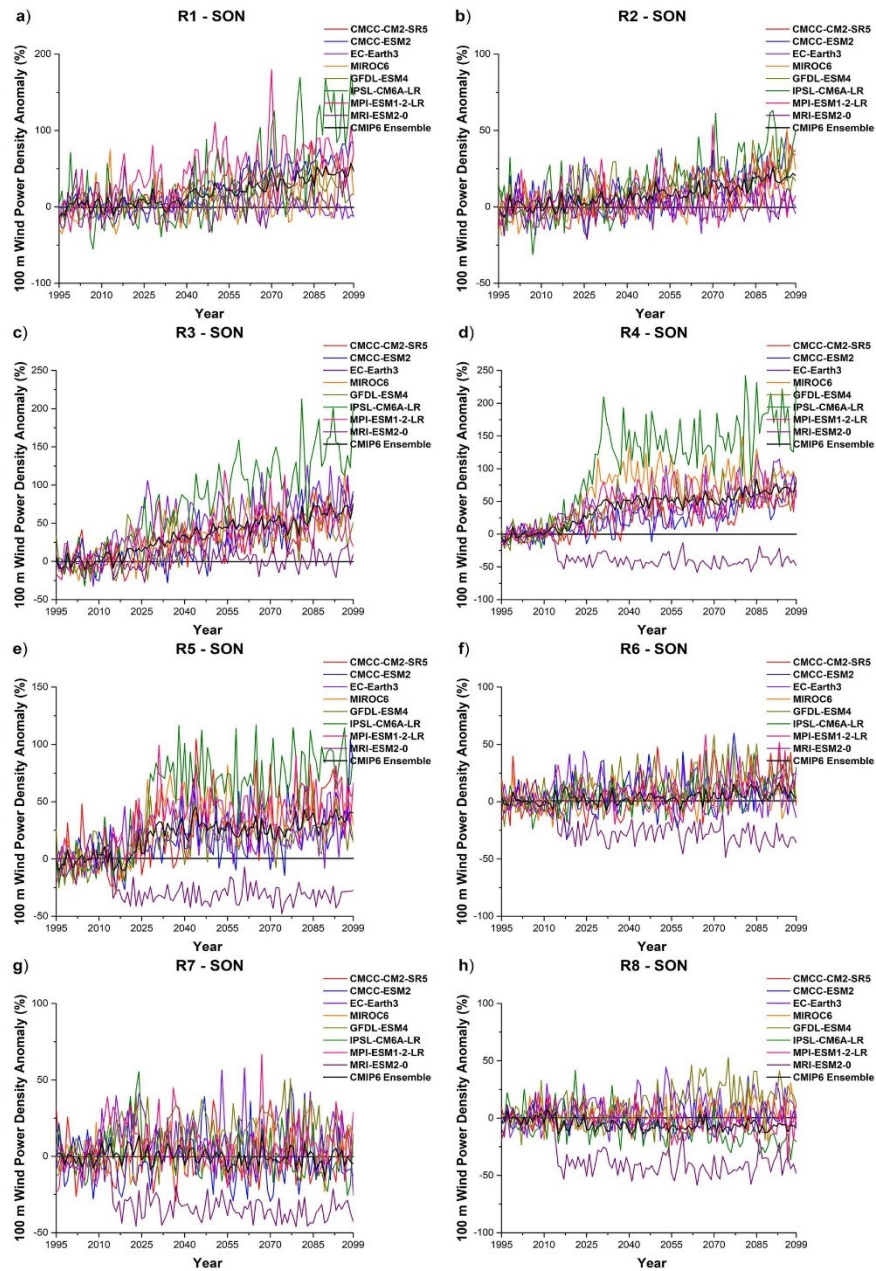


Fig. 12 Similar to Fig. 9, except for the months of SON

average anomalies relative to seasonal climatology of 1995–2014, indicating the evolution of deviations from present to future climate, highlighting the spread among the different models and associated uncertainties. As a complement to the analyses, Figure S5 in the Supplementary Material shows the seasonal cycle of wind speed and WPD at 100 m for regions R2, R3, R4, and R5 to assess the temporal variability of both indicators.

For the months of DJF (Fig. 9), about 64% of the time series indicate increasing trends in WPD at 100 m relative to the historical period (1995–2014) in the SA subdomains. In R1, virtually all models (except EC-Earth3) and ensemble project statistically significant increasing trends (Table 4), with the MPI-ESM1-2-LR model showing the highest variability (–31 to 241%). Similarly, at R2, about 66% of the projections indicate significant increasing trends, with the GFDL-ESM4 model showing the largest range of variability (–24 to 95%). GCMs from CMIP5 also showed a large spread in simulating rain and wind climatology in tropical areas such as the ITCZ and equatorial Atlantic (Huang et al. 2020).

At R3, considerable variability also occurs among projections, and virtually all models (except MRI-ESM2-0) and ensemble converge on a significant increasing trend in WPD at 100 m during the twenty-first century, with the IPSL-CM6A-LR model providing the largest variability (–27 to 271%). In R4, about 77% of the projections indicate a significant increasing trend (except EC-Earth3 and MRI-ESM2-0 models), and again, the IPSL-CM6A-LR model provides the greatest variability of projected anomalies (–19 to 199%). On the other hand, the R6, R7, and R8 sectors show mixed signals, with models indicating an increasing or decreasing trend and others with no statistically significant trend. In R6, only three models indicate an increasing trend, and most projections do not result in significant trends. In R7, almost half of the projections suggest a significant increasing trend, and there is no prominent variability of projections among the models as in the other sectors, with the IPSL-CM6A-LR model showing the greatest variation (–19 to 61%). In R8, most projections indicate a significant decreasing trend, and the GFDL-ESM4 model presents the greatest variability (–25 to 52%).

During the MAM months (Fig. 10, Table 5), approximately 55% of the projections point to a significant increasing trend in WPD at 100 m during the twenty-first century in the SA subdomains relative to the 1995–2014 period. In R1, only the EC-Earth3 model indicates a significant decreasing trend, while the IPSL-CM6A-LR model provides the largest range of anomaly projections (–39 to 374%). On the other hand, in R2, only three models and the ensemble indicate a significant increasing trend. In contrast, four others show no significant trend, and three show a decreasing trend, with the GFDL-ESM4 model resulting in the largest

variation (–22 to 119%). At R3, only the EC-Earth3 and MRI-ESM2-0 models provide no significant increasing trend, and the CMCC-ESM2 model offers the greatest variability of projections (–28 to 133%). Similarly, at R4, only the EC-Earth3 model does not result in a significant increasing trend in WPD at 100 m during the twenty-first century, with the IPSL-CM6A-LR model providing the greatest variability of projections (–15 to 311%).

Likewise, approximately 77% of the projections indicate an increasing trend at R5, and only the EC-Earth3 and MRI-ESM2-0 models indicate no trend and a decreasing trend, respectively. At R6, only four models result in an increasing trend, while the others show mixed signals of a decreasing trend or no trend. At R7, six models and the ensemble show no significant trend, and only the GFDL-ESM4 model indicates an increase in WPD at 100 m. Similarly, the GFDL-ESM4 model is the only one to show a significant increasing trend at R8. The outputs of the other eight data sets are equally distributed in significant decreasing or no trend.

During the JJA period (Fig. 11, Table 6), about 51% of the projections indicate a significant increasing trend in WPD at 100 m in the eight SA subdomains during the twenty-first century. At R1, only the EC-Earth3 and MRI-ESM2-0 models provide a decreasing trend, and the MPI-ESM1-2-LR model offers the largest range of projections (–47 to 168%). At R2, half of the models and the ensemble show an increasing trend, while only the EC-Earth3 model indicates a decreasing trend.

At R3, the data sets are unanimous in projecting a significant increasing trend, with the IPSL-CM6A-LR model presenting the largest range of projections (–33 to 209%). Similar to R2, only the EC-Earth3 model deviates from the projections of the other sets, indicating no trend in the R4 and R5 sectors. In R4, the IPSL-CM6A-LR model again stands out with the greatest range of projections (–29 to 198%), while in R5, the MIROC6 model stands out with the greatest range (–28 to 135%). Evaluation of several GCMs from CMIP5 and CMIP6 indicated that MIROC6 proved to be the least accurate model of the CMIP6 family, with a mean absolute error of 1.14 m s^{-1} and a mean underestimate of -1 m s^{-1} (Jung and Schindler 2022a). At R6, no model indicates an increasing trend, and most projections point to a decreasing trend. At R7, only the GFDL-ESM4 and MPI-ESM1-2-LR models show no trend, while all other ensembles provide a decreasing trend. Similarly, at R8, only the GFDL-ESM4 model results in an increasing trend, while five other models and the ensemble show a decreasing trend of WPD at 100 m during the twenty-first century.

Finally, considering the SON months (Fig. 12, Table 7), about 70% of the projections result in an increasing trend of WPD at 100 m in the SA subdomains. In R1, only the EC-Earth3 model indicates no trend, and the IPSL-CM6A-LR model provides the largest range of projections (–55

Assessment of the wind power density over South America simulated by CMIP6 models in the present...

Table 4. Parameters of the 100 m WPD trend time series (1995–2099) in the months of DJF, for eight subdomains of SA, obtained by the eight CMIP6-GCMs and the multi-model ensemble after applying statistical downscaling and under the SSP5-8.5 scenario

	CMCC-CM2-SR5	CMCC-ESM2	EC-EARTH3	MIROC6	GFDL-ESM4	IPSL-CM6A-LR	MPI-ESM1-2-LR	MRI-ESM2-0	ENSEMBLE
R1	Trend	I	D	I	I	I	I	I	I
	Ho	T	T	T	T	T	T	T	T
	Slope	0.487	-0.405	0.245	0.365	0.680	0.476	0.224	0.368
R2	Trend	I	D	I	I	I	NT	D	I
	Ho	T	T	T	T	T	F	T	T
	Slope	0.151	-0.150	0.182	0.599	0.180	-0.057	-0.224	0.105
R3	Trend	I	I	I	I	I	I	D	I
	Ho	T	T	T	T	T	T	T	T
	Slope	0.517	0.396	0.567	0.650	1.438	0.497	-0.123	0.513
R4	Trend	I	NT	I	I	I	I	D	I
	Ho	T	F	T	T	T	T	T	T
	Slope	0.268	-0.049	0.752	0.489	1.223	0.597	-0.220	0.406
R5	Trend	I	NT	I	I	I	I	D	I
	Ho	T	F	T	T	T	T	T	T
	Slope	0.105	-0.058	0.352	0.125	0.714	0.340	-0.199	0.179
R6	Trend	D	NT	NT	I	I	I	D	NT
	Ho	T	F	F	T	T	T	T	F
	Slope	-0.088	-0.084	0.032	0.147	0.211	0.182	-0.138	0.028
R7	Trend	D	I	I	I	I	I	D	NT
	Ho	T	T	T	T	T	T	T	F
	Slope	-0.156	0.251	0.139	0.212	0.118	0.196	-0.171	0.028
R8	Trend	D	NT	I	I	NT	D	D	D
	Ho	T	F	T	T	F	T	T	T
	Slope	-0.086	0.046	0.128	0.297	-0.056	-0.074	-0.237	-0.058

The terms I, D, NT, T, and F denote increasing trend, decreasing trend, no trend, true and false, respectively

Table 5 Similar to Table 4, except for the months of MAM

	CMCC-CM2-SR5	CMCC-ESM2	EC-EARTH3	MIROC6	GFDL-ESM4	IPSL-CM6A-LR	MPI-ESM1-2-LR	MRI-ESM2-0	ENSEMBLE
R1	Trend	I	D	I	I	I	I	I	I
	Ho	T	-0.239	T	T	T	T	T	T
	Slope	0.229	0.446	0.312	0.229	1.642	0.627	0.309	0.445
R2	Trend	I	NT	NT	I	NT	NT	D	I
	Ho	T	F	F	T	F	F	T	T
	Slope	0.155	-0.042	0.123	0.755	0.033	0.114	-0.160	0.176
R3	Trend	I	NT	I	I	I	I	D	I
	Ho	T	F	T	T	T	T	T	T
	Slope	0.199	-0.080	0.725	0.633	1.138	0.308	-0.117	0.426
R4	Trend	I	NT	I	I	I	I	I	I
	Ho	T	F	T	T	T	T	T	T
	Slope	0.196	0.032	1.362	0.863	1.351	0.797	0.206	0.596
R5	Trend	I	NT	I	I	I	I	D	I
	Ho	T	F	T	T	T	T	T	T
	Slope	0.110	-0.024	0.670	0.245	0.626	0.497	-0.242	0.254
R6	Trend	NT	D	I	I	I	I	D	NT
	Ho	F	T	T	T	T	T	T	F
	Slope	0.015	-0.164	0.110	0.154	0.086	0.176	-0.173	0.024
R7	Trend	NT	NT	NT	I	NT	NT	D	NT
	Ho	F	F	F	T	F	F	T	F
	Slope	-0.037	0.051	-0.013	0.127	-0.113	0.093	-0.254	-0.028
R8	Trend	NT	NT	NT	I	D	D	D	D
	Ho	F	F	F	T	T	T	T	T
	Slope	-0.022	-0.051	-0.065	0.244	-0.183	-0.151	-0.315	-0.126

Assessment of the wind power density over South America simulated by CMIP6 models in the present...

Table 6 Similar to Table 4, except for the months of JJA

	CMCC-CM2-SR5	CMCC-ESM2	EC-EARTH3	MIROC6	GFDL-ESM4	IPSL-CM6A-LR	MPI-ESM1-2-LR	MRI-ESM2-0	ENSEMBLE
R1	Trend	I	D	I	I	I	I	D	I
	Ho	T	T	T	T	T	T	T	T
	Slope	0.655	-0.236	0.450	0.298	0.187	0.737	-0.199	0.321
R2	Trend	I	D	I	I	NT	NT	NT	I
	Ho	T	T	T	T	F	F	F	T
	Slope	0.065	-0.117	0.150	0.650	0.019	0.031	0.012	0.093
R3	Trend	I	I	I	I	I	I	I	I
	Ho	T	T	T	T	T	T	T	T
	Slope	0.243	0.146	0.659	0.512	1.007	0.554	0.071	0.445
R4	Trend	I	NT	I	I	I	I	I	I
	Ho	T	F	T	T	T	T	T	T
	Slope	0.334	0.081	1.032	0.744	1.463	0.984	0.233	0.548
R5	Trend	I	NT	I	I	I	I	D	I
	Ho	T	F	T	T	T	T	T	T
	Slope	0.266	-0.092	0.253	0.168	0.596	0.460	-0.277	0.188
R6	Trend	NT	D	D	NT	D	NT	D	D
	Ho	F	T	T	F	T	F	T	T
	Slope	-0.028	-0.244	-0.159	0.055	-0.258	0.070	-0.321	-0.122
R7	Trend	D	D	D	NT	D	NT	D	D
	Ho	T	T	T	F	T	F	T	T
	Slope	-0.163	-0.155	-0.144	-0.008	-0.464	0.072	-0.310	-0.201
R8	Trend	NT	NT	D	I	D	D	D	D
	Ho	F	F	T	T	T	T	T	T
	Slope	-0.063	-0.028	-0.233	0.162	-0.404	-0.122	-0.359	-0.220

Table 7 Similar to Table 4, except for the months of SON

	CMCC-CM2-SR5	CMCC-ESM2	EC-EARTH3	MIROC6	GFDL-ESM4	IPSL-CM6A-LR	MPI-ESM1-2-LR	MRI-ESM2-0	ENSEMBLE
R1	Trend	I	NT	I	I	I	I	I	I
	Ho	T	F	T	T	T	T	T	T
	Slope	0.601	-0.060	0.313	0.299	1.157	0.811	0.163	0.505
R2	Trend	I	NT	I	I	I	I	NT	I
	Ho	T	F	T	T	T	T	F	T
	Slope	0.287	0.013	0.204	0.240	0.410	0.111	0.008	0.209
R3	Trend	I	I	I	I	I	I	NT	I
	Ho	T	T	T	T	T	T	F	T
	Slope	0.768	0.884	0.746	0.583	1.699	0.561	0.077	0.767
R4	Trend	I	I	I	I	I	I	D	I
	Ho	T	T	T	T	T	T	T	T
	Slope	0.598	0.788	0.988	0.726	1.954	0.710	-0.277	0.749
R5	Trend	I	I	I	I	I	I	D	I
	Ho	T	T	T	T	T	T	T	T
	Slope	0.669	0.177	0.434	0.301	0.963	0.492	-0.206	0.390
R6	Trend	I	NT	I	I	I	I	D	I
	Ho	T	F	T	T	T	T	T	T
	Slope	0.246	-0.027	0.077	0.252	0.156	0.162	-0.316	0.077
R7	Trend	NT	NT	NT	I	D	NT	D	D
	Ho	F	F	F	T	T	F	T	T
	Slope	-0.008	0.003	0.051	0.197	-0.123	0.033	-0.268	-0.031
R8	Trend	NT	I	I	I	D	D	D	D
	Ho	F	T	T	T	T	T	T	T
	Slope	0.026	0.085	0.069	0.325	-0.243	-0.110	-0.263	-0.053

to 173%). In sectors R2, R3, R4, R5, and R6, only the EC-Earth3 and MRI-ESM2-0 models indicate a decreasing trend or no trend, while all other datasets provide a significant increasing trend in WPD at 100 m. Overall, in these sectors, the model showing the greatest range of projections is IPSL-CM6A-LR, with variations from –31 to 63% at R2, from –32 to 212% at R3, from –21 to 242% at R4, and from –21 to 116% at R5. Contrarily, at R7, only the GFDL-ESM4 model indicates an increasing trend, while the other five models show no trend, and two models and the ensemble provide an increasing trend. Similarly, at R8, only three models result in an increasing trend, while most datasets project a decreasing trend in WPD at 100 m.

In summary, the analysis of 100 m WPD trends obtained after BCSD under the SSP5-8.5 emission scenario suggests that sectors R1, R2, R3, R4, and R5 tend to experience increased wind power for most of the year during the coming decades. Although some models, such as EC-Earth3 and MRI-ESM2-0, indicate a decreasing or no trend in these regions, most models converge to a favorable future scenario for wind power, considering a context of progressive warming. On the other hand, sectors R6, R7, and R8 indicate mixed signals of decrease, increase, or absence of a trend, depending on the year's seasons. However, the signs of wind power reduction prevail mainly in sectors R7 and R8. A likely reason for the models' spread in the region relates to the large GCMs spread in simulating the near-surface westerly wind jet position, given that CMIP5 models exhibit a bias towards the equator of 3.3° in the mean position of the mean zonal jet, associated with the coupling of ocean and sea ice models, which can amplify atmospheric biases and introduce biases generated by the models or the coupling procedure (Bracegirdle et al. 2013).

An analysis of the direction of the mean bias of 18 models from CMIP6 showed that half of the GCMs showed positive median mean errors, while another nine models provided a negative median (Jung and Schindler 2022a). Here, we emphasize that although the amount of GCMs used is reasonably small, such models were previously validated among 46 GCMs from CMIP6 (Dias and Reboita 2021) and were chosen due to their satisfactory performance in representing the SA climate during the historical period.

Furthermore, given the variability among GCMs, it is recommended to evaluate multi-model ensembles. Analyses demonstrated that the multi-model ensemble outperformed any individual climate model in representing the phase and amplitude of extreme winds (Kumar et al. 2015). Although the ensemble masks the poor performance of some models, using a limited number of GCMs may induce biased results. Employing a larger number of GCMs also counterbalances the use of RCMs with a better resolution, but whose number of models used in the studies is commonly smaller. However, only about 20% of global wind power

studies estimated by climate models have used more than 20 GCMs (Jung and Schindler 2022a). Finally, we reiterate that the uncertainty associated with intermodel variability is expected to be reduced with a better representation of all physical and chemical processes in the climate system. If intermodel variability is attenuated, only the climate internal variability and the variability between emission scenarios would significantly affect climate projections (Blázquez and Nuñez 2013).

3.4 Classification of wind power density

Currently, most wind turbines operate at approximately 100 m. Still, the use of wind turbines up to 160 m is expected to grow in the coming decades (Lantz et al. 2019) due to the reduced installation and maintenance costs (Barthelmie et al. 2020). Because of the structural limitations of wind turbines, wind intensity restricts the amount of wind energy available, such that weaker winds ($< 4 \text{ m s}^{-1}$) do not move turbines, while stronger winds ($> 13 \text{ m s}^{-1}$) do not increase wind power as well as winds above 25 m s^{-1} can cause structural damage to turbines (Reboita et al. 2021). Therefore, projections of increasing wind intensity do not necessarily translate into growth in wind power. Thus, it is valid to classify regions according to their potential for wind power generation.

Figures 13 and 14 illustrate the seasonal categorization of SA wind power according to the methodology proposed by Elliott et al. (1991) for the height of 100 m under the SSP2-4.5 and SSP5-8.5 scenarios, respectively. In addition, Figures S6 to S13 of the Supplementary Material present the seasonal categorization of wind power obtained individually by each GCM under the SSP5-8.5 scenario. Although the CMIP6 ensemble indicates an increase in the percentage of WPD over large parts of SA during the twenty-first century, such an increase does not determine growth in the continent's wind power.

Under the SSP2-4.5 scenario, the wind power of most of the continent is classified as poor over the twenty-first century. Exceptions occur mainly during austral spring and summer in extreme eastern Northeast Brazil and extreme southern Brazil, where moderate to excellent conditions are experienced. Additionally, other sectors, such as Uruguay, northern Venezuela, central-southern Argentina, and portions of Paraguay, show moderate to excellent conditions throughout the year. Notably, the most excellent condition in Argentine Patagonia throughout the century is impressive.

Under the SSP5-8.5 scenario, fields similar to those under SSP2-4.5 are observed, but the areas with moderate or better ratings cover slightly larger portions. Again, regions such as the eastern coast of Northeast Brazil and southern Brazil show moderate to excellent conditions, most evident during austral spring and summer. Other sectors, such as Argentine

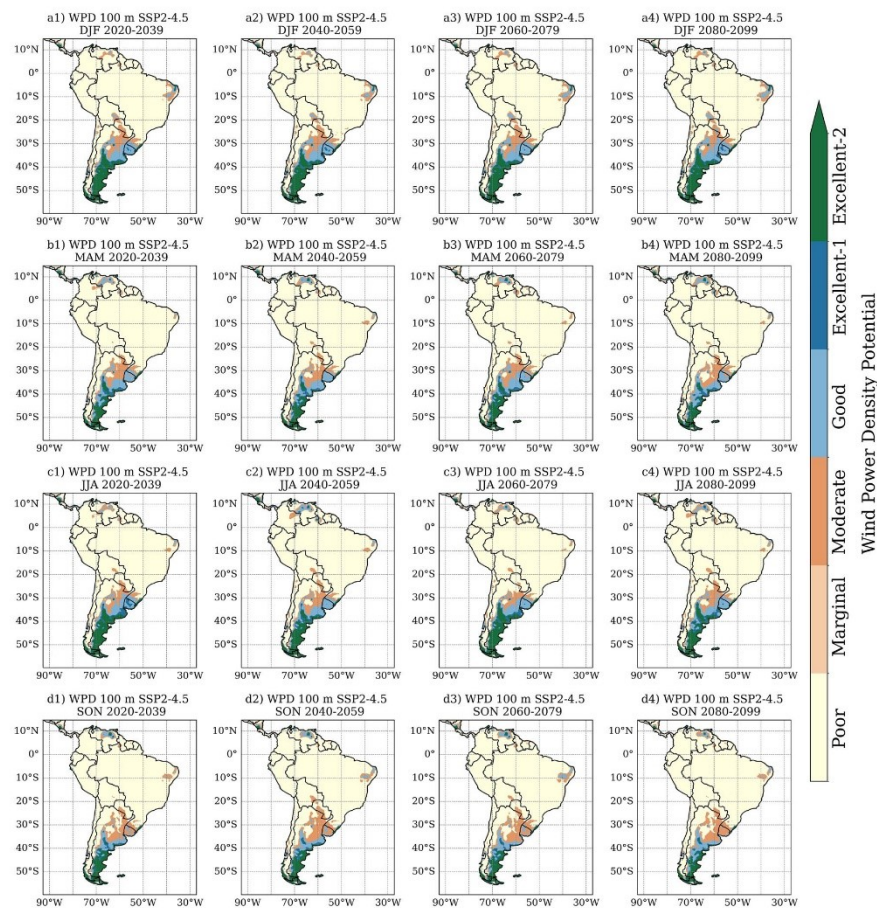


Fig. 13 Seasonal classification of areas suitable for wind power generation at the 100 m height under the SSP2-4.5 emission scenario during 2020–2099

Patagonia, Uruguay, northern Venezuela, and portions of southeastern Paraguay, indicate moderate to excellent conditions throughout the year. Importantly, although the GCMs have provided mixed WPD trend signals in Argentine Patagonia, this is not necessarily reflected in the wind power classification, as the region has the best WPD estimates on the continent. On the other hand, although the models mostly indicate a WPD-increasing trend in most of Brazil, the wind power classification suggests that the best regions for wind generation are concentrated in Northeastern and Southern Brazilian territories.

Overall, the results here reiterate the traditional wind power of countries like Argentina and Brazil. Argentina has

one of the best wind resources in the world, with high wind speeds in the country's southern, central, and northwestern provinces, potentially supplying up to 14% of total energy demand by 2030 (GWEC 2018). However, the country faces several challenges for its wind expansion, such as increased investment difficulty due to Argentina's highly volatile economy, power transmission and distribution constraints, and better local decision-making management since each Argentina province has its own power regulation (GWEC 2019).

Analogously, although Brazil's estimates are more conservative, these results reinforce the country's considerable wind energy potential. Brazilian wind power has experienced massive growth in the last decades, rising from 1

Assessment of the wind power density over South America simulated by CMIP6 models in the present...

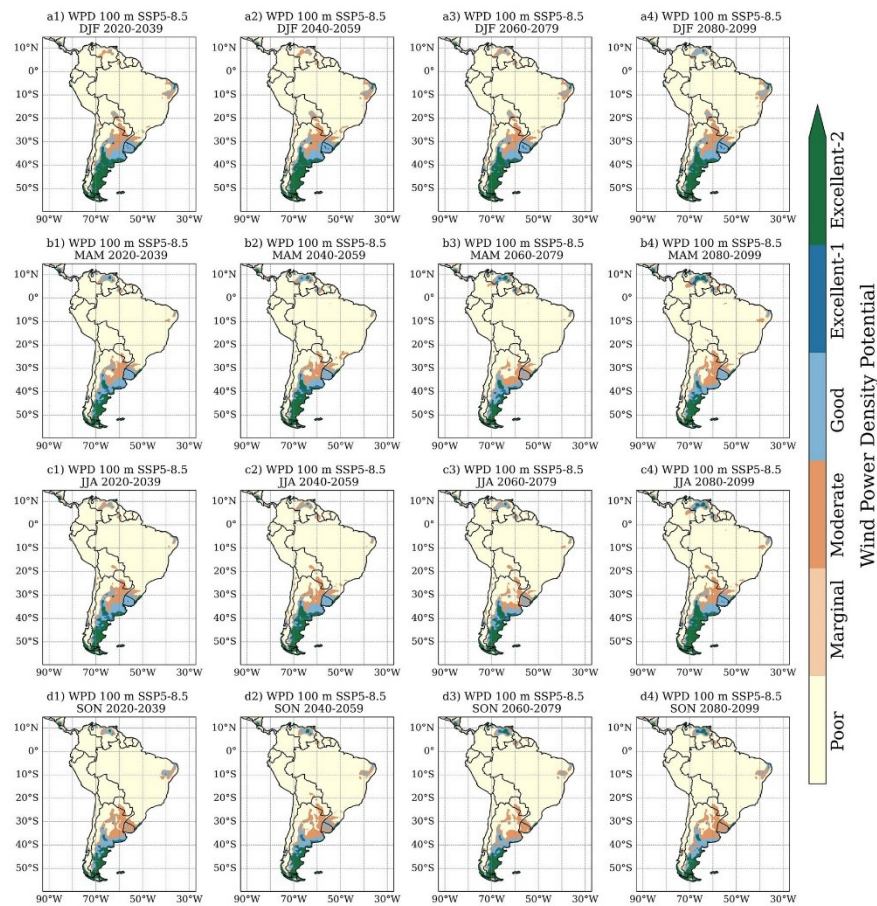


Fig. 14 Similar to Fig. 13, except for the SSP5-8.5 scenario

GW in 2011 to 21 GW in 2022 (accounting for 11% of the electricity matrix), resulting from a combination of factors such as economic recovery, increased energy demand, consolidation of the wind industry, and regulation of hybrid projects (GWEC 2022). In addition, the country presents promising offshore wind power generation capacity (Tavares et al. 2020), attracting potential investments in the sector (EPE 2022). Therefore, according to the Ten-Year Energy Expansion Plan (EPE 2022), the coming years indicate optimistic prospects for the wind sector in the country. Still, progress must also be made in strategic planning, public policies that favor a fair energy transition, and hybrid projects that contemplate wind and solar generation, offshore wind, and hydrogen (GWEC 2022). The Brazilian Northeast,

for instance, is already a relevant example of local complementarity between solar and wind sources (EPE 2021).

4 Summary and Conclusions

The growing energy demand for sustainable socio-economic development in South America during the twenty-first century and the need to mitigate the effects of climate change make it urgent to expand the renewable energy matrix in its different aspects on the continent. In this context, the present study sought to evaluate the projections of changes in wind intensity and wind power density at 100 m estimated by an ensemble composed of eight CMIP6 global climate models

for the twenty-first century under the SSP2-4.5 and SSP5-8.5 emission scenarios. ERA5 reanalysis validated the ensemble climate simulations for the historical period (1995–2014) and the application of statistical downscaling. After bias correction, the ensemble proved adept at reproducing the historical climate, although systematic biases remain in some regions of the continent.

Results indicated that regions with wind energy potential in the historical period maintain suitable conditions in the future climate. However, the potential increasing wind speed and WPD was observed over much of the South American continent during the twenty-first century. Sectors such as Northeast Brazil, portions of the Southeast, and the coast of South Brazil showed an increase of approximately 25–50% in wind energy production compared to the historical period, with excellent conditions for wind energy generation for the coming decades. Other regions such as Northern Brazil, Argentine Patagonia, Northern Venezuela, and portions of Uruguay, Bolivia, and Paraguay also suggest estimates of growth in wind energy potential. For the worst GHG emission scenario (SSP5-8.5), the CMIP6 ensemble projections indicated even more favorable conditions in those mentioned South American regions.

Projections' uncertainties were evaluated by analyzing the time series of 100 m WPD anomalies projected individually by each model of the CMIP6. A considerable spread was observed among the model projections, with more expressive variability in problematic sectors for climate modeling, such as the Brazilian north and southeast regions and western South America. Thus, caution is recommended when analyzing the projections to consider them as possible future climate conditions and perspectives for energy production and not as irrefutable truths about the climate evolution in the South American territory. In this sense, dynamical downscaling studies with RCMs driven by CMIP6-GCMs are expected to advance the knowledge of future impacts in the regions.

Within this context of uncertainties, we emphasize that this study presents limitations, which should be considered when analyzing the results. First, the study did not evaluate the impact of climate change on wind speed distribution, whose non-stationarity can mislead deductions of future wind resources. The analysis of the evolution of extreme wind speed was also not performed since this type of study would require wind data of 10-min frequency, which would demand high computational costs. However, such an investigation is essential because extreme wind events can cause structural damage to wind turbines. Furthermore, the study did not account for technological advancements and evolving energy policies, and future research should address these limitations. Moreover, we also stress that investigating the impacts of wind farm expansion on biodiversity should not be neglected. Installing increasingly

tall wind turbines may, for example, affect the distribution and habits of avian species (Therkildsen et al. 2021).

In addition, obtaining a reliable and extensive database of observed data is necessary since the validation data contains biases. Even though reanalysis products with satisfactory global performance provide consistent estimates, such data can also lead to erroneous assumptions about validating climate projections. Uncertainty is intrinsic to reanalysis since it results from data assimilation of different sources. As such, the uncertainties and systematic errors in the reference data must be considered when analyzing climate projections for wind power on the continent. Furthermore, we emphasize that the methodology used here can be replicated in dynamical downscaling studies to assess better the regional characteristics of the wind on the continent. It should be noted that there is still a scarcity of wind studies with dynamical downscaling in SA, and the methodology used in the current work proved to be satisfactory for evaluating simulations and climate projections of wind and WPD in studies with dynamical downscaling on the continent (Reboita et al. 2018).

Overall, we stress that the projections presented here have relevant implications for policymakers, energy planners, and investors in the South American wind energy sector. For example, identifying regions with high wind power density highlights potential areas for installing wind farms, developing the strategic allocation and deployment of wind energy resources, and facilitating the transition towards a cleaner and sustainable energy infrastructure in SA. In addition, these findings emphasize the importance of formulating policies encouraging wind energy deployment in favorable regions, promoting a shift towards a low-carbon economy, and reducing dependence on fossil fuels. Lastly, the study provides valuable information to policymakers, energy planners, and stakeholders involved in the development and expansion of wind energy infrastructure, as the analyses presented here represent a first look at the climate projections of the latest generation of CMIP models for SA wind power.

Supplementary Information The online version contains supplementary material available at <https://doi.org/10.1007/s00382-023-06993-3>.

Acknowledgements The authors thank the National Council for Scientific and Technological Development (CNPq), CAPES, ANEEL, and the companies Engie Brasil Energia and Energética Estreito for their financial support. The authors also thank the European Centre for Medium-Range Weather Forecasts (ECMWF), the Coupled Model Intercomparison Project (CMIP), and the National Environmental Data Organization (SONDA) for the data used in this study.

Author contributions GWSF, MSR, JGMR, PLLSS, TCB, and CAS carried out the processing and analysis of data. GWSF and MSR wrote the original draft. MSR, VSBC, and MEVS participated in the reviewing and editing process. All authors read and approved the final manuscript.

Funding This study received financial support from the R&D Program regulated by the Brazilian Electricity Regulatory Agency (ANEEL) and the companies Engie Brasil Energia and Energética Estreito (R&D-00403–54/2022), and the Coordination for the Improvement of Higher Education (CAPES, Finance Code 001).

Availability of data and materials The CMIP6 climate models are available at: <https://esgfnode.llnl.gov/search/cmip6/>. The ECMWF-ERA5 reanalysis is available at: <https://cds.climate.copernicus.eu/>. Observational data from the SONDA network is available at <http://sonda.cest.inpe.br/index.html>.

Declarations

Conflict of interest The authors have no relevant financial or non-financial interests to disclose.

Ethics approval and consent to participate Not applicable.

Consent for publication All authors read and approved the final manuscript.

References

- Admasu LM, Grant L, Thiery W (2023) Exploring global climate model downscaling based on tile-level output. *J Appl Meteorol Climatol* 62:171–190 <https://doi.org/10.1175/JAMC-D-21-0265.1>
- Akinsanola AA, Ogunjobi KO, Abolude AT, Salack S (2021) Projected changes in wind speed and wind energy potential over West Africa in CMIP6 models. *Environ Res Lett* 16:044033 <https://doi.org/10.1088/1748-9326/abed7a>
- Alkhalidi MA, Al-Dabbous SK, Neelamani S, Aldashti HA (2019) Wind energy potential at coastal and offshore locations in the state of Kuwait. *Renew Energy* 135:529–539 <https://doi.org/10.1016/j.renene.2018.12.039>
- Ambrizzi T, Reboita MS, da Rocha RP, Llopart M (2019) The state of the art and fundamental aspects of regional climate modeling in South America. *Ann NY Acad Sci* 1436:98–120 <https://doi.org/10.1111/nyas.13932>
- Anandh TS, Gopalakrishnan D, Mukhopadhyay P (2022) Analysis of future wind and solar potential over India using climate models. *Current Science* 122:1268–1278 <https://doi.org/10.18520/cs/v122/i11/1268-1278>
- Arango-Aramburo S, Ríos-Ocampo JP, Larsen ER (2020) Examining the decreasing share of renewable energy and growing thermal capacity: The case of South America. *Renew Sustain Energy Rev* 119:109648 <https://doi.org/10.1016/j.rser.2019.109648>
- Arsilan H, Baltaci H, Akkoyunlu BO, Karanfil S, Tayanc M (2020) Wind speed variability and wind power potential over Turkey: Case studies for Çanakkale and Istanbul. *Renew Energy* 145:1020–1032 <https://doi.org/10.1016/j.renene.2019.06.128>
- Ballarin AS, Sone JS, Gesualdo GC, Schwaback D, Reis A, Almagro A, Wendland EC (2023) CLIMBra - Climate change dataset for Brazil. *Sci Data* 10:47 <https://doi.org/10.1038/s41597-023-01956-z>
- Barros VR, Doyle ME (2018) Low-level circulation and precipitation simulated by CMIP5 GCMs over southeastern South America. *Int J Climatol* 38:5476–5490 <https://doi.org/10.1002/joc.5740>
- Barthelmie RJ, Shepherd TJ, Aird JA, Pryor SC (2020) Power and wind shear implications of large wind turbine scenarios in the US Central Plains. *Energies* 13:4269 <https://doi.org/10.3390/en13164269>
- Bettolli ML, Penalba OC (2018) Statistical downscaling of daily precipitation and temperatures in southern La Plata Basin. *Int J Climatol* 38:3705–3722 <https://doi.org/10.1002/joc.5531>
- Blázquez J, Nuñez MN (2013) Analysis of uncertainties in future climate projections for South America: Comparison of WCRP-CMIP3 and WCRP-CMIP5 models. *Clim Dyn* 41:1039–1056 <https://doi.org/10.1007/s00382-012-1489-7>
- Boucher O, Denvil S, Levavasseur G, Cozic A, Caubel A, Foujols MA, Meurdesoif Y, Cadule P, Devilliers M, Ghattas J, Lebas N, Lurton T, Mellul L, Musat I, Mignot J, Cheruy F (2018) IPSL IPSL-CM6A-LR model output prepared for CMIP6 CMIP historical. Version 20180803. Earth System Grid Fed <https://doi.org/10.22033/ESGF/CMIP6.5195>
- Bracegirdle TJ, Shuckburgh E, Sallee J-B, Wang Z, Meijers AJS, Bruneau N, Phillips T, Wilcox LJ (2013) Assessment of surface winds over the Atlantic, Indian, and Pacific Ocean sectors of the Southern Ocean in CMIP5 models: Historical bias, forcing response, and state dependence. *J Geophys Res Atmos* 118:547–562 <https://doi.org/10.1002/jgrd.50153>
- Braga RAHW, Santos EB, de Barros MF (2021) Validação de dados de vento da reanálise ERA5-Land para estimativa de potencial eólico no estado do Rio de Janeiro. *Rev Bras Energ* 27:142–166 <https://doi.org/10.47168/rbe.v27i4.592>
- Cannon AJ, Sobie SR, Murdock TQ (2015) Bias correction of GCM precipitation by Quantile Mapping: How well do methods preserve changes in quantiles and extremes? *J Clim* 28:6938–6959 <https://doi.org/10.1175/JCLI-D-14-00754.1>
- Carvalho D, Rocha A, Costoya X, de Castro M, Gómez-Gesteira M (2021) Wind energy resource over Europe under CMIP6 future climate projections: What changes from CMIP5 to CMIP6. *Renew Sustain Energy Rev* 151:111594 <https://doi.org/10.1016/j.rser.2021.111594>
- Casanueva A, Herrera S, Fernández J, Gutiérrez JM (2016) Towards a fair comparison of statistical and dynamical downscaling in the framework of the EURO-CORDEX initiative. *Clim Change* 137:411–426 <https://doi.org/10.1007/s10584-016-1683-4>
- Chen L (2020) Impacts of climate change on wind resources over North America based on NA-CORDEX. *Renew Energy* 153:1428–1438 <https://doi.org/10.1016/j.renene.2020.02.090>
- Chou SC, Lyra A, Mourão C, Dereczynski C, Pilotto I, Gomes J, Bustamante J, Tavares P, Silva A, Rodrigues D, Campos D, Chagas D, Sueiro G, Siqueira G, Nobre P, Marengo J (2014) Evaluation of the Eta simulations nested in three global climate models. *Am J Clim Change* 3:438–454 <https://doi.org/10.4236/AJCC.2014.35039>
- Cohen J (1998) *Statistical power analysis for the behavioral sciences*, 2 ed. Lawrence Erlbaum Associates, Hillsdale <https://doi.org/10.4324/9780203771587>
- Coriolano TR, Signorelli NT, Junior JL, Moreira MAC, da Silva MG AJ (2022) Study of the temporal variation of offshore wind energy potential in southeast Brazil. *Ciência e Natura* 44:e6 <https://doi.org/10.5902/2179460X668814>
- Custódio RS (2009) *Energia Eólica para a Produção de Energia Elétrica*. Eletrobrás, Rio de Janeiro
- da Rocha RP, Morales CA, Cuadra SV, Ambrizzi T (2009) Precipitation diurnal cycle and summer climatology assessment over South America: An evaluation of Regional Climate Model version 3 simulations. *J Geophys Res Atmos* 114:D10. <https://doi.org/10.1029/2008JD010212> <https://doi.org/10.1029/2008JD010212>
- de Jong P, Barreto TB, Tanajura CAS, Kouloukoui D, Oliveira-Esquerre KP, Kiperstok A, Torres EA (2019) Estimating the impact of climate change on wind and solar energy in Brazil using a South American regional climate model. *Renew Energy* 141: 390–401 <https://doi.org/10.1016/j.renene.2019.03.086>

- de Oliveira Filho RA, Carvalho VSB, Reboita MS (2022) Evaluating the Global Forecast System (GFS) for energy management over Minas Gerais state (Brazil) against in-situ observations. *Atmosfera* 35:357-376 <https://doi.org/10.20937/ATM.52916>
- Deng Q, Alvarado R, Toledo E, Caraguay L (2020) Greenhouse gas emissions, non-renewable energy consumption, and output in South America: The role of the productive structure. *Environ Sci Pollut Res* 27:14477-14491 <https://doi.org/10.1007/s11356-020-07693-9>
- Dias CG, Reboita MS (2021) Assessment of CMIP6 simulations over tropical South America. *Rev Bras Geogr Fis* 14:1282-1295 <https://doi.org/10.26848/rbgf.v14.3.p1282-1295>
- Donk P, Van Uytven E, Willems P (2019) Statistical methodology for on-site wind resource and power potential assessment under current and future climate conditions: A case study of Suriname. *SN Appl Sci* 1:846 <https://doi.org/10.1007/s42452-019-0885-6>
- Döscher R, Acosta M, Alessandri A, Anthoni P, Arneith A, Arsouze T, Bergman T, Bernardello R, Boussetta S, Caron LP, Carver G, Castriello M, Catalano F, Cvijanovic I, Davini P, Dekker E, Doblaser-Reyes FJ, Docquier D, Echevarria P, Fladrich U, Fuentes-Franco R, Gröger M, von Hardenberg J, Hieronymus J, Karami MP, Keskinen JP, Koenigk T, Makkonen R, Massonet F, Ménégoz M, Miller PA, Moreno-Chamarro E, Nieradzki L, van Noije T, Nolan P, O'Donnell D, Ollinaho P, van der Oord G, Ortega P, Prims OT, Ramos A, Reerink T, Rousset C, Ruprich-Robert Y, Le Sager P, Schmith T, Schrödner R, Serva F, Sicardi V, Madsen MS, Smith B, Tian T, Tourigny E, Uotila P, Vancoppenolle M, Wang S, Wärlind D, Willén U, Wyser K, Yang S, Yepes-Arbós X, Zhang Q (2022) The EC-Earth3 Earth System Model for the Climate Model Intercomparison Project 6. *Geosci Model Dev* 15:2973-3020. <https://doi.org/10.5194/gmd-15-2973-2022>
- Elliott DL, Wendell LL, Gower GL (1991) An assessment of the available windy land area and wind energy potential in the contiguous United States (No. PNL-7789). Pacific Northwest Laboratory, Richland, WA, United States
- Emeksiz C, Cetin T (2019) In case study: Investigation of tower shadow disturbance and wind shear variations effects on energy production, wind speed and power characteristics. *Sustain Energy Technol Assess* 35:148-159 <https://doi.org/10.1016/j.seta.2019.07.004>
- EPE – Empresa de Pesquisa Energética (2021). Paper combined wind and solar auctions. <https://www.epe.gov.br/sites-en/publicacoes-dados-abertos/publicacoes/Paginas/Paper-Combined-Wind-and-Solar-Auctions.aspx>. Accessed 14 Sept 2022
- EPE – Empresa de Pesquisa Energética (2022). Ten-Year Energy Expansion Plan. <https://www.epe.gov.br/sites-en/publicacoes-dados-abertos/publicacoes/Paginas/PDE-2031---English-Version.aspx>. Accessed 14 Sept 2022
- Eyring V, Bony S, Meehl GA, Senior CA, Stevens B, Stouffler RJ, Taylor KE (2016) Overview of the global coupled model intercomparison project phase 6 (CMIP6) experimental design and organization. *Geosci Model Dev* 9:1937-1958 <https://doi.org/10.5194/gmd-9-1937-2016>
- Falasca S, Gandolfi I, Argentini S, Barnaba F, Casasanta G, Di Liberto L, Petenko I, Curci G (2021) Sensitivity of near-surface meteorology to PBL schemes in WRF simulations in a port-industrial area with complex terrain. *Atmos Res* 264:105824 <https://doi.org/10.1016/j.atmosres.2021.105824>
- Ferreira GWS, Reboita MS (2022) A new look into the South America precipitation regimes: Observation and forecast. *Atmosphere* 13:873 <https://doi.org/10.3390/atmos13060873>
- Fowler HJ, Blenkinsop S, Tebaldi C (2007) Linking climate change modelling to impacts studies: recent advances in downscaling techniques for hydrological modelling. *Int J Climatol* 27:1547-1578 <https://doi.org/10.1002/joc.1556>
- Garreaud RD (2009) The Andes climate and weather. *Adv Geosci* 22:3-11 <https://doi.org/10.5194/adgeo-22-3-2009>
- Garreaud RD, Falvey M (2009) The coastal winds off western subtropical South America in future climate scenarios. *Int J Climatol* 29:543-554 <https://doi.org/10.1002/joc.1716>
- Gernaat DEHJ, de Boer HS, Daioglou V, Yalaw SG, Müller C, van Vuuren DP (2021) Climate change impacts on renewable energy supply. *Nat Clim Change* 11:119-125 <https://doi.org/10.1038/s41558-020-00949-9>
- Gilliland JM, Keim BD (2018) Position of the South Atlantic Anticyclone and its impact on surface conditions across Brazil. *J Appl Meteorol Climatol* 57:535-553 <https://doi.org/10.1175/JAMC-D-17-0178.1>
- Gomes MSS, Paiva JMF, Moris VAS, Nunes AO (2019) Proposal of a methodology to use offshore wind energy on the southeast coast of Brazil. *Energy* 185:327-336 <https://doi.org/10.1016/j.energy.2019.07.057>
- Gonçalves AR, Pes MP, Pereira EB, Martins FR, Segundo EIC, Lyra AA (2010) Statistical downscaling of Eta-HadCM3 climate model for near surface wind assessment in Brazil. *American Geophysical Union (AGU) 91:26 Meet Am Suppl, Abstract GC21A-05*
- GWEC – Global Wind Energy Council (2018) State of the wind energy industry in Argentina 2018. <https://gwec.net/state-of-the-wind-energy-industry-in-argentina/>. Accessed 14 Sept 2022
- GWEC – Global Wind Energy Council (2019) Global Wind Report 2018. <https://gwec.net/global-wind-report-2019/>. Accessed 14 September 2022.
- GWEC – Global Wind Energy Council (2022) Global Wind Report 2022. <https://gwec.net/global-wind-report-2022/>. Accessed 14 Sept 2022
- Hahmann AN, García-Santiago O, Peña A (2022) Current and future wind energy resources in the North Sea according to CMIP6. *Wind Energy Sci Discuss*. In review. <https://doi.org/10.5194/wes-2022-52>
- Hamed KH (2008) Trend detection in hydrologic data: The Mann-Kendall trend test under the scaling hypothesis. *J Hydrol* 349:350-363
- Hersbach H, Bell B, Berrisford P, Hirahara S, Horányi A, Muñoz-Sabater J, Nicolas J, Peubey C, Radu R, Schepers D, Simmons A, Soci C, Abdalla S, Abellan X, Balsamo G, Bechtold P, Biavati G, Bidlot J, Bonavita M, de Chiara G, Dahlgren P, Dee D, Diamantakis M, Dragani R, Flemming J, Forbes R, Fuentes M, Geer A, Haimberger L, Healy S, Hogan RJ, Hólm E, Janisková M, Keeley S, Lalouaux P, Lopez P, Lupu C, Radnoti G, de Rosnay P, Rozum I, Vamborg F, Villaume S, Thépaut J.N. (2020) The ERA5 global reanalysis. *Q J R Meteorol Soc* 146:1999-2049 <https://doi.org/10.1002/qj.3803>
- Huang F, Xu Z, Guo W (2020) The linkage between CMIP5 climate models' abilities to simulate precipitation and vector winds. *Clim Dyn* 54:4953-4970 <https://doi.org/10.1007/s00382-020-05259-6>
- Icaza D, Borge-Diez D, Galindo SP (2022) Analysis and proposal of energy planning and renewable energy plans in South America: Case study of Ecuador. *Renew Energy* 182:314-342 <https://doi.org/10.1016/j.renene.2021.09.126>
- IPCC – Intergovernmental Panel on Climate Change (2021) Climate change 2021: The physical science basis. In: Masson-Delmotte V, Zhai P, Pirani A, Connors SL et al. (eds) Contribution of working group I to the Sixth Assessment Report of the Intergovernmental Panel on Climate Change. Cambridge University Press. <https://www.ipcc.ch/report/ar6/wg1/#FullReport>. Accessed 10 Sept 2022
- IRENA – International Renewable Energy Agency (2019) Global Energy Transformation: a Roadmap to 2050. <https://www.irena.org/publications/2019/Apr/Global-energy-transformation-A-roadmap-to-2050-2019Edition>. Accessed 14 Sept 2022
- Jourdir B (2020) Evaluation of ERA5, MERRA-2, COSMO-REA6, NEWA and AROME to simulate wind power production

- in Brazil. *Renew Energy* 49:107-110 <https://doi.org/10.1016/j.renene.2012.01.053>
- Press WH, Teukolsky SA, Vetterling WT, Flannery BP (2007) *Numerical Recipes in C: The Art of Scientific Computing*, 1st ed.; Cambridge University Press: Cambridge
- Pryor SC, Barthelmie RJ (2021) A global assessment of extreme wind speeds for wind energy applications. *Nat Energy* 6:268-276 <https://doi.org/10.1038/s41560-020-00773-7>
- Qian H, Zhang R (2021) Future changes in wind energy resource over the Northwest Passage based on the CMIP6 climate projections. *Int J Energy Res* 45:920-937 <https://doi.org/10.1002/er.5997>
- Reboita MS, Gan MA, da Rocha RP, Ambrizzi T (2010) Regimes de precipitação na América do Sul: Uma revisão bibliográfica. *Rev Bras Meteorol* 25:185-204 <https://doi.org/10.1590/S0102-77862010000200004>
- Reboita MS, da Rocha RP, Dias CG, Ynoue RY (2014) Climate projections for South America: RegCM3 driven by HadCM3 and ECHAM5. *Adv Meteorol* 2014:376738 <https://doi.org/10.1155/2014/376738>
- Reboita MS, Dutra LMM, Dias CG (2016) Diurnal cycle of precipitation simulated by RegCM4 over South America: present and future scenarios. *Clim Res* 70:39-55 <https://doi.org/10.3354/cr01416>
- Reboita MS, Amaro TR, de Souza MR (2018) Winds: Intensity and power density simulated by RegCM4 over South America in present and future climate. *Clim Dyn* 51:187-205 <https://doi.org/10.1007/s00382-017-3913-5>
- Reboita MS, Ambrizzi T, Silva BA, Pinheiro RF, da Rocha RP (2019) The South Atlantic Subtropical Anticyclone: Present and future climate. *Front Earth Sci* 7:8 <https://doi.org/10.3389/feart.2019.00008>
- Reboita MS, Kiani RS, Ali S, Khan T (2021) Projections of wind power density in Pakistan and adjacent regions. *Clim Res* 85:177-192 <https://doi.org/10.3354/cr01679>
- Reboita MS, Teodoro TA, Ferreira GWS, Souza CA (2022) Ciclo de vida do sistema de monção da América do Sul: Clima presente e futuro. *Rev Bras Geogr Fis* 15:343-358 <https://doi.org/10.26848/rbfg.v15.1.p343-358>
- Riahi K, Van Vuuren DP, Kriegler E, Edmonds J, O'Neill BC, Fujimori S, Bauer N, Calvin K, Dellink R, Fricko O, Lutz W, Popp A, Cuaresma JC, Samir KC, Leimbach M, Jiang L, Kram T, Rao S, Emmerling J, Ebi K, Hasegawa T, Havlik P, Humenöder F, da Silva LA, Smith S, Stehfest E, Bosetti V, Eom J, Gernaat D, Masui T, Rogelj J, Strefler J, Drouet L, Krey V, Luderer G, Harmsen M, Takahashi K, Baumstark L, Doelman JC, Kainuma M, Klimont Z, Marangoni G, Lotze-Campen H, Obersteiner M, Tabeau A, Tavoni M (2017) The Shared Socioeconomic Pathways and their energy, land use, and greenhouse gas emissions implications: A review. *Glob Environ Change* 42:153-168 <https://doi.org/10.1016/j.gloenvcha.2016.05.009>
- Ruffato-Ferreira V, Barreto RC, Oscar Júnior A, Silva WL, Viana DB, Nascimento JAS, Freitas MAV (2017) A foundation for the strategic long-term planning of the renewable energy sector in Brazil: Hydroelectricity and wind energy in the face of climate change scenarios. *Renew Sustain Energy Rev* 72:1124-1137 <https://doi.org/10.1016/j.rser.2016.10.020>
- Rupp DE, Abatzoglou JT, Hegewisch KC, Mote PW (2013) Evaluation of CMIP5 20th century climate simulations for the Pacific Northwest USA. *J Geophys Res Atmos* 118:10884-10906 <https://doi.org/10.1002/jgrd.50843>
- Santos-Alamillos FJ, Pozo-Vázquez D, Ruiz-Arias JÁ, Lara-Fanego V, Tovar-Pescador J (2013) Analysis of WRF model wind estimate sensitivity to physics parameterization choice and terrain representation in Andalusia (Southern Spain). *J Appl Meteorol Climatol* 52:1592-1609 <https://doi.org/10.1175/JAMC-D-12-0204.1>
- Sawadogo W, Reboita MS, Faye A, da Rocha RP, Odoulami RC, Olusegun CF, Adeniyi MO, Abiodun BJ, Sylla MB, Diallo I, Coppola E, Giorgi F (2021) Current and future potential of solar and wind energy over Africa using the RegCM4 CORDEX-CORE ensemble. *Clim Dyn* 57:1647-1672 <https://doi.org/10.1007/s00382-020-05377-1>
- Seth A, Rojas M, Rauscher SA (2010) CMIP3 projected changes in the annual cycle of the South America monsoon. *Clim Change* 98:331-357 <https://doi.org/10.1007/s10584-009-9736-6>
- Silva AR, Pimenta FM, Assireu AT, Spyrides MHC (2016) Complementarity of Brazil's hydro and offshore wind power. *Renew Sustain Energy Rev* 56:413-427 <https://doi.org/10.1016/j.rser.2015.11.045>
- Silva NP, Crespo NM, Kaufmann CLG, Lima JAM, Andriani M, Camargo R, da Rocha RP (2022) Adjustment of extreme wind speed in regional climate downscaling over southwestern South Atlantic. *Int J Climatol* 42:9994-10008 <https://doi.org/10.1002/joc.7876>
- Silva ML, Oliveira CP, Silva CMS, Araújo JM (2023) Dynamic downscaling of climate simulations and projected changes in tropical South America using RegCM4.7. *Int J Climatol Early View* <https://doi.org/10.1002/joc.8035>
- Solman SA, Blázquez J (2019) Multiscale precipitation variability over South America: Analysis of the added value of CORDEX RCM simulations. *Clim Dyn* 53:1547-1565 <https://doi.org/10.1007/s00382-019-04689-1>
- Solman SA, Bettolli ML, Doyle ME, Olmo ME, Feijoo M, Martínez D, Blázquez J, Balmaceda Huarte R (2021) Evaluation of multiple downscaling tools for simulating extreme precipitation events over southeastern South America: A case study approach. *Clim Dyn* 57:1241-1264 <https://doi.org/10.1007/s00382-021-05770-4>
- Sulca J, Vuille M, Timm OE, Dong B, Zubieta R (2021) Empirical-statistical downscaling of austral summer precipitation over South America, with a focus on the Central Peruvian Andes and the Equatorial Amazon Basin. *J Appl Meteorol Climatol* 60:65-85 <https://doi.org/10.1175/JAMC-D-20-0066.1>
- Sweeney CP, Lynch P, Nolan P (2013) Reducing errors of wind speed forecasts by an optimal combination of post-processing methods. *Meteorol Appl* 20:32-40 <https://doi.org/10.1002/met.294>
- Tang G, Clark MP, Papalexioiu SM (2022) EM-Earth: The Ensemble Meteorological dataset for planet Earth. *Bull Am Meteorol Soc* 103:E996-E1018 <https://doi.org/10.1175/BAMS-D-21-0106.1>
- Tatebe H, Watanabe M (2018) MIROC MIROC6 model output prepared for CMIP6 CMIP historical. Version 20181212. Earth Syst Grid Fed <https://doi.org/10.22033/ESGF/CMIP6.5603>
- Tavares LFA, Shadman M, Assad LPF, Silva C, Landau L, Estefen SF (2020) Assessment of the offshore wind technical potential for the Brazilian Southeast and South regions. *Energy* 196:117097 <https://doi.org/10.1016/j.energy.2020.117097>
- Therkildsen OR, Balsby TJS, Kjeldsen JP, Due Nielsen R, Bladt J, Fox AD (2021) Changes in flight paths of large-bodied birds after construction of large terrestrial wind turbines. *J Environ Manag* 290:112647 <https://doi.org/10.1016/j.jenvman.2021.112647>
- Torres RR, Marengo JA (2014) Climate change hotspots over South America: From CMIP3 to CMIP5 multi-model datasets. *Theor Appl Climatol* 117:579-588 <https://doi.org/10.1007/s00704-013-1030-x>
- Tram-Anh Q, Ngo-Duc T, Espagne E, Trinh-Tuan L (2023) A 10-km CMIP6 downscaled dataset of temperature and precipitation for historical and future Vietnam climate. *Sci Data* 10:257 <https://doi.org/10.1038/s41597-023-02159-2>
- Viviescas C, Lima L, Diuana FA, Vasquez E, Ludovique C, Silva GN, Huback V, Magalar L, Szklo A, Lucena AFP, Schaeffer R, Paredes JR (2019) Contribution of variable renewable energy to increase energy security in Latin America: Complementarity and climate change impacts on wind and solar resources. *Renew*

Assessment of the wind power density over South America simulated by CMIP6 models in the present...

- Sustain Energy Rev 113:109232 <https://doi.org/10.1016/j.rser.2019.06.039>
- Wallace JM, Hobbs PV (2006) Atmospheric science: An introductory survey, 2nd ed. Academic Press, Cambridge
- Wang B, Jin C, Liu J (2020) Understanding future change of global monsoons projected by CMIP6 models. *J Clim* 33:6471–6489 <https://doi.org/10.1175/JCLI-D-19-0993.1>
- Washburn C, Pablo-Romero M (2019) Measures to promote renewable energies for electricity generation in Latin American countries. *Energy Policy* 128:212–222 <https://doi.org/10.1016/j.enpol.2018.12.059>
- Wieners KH, Giorgetta M, Jungclaus J, Reick C, Esch M, Bittner M, Legutke S, Schupfner M, Wachsmann F, Gayler V, Haak H, de Vrese P, Raddatz T, Mauritsen T, von Storch JS, Behrens J, Brovkin V, Claussen M, Crueger T, Fast I, Fiedler S, Hagemann S, Hohenegger C, Jahns T, Kloster S, Kinne S, Lasslop G, Kornbluh L, Marotzke J, Matei D, Meraner K, Mikolajewicz U, Modali K, Müller W, Nabel J, Notz D, Peters-von Gehlen K, Pincus R, Pohlmann H, Pongratz J, Rast S, Schmidt H, Schnur R, Schulzweida U, Six K, Stevens B, Voigt A, Roeckner E (2019) MPI-M MPI-ESM1.2-LR model output prepared for CMIP6 CMIP historical. Version 20190710. Earth Syst Grid Fed <https://doi.org/10.22033/ESGF/CMIP6.6595>
- Wiser R, Rand J, Seel J, Beiter P, Baker E, Lantz E, Gilman P (2021) Expert elicitation survey predicts 37% to 49% declines in wind energy costs by 2050. *Nat Energy* 6:555–565 <https://doi.org/10.1038/s41560-021-00810-z>
- Wu H, Lei H, Lu W, Liu Z (2022) Future changes in precipitation over the upper Yangtze River basin based on bias correction spatial downscaling of models from CMIP6. *Environ Res Commun* 4:045002 <https://doi.org/10.1088/2515-7620/ac620e>
- Xu Z, Han Y, Tam C-Y, Yang Z-L, Fu C (2021) Bias-corrected CMIP6 global dataset for dynamical downscaling of the historical and future climate (1979–2100). *Sci Data* 8:293 <https://doi.org/10.1038/s41597-021-01079-3>
- Yu E, Bai R, Chen X, Shao L (2022) Impact of physical parameterizations on wind simulation with WRF V3.9.1.1 under stable conditions at planetary boundary layer gray-zone resolution: A case study over the coastal regions of North China. *Geosci Model Dev* 15:8111–8134 <https://doi.org/10.5194/gmd-15-8111-2022>
- Yukimoto S, Koshiro T, Kawai H, Oshima N, Yoshida K, Urakawa S, Tsujino H, Deushi M, Tanaka T, Hosaka M, Yoshimura H, Shindo E, Mizuta R, Ishii M, Obata A, Adachi Y (2019) MRI MRI-ESM2.0 model output prepared for CMIP6 CMIP historical. Version 20190222. Earth Syst Grid Fed <https://doi.org/10.22033/ESGF/CMIP6.6842>
- Zhang S, Li X (2021) Future projections of offshore wind energy resources in China using CMIP6 simulations and a deep learning-based downscaling method. *Energy* 217:119321 <https://doi.org/10.1016/j.energy.2020.119321>
- Zhang MZ, Xu Z, Han Y, Guo W (2022) Evaluation of CMIP6 models toward dynamical downscaling over 14 CORDEX domains. *Clim Dyn* <https://doi.org/10.1007/s00382-022-06355-5>
- Zheng CW, Li XY, Luo X, Chen X, Qian YH, Zhang ZH, Gao ZS, Du ZB, Gao YB, Chen YG (2019) Projection of future global offshore wind energy resources using CMIP6 data. *Atmos-Ocean* 57:134–148 <https://doi.org/10.1080/07055900.2019.1624497>
- Zhou J, Lau KM (1998) Does a monsoon climate exist over South America? *J Clim* 11:1020–1040 [https://doi.org/10.1175/1520-0442\(1998\)011%3C1020:DAMCEO%3E2.0.CO;2](https://doi.org/10.1175/1520-0442(1998)011%3C1020:DAMCEO%3E2.0.CO;2)

Publisher's Note Springer Nature remains neutral with regard to jurisdictional claims in published maps and institutional affiliations.

Springer Nature or its licensor (e.g. a society or other partner) holds exclusive rights to this article under a publishing agreement with the author(s) or other rightsholder(s); author self-archiving of the accepted manuscript version of this article is solely governed by the terms of such publishing agreement and applicable law.

Supplementary Material

Assessment of the wind power density over South America simulated by CMIP6 models in the present and future climate

Ferreira, G. W. S.; Reboita, M. S.; Ribeiro, J. G. M.; Carvalho, V. S. B.; Santiago, M. E. V.; Silva, P. L. S. S.; Baldoni, T. C.; Souza, C. A.

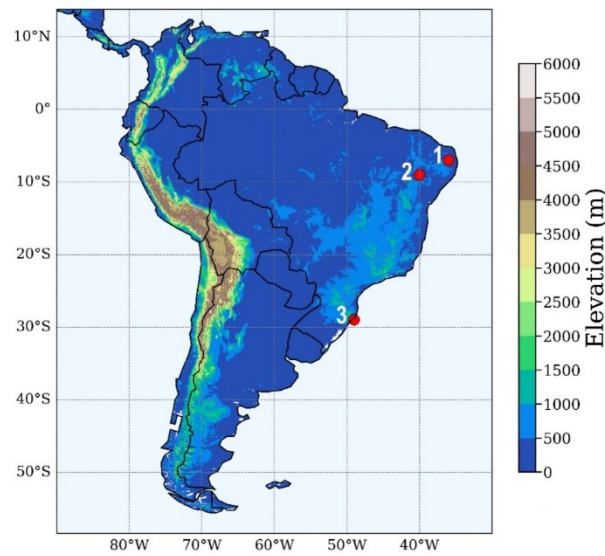


Fig. S1 Illustration of the study area with elevation (m). Red dots correspond to the locations of the weather stations from the SONDA network used to compare the ERA5 reanalysis and BCSD ensemble simulations with observational data. Source: United States Geological Survey-Earth Resources Observation System (EROS) Center.

Table S1. Information on the SONDA network stations used in the study.

Number	Station	Federal Unit	Heights of Wind (m)	Latitude	Longitude	Altitude (m)
1	São João do Cariri	PB	25 / 50	07° 22' 54'' S	36° 31' 38'' W	486
2	Petrolina	PE	10 / 25 / 50	09° 04' 08'' S	40° 19' 11'' W	387
3	Sombrio	SC	10	29° 05' 44'' S	49° 48' 48'' W	15

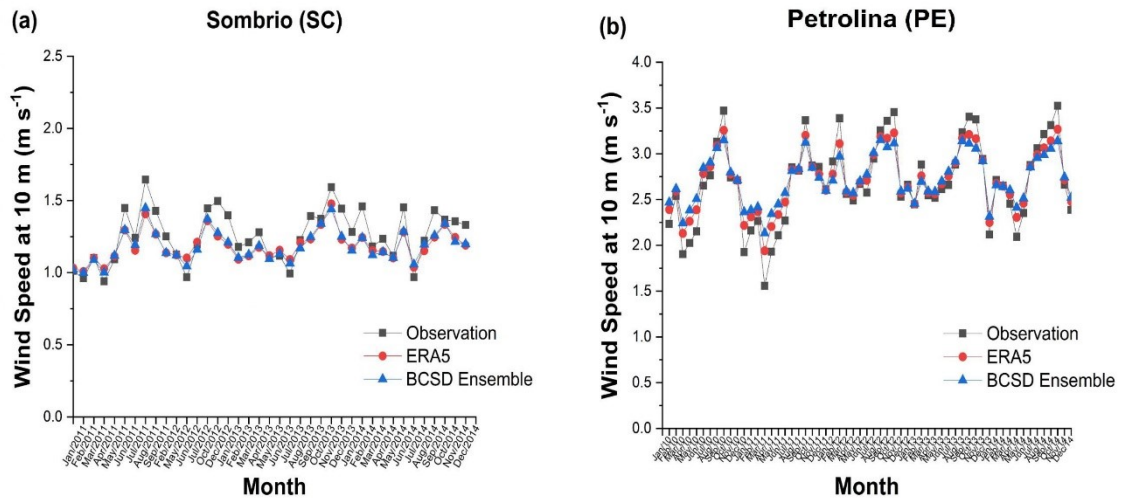


Fig. S2 Time series of wind speed (m s⁻¹) at 10 m obtained by ERA5 (red line), BCSD ensemble (blue line), and SONDA network observations (gray line) for the locations of Sombrio (a) and Petrolina (b), for the periods Jan/2011 to Dec/2014 and Jan/2010 to Dec/2014, respectively.

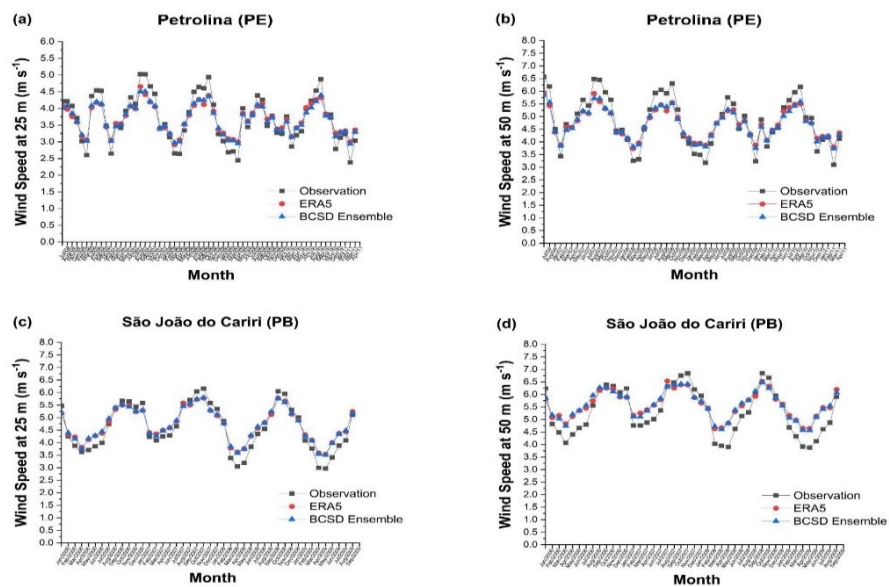


Fig. S3 Time series of wind speed (m s⁻¹) at 25 and 50 m obtained by vertical extrapolation with ERA5 (red line) and BCSD ensemble (blue line), and SONDA network observations (gray line) for the locations of Petrolina (a,b) and São João do Cariri (c,d), for the periods Jul/2004 to Apr/2011 and Jan/2006 to Sep/2009, respectively.

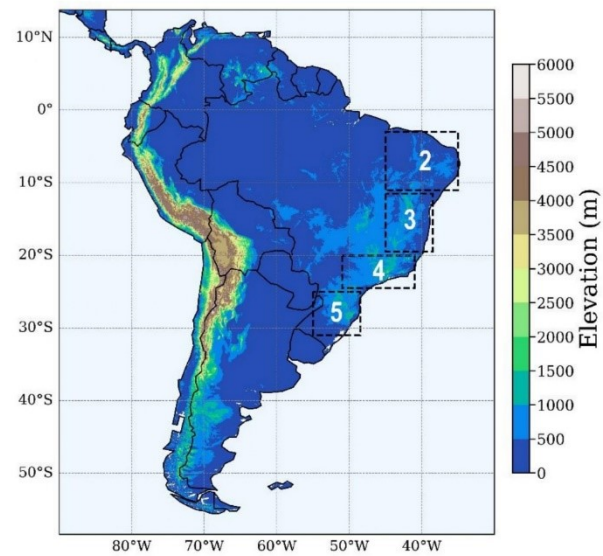


Fig. S4 Illustration of the study area with elevation (m). Black rectangles correspond to the regions used to evaluate the seasonal cycle of wind speed and WPD at 100 m obtained by the BCSD ensemble. Source: United States Geological Survey-Earth Resources Observation System (EROS) Center.

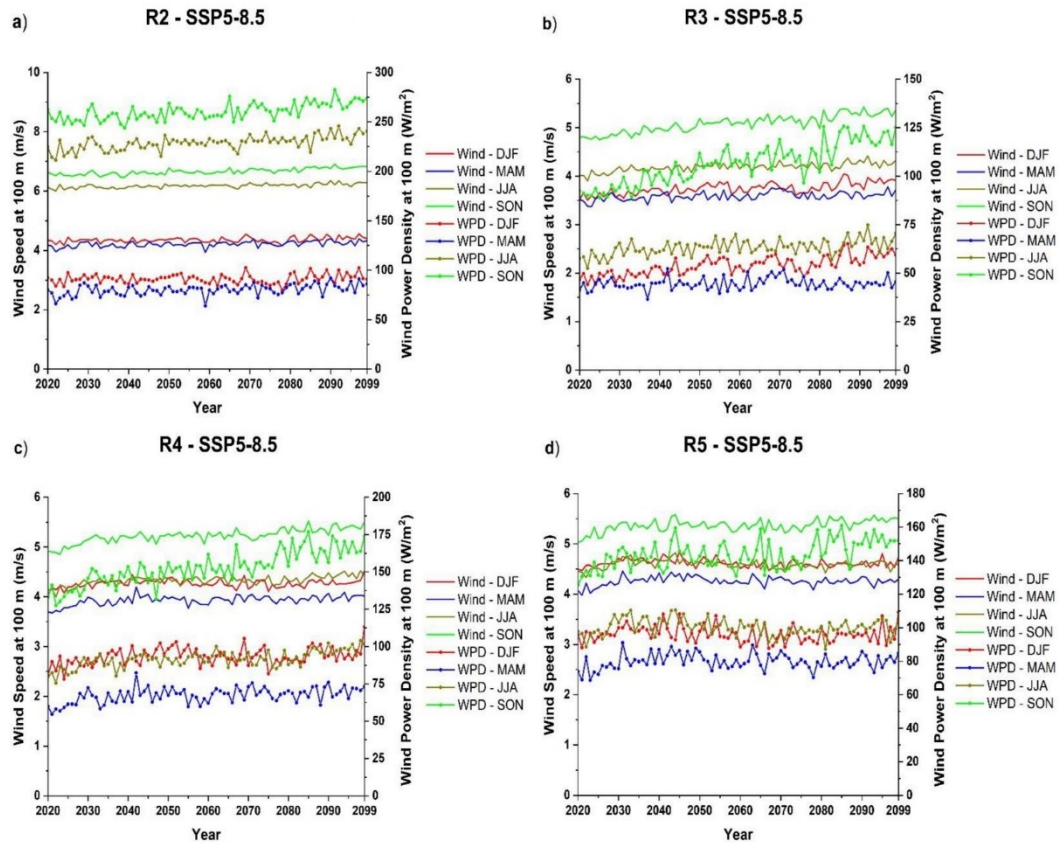


Fig. S5 Time series of the seasonal cycle of wind speed (m s^{-1}) and WPD (W m^{-2}) at 100 m obtained by the BCSO ensemble for four South America subdomains for the 2020-2099 period, under the SSP5-8.5 scenario.

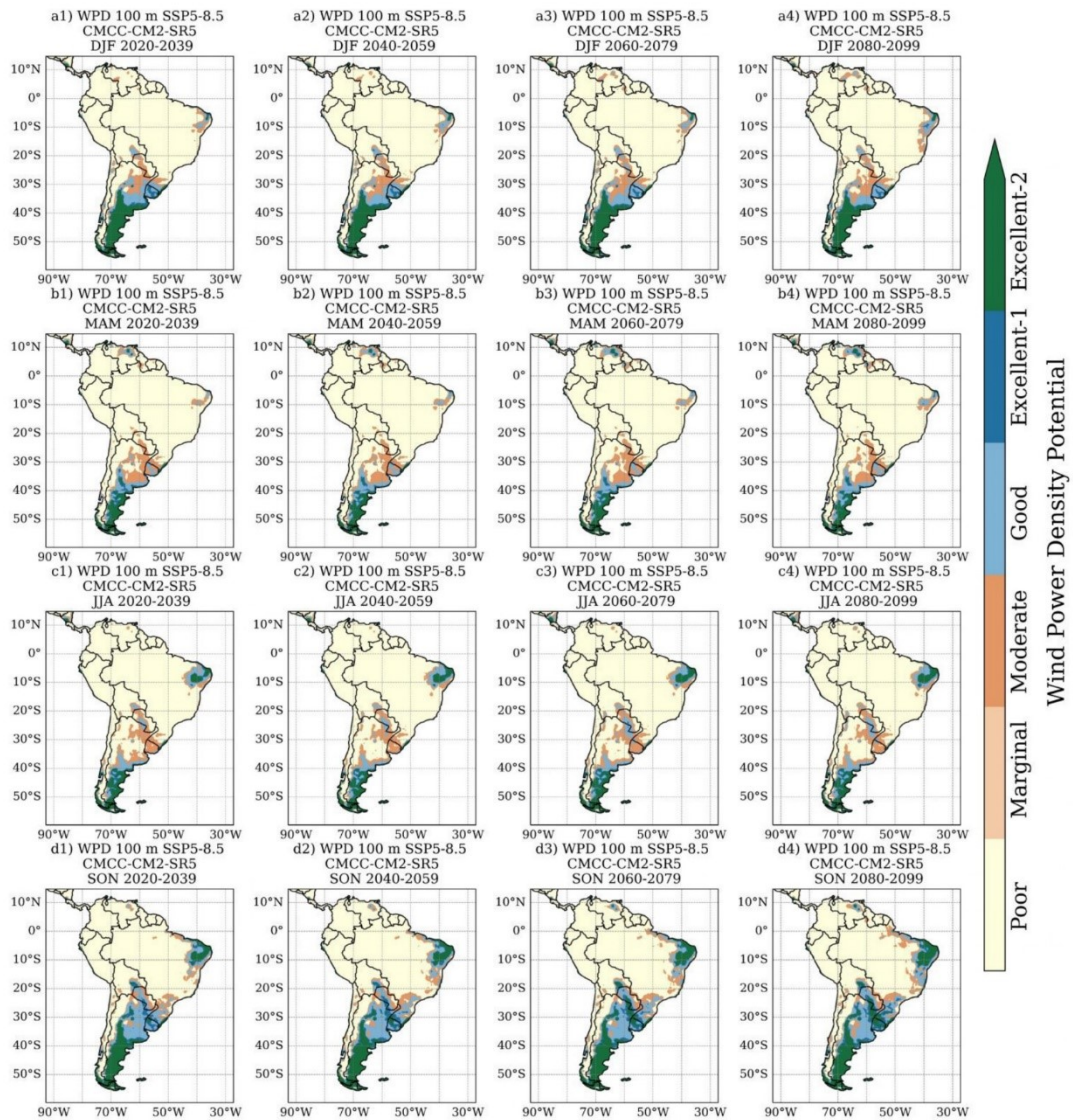


Fig. S6 Seasonal classification of areas suitable for wind power generation at the 100 m height under the SSP5-8.5 emission scenario during 2020-2099, obtained by the CMCC-CM2-SR5 model.

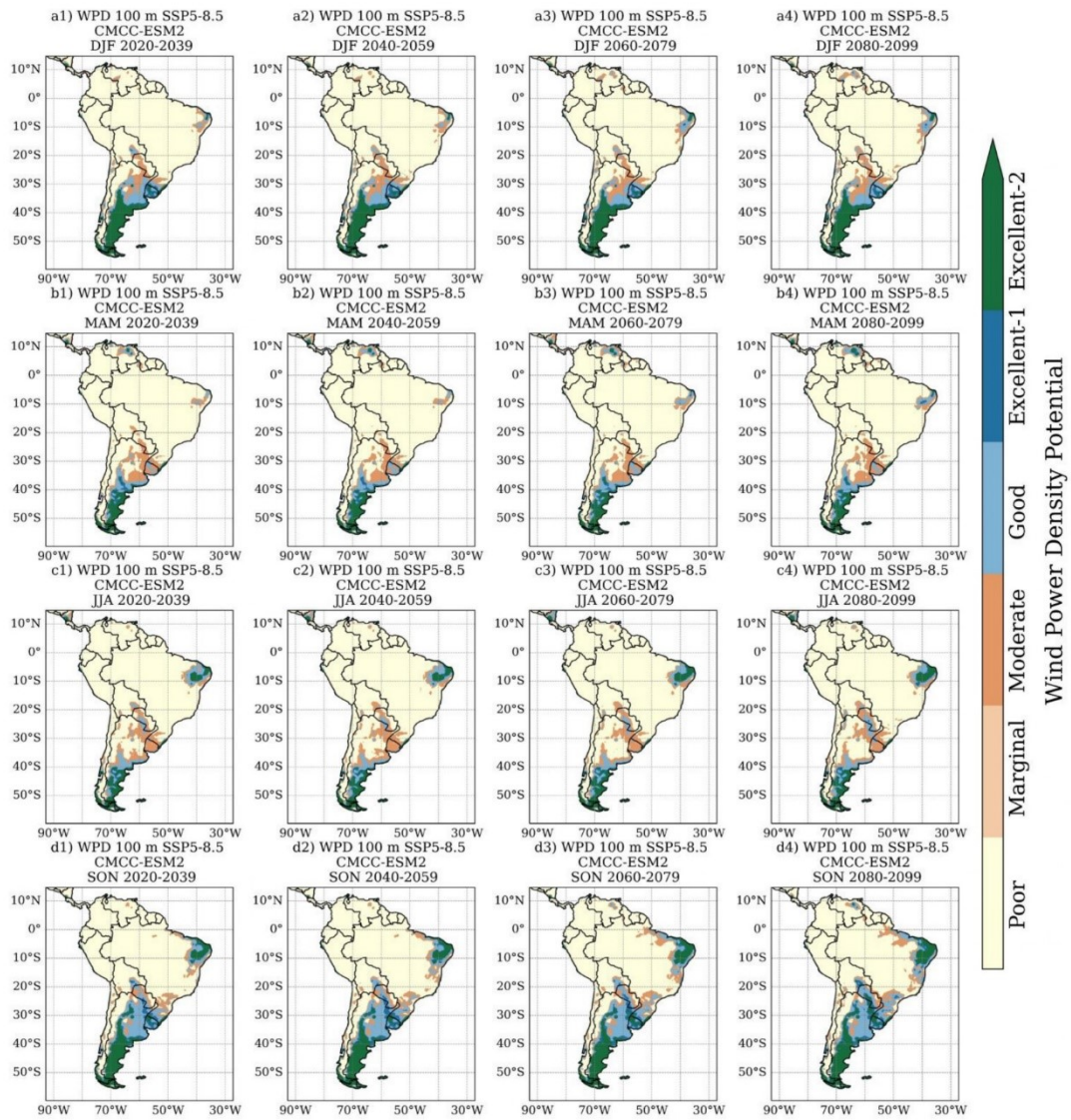


Fig. S7 Similar to Figure S6, except for the CMCC-ESM2 model.

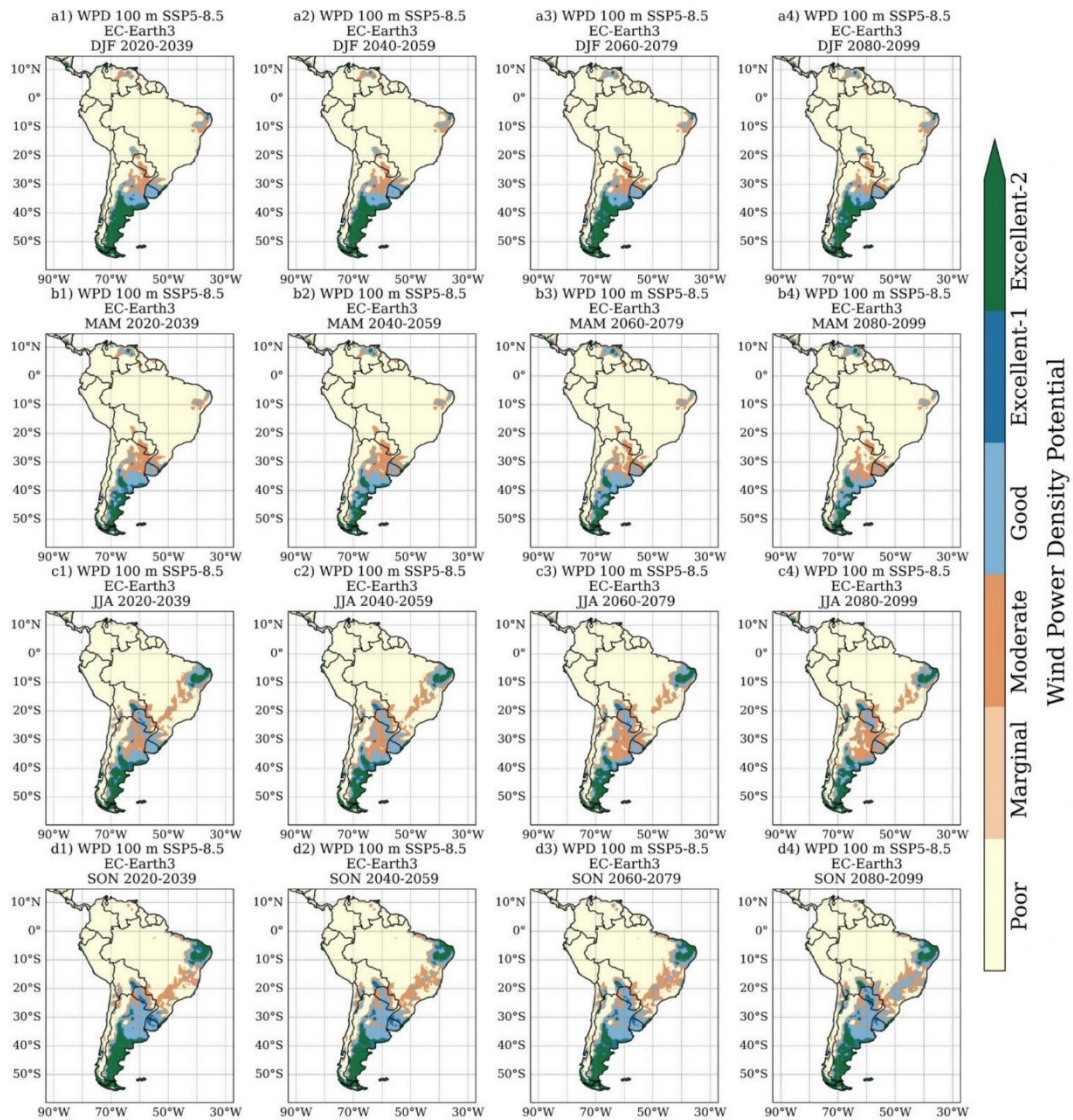


Fig. S8 Similar to Figure S6, except for the EC-Earth3 model.

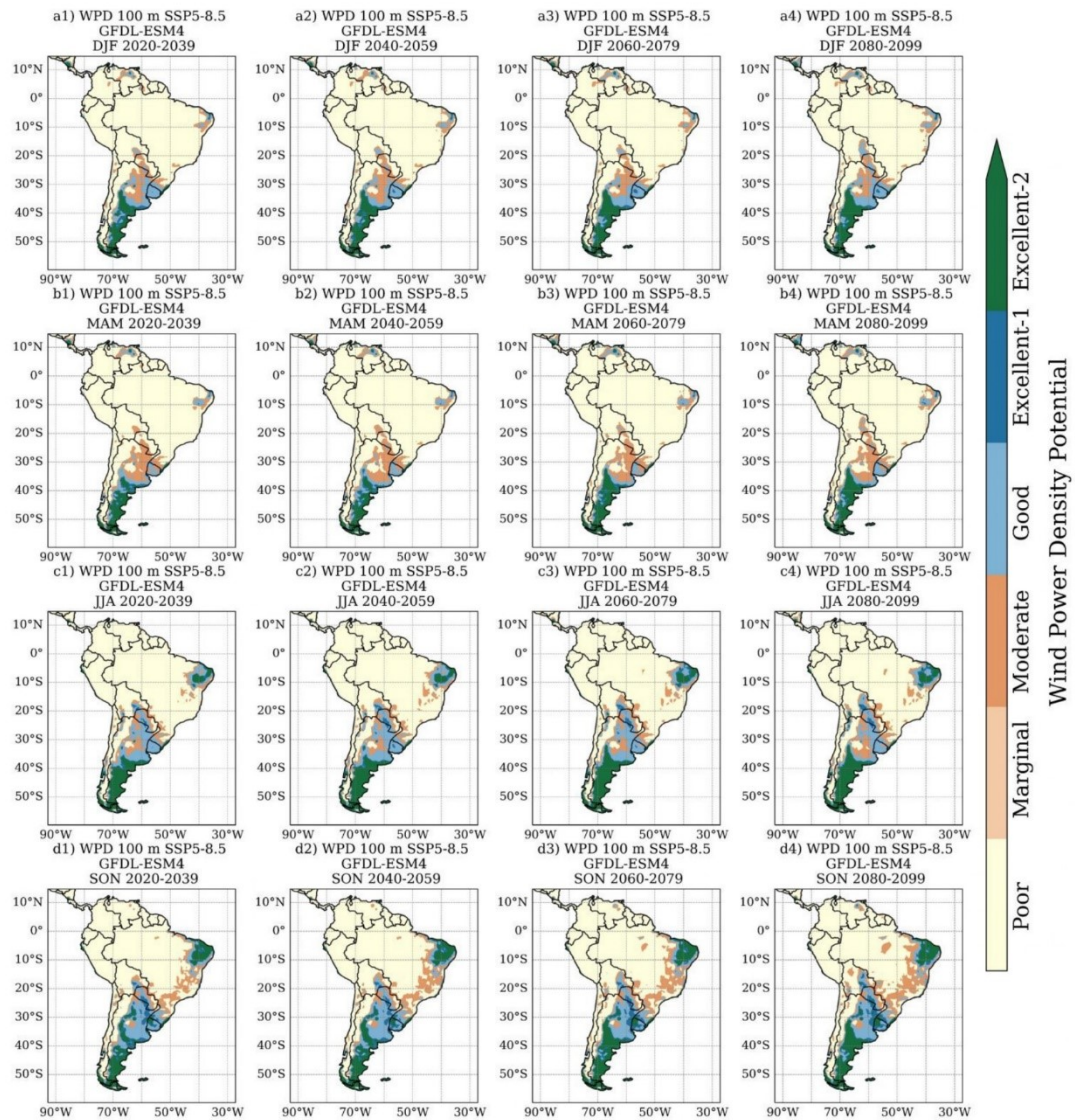


Fig. S9 Similar to Figure S6, except for the GFDL-ESM4 model.

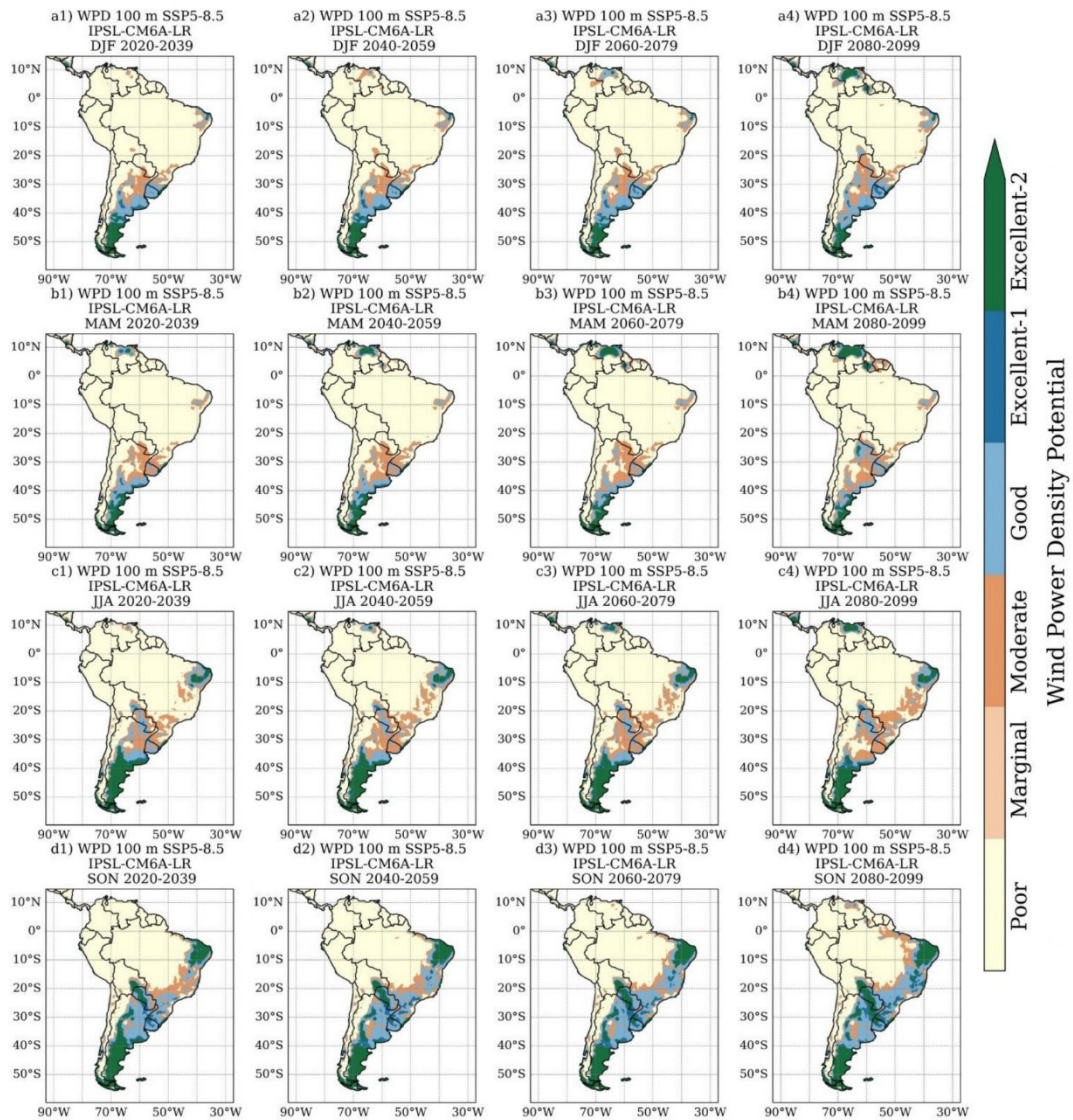


Fig. S10 Similar to Figure S6, except for the IPSL-CM6A-LR model.

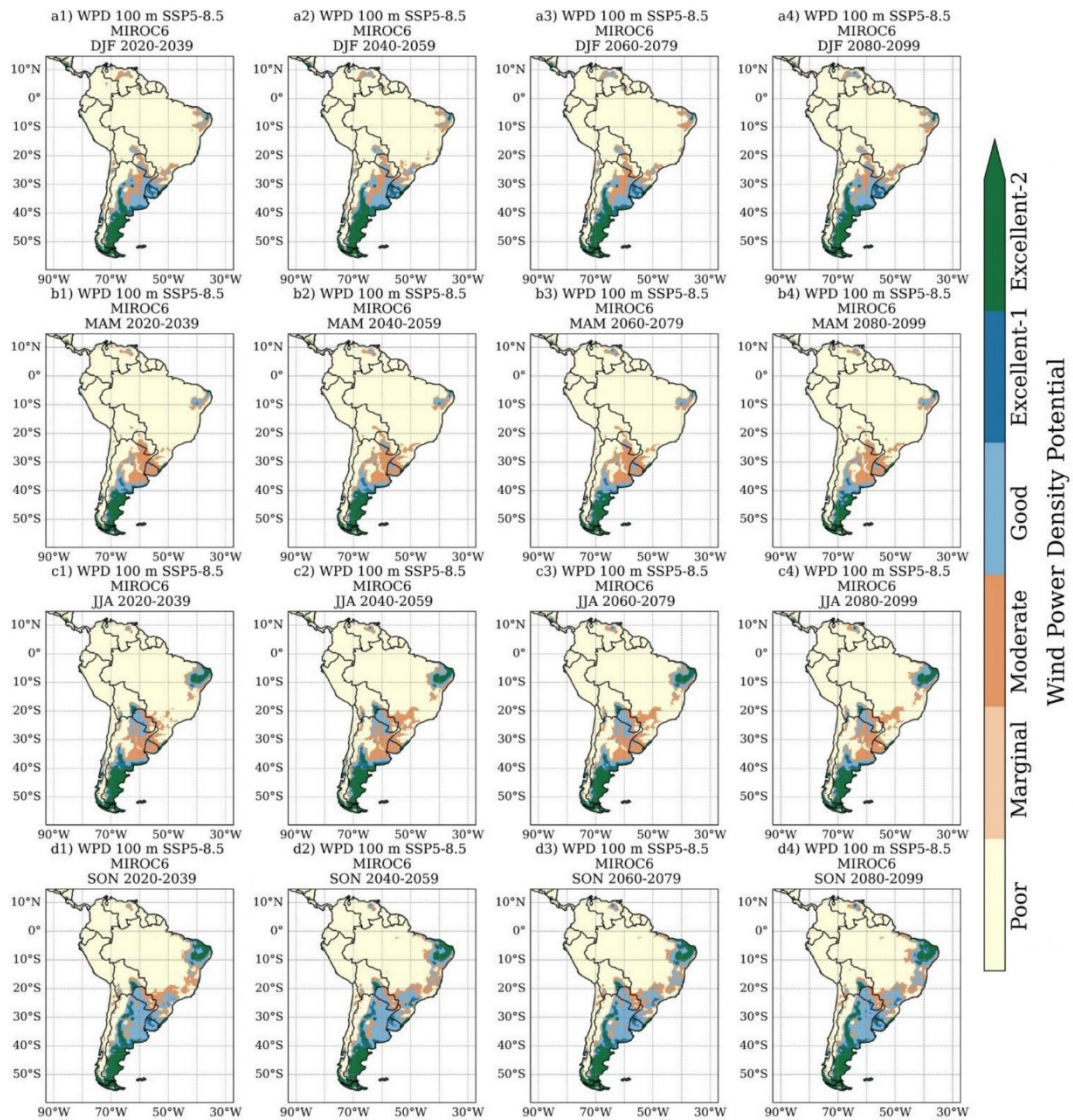


Fig. S11 Similar to Figure S6, except for the MIROC6 model.

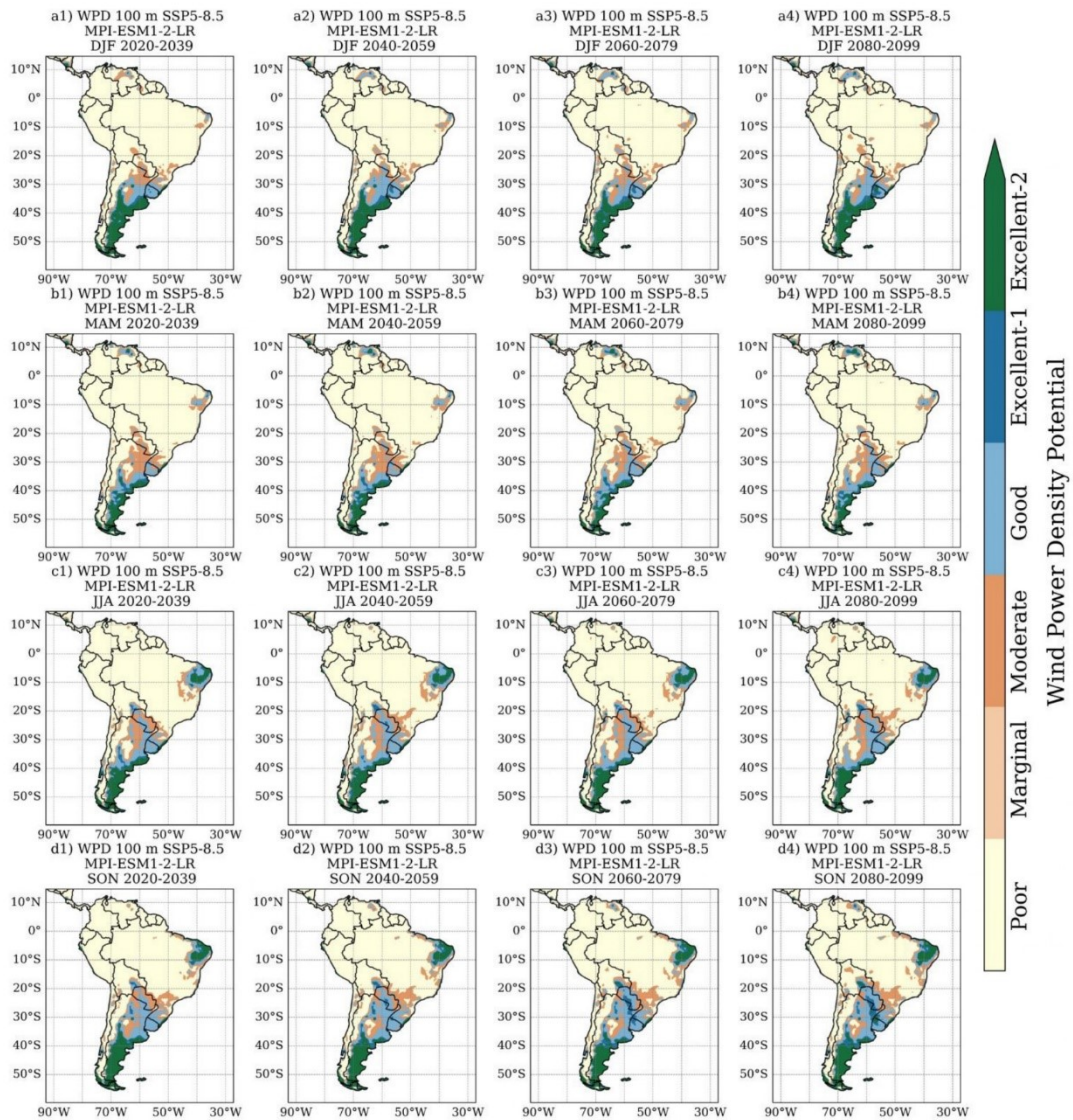


Fig. S12 Similar to Figure S6, except for the MPI-ESM1-2-LR model.

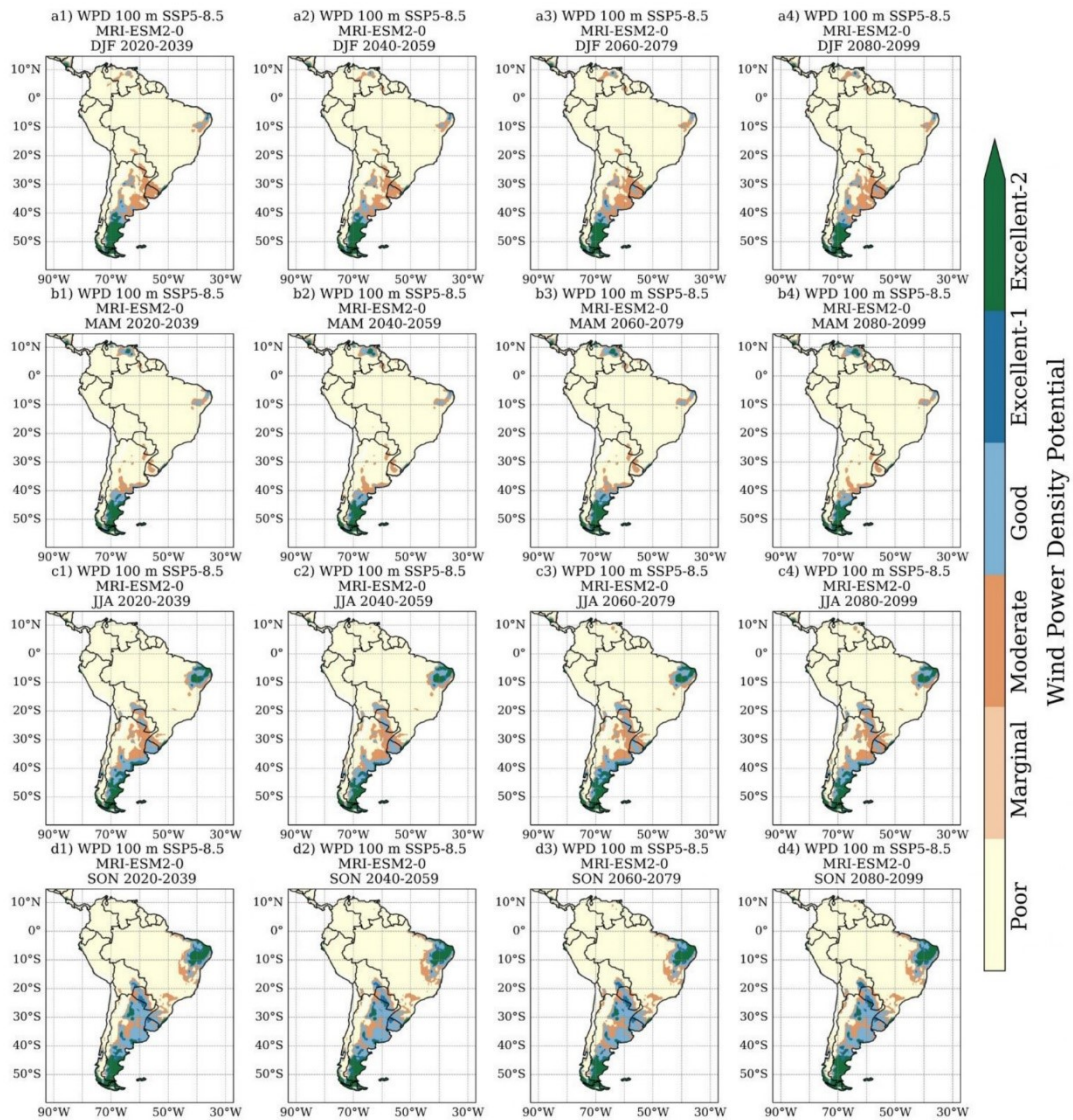


Fig. S13 Similar to Figure S6, except for the MRI-ESM2-0 model.

Acknowledgments: The authors thank the National Environmental Data Organization (SONDA) for the data used in this study. Observational data from the SONDA network is available at <http://sonda.cest.inpe.br/index.html>



7. Assessment of the solar energy potential over South America estimated by CMIP6 models in the present and future climate

23/02/2025, 18:36

E-mail de Universidade Federal de Itajubá - Permission to Include Published Article in Doctoral Dissertation



Glauber Willian de S. Ferreira <glauber_ferreira@unifei.edu.br>

Permission to Include Published Article in Doctoral Dissertation

lesley@bilpubgroup.com <lesley@bilpubgroup.com>
Para: glauber_ferreira <glauber_ferreira@unifei.edu.br>
Cc: glauber_ferreira <glauber_ferreira@unifei.edu.br>

21 de novembro de 2024 às 05:49

Dear Dr. Glauber Ferreira,

Thanks for your new email. This is Lesley Lu.

I would like to inform you that our Journal of Environmental & Earth Sciences publishes accepted manuscripts under the **Creative Commons Attribution-NonCommercial 4.0 International License (CC BY-NC 4.0)**. For non-commercial purposes, anyone may copy, redistribute material, remix, transform and construct material in any media or format, provided that the terms of the license are observed and the original source is properly cited.

Copyright for all articles published in the Journal of Environmental & Earth Sciences belongs to the author. The authors also grant permission to the publisher to publish, reproduce, distribute and transmit the articles.

If you have any other questions, please feel free to contact me.

Looking forward to receiving your new response.

Best regards,
Lesley Lu
Journal of Environmental & Earth Sciences
ISSN: 2661-3190



lesley@bilpubgroup.com

ARTICLE

Assessment of the Solar Energy Potential over South America Estimated by CMIP6 Models in the Present and Future ClimateGlauber W. S. Ferreira^{*}, Michelle S. Reboita[†], João Gabriel M. Ribeiro[‡]

Natural Resources Institute, Federal University of Itajubá, Itajubá, Minas Gerais, 37500–903, Brazil

ABSTRACT

Developing the renewable energy matrix of South America (SA) is fundamental for sustainable socioeconomic growth and mitigating climate change's adverse effects. Thus, this study estimates changes in SA's solar irradiance and solar power potential using data from eight global climate models (GCMs) belonging to the Coupled Model Intercomparison Project—Phase 6 (CMIP6). Applying statistical downscaling and bias correction with the Quantile Delta Mapping (QDM) technique, we evaluate projected changes in the Concentrated Solar Power (CSP) and Photovoltaic Power (PVP) outputs under different future climate scenarios (SSP2-4.5 and SSP5-8.5). Historical simulations (1995–2014) are validated using ERA5 reanalysis and CLARA-A3 satellite observations. The QDM method reduces the models' systematic biases, decreasing the ensemble's errors by 50% across SA throughout the year. Regarding future decades (2020–2099), the CMIP6 ensemble shows spatial and seasonal variability in solar generation. For CSP, estimates suggest that regions traditionally favorable to solar energy generation (such as the Brazilian Northeast and portions of Chile) will maintain their suitable conditions during the 21st century, projecting a potential 1–6% increase (particularly under the SSP5-8.5 scenario in southern Chile and most of Brazil). Concerning PVP generation, the CMIP6 ensemble projects a rise of 1–4% (mainly under the SSP5-8.5 scenario in the Amazonia, Midwest, and Southeast Brazilian sectors). Moreover, trend analyses projected individually by the CMIP6 GCMs converge on an increasing PVP, mainly in Brazil's Amazonia and Midwest regions. In contrast, for South Brazil, approximately 84% of the projections show a negative trend (or no trend), evidencing unfavorable or uncertain conditions for solar generation development in the region. Despite the data and processes' inherent limitations, this study yields a first analysis of statistically downscaled projections from CMIP6 for solar power generation in South America, providing valuable information for energy sector decision-makers.

Keywords: Solar power; CMIP6; Climate change; Statistical downscaling; South America

*CORRESPONDING AUTHOR:

Glauber W. S. Ferreira, Natural Resources Institute, Federal University of Itajubá, Itajubá, Minas Gerais, 37500–903, Brazil; Email: glauber_ferreira@unifei.edu.br

ARTICLE INFO

Received: 25 April 2024 | Revised: 30 May 2024 | Accepted: 13 June 2024 | Published Online: 4 July 2024

DOI: <https://doi.org/10.30564/jees.v6i2.6425>

CITATION

Ferreira, G.W.S., Reboita, M.S., Ribeiro, J.G.M., 2024. Assessment of the Solar Energy Potential over South America Estimated by CMIP6 Models in the Present and Future Climate. *Journal of Environmental & Earth Sciences*. 6(2): 110–143. DOI: <https://doi.org/10.30564/jees.v6i2.6425>

COPYRIGHT

Copyright © 2024 by the author(s). Published by Bilingual Publishing Group. This is an open access article under the Creative Commons Attribution-NonCommercial 4.0 International (CC BY-NC 4.0) License (<https://creativecommons.org/licenses/by-nc/4.0/>).

1. Introduction

Conciliating socioeconomic growth with sustainable energy development is one of the leading global urgencies. Global warming, intensified by anthropic activities that emit greenhouse gases, has caused surface temperature to rise by approximately 1.1 °C compared to pre-industrial levels^[1]. Emissions of greenhouse gases continue to grow, arising from several factors like the use of fossil fuels, land-use change, high consumption patterns etc.^[1], and in a more pessimistic scenario, global climate models (GCMs) project an increase in average global temperature of up to 5.7 °C by the end of the 21st century^[2]. Indeed, the ten warmest years in historical records have all occurred in the last decade (2014–2023), and 2023 was the warmest year since global recordings began in 1850, being approximately 1.35 °C above the pre-industrial average^[3]. In this context, executing decarbonization strategies is crucial to mitigate climate change's negative impacts and meet the Paris Agreement's commitments. For South America (SA), such actions are equally urgent because, despite its leading role worldwide in the use of renewable energies^[4], recent years have shown a growing use of non-renewable sources and greenhouse gas emissions^[5,6].

Abundant in solar and wind resources, Latin America currently has more than 319 GW of solar and wind energy production capacity (large-scale announced, in pre-construction or under construction) and could increase its production capacity by more than 460% by 2030 compared to the 69 GW (27.6 GW of solar and 41.5 GW of wind) that are currently in operation^[7]. In this scenario, Brazil stands out, as the country currently has around 40 GW of installed solar photovoltaic capacity and could reach 68 GW in the next five years, which would place it as the fifth-largest solar producer in the world and the leader in solar production in Latin America^[8,9]. However, the expansion of solar capacity in the country depends on several factors, such as the installation of solar farms, the improvement of energy transmission and storage systems, the implementation of a management system that integrates solar energy into the

Brazilian matrix, and incentives for new investments in the sector^[8].

Solar energy can be generated by two main methods: concentrated solar power (CSP) and photovoltaic solar power (PVP). Concentrated solar power stations collect and concentrate direct sunlight and use it to produce heat and drive a steam turbine to produce electricity. Two CSP technologies stand out: power towers, where flat mirrors focus sunlight on a single point on a high tower, and parabolic troughs, where curved mirrors focus sunlight onto a line running along the mirrors^[10]. Most systems use linear concentrating systems via parabolic troughs, whereas power towers are the most widely used point concentrating technology. On the other hand, solar photovoltaic technology uses solar cells to convert solar radiation into electricity directly through the photovoltaic effect^[10–12]. They can convert up to 20% of incident solar radiation into electricity, reaching a total installed capacity of 710 GW by the end of 2020^[10,11]. Among the most widely used PVP technologies, crystalline silicon devices account for 80% of the global market, while thin film technology is more recent, offering generally lower costs and more efficiency than crystalline silicon technology^[10]. In SA, solar energy has become Brazil's third largest source of electricity, and around 70% of the solar energy produced in the country comes from small crystalline silicon systems installed on the roofs of houses and commercial and rural properties^[13].

Several studies have assessed the impacts of climate change on solar radiation and, consequently, on solar energy generation in different parts of the world. Using Coupled Model Intercomparison Project—Phase 3 (CMIP3) models, Crook et al.^[14] concluded that, under the A1B scenario, there is a moderate increase (decrease) in PVP generation during the 21st century in Europe and China (the western United States and Saudi Arabia), and significant increases in CSP in the same regions. In addition, dynamically downscaled CMIP3 projections show a reduction of up to 12% in PVP in northern European countries, while southern areas may experience an increase in solar energy generation^[15]. Similarly,

CMIP5 model projections indicate favorable conditions for PVP generation in the coming decades in Spain, France, Italy, and Germany^[16–20]. In addition to Europe, other regions of the globe also suggest favorable conditions for solar power generation in the future, as projected by CMIP5 models for East Asia, Southeast North America, and Central America^[16–20]. Conversely, reduced PVP is projected by CMIP5 and CMIP6 models in Africa, the Middle East, Central Asia, Australia, and North America^[18–24].

In general, the increasing PVP generation is associated with a projected decreasing cloud cover^[16], so changes in cloud cover and the composition of atmospheric aerosols can affect PVP generation since the electricity produced does not respond linearly to changes in irradiance and depends on the ratio between direct and diffuse radiation^[17]. Globally, direct climate impacts on solar energy are expected to be modest (of the order of 5%) because the effects of changes in irradiance are also minor, while the negative impacts of warming occur mainly at higher latitudes, which already have a more limited potential for generating PVP than low latitudes^[20].

Regarding SA, it has favorable conditions for solar energy generation, given that the solar resource is evenly distributed on the continent and a large part of it is located in the Region of the Sun Belt with the highest solar radiation, with Chile, Bolivia, and Argentina among the ten countries in the world with the maximum irradiation for PVP systems^[25,26]. Some sectors of the continent stand out, such as northern Chile, which has the highest irradiation levels (with the Atacama Desert having the best global maximum irradiation), northeastern Brazil, north of Colombia, the west coast of Peru, and northern Argentina^[26]. On the other hand, climate projections from the Coordinated Regional Downscaling Experiment (CORDEX) indicate a reduction of up to 2.49% in the PVP in the central zone of Nariño (far west of Colombia) and a maximum increase of 2.52% in the southeast of the region^[27]. Furthermore, solar energy is estimated to supply up to 82% and 86% of electricity generation by 2050 in Bolivia^[28] and Chile^[29], respectively.

For Brazil, dynamically downscaled climate projections from CMIP5 suggest increased solar radiation over almost the entire country between 2030 and 2080 under the RCP8.5 scenario, resulting in an average increase of 3.6% in PVP in Northeast Brazil by 2080, as well as in locations with installed PVP solar farms in the Northeast and Southeast^[30]. In addition, statistically downscaled climate projections from CMIP5 provided three patterns of changes in global horizontal irradiance during the 21st century in Brazil: a pattern of reduction of up to 10% on the north/northeast coast, a reduction of up to 10% in the south of the country in the second half of the year, and a transversal band from the Brazilian Southeast to the Amazonia with an increase of 5 to 10% during the austral summer^[31]. On the other hand, raw climate projections from CMIP6 indicate for the 2021–2100 period an increase of up to 5% in CSP in northern Brazil and reductions in the rest of the country of more than 5%, mainly in the Southeast, Midwest, northern portion of the Northeast and portions of the Brazilian North^[32]. In contrast, raw climate projections from CMIP5 and CMIP6 suggest growth in energy generated by CSP technology, with a statistically significant average increase of up to 6% in most of Brazil (except the country's southern region) in 2071–2100^[24]. Furthermore, studies show that environmental heating caused by rising temperatures reduces the conversion efficiency of photovoltaic cells^[24,32].

GCMs are fundamental tools for evaluating climate elements, but their direct application in studies of regional impacts is inappropriate due to the outputs' coarse resolution. In this sense, statistical and dynamical downscaling techniques are essential for overcoming these limitations of global models. However, their use in studies of climate change's impacts on solar radiation in SA is still embryonic in the literature. Despite helping analyze climate phenomena on a local scale, dynamical downscaling requires high computational costs^[33]. On the other hand, statistical downscaling requires fewer computational resources but a long series of local observations^[34]. Among the sparse existing studies for the

region, there are analyses obtained by dynamical^[30] and statistical downscaling^[31], but more current studies with CMIP6 models use their raw outputs^[22,24,32]. However, a recent study^[35] used the Quantile Delta Mapping (QDM) bias correction method^[36] to statistically downscale CMIP6 simulations of irradiation in Brazil, concluding that the technique reduced the systematic biases of the models in both long-term averages and extreme values, demonstrating its potential use for studies of climate impacts in SA.

Given the above, this study aims to: (a) apply QDM bias correction and statistical downscaling to historical simulations and climate projections of solar irradiation from a CMIP6 multi-model ensemble and; (b) use the bias-corrected projections to assess the solar generation potential by CSP and PVP technologies in SA under different greenhouse gas emission scenarios. The relevance of this study is justified by the scarcity of studies on the impacts of climate change on solar energy generation in SA, as well as studies that apply statistical downscaling to CMIP6 solar radiation projections for the continent. In this context, our study fills this gap and seeks to assist policymakers, planners, and decision-makers involved in expanding the solar energy matrix in SA, as well as all those interested in the energy transition on the continent.

2. Materials and methods

2.1 Study area

The study area comprises the South American continent (**Figure 1**), located at 12°N–55°S latitudes and marked by great latitudinal extension, complex topography, and climate heterogeneity with tropical, subtropical, and extratropical regions^[37]. SA also has an intricate geography, characterized by disparate areas such as the Andes Mountains, the Atacama Desert, the Amazon Rainforest, and Brazil's semi-arid northeastern region. SA is privileged in terms of solar resources, and a large part of the continent is located in the area of the Sun Belt with the highest solar radiation^[25], with some highlighted regions,

such as northern Chile, northeastern Brazil, north of Colombia, the west coast of Peru and northern Argentina^[26].

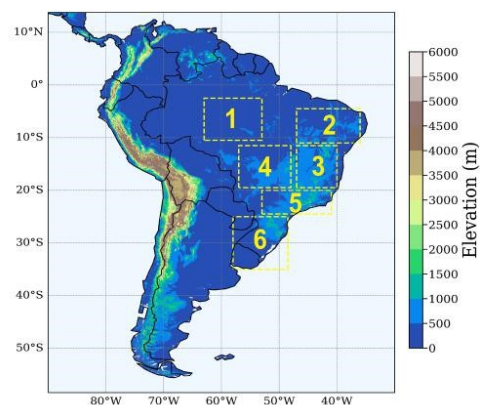


Figure 1. Illustration of the study area with elevation (m). The yellow rectangles indicate subdomains selected for individual analysis of the CMIP6 GCMs.

Source: United States Geological Survey-Earth Resources Observation System (EROS) Center.

2.2 CMIP6 GCMs

This study used surface downwelling shortwave flux, 2 m air temperature, and the zonal and meridional components of wind at 10 m from eight CMIP6 GCMs, covering the historical period (1995–2014) and two greenhouse gas emission scenarios (SSP2-4.5 and SSP5-8.5) for the future period (2020–2099). The GCMs data comprised simulations obtained every three hours provided on the Earth System Grid Federation (ESGF) platform (available at: <https://aims2.llnl.gov/search/cmip6/>). We employed the Rupp et al.^[38] methodology to select the CMIP6 GCMs, whereby various statistical metrics are used to assess the models' performance in simulating a given region's historical climate. Further details on the methodology, including the mathematical formulation and statistical parameters, can be found in Ferreira et al.^[39,40] and Reboita et al.^[41,42]. However, we emphasize that the choice of models (**Table 1**) considered the GCMs' ability to simulate historical cli-

mate and the availability of high-frequency data and projections on the ESGF platform. Furthermore, of the GCMs selected, three (EC-Earth3, IPSL-CM6A-LR, and MPI-ESM1-2-LR) had already demonstrated a fair ability to represent the South American climate^[43]. Moreover, the ensemble composed of the best-performing models produces results closer to the observations and surpasses the quality of the individual GCM simulations^[43].

2.3 Reference data

To validate the climate simulations of the CMIP6 GCMs, we used the ERA5 reanalysis product^[52] from the European Centre for Medium-Range Weather Forecasts—ERA5 (ECMWF-ERA5). The variables used were surface solar irradiance (surface downwelling shortwave flux), 2 m air temperature, zonal and meridional wind components at 10 m height, available at a temporal frequency of three hours and with a horizontal resolution of 0.25° for the 1995–2014 reference period (available at: <https://cds.climate.copernicus.eu/>). Although the ERA5 reanalysis product is an advanced dataset generated by assimilating observations and numerical simulations,

it still has systematic biases^[21,53,54].

Therefore, to complement the validation data set and overcome the limitations of the reanalysis product, we used satellite observations provided by CLARA-A3, which is a set of cloud, albedo, and surface radiation climate records generated by the Satellite Application Facility on Climate Monitoring (CM SAF), belonging to the European Organization for the Exploitation of Meteorological Satellites (EUMETSAT). CLARA-A3 is the third edition of the CLARA (CM SAF Cloud, albedo, and surface radiation) product, which provides information on cloud properties and radiation parameters derived from the Advanced Very High Resolution Radiometer (AVHRR) sensor, on board the polar-orbiting satellites of the National Oceanic and Atmosphere Administration (NOAA) and Meteorological Operational Satellite Programme (EUMETSAT Metop)^[55]. The CLARA-A3 data was obtained from the CM SAF platform, with a horizontal resolution of 0.25° and a daily frequency for the period 1995–2014 (available at https://www.cmsaf.eu/EN/Home/home_node.html). In general, satellite-based observations have fewer uncertainties than reanalysis data due to their greater accuracy^[21,56] and are widely used to evaluate solar irradiance simulated by climate models^[21].

Table 1. Information on each CMIP6-GCM employed in the study.

Model	Resolution (Lat × Lon)	Institute	Reference
CMCC-CM2-SR5	1.25 × 0.94	Fondazione Centro Euro-Mediterraneo sui Cambiamenti Climatici	Lovato and Peano ^[44]
CMCC-ESM2	1.25 × 0.94	Fondazione Centro Euro-Mediterraneo sui Cambiamenti Climatici	Lovato et al. ^[45]
EC-Earth3	0.70 × 0.70	EC-Earth Consortium	Döscher et al. ^[46]
GFDL-ESM4	1.25 × 1.00	Geophysical Fluid Dynamics Laboratory	Krasting et al. ^[47]
IPSL-CM6A-LR	2.50 × 1.26	Institut Pierre Simon Laplace	Boucher et al. ^[48]
MIROC6	1.41 × 1.41	Japan Agency for Marine-Earth Science and Technology	Tatebe and Watanabe ^[49]
MPI-ESM1-2-LR	0.94 × 0.94	Max Planck Institute for Meteorology	Wieners et al. ^[50]
MRI-ESM2-0	1.13 × 1.13	Meteorological Research Institute	Yukimoto et al. ^[51]

2.4 Bias Correction and Statistical Downscaling (BCSD)

Due to their coarse resolution, the raw output of GCMs is unsuitable for use in different applications,

such as synoptic scale studies. Given this, we applied statistical downscaling to the CMIP6 outputs (2 m air temperature and zonal and meridional wind components) using the ERA5 reanalysis as a reference set. For the solar irradiance variable, we used the

ensemble mean of CLARA-A3 observations and the ERA5 reanalysis to apply the advantages obtained by both sets. Among the different categories of statistical downscaling methods (transfer or regression models, weather generator, weather typing), we applied the transfer function, which establishes statistical relationships between the observed and modeled variables [57]. This methodology is also called Bias Correction—Statistical Downscaling (BCSD). Before BCSD, spatial disaggregation was applied to the CMIP6 outputs so that all the data from the models, the ERA5 reanalysis, and the CLARA-A3 observations were interpolated to a resolution of $0.5^\circ \times 0.5^\circ$ using bilinear interpolation since studies have shown the ability of this method to generate consistent fields [35,58].

For the BCSD method, we used the QDM technique [36] for historical simulations (1995–2014) and applied transfer functions to future projections (2015–2099) of each CMIP6 model. The QDM technique is justifiable for statistical downscaling because it preserves the relative changes and trends projected by the models and corrects systematic biases in the modeled data's quantiles concerning the observations' distribution [36]. In general, the QDM process follows three stages: first, the trend is removed from all simulated and projected quantiles individually; then, the bias is corrected using the quantile mapping technique for all quantiles with the trend removed; and finally, the projected changes are superimposed on the bias-corrected outputs [36]. The reader can find more details on the BCSD methodology in Ferreira et al. [39,40] and Reboita et al. [41,42].

The historical period (1995–2014) composed the training set to adjust the future projections (2015–2099) with the QDM algorithm to optimize computational resources and follows the same reference period used by the International Panel on Climate Change—IPCC [59]. The Python-based package xclim [60] was used to perform the calculations. According to Cannon et al. [36], the QDM technique is advantageous over quantile mapping because it is less susceptible to the inflating relative trends in extreme values, which was demonstrated in a recent study using the method to downscale different atmospheric variables simulated by CMIP6 for SA [35].

2.5 Solar energy

CSP and PVP technologies are the most widely used for generating solar energy [10–12,24]. CSP systems produce electricity with the thermal energy of sunlight through a process whereby the light is concentrated on a receiver using various mirrors or lenses and is then used to produce heat that drives the engine and electricity generator [24]. On the other hand, the PVP system converts sunlight directly into electricity through PVP panels using semiconductor materials, which absorb light and generate electricity through the photovoltaic effect [12,24]. As reported by Ha et al. [24], the empirical equations and coefficients used here evaluate the solar energy potential as a function of different atmospheric variables and how changes in climate conditions resulting from global warming can influence this potential, not considering technological advances that may alter future solar energy generation.

Concentrated Solar Power (CSP)

CSP technology can be classified into four different categories based on the type of collector: parabolic trough collector (PTC), solar power tower (SPT), linear Fresnel reflector, and parabolic dish collector [24]. In this study, the equations and coefficients used refer to the PTC system since this technology is the most mature and globally consolidated among the technologies for concentrating solar energy, both commercially and on an industrial scale [61–64], as well as being the most widespread technology in plants for thermoelectric generation from solar energy in Brazil [65].

Here, we apply the methodology proposed by Crook et al. [14], which is consolidated in the literature with various studies [20–22,24,32], whereby the CSP output (CSP_{out}) is estimated using the thermal efficiency of CSP (η_{CSP}) multiplied by the direct irradiance (R_d), see equation (1):

$$CSP_{out} = \eta_{CSP} \times R_d \quad (1)$$

η_{CSP} is expressed as a function of surface air temperature (TAS) and R_d , see equation (2):

$$\eta_{\text{CSP}} = k_0 - k_1 \times \frac{(T_i - \text{TAS})}{R_d} \quad (2)$$

The specific collector coefficients $k_0 = 0.762 \text{Wm}^{-2}\text{C}^{-1}$, $k_1 = 0.2125 \text{Wm}^{-2}\text{C}^{-1}$ and fluid temperature $T_i = 115^\circ\text{C}$ were tested on the Industrial Solar Technology parabolic trough collector at Sandia National Laboratories [21,24] and applied in several studies [14,20–22,24,32].

As R_d is not provided directly by the CMIP6 models, it is necessary to derive it from an empirical relationship between fractional cloud cover (fclt) and clear sky irradiance at the surface (R_{sc}) [21,24], see equation (3):

$$R_d = 0.75 \times R_{\text{sc}} \times (1 - \text{fclt}) \quad (3)$$

where the factor 0.75 represents the scattering effect of sunlight by air molecules and aerosols [21]. As R_{sc} is also not provided by the CMIP6 GCMs, the relationship between fclt, solar irradiance at the surface (R_s) and R_{sc} is used as follows [21,24], see equation (4):

$$\text{fclt} = 1 - \frac{R_{\text{sc}}}{R_s} \quad (4)$$

By grouping equations 3 and 4, it is possible to estimate R_d using equation (5):

$$R_d = 0.75 \times R_s \quad (5)$$

Photovoltaic Power Potential (PVP_{pot})

Following the methodology widely used in the literature [15,16,18–24,32], we estimated the photovoltaic power potential (PVP_{pot}) utilizing the energy rating method, which multiplies the total integrated solar irradiance over a period by a performance ratio [24] through the expression, see equation (6):

$$PVP_{\text{pot}} = P_R \times \frac{R_s}{R_{\text{sSTC}}} \quad (6)$$

where STC refers to the standard test conditions ($R_{\text{sSTC}} = 1000 \text{Wm}^{-2}$), under which the nominal capacity of a photovoltaic device is determined, and P_R is the performance ratio that accounts for changes in the efficiency of photovoltaic cells due to tempera-

ture changes, according to equation (7) [24]:

$$P_R = 1 + \gamma \times [T_{\text{cell}} - T_{\text{STC}}] \quad (7)$$

where T_{STC} is the ambient air temperature under standard test conditions ($T_{\text{STC}} = 25^\circ\text{C}$), γ is $-0.005^\circ\text{C}^{-1}$, following the typical response of monocrystalline silicon solar panels adopted in different studies [15,20,21,24]. Here, we consider the generation of solar energy by monocrystalline silicon solar panels since these (together with polycrystalline silicon solar panels) account for up to 80% of the global photovoltaic energy market [66], as well as being widely used in SA, given that around 70% of the solar energy produced in Brazil comes from small crystalline silicon systems installed on the roofs of houses and commercial and rural properties [13]. T_{cell} is the temperature of the photovoltaic cell, which is affected by R_s , TAS, and wind speed (WS, calculated with the zonal and meridional components of the wind). Although some studies [21,24] have shown that the contribution of wind speed is practically negligible for changes in PVP_{pot} , here we have chosen to include the variable in the estimate of photovoltaic energy generation using equation 8, widely adopted in the literature [15,16,18–24,32]:

$$T_{\text{cell}} = c_1 + c_2 \times \text{TAS} + c_3 \times R_s + c_4 \times \text{WS} \quad (8)$$

where $c_1 = 3.9^\circ\text{C}$, $c_2 = 0.942$, $c_3 = 0.028^\circ\text{C m}^{-2}\text{W}^{-1}$, and $c_4 = -1.509^\circ\text{C sm}^{-1}$. For better analysis, the value of PVP_{pot} is multiplied by 100 and is therefore referred to in %.

PVP_{pot} Anomalies and trend time series

Additionally, only for the SSP5-8.5 scenario, we present the trend and change projections estimated by each CMIP6 GCM (as well as by the multi-model ensemble) for 2020–2099 concerning the 1995–2014 period for six key regions (Figure 1) that concentrate solar energy hotspots in SA [67]: Brazilian Amazonia (R1; 2.5°S – 10°S , 53°W – 63°W), northern sector of the Brazilian Northeast (R2; 4.5°S – 11°S , 36°W – 47°W), southern and central sectors of the Brazilian Northeast (R3; 11°S – 19.5°S , 40°W – 47°W), the Brazilian Midwest (R4; 11.5°S – 19.5°S , 48°W – 57°W), the Brazilian Southeast (R5;

20°S–24.5°S, 41°W–53°W), and the Brazilian South and Uruguay (R6; 25°S–35°S, 48.5°W–58°W). This analysis assesses the temporal evolution of the spread among the different CMIP6 models' projections.

Test of statistical significance for the difference in mean climatological values and Mann-Kendall Trend Test

We used the Student's *t*-test to assess whether the differences in the mean seasonal climatological values of CSP and PVP for the future period (2020–2099) projected by the CMIP6 ensemble are statistically significant about the historical period (1995–2014), using an α significance level of 5%. Furthermore, under the SSP5-8.5 scenario, we analyzed the trend time series of PVP obtained by the eight CMIP6 models and the multi-model ensemble for six SA subdomains (Figure 1) to present the climate change signal in different solar hotspot sectors^[67]. This procedure was carried out using the Mann-Kendall test, widely used to analyze trends in climate series^[68]. In addition, Sen's slope estimation test was used to detect the linear trend of PVP_{pot} in the subdomains evaluated.

3. Results and discussion

Historical simulations

Figure 2 shows the historical seasonal climatology (1995–2014) of surface downwelling shortwave radiation ($W\ m^{-2}$) provided by the outputs of the four datasets used: the ERA5 reanalysis, the CLARA-A3 satellite observations, the simulations obtained by the ensemble composed of CLARA-A3+ERA5 and, finally, the original (pre-processed) historical simulations of the CMIP6 ensemble. The biases of the four datasets are also presented: the bias of CMIP6 statistically downscaled with the ERA5 reanalysis; the bias of CMIP6 statistically downscaled with the CLARA-A3 satellite observations; the bias of CMIP6 statistically downscaled with the CLARA-A3 + ERA5 ensemble; and bias of the original CMIP6 ensemble simulations in relation to the CLARA-A3 + ERA5 ensemble. In general, all the ensembles show their systematic biases, with a predominance of underestimates of up to $20\ W\ m^{-2}$ in much of central Brazil and northeastern

Brazil and overestimates of the same magnitude in Argentina, Chile, and northern SA during the DJF months. Similarly, in the months of MAM and JJA, overestimates of up to $20\ W\ m^{-2}$ prevail over most of the continent, including Argentina, Chile, the southern and northern sectors of Brazil, and northern SA. For the months of SON, there is a significant reduction in bias across the continent despite a persistent positive bias of up to $20\ W\ m^{-2}$ in northeast Brazil's coastal and central regions. Nevertheless, the CMIP6 downscaled simulations with the CLARA-A3 + ERA5 ensemble provide biases between -10 and $10\ W\ m^{-2}$ over most of SA (except in JJA).

Figure 3 illustrates the satisfactory performance of statistical downscaling with the CLARA-A3 + ERA5 ensemble, which shows the seasonal climatology of solar irradiance and biases (in percentages). The reduction in systematic errors by the BCSD technique with the CLARA-A3 + ERA5 ensemble is notable, indicating a decrease of up to 50% in the magnitude of the biases over most of the continent. For almost the entire year, the biases are between -5 and 5%, with the months of JJA showing more systematic errors in Brazil's central-southern and northeastern sectors, Paraguay, central-southern Peru, Suriname, and the Guianas. In addition, a positive (negative) bias of up to 10% persists in the months of JJA and SON (DJF and MAM) in northeastern Brazil. However, this Brazilian region is one of the global sectors where CLARA-A3 does not satisfactorily achieve its accuracy objective^[55].

The CSP_{out} results (Figure 4) show that the highest seasonal values of CSP in SA also occur in spring due to the higher magnitudes of solar irradiance at the surface at this time of year. During this season, the highest magnitudes of concentrated solar energy occur in northeastern Brazil and the west coast of SA, where concentrated energy exceeds $160\ W\ m^{-2}$. In other regions of Brazil, such as the center-southeast of the country, the values are between 140 and $160\ W\ m^{-2}$. In addition, the concentrated energy reaches up to $140\ W\ m^{-2}$ in the Amazonia region. In the fall and winter seasons, CSP is reduced across the continent, and the west coast of SA and the northern part of the Brazilian Northeast concentrate higher intensities, where values reach up to $180\ W\ m^{-2}$.

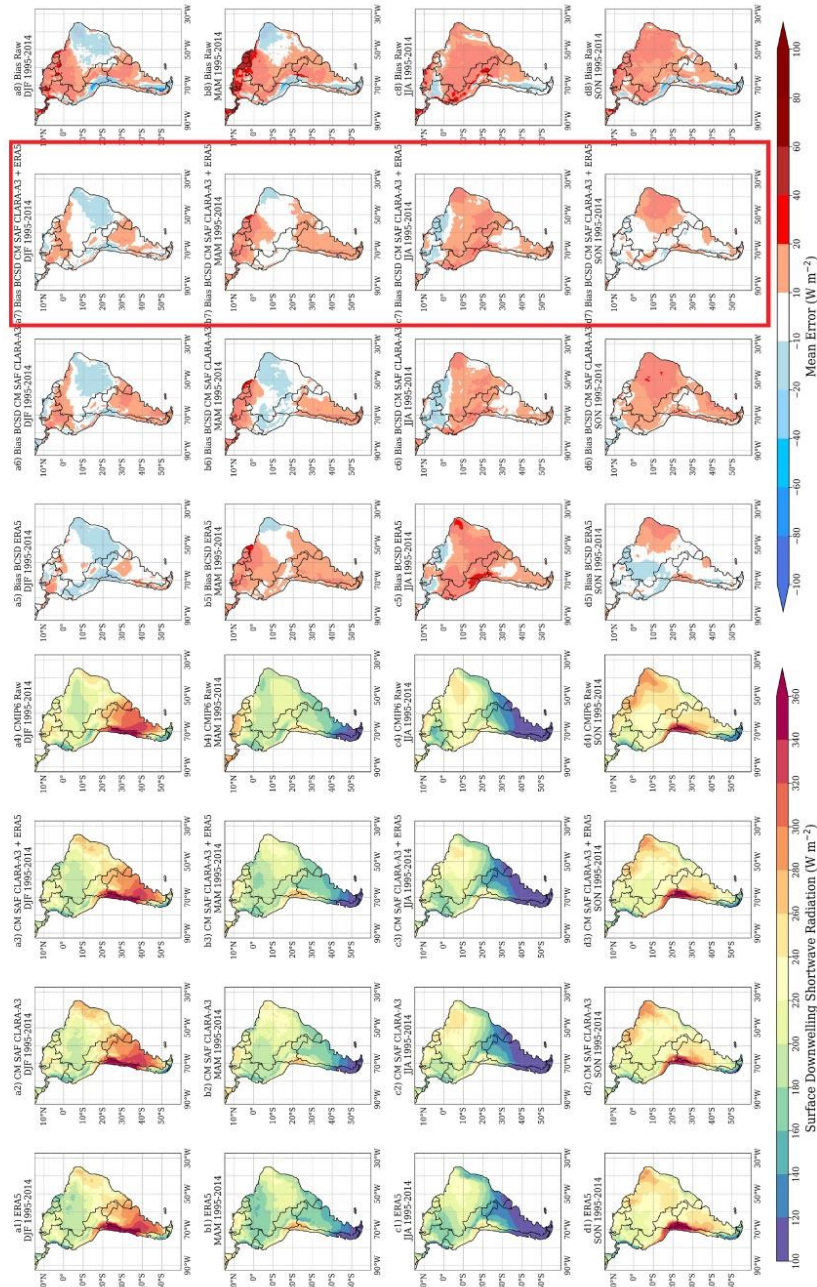


Figure 2. Seasonal climatology of surface downwelling shortwave radiation ($W m^{-2}$) over the historical period (1995–2014) obtained by ERA5 (first column on the left); CLARA-A3 satellite observations (second column on the left); CLARA-A3 + ERA5 ensemble mean (third column on the left); original CMIP6 ensemble simulations (fourth column on the left). Seasonal climatology of bias ($W m^{-2}$) in the historical period (1995–2014) between CMIP6-ERA5 statistically downscaled and ERA5 (fourth column from the right); CMIP6-CLARA-A3 statistically downscaled and CLARA-A3 (third column from the right); CMIP6-CLARA-A3 + ERA5 statistically downscaled and CLARA-A3 + ERA5 ensemble (second column from the right); original CMIP6 ensemble simulations and CLARA-A3 + ERA5 ensemble (first column from the right). The red rectangle highlights the ensemble's bias (CMIP6-CLARA-A3 + ERA5 statistically downscaled) selected to analyze the solar power projections.

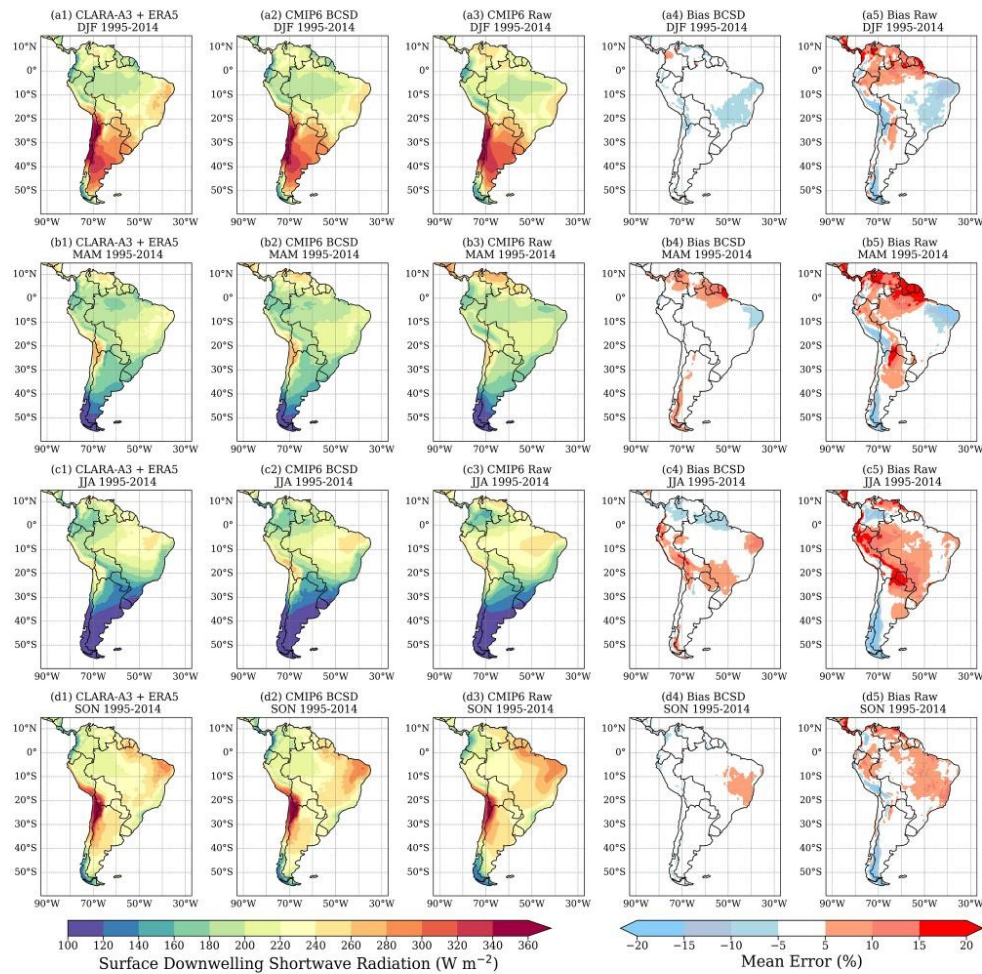


Figure 3. Seasonal climatology of surface downwelling shortwave radiation ($W m^{-2}$) in the historical period (1995–2014) obtained by the CLARA-A3 + ERA5 ensemble (first column on the left), CMIP6-CLARA-A3 + ERA5 statistically downscaled (second column on the left), original CMIP6 ensemble simulations (middle column); and seasonal bias (%) between the CMIP6-CLARA-A3 + ERA5 statistically downscaled and the CLARA-A3 + ERA5 ensemble (second column from the right), and between the original CMIP6 ensemble's simulations and the CLARA-A3 + ERA5 ensemble (first column from the right).

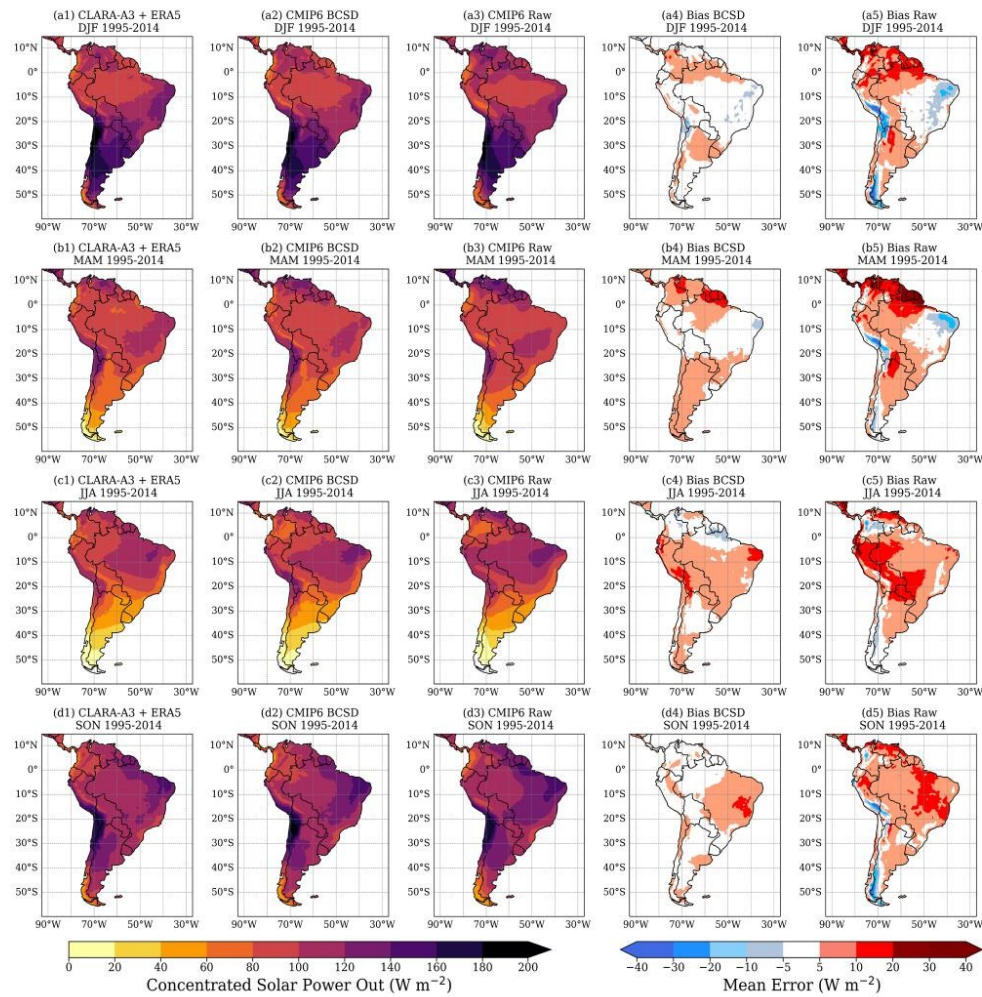


Figure 4. Seasonal climatology of CSP_{out} (W m^{-2}) in the historical period (1995–2014) obtained by the CLARA-A3 + ERA5 ensemble (first column on the left), CMIP6-CLARA-A3 + ERA5 statistically downscaled (second column on the left), original CMIP6 ensemble simulations (middle column) and seasonal bias (W m^{-2}) between the CMIP6-CLARA-A3 + ERA5 statistically downscaled and the CLARA-A3 + ERA5 ensemble (second column on the right) and original CMIP6 ensemble's simulations and the CLARA-A3 + ERA5 ensemble (first column on the right).

The bias fields show that the CMIP6 ensemble tends to overestimate CSP over practically the whole of SA, with positive biases of up to 20 W m^{-2} north of 20°S throughout the year. Additionally, underestimates of up to 20 W m^{-2} occur in the northern sector of the Brazilian Northeast during the first half of the year. Furthermore, underestimates of up to 30 W m^{-2} occur on the west coast of SA throughout the year. The BCSD technique significantly reduces the GCMs' systematic errors, especially in the austral spring and summer. After applying BCSD during the summer, the ensemble biases are between -5 and 5 W m^{-2} over practically the entire continent. However, underestimates (overestimates) of up to 10 W m^{-2} (-10 W m^{-2}) remain in the Northeast region during the summer (spring). In the fall and winter seasons, the prevalence of CSP overestimates remains throughout the continent despite BCSD reducing errors, especially in the Amazonia region and northern SA.

The PVP_{pot} results (Figure 5) indicate spatial fields similar to CSP_{out} 's. The highest PVP occurs during spring and regions such as the Brazilian Northeast and the west coast of SA show values of up to 36%. In other areas of Brazil, the values are between 20 and 28% for most of the year. Similarly to the CSP bias fields, the CMIP6 raw ensemble shows systematic overestimates in northern Brazil and northern SA, with a positive bias of up to 6%. Conversely, underestimates of up to 4% occur in northeastern Brazil during the summer and fall, while the Andean region shows underestimates of up to 6%. The BCSD technique considerably reduces the systematic errors of the models, especially in the spring and summer months, when biases of between -1 and 1% are found in practically all of SA. On the other hand, positive biases of up to 2% predominate on the continent in the fall and winter months.

CSP_{out} and PVP_{pot} projections

Figures 6 and 7 show the seasonal difference (in percent) in CSP_{out} after applying statistical downscaling with the CLARA-A3 + ERA5 ensemble under the SSP2-4.5 and SSP5-8.5 scenarios, respectively. The seasonal differences refer to the changes in the 2020–2039, 2040–2059, 2060–2079, and 2080–2099 periods compared to the 1995–2014 historical period. For the DJF months, the projections indicate statistically significant increases in CSP of up to 4% in Brazil's southern and northern regions by 2059 under the SSP2-4.5 scenario. Under the SSP5-8.5 scenario, there is a statistically significant increase of over 3% in the Brazilian Amazonia from 2040 onwards. From 2060 onwards, the SSP2-4.5 scenario projects increased CSP by up to 4% in almost all Brazil. On the other hand, the SSP5-8.5 scenario projects more intense increases (above 4%) for summer from 2060 onwards in a large part of the northern region of Brazil, Peru, Ecuador, southern Colombia, Venezuela, Suriname, and the Guianas, and reductions of up to 2% in the northern part of the Brazilian Northeast.

For the MAM months, the SSP2-4.5 scenario shows no statistically significant increase until 2059, while the SSP5-8.5 scenario indicates increases of up to 4% in northwestern SA. From 2060 onwards, both scenarios show increases of over 3% in the Amazonia region and a reduction of the same intensity in north-central Argentina.

Considering the months of JJA, both scenarios indicate a statistically significant increase of up to 2% in areas of the north and northeast of Brazil by 2059. From 2060 onwards, both scenarios maintain their projections of a significant increase of over 3% in Brazil's Southeast, Northeast, and North regions, with a more intense signal under the SSP5-8.5 scenario.

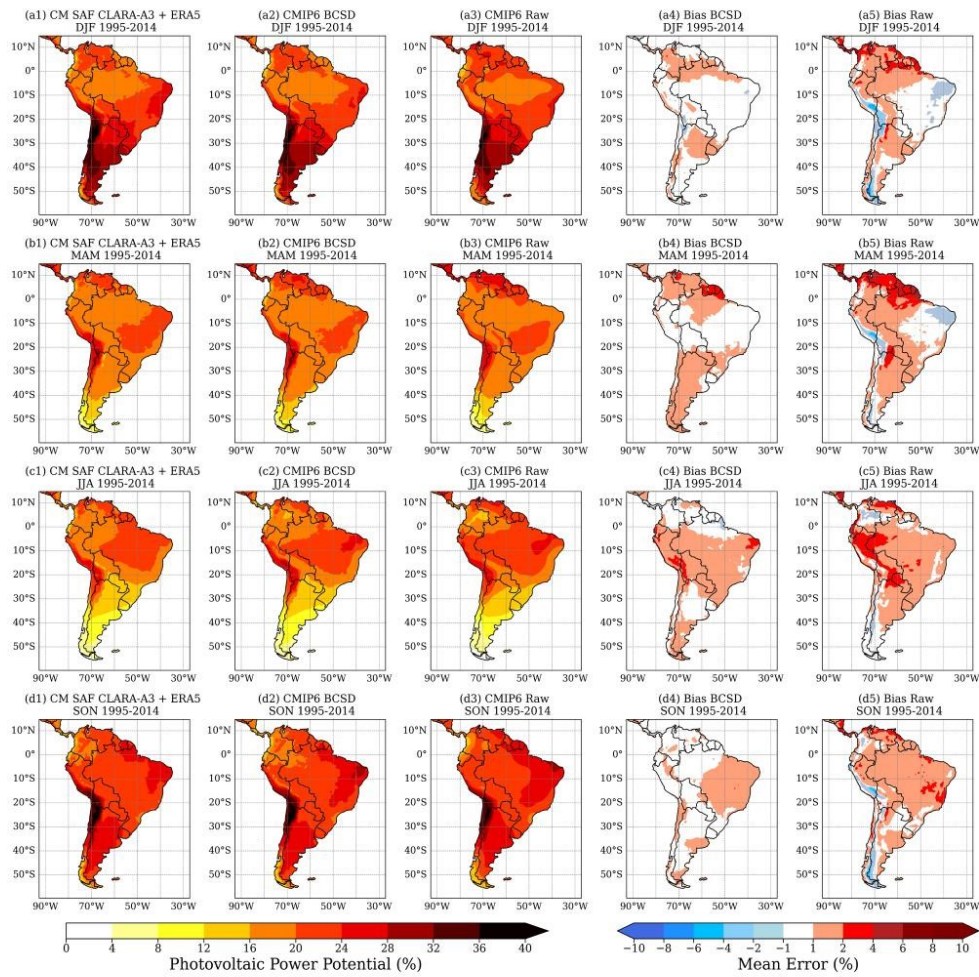


Figure 5. Seasonal climatology of PVP_{pot} (%) in the historical period (1995–2014) obtained by the CLARA-A3 + ERA5 ensemble (first column on the left), CMIP6-CLARA-A3 + ERA5 statistical downscaling (second column on the left), original CMIP6 ensemble simulations (middle column) and seasonal bias (%) between the CMIP6-CLARA-A3 + ERA5 statistical downscaling and the CLARA-A3 + ERA5 ensemble (second column on the right) and original CMIP6 ensemble's simulations and the CLARA-A3+ERA5 ensemble (first column on the right).

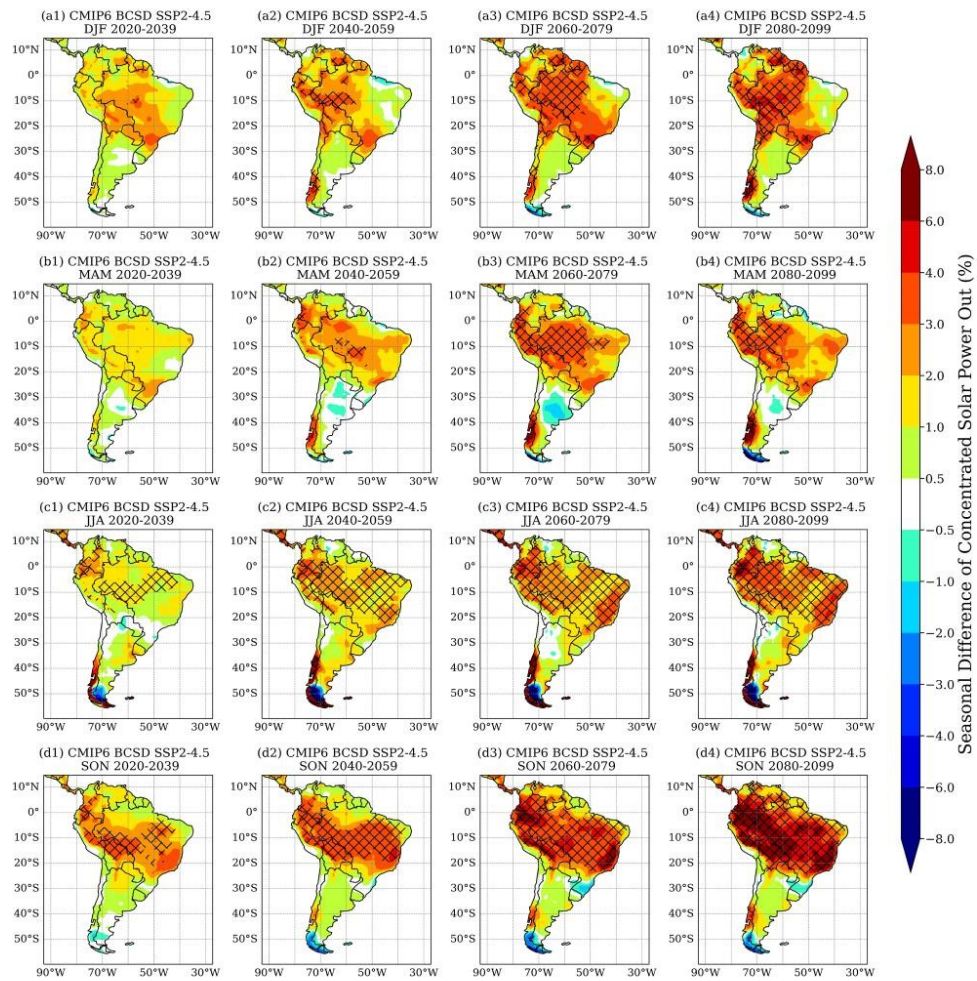


Figure 6. Seasonal difference (%) in CSP_{out} projected by the CMIP6 ensemble after BCSD with the CLARA-A3 + ERA5 ensemble under the SSP2-4.5 emission scenario for the periods 2020–2039, 2040–2059, 2060–2079, and 2080–2099 in relation to the historical period (1995–2014). Hatched areas indicate a statistical significance of 95%, based on the Student's *t*-test.

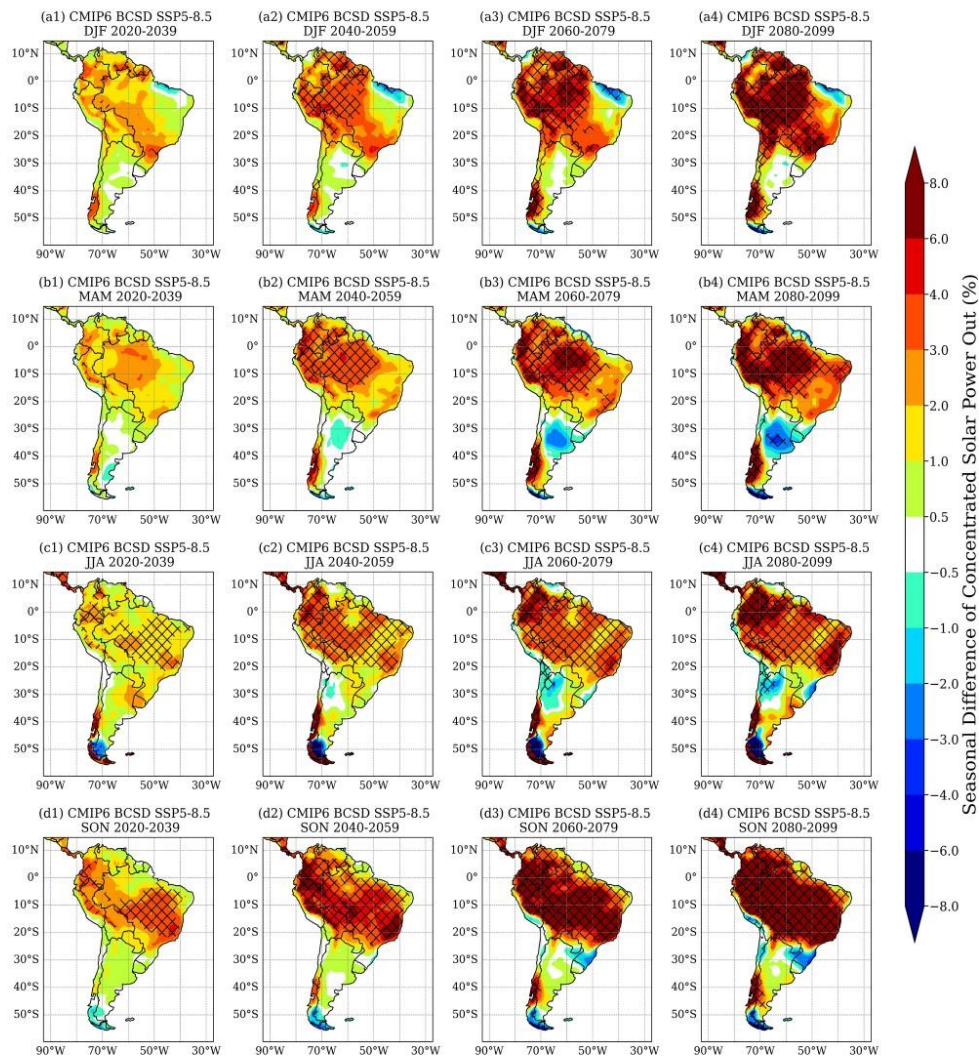


Figure 7. Similar to Figure 6, except for the SSP5-8.5 scenario.

About SON months, both scenarios show a significant increase of over 3% in the Southeast, Northeast, and North regions by 2059, as well as in Peru, Bolivia, Ecuador, and Colombia. From 2060 onwards, the two scenarios suggest an intensified increase in almost all of Brazil (as well as the other countries mentioned and Venezuela) and a reduction in the extreme south of Chile and Rio Grande do Sul (Brazil). In general, CSP projections suggest a favorable scenario for solar power generation in SA, mainly in sectors of Brazil such as the Southeast, Midwest, and Northeast coast (depending on the season and emission scenario), Bolivia, Peru, Ecuador, Colombia, and Venezuela. At the same time, reductions are estimated for the southern region of Brazil. These results corroborate projections of concentrated solar energy provided by CMIP3 models for the second half of the 21st century^[14].

Figures 8 and 9 show the seasonal difference (in percentage) in PVP_{pot} under the SSP2-4.5 and SSP5-8.5 scenarios, respectively. To the DJF months of the 2020–2059 period, both scenarios project an increase of up to 2% in the Brazilian Amazonia and northern Peru, a pattern also obtained by an ensemble made up of five CMIP6 GCMs under the same scenarios for the DJF months of the 2015–2040 period^[22], as well as by an ensemble of seven CMIP5 GCMs under the RCP-4.5 scenario for the summer of 2036–2065^[19].

From 2060 onwards, both scenarios maintain their trend of a significant increase of more than 1% in a large part of the Midwest and North regions and portions of the Brazilian Southeast, as well as Bolivia, Peru, Ecuador and Venezuela. The SSP5-8.5 scenario projects a more intense sign of change, indicating a significant increase of over 3% in practically all of northwestern SA from 2080 onwards. Similarly, ensemble projections of five CMIP6 GCMs

indicate an increase of approximately 6% in PVP at latitudes above 20°S under the SSP1-2.6, SSP2-4.5, and SSP5-8.5 scenarios for the period 2041–2100^[22]. In addition, there are up to 2% reductions in the northern sector of northeastern Brazil, southern Brazil, Uruguay, and south-central Argentina, previously obtained with CMIP6 projections^[24,32].

For the MAM months, the projected changes are more modest during the 2020–2059 period, with both scenarios indicating non-significant increases of up to 2%. For the decades from 2060 onwards, the scenarios reinforce the pattern of change, with the SSP5-8.5 scenario extending the areas with an increase of more than 2% to the Brazilian Northeast from 2080 onwards, and extending the core of maximum increase in central Amazonia, as well as a reduction of the same magnitude in central Argentina. These results corroborate CMIP6 projections previously analyzed for the austral autumn of 2015–2100^[22].

Considering the months of JJA, the scenarios show significant increases of up to 1% in most of Brazil, Peru, and Colombia by 2059, with more evident increases projected by the SSP5-8.5 scenario. These results reiterate those of Dutta et al.^[22], which found an increase of up to 4% in photovoltaic energy potential in Brazil during JJA of 2015–2040. For the decades from 2060 onwards, the increases persist in the areas already mentioned, including significant increases of over 2% in the Brazilian Southeast and Northeast coastal areas, projected by both scenarios. Similarly, these areas also showed a rise of over 2% in the austral winter of 2041–2100 under the SSP1-2.6, SSP2-4.5, and SSP5-8.5 scenarios^[22]. Furthermore, reductions of up to 3% persist in central-southern Brazil, central-northern Argentina, and the west coast of SA.

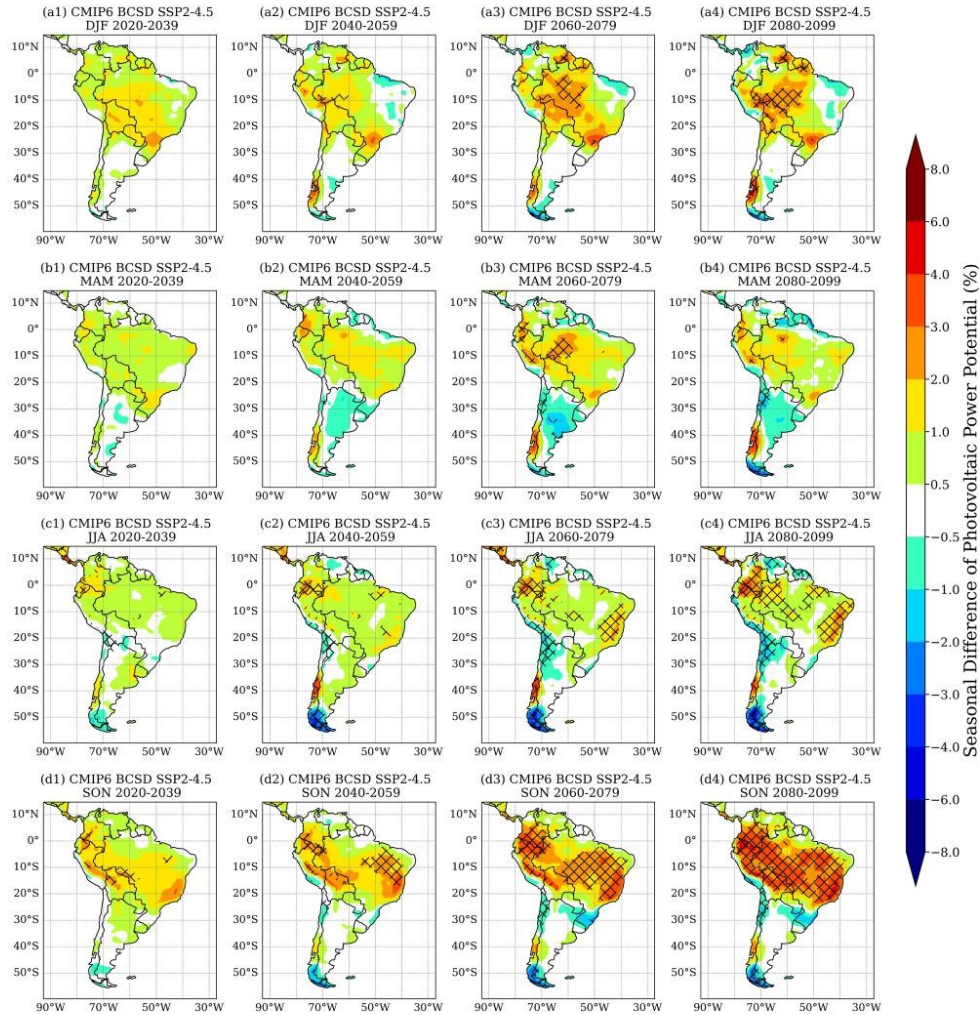


Figure 8. Seasonal difference (%) in PVP_{pot} projected by the CMIP6 ensemble after BCSd with the CLARA-A3 + ERA5 ensemble under the SSP2-4.5 emission scenario for the periods 2020–2039, 2040–2059, 2060–2079, and 2080–2099 in relation to the historical period (1995–2014). Hatched areas indicate a statistical significance of 95%, based on the Student's *t*-test.

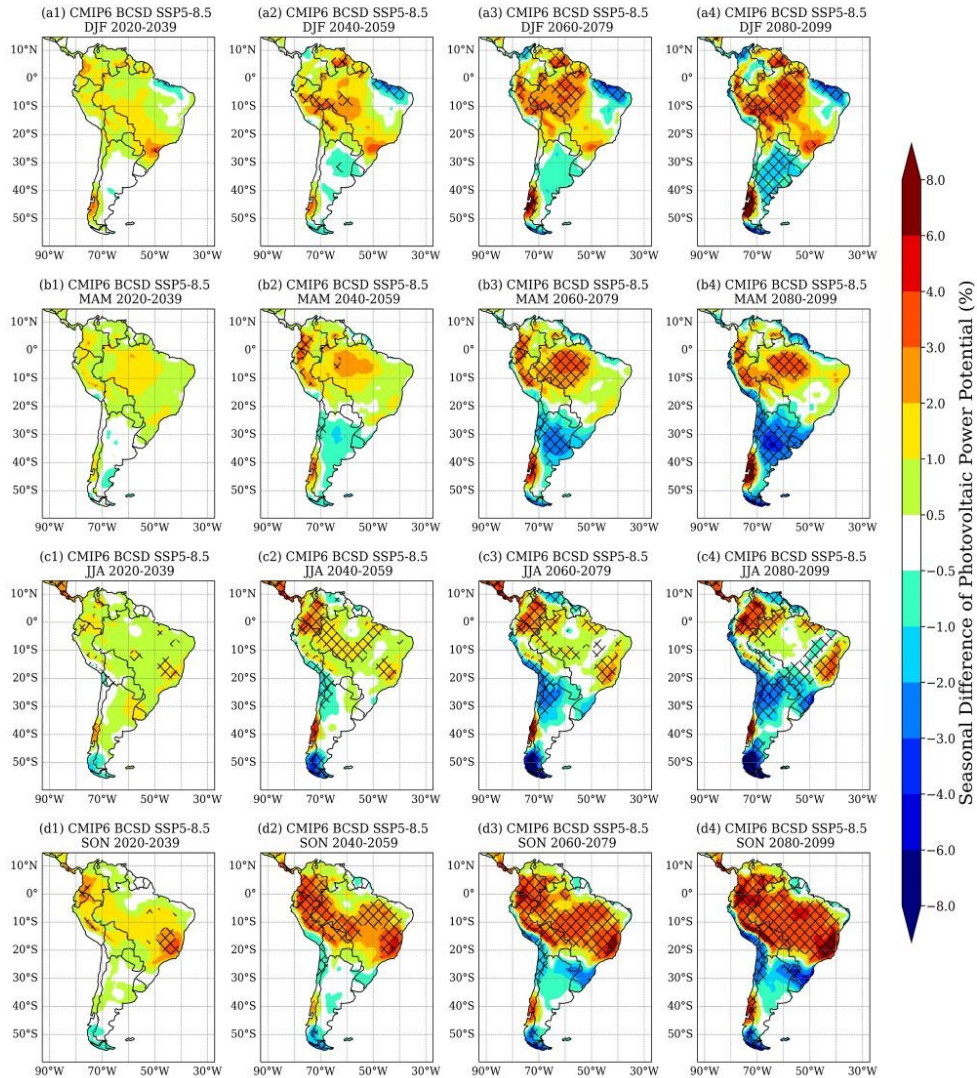


Figure 9. Similar to Figure 8, except for the SSP5-8.5 scenario.

For the SON months, under both scenarios, the CMIP6 ensemble shows significant increases of 2 to 6% by 2059 in the Brazilian Midwest, the northern portion of Northeast Brazil, the coast of Southeast Brazil, Brazilian Amazonia, Bolivia, Peru, Ecuador, and Colombia, reiterating previous CMIP6 results for 2015–2040 under the same scenarios [22]. From 2060 onwards, both scenarios amplify the regions with a significant increase above 3%, covering practically all of Brazil, Bolivia, Peru, Colombia, Ecuador, and Venezuela, with the SSP5-8.5 scenario showing a more intense sign of change. These results corroborate CMIP6 projections already made for 2041–2100, which indicate a transversal range of increasing PVP of up to 8% extending from the coast of southeastern Brazil to the north of SA [22].

In summary, results indicated that regions with solar energy potential in the historical period maintain suitable conditions in the future climate. Furthermore, the projections of CSP suggest an increasing generation in most SA (mainly Brazil, Peru, Bolivia, Ecuador, and Colombia). On the other hand, although PVP projections also majoritarily indicate favorable conditions for solar energy generation (especially during SON and under the SSP5-8.5 scenario), there are decreasing estimates in areas such as the northern sector of the Brazilian Northeast (during DJF), southern Brazil, Argentina and north Chile (all year round), whose reduction sign is more intense under the SSP5-8.5 scenario, which was also observed in studies with projections of CMIP3 [14], CMIP5 [18,19,30,31] and CMIP6 [22,24,32] models. In general, the negative PVP anomalies obtained here partially agree with those of other studies, which found that a thermal increase of up to 5 °C under the RCP-8.5 scenario can promote a reduction of up to 3% in PVP generation [15,17]. Thus, we suggest that the decreasing PVP in these regions may stem from the increasing local warming, given that the efficiency of PVP solar panels reduces by approximately 0.2–0.5% for every 1 °C increase in temperature [10,69]. However, in other regions where local warming does not result in neg-

ative PVP projections, it is likely that other factors, such as increased solar irradiance at the surface and reduced cloud cover, can compensate for this decrease in the PVP panels' efficiency due to thermal warming [15,24]. In this sense, the decreasing cloud cover projected for low latitudes [70] and the increasing average surface wind speed of 0.5–1.0 m s⁻¹ estimated for SA [40] may enhance the PVP generation, contributing to greater solar panel efficiency (through the higher incidence of solar radiation and the cooling effect). Moreover, the projections of increasing cloud cover in mid-latitudes [70] and precipitation in southern Brazil [39] may intensify the decreasing PVP in South Brazil for the coming decades.

We stress that errors persist in climate simulations even after bias correction of the original CMIP6 data. One reason for this arises from the CM SAF CLARA-A3 solar irradiance at the surface being derived from other parameters such as the cloud cover index (extracted from satellite observations), vertically integrated water vapor, ozone, and surface albedo (obtained from climatological data from ERA5) through a radiative transfer model, which also has their associated biases and uncertainties [21,54]. However, we highlight the good performance of the QDM technique in reducing the systematic errors of CMIP6 simulations by up to 50% when using the CLARA-A3 + ERA5 ensemble mean for statistical downscaling.

Anomalies time series and trends

Figures 10 to 13 present the seasonal PVP_{pot} anomalies (in percentage) in six subdomains of SA projected by each CMIP6 GCM and the multi-model ensemble under the SSP5-8.5 scenario and after BCSD with the CLARA-A3 + ERA5 ensemble mean. The series represents seasonal anomalies projected for 2020-2099 relative to the climatological period (1995–2014). In addition, Tables 2 to 5 also present the results of the Mann-Kendall and Sen's slope tests, provided by each model and the multi-model ensemble for the six subdomains under the SSP5-8.5 scenario.

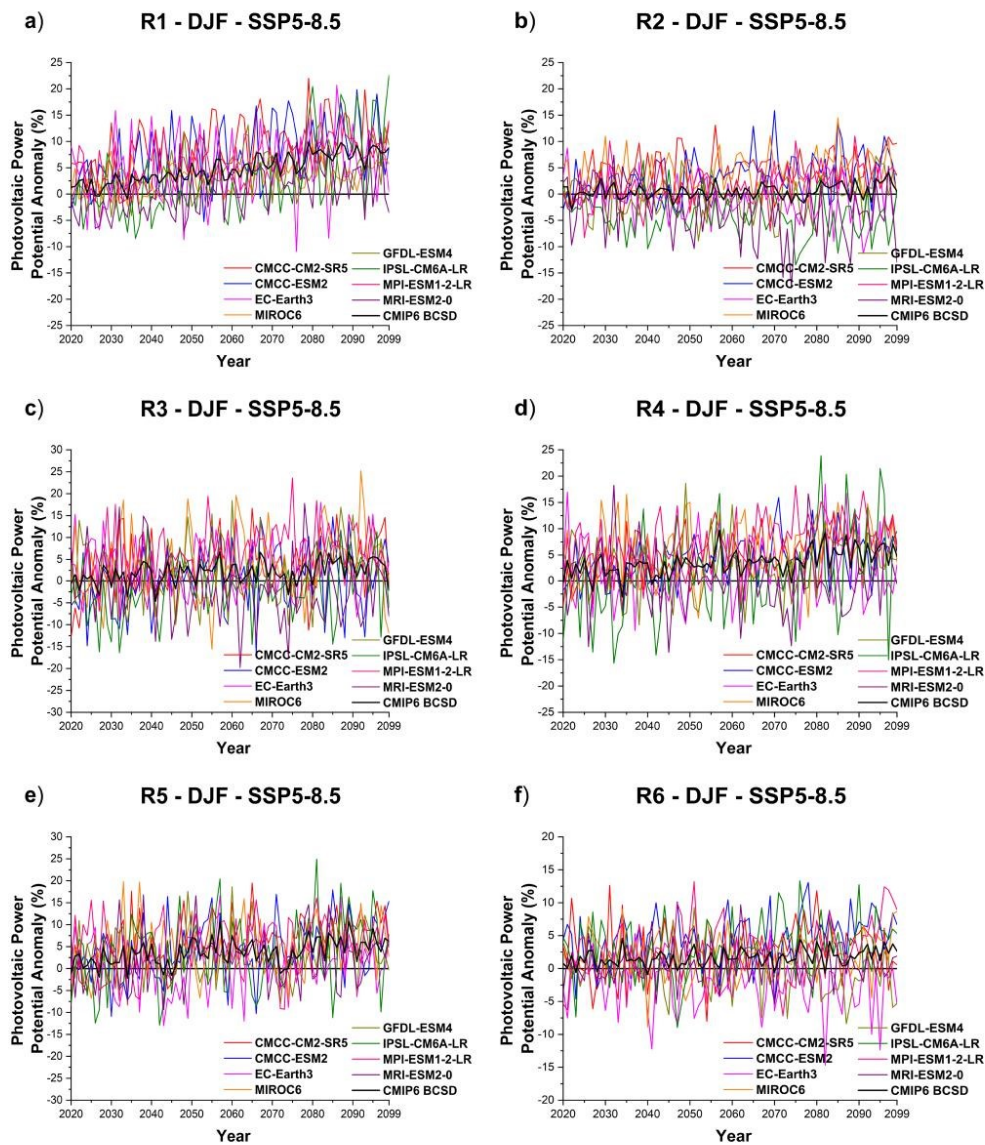


Figure 10. Time series (2020–2099) of PVP_{pot} anomalies (%) in the DJF months for six SA subdomains (R1-R6) relative to the climatological period (1995–2014), obtained after BCSDe with the CLARA-A3 + ERA5 ensemble under the SSP5-8.5 scenario.

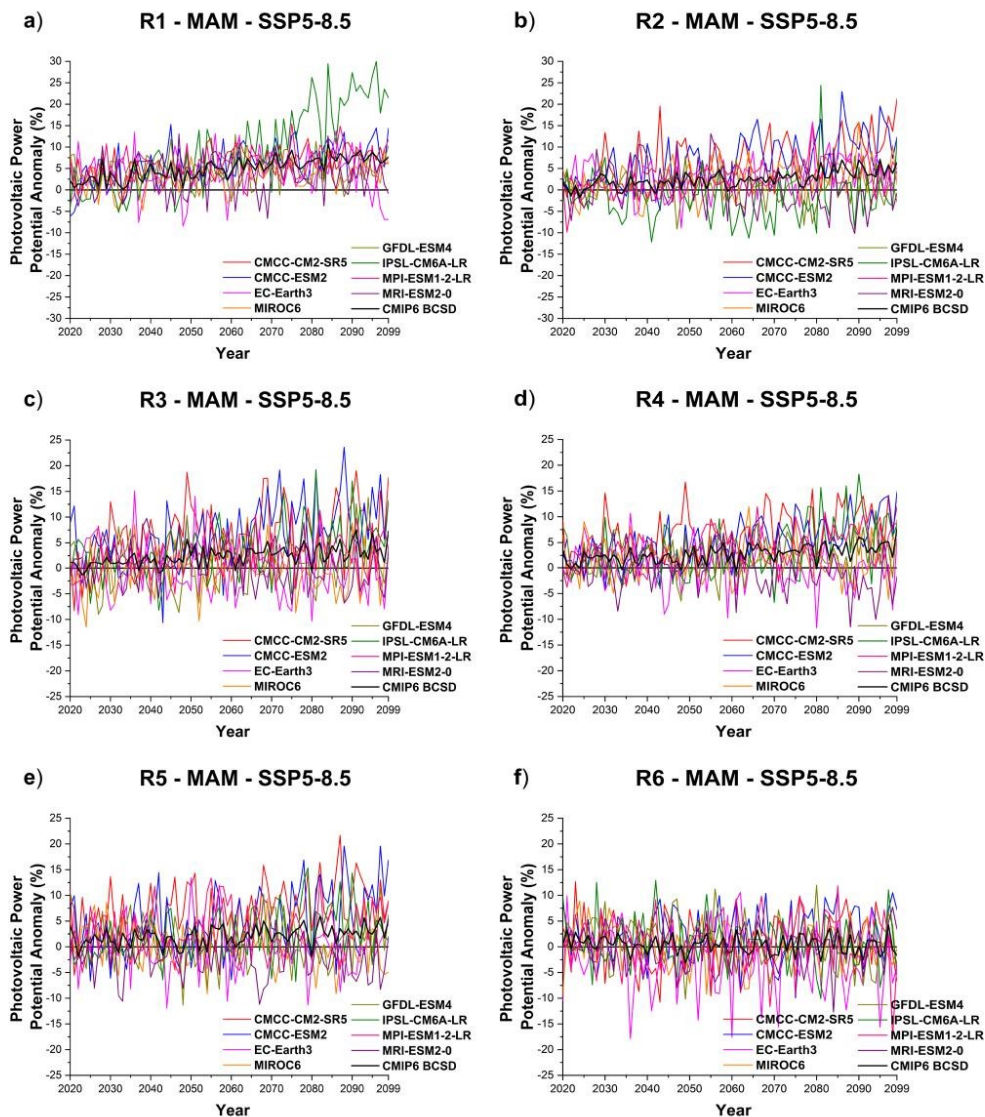


Figure 11. Similar to Figure 10, except for MAM.

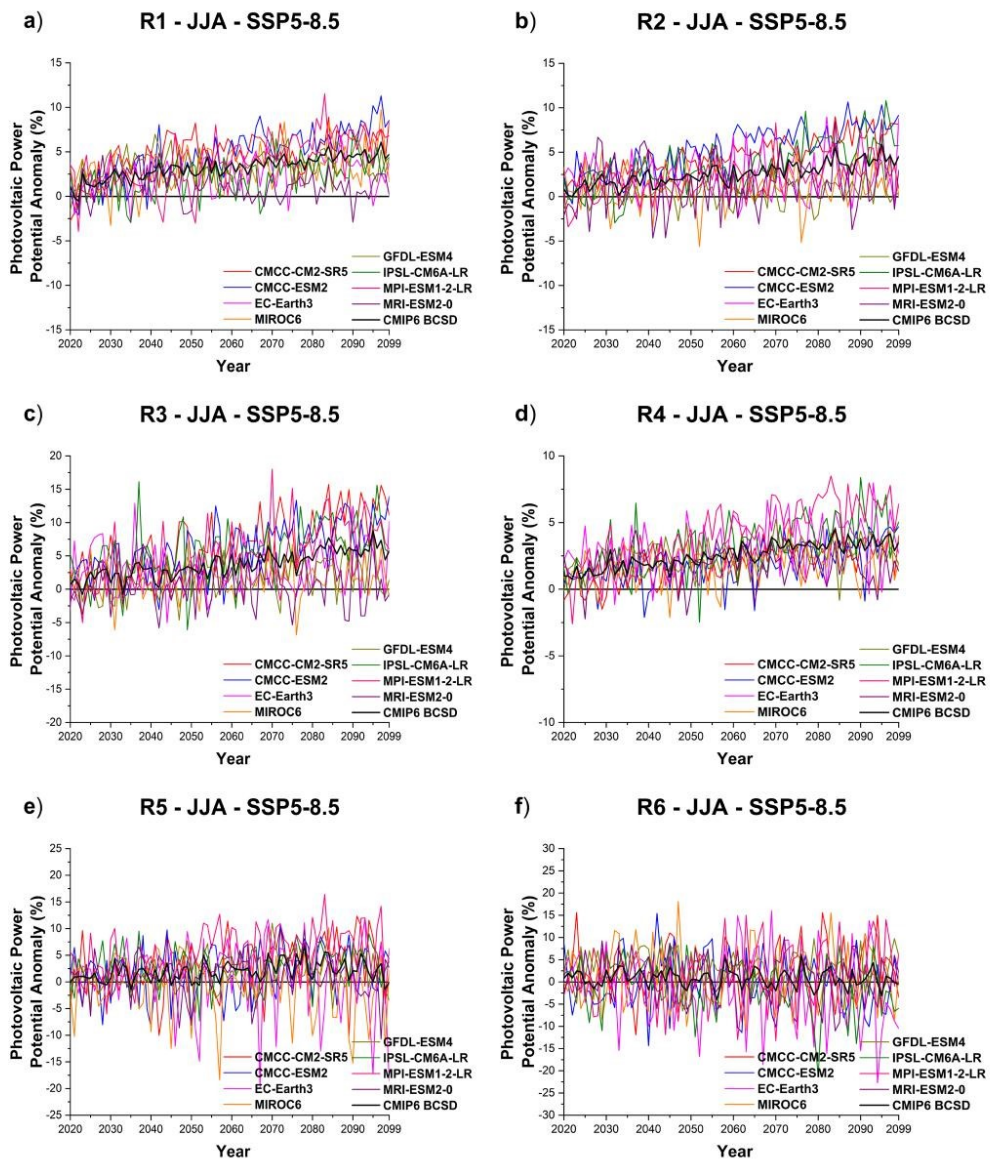


Figure 12. Similar to Figure 10, except for JJA.

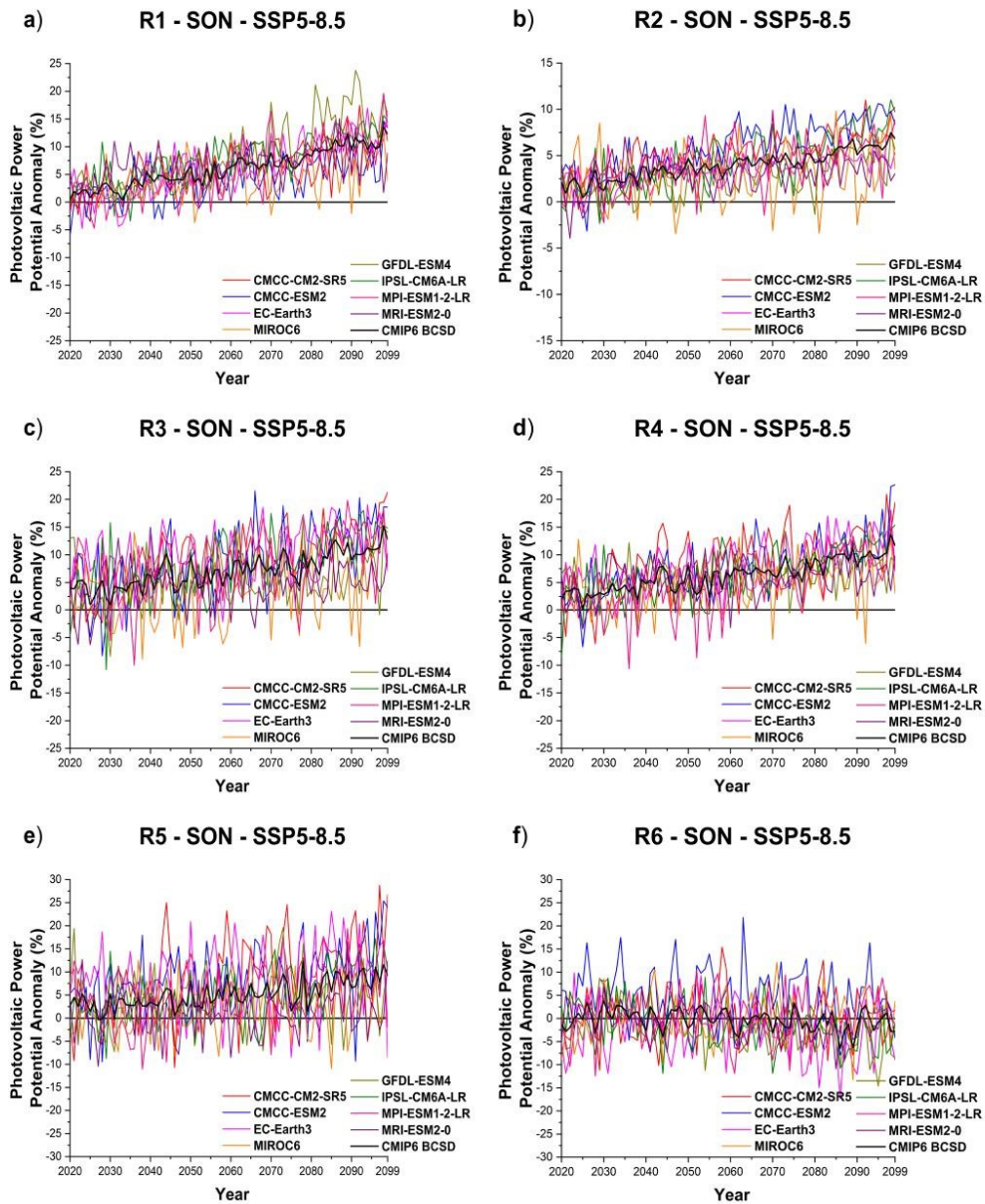


Figure 13. Similar to Figure 10, except for SON.

Table 2. Parameters of the Mann-Kendall and Sen’s Slope tests for the PVP_{pot} time series in the months of DJF (2020–2099) for six SA subdomains obtained by each GCM and CMIP6 multi-model ensemble after BCSD and under the SSP5-8.5 scenario. P, N, NT, T, and F denote positive, negative, no trend, true and false, respectively.

		CMCC-SR5	CMCC-ESM2	EC-EARTH3	MIROC6	GFDL-ESM4	IPSL-CM6A-LR	MPI-ESM1-2-LR	MRI-ESM2-0	CMIP6 BCSD
R1	Trend	P	P	NT	P	NT	P	P	P	P
	Ho	T	T	F	T	F	T	T	T	T
	Slope	0.0295	0.0241	0.0127	0.0100	0.0173	0.0324	0.0245	0.0162	0.0192
R2	Trend	P	P	NT	P	NT	N	P	N	NT
	Ho	T	T	F	T	F	T	T	T	F
	Slope	0.0133	0.0178	-0.0059	0.0098	0.0068	-0.0087	0.0151	-0.0181	0.0035
R3	Trend	P	P	NT	NT	NT	P	P	N	P
	Ho	T	T	F	F	F	T	T	T	T
	Slope	0.0228	0.0200	0.0022	0.0153	0.0138	0.0173	0.0200	0.0196	0.0105
R4	Trend	P	P	NT	NT	NT	P	P	NT	P
	Ho	T	T	F	F	F	T	T	F	T
	Slope	0.0182	0.0164	-0.0024	0.0106	0.0064	0.0283	0.0247	-0.0050	0.0119
R5	Trend	P	P	NT	NT	NT	P	NT	NT	P
	Ho	T	T	F	F	F	T	F	F	T
	Slope	0.0342	0.0221	0.0054	0.0113	0.0081	0.0223	0.0101	0.0074	0.0145
R6	Trend	P	P	NT	NT	N	P	P	NT	P
	Ho	T	T	F	F	T	T	T	F	T
	Slope	0.0115	0.0123	0.0058	0.0041	-0.0119	0.0139	0.0169	0.0030	0.0053

Table 3. Similar to Table 2, except for the MAM months.

		CMCC-SR5	CMCC-ESM2	EC-EARTH3	MIROC6	GFDL-ESM4	IPSL-CM6A-LR	MPI-ESM1-2-LR	MRI-ESM2-0	CMIP6 BCSD
R1	Trend	P	P	NT	P	NT	P	P	NT	P
	Ho	T	T	F	T	F	T	T	F	T
	Slope	0.0133	0.0211	0.0035	0.0085	0.0030	0.0619	0.0169	0.0025	0.0100
R2	Trend	P	P	NT	P	NT	NT	P	NT	P
	Ho	T	T	F	T	F	F	T	F	T
	Slope	0.0277	0.0306	0.0079	0.0140	-0.0004	-0.0005	0.0166	-0.0076	0.0114
R3	Trend	P	P	NT	NT	NT	P	NT	NT	P
	Ho	T	T	F	F	F	T	F	F	T
	Slope	0.0226	0.0254	-0.0032	0.0001	0.0078	0.0171	0.0143	-0.0098	0.0098
R4	Trend	P	P	NT	NT	NT	P	P	N	P
	Ho	T	T	F	F	F	T	T	T	T
	Slope	0.0188	0.0244	-0.0053	-0.0015	0.0047	0.0235	0.0172	-0.0103	0.0089
R5	Trend	P	P	NT	N	NT	P	NT	NT	P
	Ho	T	T	F	T	F	T	F	F	T
	Slope	0.0194	0.0236	-0.0031	-0.0085	-0.0001	0.0153	0.0081	-0.0049	0.0062
R6	Trend	NT	NT	NT	NT	N	NT	NT	NT	NT
	Ho	F	F	F	F	T	F	F	F	F
	Slope	0.0057	0.0065	-0.0044	-0.0033	-0.0092	-0.0026	-0.0028	0.0006	-0.0023

Table 4. Similar to Table 2, except for the JJA months.

		CMCC-SR5	CMCC-ESM2	EC-EARTH3	MIROC6	GFDL-ESM4	IPSL-CM6A-LR	MPI-ESM1-2-LR	MRI-ESM2-0	CMIP6 BCS
R1	Trend	P	P	P	P	P	P	P	NT	P
	Ho	T	T	T	T	T	T	T	F	T
	Slope	0.0139	0.0220	0.0065	0.0063	0.0044	0.0099	0.0187	-0.0019	0.0100
R2	Trend	P	P	NT	NT	P	P	P	NT	P
	Ho	T	T	F	F	T	T	T	F	T
	Slope	0.0195	0.0220	0.0009	0.0029	0.0034	0.0187	0.0116	0.0038	0.0108
R3	Trend	P	P	NT	NT	P	P	P	NT	P
	Ho	T	T	F	F	T	T	T	F	T
	Slope	0.0281	0.0234	0.0044	0.0043	0.0072	0.0166	0.0267	0.0014	0.0136
R4	Trend	P	P	P	NT	P	P	P	NT	P
	Ho	T	T	T	F	T	T	T	F	T
	Slope	0.0101	0.0092	0.0067	0.0031	0.0046	0.0118	0.0167	0.0002	0.0078
R5	Trend	P	NT	NT	NT	NT	P	P	NT	P
	Ho	T	F	F	F	F	T	T	F	T
	Slope	0.0172	0.0063	-0.0005	-0.0024	0.0050	0.0075	0.0167	0.0147	0.0045
R6	Trend	NT	NT	NT	NT	NT	N	P	NT	NT
	Ho	F	F	F	F	F	T	T	F	F
	Slope	0.0021	-0.0028	-0.0098	0.0006	-0.0018	-0.0067	0.0106	-0.0015	-0.0013

Table 5. Similar to Table 2, except for the SON months.

		CMCC-SR5	CMCC-ESM2	EC-EARTH3	MIROC6	GFDL-ESM4	IPSL-CM6A-LR	MPI-ESM1-2-LR	MRI-ESM2-0	CMIP6 BCS
R1	Trend	P	P	P	P	P	P	P	P	P
	Ho	T	T	T	T	T	T	T	T	T
	Slope	0.0295	0.0227	0.0389	0.0133	0.0449	0.0379	0.0379	0.0171	0.0304
R2	Trend	P	P	P	NT	P	P	P	NT	P
	Ho	T	T	T	F	T	T	T	F	T
	Slope	0.0211	0.0291	0.0119	0.0038	0.0162	0.0290	0.0184	0.0047	0.0169
R3	Trend	P	P	P	P	P	P	P	NT	P
	Ho	T	T	T	T	T	T	T	F	T
	Slope	0.0413	0.0404	0.0261	0.0169	0.0137	0.0416	0.0288	0.0097	0.0279
R4	Trend	P	P	P	P	P	P	P	NT	P
	Ho	T	T	T	T	T	T	T	F	T
	Slope	0.0368	0.0337	0.0292	0.00139	0.0186	0.0378	0.0282	0.0079	0.0261
R5	Trend	P	P	NT	NT	NT	P	P	NT	P
	Ho	T	T	F	F	F	T	T	F	T
	Slope	0.0465	0.0318	0.0141	0.0105	0.0095	0.0324	0.0184	0.0017	0.0203
R6	Trend	NT	NT	NT	NT	N	N	NT	N	N
	Ho	F	F	F	F	T	T	F	T	T
	Slope	0.0007	-0.0081	-0.0056	0.0058	-0.0179	-0.0161	0.0072	-0.0101	-0.0063

For R1, approximately 83% of PVP anomaly projections are positive, indicating year-round solar potential growth in the region throughout the 21st century. Considering all seasons, only the EC-Earth3, GFDL-ESM4, and MRI-ESM2-0 models do not project a significant positive trend in PVP in the Amazonia sector. Similarly, the multi-model ensemble projects a significant increase in year-round PVP throughout the 21st century, with anomalies of up to 13.5% in SON months. EC-Earth3, IPSL-CM6A-LR, and MPI-ESM1-2-LR models present the largest amplitude of projected PVP anomalies in the months of DJF, MAM, JJA, and SON, respectively. On the other hand, the maximum PVP anomalies are projected by the models IPSL-CM6A-LR (~23% in DJF 2099 and ~30% in MAM 2096), MPI-ESM1-2-LR (~11.5% in JJA from 2083) and GFDL-ESM4 (~28% in SON from 2091). Other studies also indicate a significant increase in PVP in the region throughout the century, projected by CMIP3^[14], CMIP5^[18,19,24,30,31], and CMIP6^[22,24] models.

For R2, approximately 61% of projections indicate a statistically significant increase in year-round PVP during the 21st century. EC-Earth3, GFDL-ESM4, IPSL-CM6A-LR, and MRI-ESM2-0 models indicate no trend or negative trend in the months of DJF and MAM, while in the months of JJA and SON, EC-Earth3, MIROC6, and MRI-ESM2-0 models do not indicate a significant trend. Similarly, the CMIP6 multi-model ensemble projects a statistically significant increase in PVP in all months, with a positive anomaly of up to 7.5% in MAM 2098. MRI-ESM2-0, CMCC-ESM2, and IPSL-CM6A-LR models present the largest range of projections, while the largest seasonal PVP anomalies show increases of up to 16% in 2070 DJF (CMCC-ESM2), 23% in 2081 MAM (CMCC-ESM2), 11% in 2096 JJA (IPSL-CM6A-LR) and 11% in 2092 SON (IPSL-CM6A-LR).

Regarding R3, around 64% of projections indicate a statistically significant increase in PVP throughout the year during the 21st century. EC-Earth3, GFDL-ESM4, MIROC6, IPSL-CM6A-LR, MPI-ESM1-2-LR, and MRI-ESM2-0 show no trend in practically

the entire year, while for the SON months, only the MRI-ESM2-0 model does not indicate a significant positive trend. Furthermore, the ensemble projects an increase of up to 17% in the SON months of 2098. The CMCC-ESM2, MIROC6, and MPI-ESM1-2-LR models have the largest range of projections, with the MPI-ESM1-2-LR model projecting a positive PVP anomaly of ~25% in DJF of 2092. In general, the anomalies projected by the models and ensemble agree with those of other studies that show an average increase of 5% in the PVP of the northeastern region for the following decades, projected by models of CMIP5^[19,30,24] and CMIP6^[22].

For R4, approximately 70% of projections estimate a significant increase in PVP throughout the year during the following decades, while EC-Earth3, MIROC6, GFDL-ESM4, and MRI-ESM2-0 models indicate no trend or negative trend in practically all year. Furthermore, the ensemble projects a statistically significant increase in PVP throughout the year, with a positive anomaly of up to 14% during SON of 2098. CMCC-ESM2, IPSL-CM6A-LR, and MPI-ESM1-2-LR models present greater amplitude of projections, estimating up to 24% increases in the DJF months. The anomalies obtained corroborate the average growth of approximately 5% in the PVP of the Brazilian Midwest during the 21st century, estimated by CMIP5 models under the RCP4.5^[19] and RCP8.5^[30] scenarios and CMIP6 under the SSP2-4.5 and SSP5-8.5 scenarios^[22].

Regarding R5, approximately 47% of projections indicate a statistically significant increase in PVP throughout the year during the 21st century. Similar to regions R3 and R4, in this sector, EC-Earth3, GFDL-ESM4, MIROC6, IPSL-CM6A-LR, MPI-ESM1-2-LR, and MRI-ESM2-0 result in no trend in seasonal PVP projections across most of the year. Furthermore, the CMIP6 ensemble projects a statistically significant increase in PVP throughout the year, with a positive anomaly of up to 12% in the SON months. IPSL-CM6A-LR, CMCC-CM2-SR5, and EC-Earth3 models present the largest range of projections, with the CMCC-CM2-SR5 and IPSL-CM6A-LR GCMs estimating increases of up to 28% and 25% in the

months of SON and DJF, respectively. Similarly, the anomalies found here reiterate those of other studies, which obtained an average increase of 5% in PVP for the coming decades in Southeast Brazil, projected by CMIP5^[19,30,31] and CMIP6^[22,24] models.

Finally, for R6, only 16% of projections estimate a significant increase in PVP, concentrated in the DJF months. Unlike the other five regions evaluated, the projections obtained for South Brazil and Uruguay mainly indicate a non-significant or negative trend in PVP throughout the year for the coming decades. Furthermore, the CMIP6 ensemble projects a statistically significant increase (reduction) in PVP only in DJF (SON). In general, these results corroborate the literature since the considerable decrease of PVP in South Brazil was also estimated by projections from CMIP3^[14], CMIP5^[18,19,24,30], and CMIP6^[22,24,32].

In summary, PVP trend analyses in different subdomains of SA show that practically all regions (except the southern region of Brazil and Uruguay) show a tendency for an increasing solar potential during the 21st century throughout the year (with better estimates for the austral spring and summer and sectors R1 and R4). The anomaly projections obtained by the ensemble show that, in descending order, the most significant increases in PVP occur in northern Brazil (R1), Brazilian Midwest (R4), southern and central sectors of Northeast Brazil (R3), north sector of Northeast Brazil (R2) and Southeast Brazil (R5). On the other hand, southern Brazil (R6) presents around 84% of projections with a negative trend or no signal, highlighting an unfavorable or uncertain scenario for the PVP development in the region.

In general, the models mostly converge to an increasing PVP throughout the century in practically all of Brazil. On the other hand, while models such as EC-Earth3 and MIROC6 result in no trend in almost all analyses, other GCMs such as GFDL-ESM4 and MRI-ESM2-0 project mixed signals, depending on the regions and seasons. In any case, the projections reiterate the literature, which shows a significant increasing tendency for PVP over the next decades in the Amazonia region^[14,18,19,22,24,30,31,32], the Northeast, Midwest, and Southeast Brazil^[19,22,24,30,31].

Conversely, projections for South Brazil predominantly suggest the absence of a signal or a tendency towards a decreasing PVP, corroborating previous results^[14,19,22,24,30,31,32].

4. Conclusions

The growing demand for energy makes it urgent to promote sustainable development in response to climate change. In this context, adopting measures to mitigate environmental impacts is essential to promote the efficient use of resources and the clean energy transition. Therefore, this study sought to evaluate the projections of change in solar irradiance, concentrated solar energy, and photovoltaic energy potential estimated by an ensemble of eight CMIP6 GCMs for SA during the 21st century under the SSP2-4.5 and SSP5-8.5 scenarios. To this end, we applied statistical downscaling to the simulations and projections of the CMIP6 models using the ERA5 reanalysis and CLARA-A3 satellite observations as reference data. The ERA5 + CLARA-A3 ensemble mean validated the climate simulations for the historical period (1995–2014) and the application of statistical downscaling. The QDM technique effectively reduced the systematic biases of the original CMIP6 solar irradiance simulations, reducing errors by approximately 50% over practically the entire continent throughout the year. However, even after the BCSD method, biases persist in regions such as northeastern Brazil and northern SA.

The projections of CSP show that regions traditionally favorable to its generation (mainly the Brazilian Northeast) may maintain suitable conditions in the coming decades. On the other hand, projections of decreasing PVP in sectors such as the north of the Brazilian Northeast, Argentina, the west coast of SA, and southern Brazil suggest that other climate factors such as local warming, cloud cover, aerosols, and wind speed may influence solar energy generation in these regions. In general, the results indicate spatial and seasonal variability of solar generation in SA, pointing to increases of approximately 1–6% in CSP (mainly under the SSP5-8.5 scenario in southern Chile and most of Brazil) and 1–4% in PVP gen-

eration (mainly under the SSP5-8.5 scenario in the Amazon, Midwest and Southeast Brazilian sectors). In addition, trend analyses projected individually by the CMIP6 GCMs converge on an increasing PVP, mainly in Brazil's Amazonia and Midwest regions. Conversely, for the country's southern sector, approximately 84% of the projections show a negative trend (or no trend), showing unfavorable or uncertain conditions for the development of PVP generation in the region.

It is also worth mentioning some limitations of this study. Firstly, this analysis investigates the possible changes in solar energy generation in SA from a purely atmospheric perspective without considering other relevant economic, technological, and political factors. In this sense, future research should consider the feasibility of expanding the solar matrix on the continent through incentive policies for the sector that favor strategic planning, foreign investment, solar industry consolidation, and energy storage. Furthermore, there is no analysis of the technological advances that may improve the photovoltaic panels' efficiency (including their performance concerning thermal heating) and the reduced cost of solar technology, factors that could encourage its implementation in SA over the coming decades. In addition, we highlight the importance of studies that evaluate the relationship between solar energy generation and cloud cover, given that in SA, this correspondence is well corroborated during the austral fall and inconsistent for the other seasons^[22]. In this context, regional climate models are valuable tools for analyzing this issue, and we expect to see increasing use of these models driven by CMIP6 GCMs in future research.

Finally, we point out that the datasets used to validate climate simulations also have their systematic biases. Although the reanalysis products have satisfactory overall performance, these data result from the assimilation of observations and numerical simulations through radiative transfer models^[52], so uncertainties and biases are inherent to this source of information. For example, the solar energy derived from the ERA5 reanalysis is overestimated by ap-

proximately 23% during the boreal winter in North America^[54]. Furthermore, one of SA's solar hotspots (Northeast Brazil) corresponds to one of the global sectors where CLARA-A3 presents uncertainties^[55]. Here, we stress that the satellite dataset also has systematic biases since it derives from the assimilation of different sources, such as reanalysis and numerical simulations^[21,55]. Given this, we reiterate that the projections must be analyzed considering the uncertainties and systematic biases of the reference data.

Moreover, this study uses CMIP6 climate projections with bias correction and statistical downscaling to assess solar potential in SA. Generally, studies analyze raw model outputs with coarse resolution and without bias correction, which is inappropriate for studies focused on renewable energy and climate change impacts. In this context, our results advance knowledge about future solar generation scenarios on the continent and represent a first look at solar energy potential in SA with corrected state-of-the-art projections. Furthermore, the few existing studies on the future potential of solar energy with CMIP6 models in South America evaluate shorter time horizons, such as the near future of 2021–2050^[32] and the distant future of 2071–2100^[24]. In this sense, our study differs by presenting projections for the entire 21st century, using four time horizons of interest to the South American energy sector.

Nevertheless, the projections presented here may have significant implications for policymakers, energy planners, and South American energy sector investors. For instance, indicating areas with high solar power potential underscores promising locales for establishing solar farms, fostering strategic planning, and assisting the transition towards a low-carbon and sustainable energy grid across SA. Lastly, this study gives helpful insights to stakeholders engaged in developing the solar energy infrastructure, as the analyses herein mark a fresh analysis of statistically downscaled climate projections from CMIP6 models tailored to SA's solar potential.

Author Contributions

Glauber W.S. Ferreira, Michelle S. Reboita, and

J.G.M. Ribeiro processed and analyzed the data. Glauber W.S. Ferreira and Michelle S. Reboita wrote the original draft. All authors read and approved the final manuscript.

Conflict of Interest

The authors have no relevant financial or non-financial interests to disclose.

Funding

This research was funded by Engie Brasil Energia (R&D00403–54/2022) through the R&D Program regulated by the Brazilian Electricity Regulatory Agency (ANEEL) and the Coordination for the Improvement of Higher Education (CAPES, Finance Code 001).

Acknowledgments

The authors thank the National Council for Scientific and Technological Development (CNPq), Coordination for the Improvement of Higher Education (CAPES), and Engie Brasil Energia for their financial support. The authors also thank the European Centre for Medium-Range Weather Forecasts (ECMWF), the Coupled Model Intercomparison Project (CMIP), and the Satellite Application Facility on Climate Monitoring (CM SAF) from the European Organization for the Exploitation of Meteorological Satellites (EUMETSAT) for the data used in this study.

Data Availability Statement

The CMIP6 climate models are available at: <https://aims2.llnl.gov/search/cmip6/>. The ECMWF-ERA5 reanalysis is available at: <https://cds.climate.copernicus.eu/>. Satellite observations from CLARA-A3 are available at: <https://wui.cmsaf.eu/safira/action/viewProduktList?dId=2>

References

[1] Climate Change 2023: Synthesis Report. IPCC:

Geneva, Switzerland. pp. 1–34.

DOI: <https://doi.org/10.59327/IPCC/AR6-9789291691647.001>

- [2] Reboita, M.S., Ambrizzi, T., 2022. Climate system in a nutshell: an overview for understanding climate change. *International Journal of Development Research*. 12, 53365-53378. Available from: <https://www.journalijdr.com/sites/default/files/issue-pdf/23731.pdf>
- [3] Climate Change: Global Temperature [Internet] [cited 2024 Apr 3]. Available from: https://www.energy.gov/sites/default/files/2024-02/093.%20Rebecca%20Lindsey%20and%20Luann%20Dahlman%2C%20NOAA%2C%20Climate%20Change_%20Global%20Temperature.pdf
- [4] Icaza, D., Borge-Diez, D., Galindo, S.P., 2022. Analysis and proposal of energy planning and renewable energy plans in South America: Case study of Ecuador. *Renewable Energy*. 182, 314–342. DOI: <https://doi.org/10.1016/j.renene.2021.09.126>
- [5] Arango-Aramburo, S., Ríos-Ocampo, J.P., Larsen, E.R., 2020. Examining the decreasing share of renewable energy and growing thermal capacity: The case of South America. *Renewable and Sustainable Energy Review*. 119, 109648. DOI: <https://doi.org/10.1016/j.rser.2019.109648>
- [6] Deng, Q., Alvarado, R., Toledo, E., Caraguay, L., 2020. Greenhouse gas emissions, non-renewable energy consumption, and output in South America: the role of the productive structure. *Environmental Science and Pollution Research*. 27, 14477–14491. DOI: <https://doi.org/10.1007/s11356-020-07693-9>
- [7] A Race to the Top Latin America 2023: Wind and Solar Utility-Scale Buildout Gains Speed in Brazil, Chile and Colombia, while Mexico Falls Behind [Internet] [cited 2024 Apr 5]. Available from: <https://globalenergymonitor.org/report/a-race-to-the-top-latin-america/>
- [8] Brazil Holds the Key to Latin America’s Solar Potential [Internet] [cited 2024 Apr 5].

- Available from: <https://www.reuters.com/markets/commodities/brazil-holds-key-latin-america-solar-potential-2024-02-29/#:~:text=PV%20PLANS,of%20Latin%20America's%20solar%20generation>
- [9] Exame, E.S.G., 2024. Solar Energy Reaches 40 GW of Installed Capacity in Brazil. Retrieved from Exame ESG [Internet] [cited 2024 Apr 5]. Available from: <https://exame.com/esg/energia-solar-alcanca-40-gw-de-capacidade-instalada-no-brasil/> (In Portuguese)
- [10] Patt, A., Pfenninger, S., Lilliestam, J., 2013. Vulnerability of solar energy infrastructure and output to climate change. *Climatic Change*. 121, 93–102.
DOI: <https://doi.org/10.1007/s10584-013-0887-0>
- [11] Solar Energy [Internet] [cited 2024 Apr 5]. Available from: <https://www.irena.org/Energy-Transition/Technology/Solar-energy>
- [12] Letcher, T.M., 2022. *Comprehensive renewable energy*, 2nd ed. Elsevier: Amsterdam, Netherlands. pp. 796.
- [13] Solar Energy Becomes the Third Largest Source in Brazil [Internet] [cited 2024 Apr 5]. Available from: <https://www.gov.br/en/government-of-brazil/latest-news/solar-energy-becomes-the-third-largest-source-in-brazil>
- [14] Crook, J.A., Jones, L.A., Forster, P.M., et al., 2011. Climate change impacts on future photovoltaic and concentrated solar power energy output. *Energy & Environmental Science*. 4, 3101.
DOI: <https://doi.org/10.1039/c1ee01495a>
- [15] Jerez, S., Tobin, I., Vautard, R., et al, 2015. The impact of climate change on photovoltaic power generation in Europe. *Nature Communications*. 6, 10014.
DOI: <https://doi.org/10.1038/ncomms10014>
- [16] Wild, M., Folini, D., Henschel, F., Fischer, N., Müller, B., 2015. Projections of long-term changes in solar radiation based on CMIP5 climate models and their influence on energy yields of photovoltaic systems. *Solar Energy*. 116, 12–24.
DOI: <https://doi.org/10.1016/j.solener.2015.03.039>
- [17] Müller, J., Folini, D., Wild, M., et al., 2019. CMIP-5 models project photovoltaics are a no-regrets investment in Europe irrespective of climate change. *Energy*. 171, 135–148.
DOI: <https://doi.org/10.1016/j.energy.2018.12.139>
- [18] Zou, L., Wang, L., Li, J., et al., 2019. Global surface solar radiation and photovoltaic power from Coupled Model Intercomparison Project Phase 5 climate models. *Journal of Cleaner Production*. 224, 304–324.
DOI: <https://doi.org/10.1016/j.jclepro.2019.03.268>
- [19] Feron, S., Cordero, R.R., Damiani, A., et al., 2021. Climate change extremes and photovoltaic power output. *Nature Sustainability*. 4, 270–276.
DOI: <https://doi.org/10.1038/s41893-020-00643-w>
- [20] Gernaat, D.E.H.J., de Boer, H.S., Daioglou, V., Yalew, S.G., Müller, C., van Vuuren, D.P., 2021. Climate change impacts on renewable energy supply. *Nature Climate Change*. 11, 119–125.
DOI: <https://doi.org/10.1038/s41558-020-00949-9>
- [21] Sawadogo, W., Reboita, M.S., Faye, A., et al, 2021. Current and future potential of solar and wind energy over Africa using the RegCM4 CORDEX-CORE ensemble. *Climate Dynamics*. 57, 1647–1672.
DOI: <https://doi.org/10.1007/s00382-020-05377-1>
- [22] Dutta, R., Chanda, K., Maity, R., 2022. Future of solar energy potential in a changing climate across the world: A CMIP6 multimodel ensemble analysis. *Renewable Energy*. 188, 819–829.
DOI: <https://doi.org/10.1016/j.renene.2022.02.023>
- [23] Ndiaye, A., Moussa, M.S., Dione, C., et al., 2023. Projected changes in solar PV and wind energy potential over West Africa: an analysis of CORDEX-CORE simulations. *Energies*. 15,

9602.
DOI: <https://doi.org/10.3390/en15249602>
- [24] Ha, S., Zhou, Z., Im, E.-S., et al., 2023. Comparative assessment of future solar power potential based on CMIP5 and CMIP6 multimodel ensembles. *Renewable Energy*. 206, 324–335.
DOI: <https://doi.org/10.1016/j.renene.2023.02.039>
- [25] Barbosa, L.S.N.S., Bogdanov, D., Vainikka, P., et al., 2017. Hydro, wind and solar power as a base for a 100% renewable energy supply for South and Central America. *PLoS ONE*. 12, e0173820.
DOI: <https://doi.org/10.1371/journal.pone.0173820>
- [26] Gil, G.M.V., Cunha, R.B.A., Di Santo, S.G., et al., 2020. Photovoltaic energy in South America: Current state and grid regulation for large-scale and distributed photovoltaic systems. *Renewable Energy*. 162, 1307–1320.
DOI: <https://doi.org/10.1016/j.renene.2020.08.022>
- [27] Narvaez, G., Giraldo, L.F., Bressan, M., 2022. The impact of climate change on photovoltaic power potential in Southwestern Colombia. *Heliyon*. 8, e11122.
DOI: <https://doi.org/10.1016/j.heliyon.2022.e11122>
- [28] Lopez, G., Aghahosseini, A., Bogdanov, D., et al., 2021. Pathway to a fully sustainable energy system for Bolivia across power, heat, and transport sectors by 2050. *Journal of Cleaner Production*. 293, 126195.
DOI: <https://doi.org/10.1016/j.jclepro.2021.126195>
- [29] Osorio-Aravena, J.C., Aghahosseini, A., Bogdanov, D., et al., 2021. The impact of renewable energy and sector coupling on the pathway towards a sustainable energy system in Chile. *Renewable and Sustainable Energy Reviews*. 151, 111557.
DOI: <https://doi.org/10.1016/j.rser.2021.111557>
- [30] de Jong, P., Barreto, T.B., Tanajura, C.A.S., et al., 2019. Estimating the impact of climate change on wind and solar energy in Brazil using a South American regional climate model. *Renewable Energy*. 141, 390–401.
DOI: <https://doi.org/10.1016/j.renene.2019.03.086>
- [31] Costa, R.S., da Costa, G.L., de Lima, F.J.L., et al., 2020. Impacts of climate change on the availability of solar energy resources. *Revista Brasileira de Energia*. 26, 39–50. (In Portuguese)
DOI: <https://doi.org/10.47168/rbe.v26i4.579>
- [32] Zuluaga, C.F., Avila-Diaz, A., Justino, F.B., et al., 2022. The climate change perspective of photovoltaic power potential in Brazil. *Renewable Energy*. 193, 1019–1031.
DOI: <https://doi.org/10.1016/j.renene.2022.05.029>
- [33] Ambrizzi, T., Reboita, M.S., da Rocha, R.P., et al., 2019. The state of the art and fundamental aspects of regional climate modeling in South America. *Annals of the New York Academy of Sciences*. 1436, 98–120.
DOI: <https://doi.org/10.1111/nyas.13932>
- [34] Mutz, S.G., Scherrer, S., Muceniece, I., et al., 2021. Twenty-first century regional temperature response in Chile based on empirical-statistical downscaling. *Climate Dynamics*. 56, 2881–2894.
DOI: <https://doi.org/10.1007/s00382-020-05620-9>
- [35] Ballarin, A.S., Sone, J.S., Gesualdo, G.C., et al., 2023. CLIMBra—Climate change dataset for Brazil. *Scientific Data*. 10, 47.
DOI: <https://doi.org/10.1038/s41597-023-01956-z>
- [36] Cannon, A.J., Sobie, S.R., Murdock, T.Q., 2015. Bias correction of GCM precipitation by Quantile Mapping: How well do methods preserve changes in quantiles and extremes? *Journal of Climate*. 28, 6938–6959.
DOI: <https://doi.org/10.1175/JCLI-D-14-00754.1>
- [37] Ferreira, G.W.S., Reboita, M.S., 2022. A new look into the South America precipitation regimes: Observation and forecast. *Atmosphere*. 13, 873.

- DOI: <https://doi.org/10.3390/atmos13060873>
- [38] Rupp, D.E., Abatzoglou, J.T., Hegewisch, K.C., et al., 2013. Evaluation of CMIP5 20th century climate simulations for the Pacific Northwest USA. *Journal of Geophysical Research: Atmosphere*. 118, 10884–10906.
DOI: <https://doi.org/10.1002/jgrd.50843>
- [39] Ferreira, G.W.S., Reboita, M.S., Ribeiro, J.G.M., et al., 2023. Assessment of precipitation and hydrological droughts in South America through statistically downscaled CMIP6 projections. *Climate*. 11, 166.
DOI: <https://doi.org/10.3390/cli11080166>
- [40] Ferreira, G.W.S., Reboita, M.S., Ribeiro, J.G.M., et al., 2024. Assessment of the wind power density over South America simulated by CMIP6 models in the present and future climate. *Climate Dynamics*. 62, 1729–1763.
DOI: <https://doi.org/10.1007/s00382-023-06993-3>
- [41] Reboita, M.S., Ferreira, G.W.S., Ribeiro, J.G.M., et al., 2023. South American monsoon lifecycle projected by statistical downscaling with CMIP6-GCMs. *Atmosphere*. 14, 1380.
DOI: <https://doi.org/10.3390/atmos14091380>
- [42] Reboita, M.S., Ferreira, G.W.S., Ribeiro, J.G.M., et al., 2024. Assessment of precipitation and near-surface temperature simulation by CMIP6 models in South America. *Environmental Research: Climate*. 3(2), 025001.
DOI: <https://doi.org/10.1088/2752-5295/ad3fdb>
- [43] Dias, C.G., Reboita, M.S., 2021. Assessment of CMIP6 simulations over tropical South America. *Revista Brasileira de Geografia Física*. 14, 1282–1295.
DOI: <https://doi.org/10.26848/rbgf.v14.3.p1282-1295>
- [44] Lovato, T., Peano, D., 2020. CMCC CMCC-CM2-SR5 model output prepared for CMIP6 CMIP historical Version 20200616. Earth System Grid Federation.
DOI: <https://doi.org/10.22033/ESGF/CMIP6.3825>
- [45] Lovato, T., Peano, D., Butenschön, M., et al., 2022. CMIP6 simulations with the CMCC Earth System Model (CMCC-ESM2). *Journal of Advances in Modeling Earth Systems*. 14, e2021MS002814.
DOI: <https://doi.org/10.1029/2021MS002814>
- [46] Döscher, R., Acosta, M., Alessandri, A., et al., 2022. The EC-Earth3 Earth System Model for the climate model intercomparison project 6. *Geoscience Model Development*. 15, 2973–3020.
DOI: <https://doi.org/10.5194/gmd-15-2973-2022>
- [47] Krasting, J.P., John, J.G., Blanton, C., et al., 2018. NOAA-GFDL GFDL-ESM4 model output prepared for CMIP6 CMIP historical. Version 20190726. Earth System Grid Federation.
DOI: <https://doi.org/10.22033/ESGF/CMIP6.8597>
- [48] Boucher, O., Denvil, S., Levassasseur, G., et al., 2018. IPSL IPSL-CM6A-LR model output prepared for CMIP6 CMIP historical. Version 20180803. Earth System Grid Federation.
DOI: <https://doi.org/10.22033/ESGF/CMIP6.5195>
- [49] Tatebe, H., Watanabe, M., 2018. MIROC MIROC6 model output prepared for CMIP6 CMIP historical. Version 20181212. Earth System Grid Federation.
DOI: <https://doi.org/10.22033/ESGF/CMIP6.5603>
- [50] Wieners, K.H., Giorgetta, M., Jungclaus, J., et al., 2019. MPI-M MPI-ESM1.2-LR model output prepared for CMIP6 CMIP historical. Version 20190710. Earth System Grid Federation.
DOI: <https://doi.org/10.22033/ESGF/CMIP6.6595>
- [51] Yukimoto, S., Koshiro, T., Kawai, H., et al., 2019. MRI MRI-ESM2.0 model output prepared for CMIP6 CMIP historical. Version 20190222. Earth System Grid Federation.
DOI: <https://doi.org/10.22033/ESGF/CMIP6.6842>
- [52] Hersbach, H., Bell, B., Berrisford, P., et al., 2020. The ERA5 global reanalysis. *Quarterly Journal of Royal Meteorological Society*. 146, 1999–2049.
DOI: <https://doi.org/10.1002/qj.3803>
- [53] Dullaart, J.C., Muis, S., Bloemendaal, N., et

- al., 2020. Advancing global storm surge modelling using the new ERA5 climate reanalysis. *Climate Dynamics*. 54, 1007–1021. DOI: <https://doi.org/10.1007/s00382-019-05044-0>
- [54] Wilczak, J.M., Akish, E., Capotondi, A., et al., 2024. Evaluation and bias correction of the ERA5 reanalysis over the United States for wind and solar energy applications. *Energies*. 17, 1667. DOI: <https://doi.org/10.3390/en17071667>
- [55] Karlsson, K.-G., Stengel, M., Meirink, J.F., et al., 2023. CLARA-A3: The third edition of the AVHRR-based CM SAF climate data record on clouds, radiation and surface albedo covering the period 1979 to 2023. *Earth System Science Data*. 15, 4901–4926. DOI: <https://doi.org/10.5194/essd-15-4901-2023>
- [56] Boilley, A., Wald, L., 2015. Comparison between meteorological re-analyses from ERA-Interim and MERRA and measurements of daily solar irradiation at surface. *Renewable Energy*. 75, 135–143. DOI: <https://doi.org/10.1016/j.renene.2014.09.042>
- [57] Lee, T., Singh, V.P., 2018. Statistical downscaling for hydrological and environmental applications, 1st edition. CRC Press: Florida, USA. pp. 181. DOI: <https://doi.org/10.1201/9780429459580>
- [58] Tram-Anh, Q., Ngo-Duc, T., Espagne, E., et al., 2023. A 10-km CMIP6 downscaled dataset of temperature and precipitation for historical and future Vietnam climate. *Scientific Data*. 10, 257. DOI: <https://doi.org/10.1038/s41597-023-02159-2>
- [59] Climate change 2021: The Physical Science Basis [Internet] [cited 2024 Mar 10]. Available from: <https://www.ipcc.ch/report/ar6/wg1/#-FullReport>
- [60] Logan, T., Aoun, A., Bourgault, P., et al., 2022. Ouranosinc/xclim: v0.37.0 (v0.37.0). Zenodo. DOI: <https://doi.org/10.5281/zenodo.6671565>
- [61] Yilmaz, I.H., Mwesigye, A., 2018. Modeling simulation and performance analysis of parabolic trough solar collectors: A comprehensive review. *Applied Energy*. 225, 135–174. DOI: <https://doi.org/10.1016/j.apenergy.2018.05.014>
- [62] Bellos, E., Tzivanidis, C., Tsimpoukis, D., 2018. Enhancing the performance of parabolic trough collectors using nanofluids and turbulators. *Renewable and Sustainable Energy Reviews*. 91, 358–375. DOI: <https://doi.org/10.1016/j.rser.2018.03.091>
- [63] He, Y., Yang, K., Wild, M., et al., 2023. Constrained future brightening of solar radiation and its implication for China’s solar power. *National Science Review*. 10, nwac242. DOI: <https://doi.org/10.1093/nsr/nwac242>
- [64] Solar Thermal Electricity: Global Outlook 2016—Full Report [Internet] [cited 2024 Mar 25]. Available from: https://www.estelasolar.org/wp-content/uploads/2016/02/GP-ESTELA-SolarPACES_Solar-Thermal-Electricity-Global-Outlook-2016_Full-report.pdf
- [65] Pereira, E.B., Martins, F.R., Gonçalves, A.R., et al., 2017. Brazilian solar energy atlas, 2nd Edition. (In Portuguese) DOI: <http://doi.org/10.34024/978851700089>
- [66] Renewable Energy Sources and Climate Change Mitigation—Special Report of the Intergovernmental Panel on Climate Change (IPCC) [Internet] [Accessed 2024 Mar 25]. Available from: <https://www.ipcc.ch/report/renewable-energy-sources-and-climate-change-mitigation/>
- [67] Viviescas, C., Lima, L., Diuana, F.A., et al., 2019. Contribution of variable renewable energy to increase energy security in Latin America: Complementarity and climate change impacts on wind and solar resources. *Renewable and Sustainable Energy Reviews*. 113, 109232. DOI: <https://doi.org/10.1016/j.rser.2019.06.039>
- [68] Li, J., Huo, R., Chen, H., et al., 2021. Comparative assessment and future prediction using CMIP6 and CMIP5 for annual precipitation and extreme precipitation simulation. *Frontiers*



- in Earth Science. 9, 2021.
DOI: <https://doi.org/10.3389/feart.2021.687976>
- [69] Anderson, T., Duke, M., Morrison, G., et al., 2009. Performance of a building integrated photovoltaic/thermal (BIPVT) solar collector. *Solar Energy*. 83, 445–455.
DOI: <https://doi.org/10.1016/j.solener.2008.08.013>
- [70] Trenberth, K.E., Fasullo, J., 2009. Global warming due to increasing absorbed solar radiation. *Geophysical Research Letters*. 36, L07706.
DOI: <https://doi.org/10.1029/2009GL037527>

8. Assessing renewable resources complementarity in South America with statistically downscaled CMIP6 projections

Assessing renewable resources complementarity in South America with statistically downscaled CMIP6 projections

Glauber Willian de Souza Ferreira^{1,*}, Michelle Simões Reboita¹, João Gabriel Martins Ribeiro¹

¹Natural Resources Institute, Federal University of Itajubá, Itajubá, MG, Brazil

Corresponding author*:

Glauber Willian de Souza Ferreira
glauber_ferreira@unifei.edu.br
Natural Resources Institute, Federal University of Itajubá
Avenida BPS, 1303. Prédio M3. 37500-903, Itajubá, Minas Gerais, Brasil

ORCID

Glauber Willian de Souza Ferreira: 0000-0003-1979-7120

Michelle Simões Reboita: 0000-0002-1734-2395

João Gabriel Martins Ribeiro: 0000-0002-9854-8693

Abstract

The diversification and complementarity of renewable energy resources are essential for ensuring energy security in South America, particularly regarding climate change. This study analyzes projected changes in energy complementarity among precipitation, global horizontal irradiance, and wind speed at 100 m throughout the 21st century using statistically downscaled CMIP6 projections. The findings indicate substantial transformations in these relationships, with increased precipitation-solar complementarity in the Midwest and Southeast Brazil during summer (DJF) and fall (MAM), while declining rainfall in Amazonia may weaken this effect. Similarly, precipitation-wind complementarity strengthens in North and Northeast Brazil, favoring hybrid energy generation during dry periods. Conversely, strong solar-wind similarity is projected across Northern South America and the Brazilian Northeast, corroborating the region's potential for hybrid solar-wind systems. The expansion of run-of-river hydropower in Brazil, particularly in the North, poses operational challenges due to its vulnerability to seasonal rainfall variability. However, integrating solar energy with hydropower could mitigate fluctuations, ensuring a more stable supply. Despite the challenges of increasing renewable intermittency and reduced water storage capacity, South America's vast availability of hydropower, solar, and wind resources presents a unique opportunity to optimize its energy matrix. Strategic integration of hybrid systems and improved transmission infrastructure can enhance grid stability and resilience in the face of climate change, positioning South America as a global leader in sustainable energy.

Keywords: Climate change; Renewable energy; Energy complementarity; CMIP6; South America.

1. Introduction

Climate change is impacting every corner of the globe. 2024 was the hottest year, marking the first time the global average temperature exceeded the Paris Agreement's 1.5°C threshold (Copernicus Climate Change Service, 2025). Extreme precipitation events struck Brazil (Reboita et al. 2024a), Spain and Central

Europe (Amiri et al. 2025; Zhang et al. 2025), Africa (Li et al. 2025; Zhang et al. 2025), the Middle East (Sian et al. 2025; Zhang et al. 2025), Asia (Zhang et al. 2025; Zhou et al. 2025), and Australia (Climate Council, 2024), while wildfires, droughts, and heatwaves further underscored the intensifying climate crisis (European Commission, 2024; NOAA/NIDIS, 2025; Zhang et al. 2025). Despite these warnings, some global leaders continue propagating scientific denialism, obstructing decarbonization efforts and reinforcing fossil fuel dependency (Sivin, 2025).

Amid these challenges, the global energy transition is advancing. Europe leads the shift to renewables, but China's solar and wind capacity is expanding by 30% annually, while India aims for 40% renewables by 2030 (Hassan et al. 2024). In South America (SA), countries such as Chile, Brazil, and Argentina stand out, with renewable resources accounting for approximately 68%, 49%, and 40% of their energy matrices, respectively (Brazilian Energy Balance 2024; Global Electricity Review 2024; IRENA 2024). On the other hand, North America shows mixed progress, and regions like Africa and the Middle East have structural challenges and incipient energy diversification (Hassan et al. 2024).

Hydropower dominates SA's renewable sector, supplying 45% of the continent's electricity – far above the global average of 16% (Cacciuttolo et al. 2024). Yet, climate change threatens hydropower reliability through intensified droughts (Ferreira et al. 2023) and shifts in the South American monsoon cycle (Reboita et al. 2023), besides environmental damage resulting from its implementation (Araujo 2024; Costa et al. 2025). Hybrid energy systems combining wind, solar, and hydro offer a solution, enhancing system resilience against intermittency and variability (da Luz and Moura, 2018). Brazil's Northeast exemplifies this approach, with over half of its electricity derived from wind-solar integration (Campos et al. 2020).

In sum, energy complementarity is the ability of two or more renewable energy resources to balance each other across time and space (Beluco et al. 2008). Temporal complementarity ensures stability within a given period, while spatial complementarity distributes generation across regions (Engeland et al. 2017; da Silva et al. 2024).

Studies of energy complementarity employ various methodologies, including statistical metrics – like Pearson and Spearman correlations (Monforti et al. 2014; Bett and Thornton 2016; François et al. 2016; Silva et al. 2016; Cantão et al. 2017; Rosa et al. 2017; Gallardo et al. 2020; Guezgouz et al. 2021; Soukissian et al. 2021; da Silva et al. 2024; Silva et al. 2024) –, cross-correlation and coherence analyses (dos Anjos et al. 2015; Silva et al. 2016), spatiotemporal complementarity indices (Beluco et al. 2008; Bagatini et al. 2017; Risso et al. 2018) and optimization models (da Luz and Moura 2018; Campos et al. 2020). Research on energy complementarity spans North America (Hoicka and Rowlands, 2011; Solomon et al. 2016), Europe (Bett and Thornton 2016; François et al. 2016; Dalbeke et al. 2023), Asia (Liu et al. 2013; Min and Kim 2017), Oceania (Prasad et al. 2017), Africa (Guezgouz et al. 2021), and SA (Riscoti and Sauer 2013; Schmidt et al. 2016; Silva et al. 2016; Cantão et al. 2017; Rosa et al. 2017; Viviescas et al. 2019; Cantor et al. 2022; Nascimento et al. 2022).

In Brazil, studies on energy complementarity began with the development of a spatiotemporal index for the South (Beluco et al. 2008), laying the groundwork for subsequent regional assessments (Bagatini et al. 2017; Risso et al. 2018; Pimentel and Rosário 2024; Rosa et al. 2017; Campos et al. 2020; da Silva et al. 2024; Silva et al. 2024). These studies emphasize Brazil's potential to optimize renewable energy integration, mitigating generation intermittency and strengthening energy security. Moreover, climate projections indicate favorable trends for wind and solar resources, particularly in Northeast Brazil (Ferreira et al. 2024a,b), suggesting new opportunities for energy planning. However, despite the growing importance of long-term climate variability in power system resilience, research on energy complementarity under future climate conditions remains limited. Therefore, this study addresses this gap by employing a multi-model ensemble of statistically downscaled CMIP6 projections to assess future complementarity patterns. Additionally, it contributes to a broader initiative aligned with Brazil's renewable energy strategy, providing insights for more adaptive and resilient energy planning.

2. Material and Methods

2.1 Study Area

SA (12°N-55°S) is a continent characterized by remarkable climate diversity, shaped by its vast latitudinal span and complex topography (Figure 1). This unique setting provides the region abundant renewable energy resources – hydropower, wind, and solar – making it highly favorable for sustainable energy

development. The continent's water availability is primarily governed by the South American Monsoon System (SAMS), which drives intense seasonal rainfall over central and eastern regions (Reboita et al., 2023). In contrast, southern latitudes experience peak precipitation during winter due to the passage of cold fronts and extratropical cyclones, while the northeastern semiarid region frequently faces droughts influenced by Intertropical Convergence Zone (ITCZ) variability and large-scale teleconnection patterns (Ferreira and Reboita, 2022).

Wind energy potential in SA is striking and influenced by key atmospheric circulation features. The trade winds provide persistent airflow over the Brazilian Northeast, making it one of the most promising regions for wind power generation. Low-level jets and extratropical cyclones generate high speeds in southern SA, particularly in Argentina and Uruguay. Additionally, the influence of the South Atlantic Subtropical Anticyclone (SASA) enhances wind energy potential along the eastern coast, reinforcing the viability of large-scale wind farms (Ferreira et al., 2024a).

Solar energy availability across the continent is equally remarkable, as much of SA lies within the Sun Belt (Barbosa et al. 2017), a latitudinal zone of consistently high solar irradiance. This feature is particularly evident in northern Chile, northeastern Brazil, and northern Argentina, where arid conditions and predominantly clear skies contribute to some of the highest solar radiation levels globally (Ferreira et al., 2024b). The abundant availability of water, wind, and solar resources establishes SA as a pivotal region in the shift toward a more sustainable and resilient energy matrix, offering extensive opportunities for hybrid energy integration and long-term energy stability.

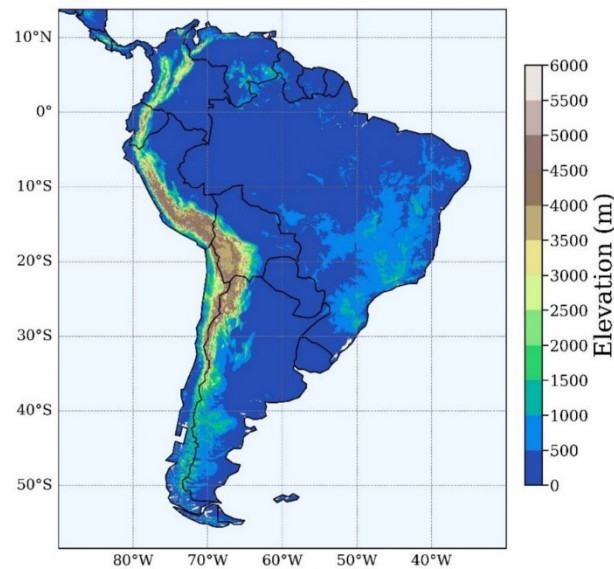


Figure 1: Illustration of the study area with elevation (m). Source: United States Geological Survey-Earth Resources Observation System (EROS) Center.

2.2 CMIP6 Models

This study utilized data from eight global climate models (GCMs) of CMIP6 (Table 1), including precipitation, global horizontal irradiance, 2 m air temperature, and the zonal and meridional wind components at 10 m. The dataset covers the historical period (1995-2014) and future projections (2020-2099) under two greenhouse gas emission scenarios (SSP2-4.5 and SSP5-8.5). The simulations, available at three-hour intervals, were obtained from the Earth System Grid Federation (ESGF) platform (<https://aims2.llnl.gov/search/cmip6/>).

The GCMs selection followed the methodology proposed by Rupp et al. (2013), which employs statistical metrics to evaluate model performance in reproducing the historical climate of a given region. Further methodological details, including mathematical formulations and statistical parameters, are provided in Reboita et al. (2024b). The model selection prioritized their ability to simulate historical climate conditions, the availability of high-frequency data, and their projections on the ESGF platform. Additionally, the ensemble of the best-performing models yielded results that aligned more closely with observations and outperformed individual GCM simulations (Reboita et al. 2024b).

Table 1 – CMIP6 GCMs used in the study.

Model	Resolution (°Lat × °Lon)	Institute	Reference
CMCC-CM2-SR5	1.25 × 0.94	Fondazione Centro Euro-Mediterraneo sui Cambiamenti Climatici	Lovato and Peano (2020)
CMCC-ESM2	1.25 × 0.94	Fondazione Centro Euro-Mediterraneo sui Cambiamenti Climatici	Lovato et al. (2022)
EC-Earth3	0.70 × 0.70	EC-Earth Consortium	Döscher et al. (2022)
GFDL-ESM4	1.25 × 1.00	Geophysical Fluid Dynamics Laboratory	Krasting et al. (2018)
IPSL-CM6A-LR	2.50 × 1.26	Institut Pierre Simon Laplace	Boucher et al. (2018)
MIROC-6	1.41 × 1.41	Japan Agency for Marine-Earth Science and Technology	Tatebe and Watanabe (2018)
MPI-ESM1-2-LR	0.94 × 0.94	Max Planck Institute for Meteorology	Wieners et al. (2019)
MRI-ESM2-0	1.13 × 1.13	Meteorological Research Institute	Yukimoto et al. (2019)

2.3 Reference Dataset

Multiple reference datasets were used to validate the historical simulations of the CMIP6 GCMs. Precipitation data were obtained from the Climate Prediction Center (CPC) gauge-based global daily precipitation analysis (Chen et al. 2008), covering the 1995-2014 period with a 0.5° horizontal resolution (https://ftp.cpc.ncep.noaa.gov/precip/CPC_UNI_PRCP/GAUGE_GLB/RT/). While CPC data effectively capture seasonal and mean precipitation patterns over most of SA, uncertainties persist in regions with complex topography, such as the Andes (Lagos-Zuñiga et al. 2024). For temperature and wind validation, the ERA5 reanalysis from the European Centre for Medium-Range Weather Forecasts (ECMWF) was used (<https://cds.climate.copernicus.eu/>), which provides 2 m air temperature and 10 m wind components at three-hour intervals with a 0.25° resolution (Hersbach et al. 2020).

Despite ERA5's high quality, reanalysis products can exhibit systematic biases (Dullaart et al. 2020; Sawadogo et al. 2021; Wilczak et al. 2024; Khan et al. 2025). To enhance the validation dataset and address the limitations of the reanalysis product, satellite observations from CLARA-A3 (Karlsson et al. 2023) were incorporated, which comprises a collection of climate records on cloud properties, albedo, and surface radiation produced by the Satellite Application Facility on Climate Monitoring (CM SAF) under EUMETSAT (https://www.cmsaf.eu/EN/Home/home_node.html). This dataset includes surface solar irradiance and cloud properties derived from AVHRR sensors aboard NOAA and Metop satellites, offering daily data at 0.25° resolution for 1995-2014. Satellite-based products generally provide higher accuracy than reanalysis data, making them valuable for evaluating solar radiation estimates in climate models (Boilley and Wald 2015; Sawadogo et al. 2021).

2.4 Bias Correction/Statistical Downscaling

GCMs have a coarse spatial resolution, making their raw outputs unsuitable for applications requiring finer detail, such as synoptic-scale studies. Hence, statistical downscaling was applied to refine the CMIP6 outputs using previously mentioned datasets. For solar irradiance, both CLARA-A3 satellite observations and ERA5 reanalysis were averaged to compose an ensemble mean capturing the strengths of each dataset. Among various statistical downscaling approaches, the Bias Correction–Statistical Downscaling (BCSD) method was employed, precisely the transfer function technique, which establishes statistical relationships between observed and simulated variables.

Before applying BCSD, spatial disaggregation was performed on all datasets to $0.5^\circ \times 0.5^\circ$ using bilinear interpolation, a method known for producing consistent fields (Tram-Anh et al. 2023). For bias correction, we used the Quantile Delta Mapping (QDM) technique for historical simulations (1995-2014) and transfer functions for future projections (2020-2099). QDM is particularly effective in statistical downscaling as it preserves relative trends projected by models while correcting systematic biases in the data's quantile distribution (Cannon et al. 2015). This process involves three key steps: removing the trend from all quantiles, applying quantile mapping for bias correction, and reintroducing projected changes onto the corrected data. The historical period (1995-2014) served as the training dataset to calibrate future projections (2020-2099) using the QDM algorithm, aligning with the reference period established by the Intergovernmental Panel on Climate Change (IPCC).

After bias-correcting the simulations, the wind intensity at 10 m was vertically extrapolated to 100 m since most wind turbines are installed at this height to reduce friction effects in wind intensity (Custódio 2009). Equation 1 (Reboita et al. 2021a; Ferreira et al. 2024a) was used to calculate the wind extrapolation:

$$W_H = W_{10} \left(\frac{Z_H}{Z_{10m}} \right)^{\frac{1}{7}} \quad (1)$$

where W_H is the wind speed ($m\ s^{-1}$) at the desired height (Z_H , 100 m), and W_{10} is the wind speed ($m\ s^{-1}$) at the reference height of 10 m.

2.5 Complementarity Analysis

This study analyzes three types of renewable resource complementarity: precipitation-wind, precipitation-solar and wind-solar. Pearson's linear correlation coefficient, a metric widely used to assess the relationship between linear series of environmental variables – including water, wind, and solar resources (Silva et al. 2016; Cantão et al. 2017; Rosa et al. 2017; da Silva et al. 2024; Silva et al. 2024) –, was applied to achieve this goal. The coefficient was obtained according to Equation 2 on a seasonal scale, and it measures the intensity of the correlation (r), ranging from -1 to 1. The correlation intensity can be interpreted according to Table 1 (Cantão et al. 2017).

$$r = \frac{\sum_{i=1}^n (x_i - \bar{x})(y_i - \bar{y})}{\sqrt{\sum_{i=1}^n (x_i - \bar{x})^2} \sqrt{\sum_{i=1}^n (y_i - \bar{y})^2}} \quad (2)$$

where n is the number of samples, i is the monthly period, x_i is the monthly precipitation value at time i (or wind, in the case of wind-solar complementarity), \bar{x} is the seasonal average precipitation, y_i is the monthly wind or solar irradiance value at time i , and \bar{y} is the seasonal average wind (or solar irradiance).

Table 2 – Interpretation of correlation coefficient values (adapted from Cantão et al. 2017).

Behavior	Values of r	Interpretation
Similarity	$0.9 \leq r \leq 1.0$	Very strong similarity
	$0.6 \leq r \leq 0.9$	Strong similarity
	$0.3 \leq r \leq 0.6$	Moderate similarity
	$0.0 \leq r \leq 0.3$	Weak similarity
Complementarity	$-0.3 \leq r \leq 0.0$	Weak complementarity
	$-0.6 \leq r \leq -0.3$	Moderate complementarity
	$-0.9 \leq r \leq -0.6$	Strong complementarity
	$-1.0 \leq r \leq -0.9$	Very strong complementarity

Negative values indicate complementarity between the resources, as they behave in opposite ways since when one resource's availability decreases, the other's availability increases. On the other hand, positive values indicate that the resources behave similarly and that the availability curves tend to be similar (Cantão et al. 2017; da Silva et al. 2024). In this way, applying the coefficient makes it possible to quantify the interrelationship between renewable resources and identify seasonal availability patterns. Based on these analyses, it is possible to identify regions with greater potential for complementarity between renewable resources and thus contribute to more efficient and resilient energy planning.

3. Results and Discussion

3.1 Historical period

Figure 2 illustrates the results of Pearson's linear correlation (r) between the seasonal anomalies of renewable sources (precipitation, wind at 100 m, and global horizontal irradiance) simulated by the CMIP6 ensemble in the historical period (considering the climatological period 1995-2014) and those obtained by the reference data sets. The first row (Figure 2a1-2a4) shows the correlations between the seasonal precipitation anomalies of the CMIP6 ensemble and those of the CPC; the second row (Figure 2b1-2b4) shows the correlations between the seasonal anomalies of global horizontal irradiance from the CMIP6 ensemble and those obtained by the ERA5+CLARA-A3 mean ensemble; finally, the third row (Figure 2c1-2c4) shows the correlations between the seasonal wind anomalies at 100 m simulated by the CMIP6 ensemble and those provided by ERA5. It is worth noting that the correlations shown in Figure 2 are not associated with complementarity between renewable resources but rather indicate the simulation performance of the CMIP6 ensemble through the linear correlation between simulated and observed climate anomalies.

Regarding the CMIP6 ensemble skill in simulating the seasonal precipitation anomalies of the historical period, in the austral summer (DJF), there are statistically significant correlations ($\alpha = 0.05$) above 0.4 in northeastern and central-southern Brazil sectors. On the other hand, low correlations occur in much of the Amazonia and western SA, sectors in which GCMs show considerable systematic biases resulting from an unsatisfactory representation of the position and intensity of the ITCZ, as well as insufficient representation of biosphere-atmosphere interactions and orographic effects, especially in the northern SA and the Andes (Torres and Marengo 2011; Rivera and Arnould 2020; Almazroui et al. 2021; Arias et al. 2021; Ortega et al. 2021; Ferreira et al. 2023). A similar pattern occurs in the MAM and JJA seasons, with statistically significant moderate correlations in a few southeastern and central-western Brazil regions. On the other hand, the pattern obtained in SON shows statistically significant moderate correlations in sectors of the Brazilian Southeast and Northeast. Similarly, other studies (Coelho et al. 2006; Chou et al. 2020; Reboita et al. 2021b; Ferreira et al. 2022) have indicated a good performance of GCMs in simulating precipitation anomalies in these sectors during SON, associated with a better predictability of the teleconnection effects of El Niño – Southern Oscillation (ENSO) and the Tropical Atlantic Dipole.

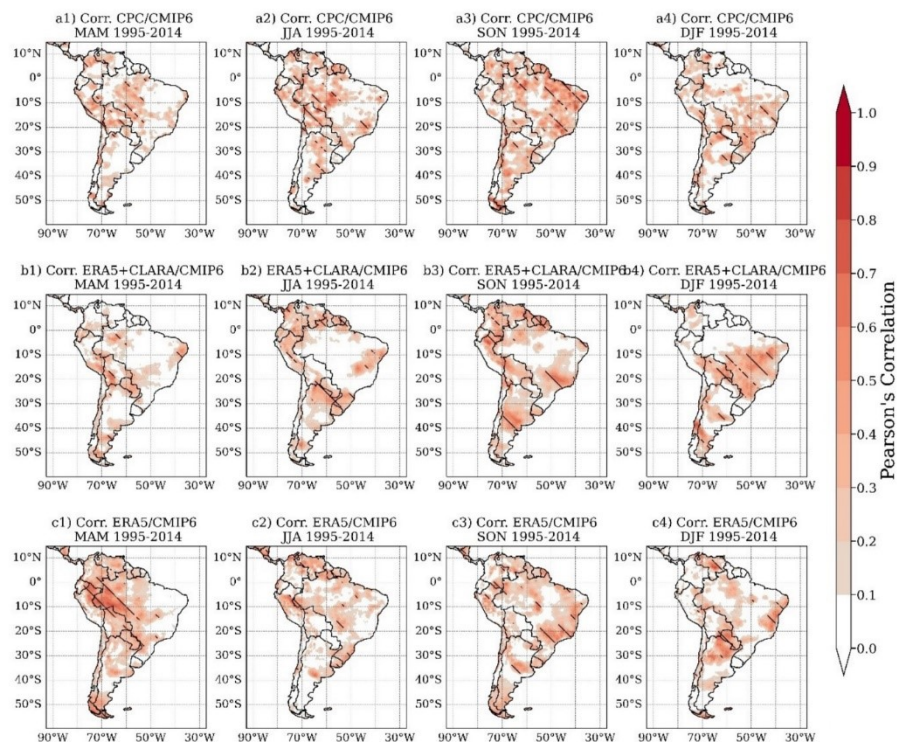


Figure 2: Pearson's correlation between the seasonal anomalies of renewable resources (precipitation, wind at 100 m, and global horizontal irradiance) simulated by the CMIP6 ensemble and the reference data for the historical period (1995-2014). Hatched areas indicate statistical significance at the 95% level.

Regarding the representation of seasonal anomalies in global horizontal irradiance, the GCMs perform better at simulating the variable in the months of SON and DJF in central Argentina and Brazil's Northeast and central-southeast regions. In contrast, sectors such as the Amazonia, western SA, and northern SA show low correlation values ($r < 0.4$) for much of the year, reflecting systematic biases, especially in areas of intense convection. In fact, even after the reduction of up to 50% of the errors in the CMIP6 ensemble simulations after the BCSD application, average overestimates of up to 10 W m^{-2} occur in most of SA in the months of MAM and JJA (Ferreira et al. 2024b).

Considering the wind simulation, the highest statistically significant correlation values ($r > 0.4$) occur in the months of SON and DJF in northeast Brazil and on the ocean coast of the Rio de Janeiro and São Paulo states. A statistically significant moderate correlation exists during MAM in the region where the low-level jets east of the Andes (LLJ) act. Still, this performance does not occur in the other months due to the systematic biases of the GCMs and their poor representation of the complex topography of the region (Kumar et al. 2015; Barros and Doyle 2018; Reboita et al. 2018; Huang et al. 2020; Ferreira et al. 2024a).

Moreover, Figures S1, S2, and S3 of the Supplementary Material present an additional analysis of the CMIP6 ensemble performance in simulating the seasonal patterns of renewable resources in SA during the reference period. Figure S1 illustrates the complementarity obtained with the CMIP6 ensemble simulations (i.e., the complementarity between the precipitation, wind at 100 m, and global horizontal irradiance of the selected GCMs were calculated), while Figure S2 presents the complementarity resulting from the reference data (i.e., the complementarity between the CPC precipitation analyses, the wind from the ERA5 reanalysis and the global horizontal irradiance of the ERA5+CLARA-A3 mean ensemble). Moreover, Figure S3 shows the bias of correlations between the complementarity of the CMIP6 GCMs and that of the reference data.

CMIP6 GCMs generally provide spatial and temporal complementarity fields similar to those of the reference ensembles. The most expressive deviations occur in the central-southern sectors of Brazil and northern SA for the precipitation-wind complementarity at 100 m (Figure S3b) and in Brazil's southern and northeastern sectors for the solar irradiance-wind complementarity. These findings endorse previous results, which showed persistent errors in the CMIP6 ensemble's representation of wind and solar radiation in Brazil's southern and northeastern regions, even after applying BCSD (Ferreira et al. 2024a, 2024b). It is worth noting that the observed data used also has uncertainties and constraints, making validating CMIP6 GCMs climate simulations in SA more problematic.

3.2 Renewable Complementarity in the Future

3.2.1 Complementarity Precipitation-Solar

Figure 3 illustrates the complementarity between precipitation and global horizontal irradiance in SA throughout the 21st century, based on CMIP6 ensemble projections under the SSP5-8.5 scenario. The analysis considers seasonal precipitation and global horizontal irradiance anomalies relative to their climatological means of the period analyzed. The uncertainties and variability associated with individual ensemble members (i.e., individual GCM projections) are comprehensively discussed in studies that assess each renewable energy resource separately (Ferreira et al. 2023; Reboita et al. 2023; Ferreira et al. 2024a, 2024b), which provide detailed evaluations of the spread and biases among models. This analysis focuses on the general pattern provided by the ensemble mean, representing the collective signal of multiple models, smoothing individual model deviations, and highlighting the overarching trends in renewable energy complementarity across SA.

A strengthened negative correlation between these variables becomes more pronounced from 2040 onwards. This pattern, driven by projected changes in precipitation and cloud cover, enhances the availability of one resource when the other declines. The Midwest and Southeast of Brazil exhibit increasing negative correlations, particularly in summer (DJF) and fall (MAM), due to the influence of the SAMS and the associated seasonal rainfall peaks. Similarly, the Amazonian region shows strong precipitation-solar complementarity between December and May, but this effect is expected to weaken due to land-use changes and declining rainfall (Reboita et al. 2021b, 2023; Ferreira et al. 2023). In winter (JJA), complementarity is generally weak across the continent, except in Northeast Brazil and northern SA, where seasonal variability is more pronounced. Under the SSP2-4.5 scenario (Figure S4), the spatial patterns show slight differences, such as the more extensive areas of strong complementarity in Brazil in the months of DJF (2020-2039) and MAM (2060-2099). However, this scenario generally shows a weaker signal intensity compared to SSP5-8.5.

Southern Brazil, in contrast, exhibits strong precipitation-solar complementarity throughout most of the year, with a moderate relationship in winter. This stability is attributed to well-distributed precipitation patterns, which support hydroelectric generation when solar radiation is lower (Ferreira and Reboita, 2022). Studies indicate that nearly half of Rio Grande do Sul shows significant temporal hydro-solar complementarity, with over 72 days separating the minimum availability of the two energy resources (Beluco et al. 2008).

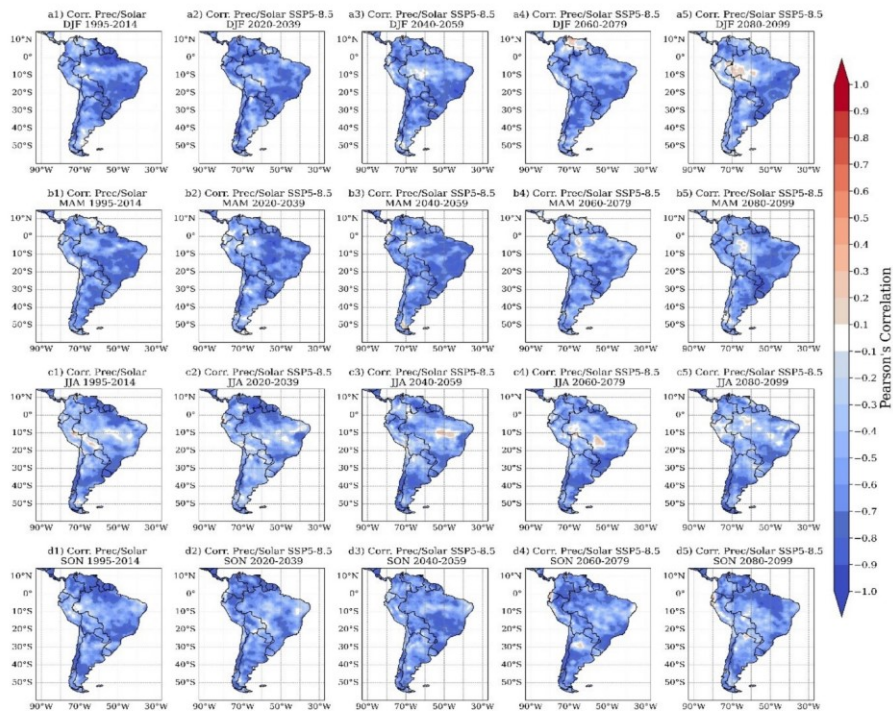


Figure 3: Seasonal correlations between precipitation and global horizontal irradiance anomalies provided by statistically downscaled CMIP6 projections for the historical and future periods under the SSP5-8.5 scenario.

CMIP6 projections under SSP5-8.5 suggest substantial precipitation changes across the century. While precipitation is expected to increase in the Southeast and South during DJF and MAM, reinforcing the inverse relationship with solar radiation (Ferreira et al. 2023; Reboita et al. 2023), JJA and SON are projected to experience considerable rainfall reductions in much of central and Northeast Brazil (Ferreira et al. 2023). These reductions may undermine hydro-solar complementarity in these regions, necessitating stronger integration with wind and solar energy resources to stabilize generation. The Southeast and South are likely to maintain high precipitation levels (Almazroui et al. 2021; Reboita et al. 2021b), whereas the Midwest and Northeast could face severe rainfall declines, impacting hydroelectric output and increasing reliance on alternative renewables.

The expansion of run-of-river hydroelectric plants, particularly in North Brazil, must be assessed in the context of climate change and renewable energy complementarity. These plants, which lack large reservoirs, are susceptible to seasonal and interannual rainfall variability, posing risks to their operational reliability (Alencar et al. 2019). However, their integration with solar energy can mitigate these challenges, as photovoltaic generation thrives in dry conditions with reduced cloud cover, while hydropower peaks during rainy periods. This synergy enables more efficient water use, reducing daily reservoir withdrawals and enhancing energy security.

Given growing environmental restrictions and the high costs of new hydroelectric projects, retrofitting existing plants with solar generation is a practical and cost-effective alternative. Solutions like floating photovoltaic modules and secondary reservoirs for irrigation and supply can further optimize efficiency (Teixeira et al. 2015). Additionally, integrating solar energy with run-of-river plants can reduce the

extent of flooding, improve dam safety, and ensure a more stable energy supply throughout the year (Alencar et al. 2019).

The findings indicate that hydro-solar complementarity will remain a key factor in optimizing Brazil's energy matrix throughout the 21st century. Strengthening negative correlations across regions supports expanding hybrid generation systems, particularly in the South and Southeast, where climate stability favors a balanced energy mix. However, the growing reliance on run-of-river hydropower necessitates careful energy planning to maintain grid reliability. Reduced water storage capacity and shifting rainfall patterns could destabilize hydroelectric generation, making integrating wind and solar energy crucial to compensating for seasonal fluctuations. Thus, hybrid strategies, including solar retrofitting at hydroelectric plants and the development of secondary reservoirs, represent viable solutions to enhance resource utilization and bolster the resilience of Brazil's energy system in the face of climate change.

3.2.2 Complementarity Precipitation-Wind

Figure 4 presents the complementarity between precipitation and wind speed at 100 m in SA over the 21st century, based on BSCD projections from the CMIP6 ensemble under the SSP5-8.5 scenario. Compared to the historical period (1995-2014), future projections indicate a strengthening of the negative correlation between precipitation and wind speed across various regions, highlighting an increasing potential for energy complementarity. This effect is more pronounced in SON and DJF, with more apparent patterns of alternating phases – higher precipitation coinciding with weaker winds and vice versa. Additionally, some areas exhibit a more pronounced positive correlation, suggesting potential for joint energy production throughout the year. Under the SSP2-4.5 scenario (Figure S5), the spatial patterns are similar, and the sign of change is less intense. Still, there is stronger complementarity along the coast of northern Brazil in DJF (2040-2059) and MAM (from 2040).

Moderate to strong precipitation-wind complementarity is primarily observed in North and Northeast Brazil and northern SA during DJF and MAM, where alternating periods of intense winds and heavy rainfall create favorable conditions for hybrid energy generation systems. Conversely, regions such as the South and Midwest of Brazil exhibit moderate to strong similarity, indicating that wind and precipitation co-occur, particularly in the first half of the year. Similar areas include central-southern Chile (year-round) and central Argentina (JJA).

These findings reinforce previously identified patterns of strong precipitation-wind complementarity in Northern and Northeastern Brazil (Cantão et al. 2017). Similarly, the observed hydro-wind similarity in Southern Brazil, particularly from May to November and in the Northeast during JJA, aligns with the study above, suggesting that these regions exhibit favorable conditions for integrating hydropower and wind energy. Additionally, hydro-wind complementarity is particularly strong in the Northeast basins, including São Francisco, Parnaíba, and the eastern and western northeast Atlantic basins, as well as in areas near the São Francisco River's power plants (Cantão et al. 2017). In contrast, in the Southern region, hydro-wind similarity tends to dominate, although some areas show moderate or weak alignment between these energy resources.

CMIP6 projections under the SSP5-8.5 scenario indicate that precipitation is expected to increase over Southern Brazil and the La Plata Basin throughout the 21st century, while wind speeds are projected to intensify in Northern and Northeastern Brazil and along the western coast of SA (Reboita et al., 2021; Almazroui et al., 2021; Ferreira et al. 2023). This configuration reinforces the complementarity between these regions, highlighting strategic opportunities for integrating hydropower and wind energy production. Additionally, projections suggest that wind speeds in central and southern Brazil may become stronger during spring and winter (de Jong et al., 2019; Rufato-Ferreira et al., 2017; Ferreira et al., 2024a), while precipitation may decline in parts of the Midwest and Northeast (Reboita et al., 2021; Ferreira et al., 2023), further enhancing the potential for energy compensation between these resources. Conversely, the projected decline in wind speeds over Patagonia and extreme southern Argentina throughout the century (Ferreira et al., 2024a) may pose challenges for wind energy generation in the region, necessitating adaptive energy strategies.

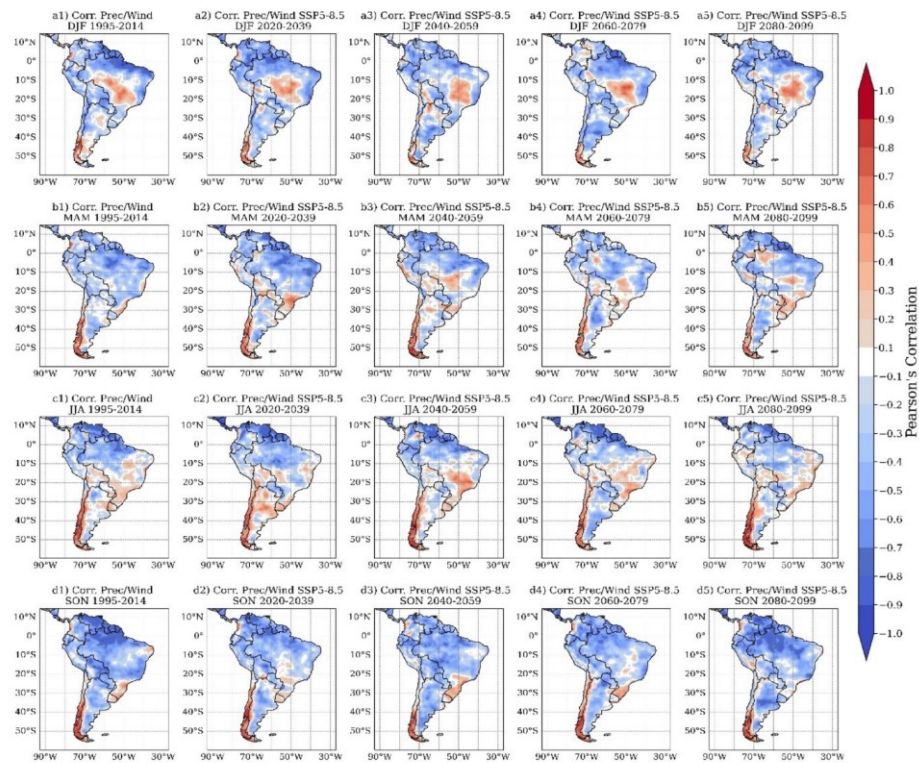


Figure 4: Seasonal correlations between precipitation and wind intensity at 100 m anomalies provided by statistically downscaled CMIP6 projections for the historical and future periods under the SSP5-8.5 scenario.

3.2.3 Complementarity Solar-Wind

Figure 5 illustrates the solar-wind complementarity in SA over the 21st century, based on statistically downscaled projections from the CMIP6 ensemble under the SSP5-8.5 scenario. The results highlight that the similarity between global horizontal irradiance and wind speed at 100 m is more pronounced than other renewable energy combinations, suggesting a high potential for the joint operation of solar and wind farms throughout the year. Compared to the historical period (1995-2014), future projections indicate a strengthening positive correlation between global horizontal irradiance and wind across much of the continent. This pattern suggests a growing simultaneous availability of these resources, which could further support the integration of solar and wind power plants. The intensification of this trend is particularly evident during spring (SON) and summer (DJF), while in winter (JJA) and autumn (MAM), certain regions exhibit greater complementarity (negative correlation). Under the SSP2-4.5 scenario (Figure S6), again the spatial patterns are similar, but stronger complementarity is projected for the northern coast of Brazil in DJF and MAM.

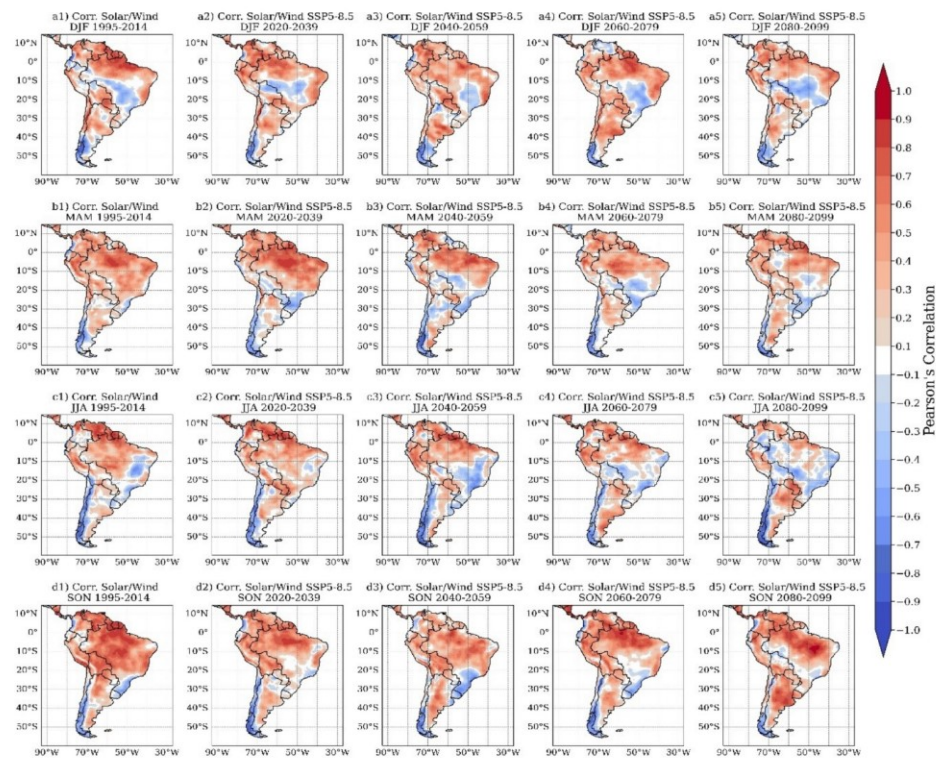


Figure 5: Seasonal correlations between horizontal global irradiance and wind intensity at 100 m anomalies provided by statistically downscaled CMIP6 projections for the historical and future periods under the SSP5-8.5 scenario.

Regions exhibiting strong similarity include northern SA, encompassing parts of the Brazilian Amazonia, Colombia, Venezuela, and the Guianas, where energy resources are simultaneously available throughout the year. Additionally, Northeast Brazil displays a consistent pattern of similarity nearly year-round, reinforcing findings from previous studies that identified a high degree of solar-wind synergy in the region (da Silva et al. 2024; Silva et al. 2024). Moreover, Southeast Brazil presents strong similarity during SON, while moderate-to-strong similarities are also observed in Argentina and Uruguay. Conversely, Southern Brazil and Chile exhibit moderate-to-strong complementarity (negative correlation) for much of the year, suggesting that wind energy availability may compensate for solar intermittency in these regions.

CMIP6 projections under SSP5-8.5 indicate substantial changes in solar radiation and wind patterns across SA. Global horizontal irradiance is expected to increase throughout the 21st century in North and Northeast Brazil, as well as in parts of the Amazonia and the Andean region, reinforcing its alignment with projected wind trends in these areas (Dutta et al., 2022; Ha et al., 2023). Additionally, wind speeds in Northeast and Southeast Brazil and the western coast of SA are projected to intensify, further supporting the simultaneous generation of solar and wind energy (Reboita et al., 2018; de Jong et al., 2019). These findings indicate that the strong solar-wind similarity observed in various regions, particularly in northern, northeastern, and southeastern Brazil, presents a significant advantage for the integrated operation of hybrid solar and wind power plants throughout the 21st century. However, in regions such as Southern Brazil, Uruguay, and Chile, the complementarity between these resources suggests that energy storage solutions and enhanced grid integration may be necessary to optimize energy utilization and ensure year-round stability.

4. Conclusion

This study analyzed projected changes in the complementarity of renewable energy resources across South America, using statistically downscaled projections from the CMIP6 ensemble. The results indicate substantial transformations in the relationships between precipitation, global horizontal irradiance, and wind speed throughout the 21st century, with potential implications for energy planning and integration. The increasing complementarity between precipitation and global horizontal irradiance, particularly in Brazil's Midwest and Southeast regions, highlights opportunities for hydro-solar hybrid systems, especially during summer and fall. However, this complementarity is expected to weaken in Amazonia due to declining rainfall and land-use changes. Conversely, precipitation-wind complementarity is projected to strengthen in North and Northeast Brazil, where alternating intense wind and rainfall phases could optimize energy generation throughout DJF and MAM. In contrast, regions like Southern Brazil, Uruguay, and Chile show more substantial wind-solar complementarity, where wind energy could offset solar intermittency during certain seasons.

The projections further indicate that the spatial extent of complementarity will evolve throughout the century. Precipitation-solar complementarity is expected to persist in the Southeast and South, where precipitation increases during DJF and MAM, reinforcing the inverse relationship with solar radiation. However, precipitation reductions in the Midwest and Northeast could undermine the efficiency of hydro-solar integration in these regions, necessitating greater reliance on wind and solar energy. Similarly, the increasing wind potential in North and Northeast Brazil and precipitation gains in the South enhance the feasibility of balancing energy supply across these regions. Additionally, the hydro-wind similarity in South Brazil indicates that the combined hydrologic and wind resources could supply energy to the southeastern region, the country's highest consumption center.

The outcomes also emphasize the growing role of run-of-river hydropower in Brazil's energy matrix, particularly in the North, where the absence of large reservoirs makes these plants highly vulnerable to seasonal and interannual rainfall variability. While this poses operational challenges, integrating solar energy with hydropower could mitigate fluctuations, as photovoltaic generation is enhanced in dry periods, whereas hydropower is favored during the rainy season. This synergy supports more efficient water use, reduces reservoir withdrawals, and improves energy security. Furthermore, the observed similarity between wind and solar resources in regions such as Northeast Brazil reinforces previous findings, confirming the region's high potential for hybrid solar-wind systems. Wind energy could supplement solar power during nighttime and low-insolation periods in these areas, ensuring a more stable supply.

Despite these advantages, transitioning to a more renewable-based energy system in South America presents several challenges. The increasing deployment of run-of-river hydropower reduces the country's capacity to store water, making the system more dependent on variable resources such as wind and solar. These resources' spatial and temporal variability also necessitates improved grid integration and energy storage solutions to manage fluctuations. While regions like the Northeast and Midwest Brazil and Andean territories exhibit strong renewable potential, ensuring efficient energy transmission to consumption centers remains a crucial challenge. Nevertheless, the vast availability of hydropower, solar, and wind resources across the continent offers unique opportunities for a diversified and resilient energy matrix. By strategically leveraging these complementary resources and adopting hybrid energy strategies – such as retrofitting hydro plants with solar modules and developing secondary reservoirs – South America, particularly Brazil, can enhance its energy security and adaptability in the face of climate change.

Declarations

Ethics approval and consent to participate: Not applicable.

Consent for publication: All authors read and approved the final manuscript.

Competing interests: The authors have no relevant financial or non-financial interests to disclose.

Funding: This study received financial support from the R&D Program regulated by the Brazilian Electricity Regulatory Agency (ANEEL) and the companies Engie Brasil Energia and Energética Estreito (R&D-00403-54/2022), and the Coordination for the Improvement of Higher Education (CAPES, Finance Code 001).

Acknowledgments: The authors thank the National Council for Scientific and Technological Development (CNPq), CAPES, ANEEL, and the companies Engie Brasil Energia and Energética Estreito for their financial support. The authors also thank the the European Centre for Medium-Range Weather Forecasts (ECMWF), the Climate Prediction Center (CPC), and the Satellite Application Facility on Climate Monitoring (CM SAF) from the European Organization for the Exploitation of Meteorological Satellites (EUMETSAT) for the data used in this study.

Authors' contributions: Glauber Ferreira and João Gabriel Ribeiro carried out the processing and analysis of data. Glauber Ferreira wrote the original draft. Glauber Ferreira and Michelle Reboita reviewed and edited the original draft. All authors read and approved the final manuscript.

References

- Alencar CA, Stedile R, Junior JU (2019) Estudo da complementariedade da geração de energia entre as fontes solar e hidráulica. *Revista Brasileira de Energia Solar* 9:58-67. <https://doi.org/10.59627/rbens.2018v9i1.235>
- Almazroui M, Ashfaq M, Islam MN, Kamil S, Abid MA, O'Brien E, Ismail M, Reboita MS, Sörensson AA, Arias PA, Alves LM, Tippet MK, Saeed S, Haarsma R, Doblas-Reyes FJ, Saeed F, Kucharski F, Nadeem I, Silva-Vidal Y, Rivera JA, Ehsan MA, Martínez-Castro D, Muñoz AG, Ali MA, Coppola E, Sylla MB (2021) Assessment of CMIP6 performance and projected temperature and precipitation changes over South America. *Earth Systems and Environment* 5:155-183. <https://doi.org/10.1007/s41748-021-00233-6>
- Amiri A, Gumiere SJ, Gharabaghi B, Bonakdari H (2025) From warm seas to flooded streets: The impact of sea surface temperature on cutoff low and extreme rainfall in Valencia, Spain. *Journal of Flood Risk Management* 18:e13055. <https://doi.org/10.1111/jfr3.13055>
- Araujo R (2024) The value of tropical forests to hydropower. *Energy Economics* 129:107205. <https://doi.org/10.1016/j.eneco.2023.107205>
- Arias PA, Ortega G, Villegas LD, Martínez J (2021) Colombian climatology in CMIP5/CMIP6 models: Persistent biases and improvements. *Revista Facultad de Ingeniería* 100:75-96. <https://doi.org/10.17533/udea.redin.20210525>
- Bagatini M, Benevit MG, Beluco A, Risso A (2017) Complementarity in time between hydro, wind and solar energy resources in the state of Rio Grande do Sul, in southern Brazil. *Energy and Power Engineering* 9:515-526. <https://doi.org/10.4236/epe.2017.99036>
- Barbosa LSNS, Bogdanov D, Vainikka, P, Breyer C (2017) Hydro, wind and solar power as a base for a 100% renewable energy supply for South and Central America. *PLoS ONE* 12:e0173820. <https://doi.org/10.1371/journal.pone.0173820>
- Barros VR, Doyle ME (2018) Low-level circulation and precipitation simulated by CMIP5 CGMs over southeastern South America. *International Journal of Climatology* 38:5476-5490. <https://doi.org/10.1002/joc.5740>
- Beluco A, Souza PK, Krenzinger A (2008) A dimensionless index evaluating the time complementarity between solar and hydraulic energies. *Renewable Energy* 33:2157-2165. <https://doi.org/10.1016/j.renene.2008.01.019>



- Bett PE, Thornton HE (2016) The climatological relationships between wind and solar energy supply in Britain. *Renewable Energy* 87:96-110. <https://doi.org/10.1016/j.renene.2015.10.006>
- Boilley A, Wald L (2015) Comparison between meteorological re-analyses from ERA-Interim and MERRA and measurements of daily solar irradiation at surface. *Renewable Energy* 75:135-143. <https://doi.org/10.1016/j.renene.2014.09.042>
- Boucher O, Denvil S, Levavasseur G, Cozic A, Caubel A, Foujols MA, Meurdesoif Y, Cadule P, Devilliers M, Ghattas J, Lebas N, Lurton T, Mellul L, Musat I, Mignot J, Cheruy F (2018) IPSL IPSL-CM6A-LR model output prepared for CMIP6 CMIP historical. Version 20180803. Earth System Grid Federation. <https://doi.org/10.22033/ESGF/CMIP6.5195>
- Brazilian Energy Balance (2024) Summary Report 2024 – Reference Year 2023. Energy Research Office (EPE). Available at: <https://www.epe.gov.br/pt/publicacoes-dados-abertos/publicacoes/balanco-energetico-nacional-2024> (accessed on 01 Feb 2025)
- Cacciuttolo C, Navarrete M, Atencio E (2024) Renewable wind energy implementation in South America: A comprehensive review and sustainable prospects. *Sustainability* 16:6082. <https://doi.org/10.3390/su16146082>
- Campos RA, Nascimento LR, Rüther R (2020) The complementary nature between wind and photovoltaic generation in Brazil and the role of energy storage in utility-scale hybrid power plants. *Energy Conversion and Management* 221:113160. <https://doi.org/10.1016/j.enconman.2020.113160>
- Cannon AJ, Sobie SR, Murdock TQ (2015) Bias correction of GCM precipitation by Quantile Mapping: How well do methods preserve changes in quantiles and extremes? *Journal of Climate* 28:6938-6959. <https://doi.org/10.1175/JCLI-D-14-00754.1>
- Cantão MP, Bess MR, Bettega R, Detzel DHM, Lima JM (2017) Evaluation of hydro-wind complementarity in the Brazilian territory by means of correlation maps. *Renewable Energy* 101:1215-1225. <https://doi.org/10.1016/j.renene.2016.10.012>
- Cantor D, Ochoa A, Mesa O (2022) Total variation-based metrics for assessing complementarity in energy resources time series. *Sustainability* 14:8514. <https://doi.org/10.3390/su14148514>
- Chen M, Shi W, Xie P, Silva VBS, Kousky VE, Higgins RW, Janowiak JE (2008) Assessing objective techniques for gauge-based analyses of global daily precipitation. *Journal of Geophysical Research* 113:D04110. <https://doi.org/10.1029/2007JD009132>
- Chou SC, Lyra A, Mourão C, Dereczynski C, Pilotto I, Gomes J, Bustamante J, Tavares P, Silva A, Rodrigues D, Campos D, Chagas D, Sueiro G, Siqueira G, Nobre P, Marengo J (2014) Evaluation of the Eta simulations nested in three global climate models. *American Journal of Climate Change* 3:438-454 <https://doi.org/10.4236/AJCC.2014.35039>
- Climate Council (2024) Climate whiplash: Wild swings between weather extremes. Climate Council of Australia. Available at: <https://www.climatecouncil.org.au/resources/climate-whiplash-wild-swings-between-weather-extremes/> (accessed on 01 Feb 2025).
- Coelho CAS, Stephenson DB, Balsameda M, Doblas-Reyes FJ, Van Oldenborgh GJ (2006) Toward an integrated seasonal forecasting system for South America. *Journal of Climate* 19:3704-3721. <https://doi.org/10.1175/JCLI3801.1>
- Copernicus Climate Change Service (2025) Global Climate Highlights 2024. Copernicus Climate Change Service (C3S). Available at: <https://climate.copernicus.eu/global-climate-highlights-2024> (accessed on 01 Feb 2025).
- Costa F, Szman D, Assunção J (2025) The environmental costs of political interference: Evidence from power plants in the Amazon. *Journal of Public Economics* 242: 105314. <https://doi.org/10.1016/j.jpubeco.2025.105314>
- Custódio RS (2009) Energia Eólica para a Produção de Energia Elétrica. Eletrobrás, Rio de Janeiro.

- da Luz T, Moura P (2018) Power generation expansion planning with complementarity between renewable sources and regions for 100% renewable energy systems. *International Transactions on Electrical Energy Systems* 29: e2817. <https://doi.org/10.1002/2050-7038.2817>
- da Silva SL, Linard MA, Almeida AR, Santos Junior BF (2024) Análise da complementaridade de fontes intermitentes no nordeste brasileiro. *Latin American Journal of Energy Research* 11:154-166. <https://doi.org/10.21712/lajer.2024.v11.n1.p154-166>
- Delbeke O, Moschner JD, Driesen J (2023) The complementarity of offshore wind and floating photovoltaics in the Belgian North Sea, an analysis up to 2100. *Renewable Energy* 218: 119253. <https://doi.org/10.1016/j.renene.2023.119253>
- dos Anjos PS, da Silva ASA, Stošić B, Stošić T (2015) Long-term correlations and cross-correlations in wind speed and solar radiation temporal series from Fernando de Noronha Island, Brazil. *Physica A: Statistical Mechanics and its Applications* 424: 90-96. <https://doi.org/10.1016/j.physa.2015.01.003>
- Döscher R, Acosta M, Alessandri A, Anthoni P, Arneth A, Arsouze T, Bergman T, Bernardello R, Bousetta S, Caron LP, Carver G, Castrillo M, Catalano F, Cvijanovic I, Davini P, Dekker E, DoblasReyes FJ, Docquier D, Echevarria P, Fladrich U, Fuentes-Franco R, Gröger M, von Hardenberg J, Hieronymus J, Karami MP, Keskinen JP, Koenig T, Makkonen R, Massonet F, Ménégos M, Miller PA, Moreno-Chamarro E, Nieradzki L, van Noije T, Nolan P, O'Donnell D, Ollinaho P, van der Oord G, Ortega P, Prims OT, Ramos A, Reerink T, Rousset C, Ruprich-Robert Y, Le Sager P, Schmith T, Schrödner R, Serva F, Sicardi V, Madsen MS, Smith B, Tian T, Tourigny E, Uotila P, Vancoppenolle M, Wang S, Wärlind D, Willén U, Wyser K, Yang S, Yepes-Arbós X, Zhang Q (2022) The EC-Earth3 Earth System Model for the Climate Model Intercomparison Project 6. *Geoscientific Model Development* 15:2973-3020. <https://doi.org/10.5194/gmd-15-2973-2022>
- Dullaart JC, Muis S, Bloemendaal N, Aerts JCJH (2020) Advancing global storm surge modelling using the new ERA5 climate reanalysis. *Climate Dynamics* 54:1007-1021. <https://doi.org/10.1007/s00382-019-05044-0>
- Engeland K, Borga M, Creutin J-D, François B, Ramos M-H, Vidal J-P (2017) Space-time variability of climate variables and intermittent renewable electricity production – A review. *Renewable and Sustainable Energy Reviews* 79: 600-617. <https://doi.org/10.1016/j.rser.2017.05.046>
- European Commission, Joint Research Centre, Toreti, A., Bavera, D., Acosta Navarro, J. et al. (2024a) Drought in the Amazon and the La Plata Basins: December 2024: GDO analytical report. Publications Office of the European Union. Available at: <https://data.europa.eu/doi/10.2760/9524487> (accessed on 01 Feb 2025)
- European Commission, Joint Research Centre, Toreti, A., Bavera, D., Acosta Navarro, J., et al. (2024b) Drought in Southern Africa: April 2024. Publications Office of the European Union Available at: <https://data.europa.eu/doi/10.2760/960341>
- Ferreira GWS, Reboita MS (2022) A new look into the South America precipitation regimes: Observation and forecast. *Atmosphere* 13:873. <https://doi.org/10.3390/atmos13060873>
- Ferreira GWS, Reboita MS, Drumond A (2022) Evaluation of ECMWF-SEAS5 seasonal temperature and precipitation predictions over South America. *Climate* 10:128. <https://doi.org/10.3390/cli10090128>
- Ferreira GWS, Reboita MS, Ribeiro JGM, Souza CA (2023) Assessment of precipitation and hydrological droughts in South America through statistically downscaled CMIP6 projections. *Climate* 11: 166. <https://doi.org/10.3390/cli11080166>
- Ferreira GWS, Reboita MS, Ribeiro JGM, Carvalho VSB, Santiago MEV, Silva PLLS, Baldoni TC, Souza CA (2024a) Assessment of the wind power density over South America simulated by CMIP6 models in the present and future climate. *Climate Dynamics* 62: 1729-1763. <https://doi.org/10.1007/s00382-023-06993-3>
- Ferreira GWS, Reboita MS, Ribeiro JGM (2024b) Assessment of the solar energy potential over South America estimated by CMIP6 models in the present and future climate. *Journal of Environmental & Earth Sciences*, 6: 110-143. <https://doi.org/10.30564/jees.v6i2.6425>

- François B, Hingray B, Raynaud D, Borga M, Creutin JD (2016) Increasing climate-related-energy penetration by integrating run-of-the river hydropower to wind/solar mix. *Renewable Energy* 87: 686-696. <https://doi.org/10.1016/j.renene.2015.10.064>
- Gallardo RP, Rios AM, Ramirez JS (2020) Analysis of the solar and wind energetic complementarity in Mexico. *Journal of Cleaner Production* 268: 122323. <https://doi.org/10.1016/j.jclepro.2020.122323>
- Global Electricity Review (2024) Global Electricity Review 2024. Ember Energy. Available at: <https://ember-energy.org/latest-insights/global-electricity-review-2024/> (accessed on 01 Feb 2025)
- Guezgouz M, Jurasz J, Chouai M, Bloomfield H, Bekkouche B (2021) Assessment of solar and wind energy complementarity in Algeria. *Energy Conversion and Management* 238: 114170. <https://doi.org/10.1016/j.enconman.2021.114170>
- Hassan Q, Viktor P, Al-Musawi TJ, Ali BM, Algburi S, Alzoubi HM, Al-Jiboory AK, Sameen AZ, Salman HM, Jaszczur M (2024) The renewable energy role in the global energy Transformations. *Renewable Energy Focus* 48: 100545. <https://doi.org/10.1016/j.ref.2024.100545>
- Hersbach H, Bell B, Berrisford P, Hirahara S, Horányi A, MuñozSabater J, Nicolas J, Peubey C, Radu R, Schepers D, Simmons A, Soci C, Abdalla S, Abellan X, Balsamo G, Bechtold P, Biavati G, Bidlot J, Bonavita M, de Chiara G, Dahlgren P, Dee D, Diamantakis M, Dragani R, Flemming J, Forbes R, Fuentes M, Geer A, Haimberger L, Healy S, Hogan RJ, Hólm E, Janisková M, Keeley S, Laloyaux P, Lopez P, Lupu C, Radnoti G, de Rosnay P, Rozum I, Vamborg F, Villaume S, Thépaut J.N. (2020) The ERA5 global reanalysis. *Quarterly Journal of the Royal Meteorological Society* 146:1999-2049. <https://doi.org/10.1002/qj.3803>
- Hoicka CE, Rowlands IH (2011) Solar and wind resource complementarity: Advancing options for renewable electricity integration in Ontario, Canada. *Renewable Energy* 36: 97-107. <https://doi.org/10.1016/j.renene.2010.06.004>
- Huang F, Xu Z, Guo W (2020) The linkage between CMIP5 climate models' abilities to simulate precipitation and vector winds. *Climate Dynamics* 54:4953-4970. <https://doi.org/10.1007/s00382-020-05259-6>
- IRENA (2024) Renewable energy statistics 2024. International Renewable Energy Agency (IRENA). Available at: <https://www.irena.org/Publications/2024/Jul/Renewable-energy-statistics-2024> (accessed on 01 Feb 2025).
- Karlsson K-G, Stengel M, Meirink JF, Riihelä A, Trentmann J, Akkermans T, Stein D, Devasthale A, Eliasson S, Johansson E, Håkansson N, Solodovnik I, Benas N, Clerbaux N, Selbach N, Schröder M, Hollmann R (2023) CLARA-A3: The third edition of the AVHRR-based CM SAF climate data record on clouds, radiation and surface albedo covering the period 1979 to 2023. *Earth System Science Data* 15:4901-4926. <https://doi.org/10.5194/essd-15-4901-2023>
- Khan MA, Dairaku K, Kelkar S (2025) Assessing wind power generation potential over South Asia using wind speed observation and reanalysis datasets. *Stochastic Environmental Research and Risk Assessment*. <https://doi.org/10.1007/s00477-025-02918-0>
- Krasting JP, John JG, Blanton C, McHugh C, Nikonov S, Radhakrishnan A, Rand K, Zadeh NT, Balaji V, Durachta J, Dupuis C, Menzel R, Robinson T, Underwood S, Vahlenkamp, H, Dunne KA, Gauthier PPG, Ginoux P, Grifès SM, Hallberg R, Harrison M, Hurlin W, Malyshev S, Naik V, Paulot F, Paynter DJ, Ploshay J, Reichl BG, Schwarzkopf DM, Seman CJ, Silvers L, Wyman B, Zeng Y, Adcroft A, Dunne JP, Dussin R, Guo H, He J, Held IM, Horowitz LW, Lin P, Milly PCD, Shevliakova E, Stock C, Winton M, Wittenberg AT, Xie Y, Zhao M (2018) NOAA-GFDL GFDL-ESM4 model output prepared for CMIP6 CMIP historical. Version 20190726. Earth System Grid Federation. <https://doi.org/10.22033/ESGF/CMIP6.8597>
- Kumar D, Mishra V, Ganguly AR (2015) Evaluating wind extremes in CMIP5 climate models. *Climate Dynamics* 45:441-453 <https://doi.org/10.1007/s00382-014-2306-2>
- Lagos-Zúñiga MA, Balmaceda-Huarte R, Regoto P, Torrez L, Olmo M, Lyra A, Pareja-Quispe D, Bettolli ML (2024) Extreme indices of temperature and precipitation in South America: Trends and intercomparison of regional climate models. *Climate Dynamics* 62:4541-4562. <https://doi.org/10.1007/s00382-022-06598-2>



- Lovato T, Peano D (2020) CMCC CMCC-CM2-SR5 model output prepared for CMIP6 CMIP historical Version 20200616. Earth Syst Grid Federation. <https://doi.org/10.22033/ESGF/CMIP6.3825>
- Lovato T, Peano D, Butenschön M, Materia S, Iovino D, Scoccimarro E, Fogli PG, Cherchi A, Bellucci A, Gualdi S, Masina S, Navarra S (2022) CMIP6 simulations with the CMCC Earth System Model (CMCC-ESM2). *Journal of Advances in Modeling Earth Systems* 14:e2021MS002814. <https://doi.org/10.1029/2021MS002814>
- Li Q, Xue Y, Kong X, Lau WK-M, Wang A, Li Q, Cao Z, Nayak H, Xu G, Guo W, Vasic R (2025) Excessive Tibetan Plateau spring warming found to cause catastrophic June 2024 heavy rainfall in China. *Science Bulletin*. <https://doi.org/10.1016/j.scib.2025.01.011>
- Li T, Ma J, Huang Y, Zhang S, Gao H, Xu C (2025) Disaster analysis and lessons learned from the July 22, 2024, Ethiopian landslide. *Earthquake Research Advances*. <https://doi.org/10.1016/j.eqrea.2025.100358>
- Liu Y, Xiao L, Wang H, Dai S, Qi Z (2013) Analysis on the hourly spatiotemporal complementarities between China's solar and wind energy resources spreading in a wide area. *Science China Technological Sciences* 56: 683-692. <https://doi.org/10.1007/s11431-012-5105-1>
- Min C-G, Kim M-K (2017) Impact of the complementarity between variable generation resources and load on the flexibility of the Korean power system. *Energies* 10: 1719. <https://doi.org/10.3390/en10111719>
- Monforti F, Huld T, Bódis K, Vitali L, D'Isidoro M, Lacal-Arántegui R (2014) Assessing complementarity of wind and solar resources for energy production in Italy. A Monte Carlo approach. *Renewable Energy* 63: 576-586. <https://doi.org/10.1016/j.renene.2013.10.028>
- Nascimento MMS, Shadman M, Silva C, Assad LPF, Estefen SF, Landau L (2022) Offshore wind and solar complementarity in Brazil: A theoretical and technical potential assessment. *Energy Conversion and Management* 270: 116194. <https://doi.org/10.1016/j.enconman.2022.116194>
- NOAA/NIDIS (2025) Drought Report Annual 2024. National Oceanic and Atmospheric Administration/ National Integrated Drought Information System (NOAA/NIDIS). Available at: <https://www.ncei.noaa.gov/access/monitoring/monthly-report/drought/202413> (accessed on 01 Feb 2025)
- Ortega G, Arias PA, Villegas JC, Marquet PA, Nobre P (2021) Present-day and future climate over Central and South America according to CMIP5/CMIP6 models. *International Journal of Climatology* 41:6713-6735. <https://doi.org/10.1002/joc.7221>
- Pimentel LO, Rosário JA (2024) Evaluation of energy complementarity between wind, solar and water resources in the municipality of Lages (Santa Catarina, Brazil). *Revista de Gestão Social e Ambiental* 18: e05462. <https://doi.org/10.24857/rgsa.v18n5-030>
- Prasad AA, Taylor RA, Kay M (2017) Assessment of solar and wind resource synergy in Australia. *Applied Energy* 190: 354-367. <https://doi.org/10.1016/j.apenergy.2016.12.135>
- Reboita MS, Amaro TR, de Souza MR (2018) Winds: Intensity and power density simulated by RegCM4 over South America in present and future climate. *Climate Dynamics* 51:187-205. <https://doi.org/10.1007/s00382-017-3913-5>
- Reboita MS, Kiani RS, Ali S, Khan T (2021a) Projections of wind power density in Pakistan and adjacent regions. *Climate Research* 85:177-192. <https://doi.org/10.3354/cr01679>
- Reboita MS, Kuki CAC, Marrafon VH, Souza CA, Ferreira GWS, Teodoro T, Lima JWM (2021b) South America climate change revealed through climate indices projected by GCMs and Eta-RCM ensembles. *Climate Dynamics* 58:459-485. <https://doi.org/10.1007/s00382-021-05918-2>
- Reboita MS, Ferreira GWS, Ribeiro JGM, da Rocha RP, Rao VB (2023) South American monsoon lifecycle projected by statistical downscaling with CMIP6-GCMs. *Atmosphere* 14:1380. <https://doi.org/10.3390/atmos14091380>

- Reboita MS, Mattos EV, Capucin BC, Souza DO, Ferreira GWS (2024a) A multi-scale analysis of the extreme precipitation in southern Brazil in April/May 2024. *Atmosphere* 15: 1123. <https://doi.org/10.3390/atmos15091123>
- Reboita MS, Ferreira GWS, Ribeiro JGM, Ali S (2024b) Assessment of precipitation and near-surface temperature simulation by CMIP6 models in South America. *Environmental Research: Climate* 3:025011. <https://doi.org/10.1088/2752-5295/ad3fdb>
- Requia WJ (2024) Fires in Brazil: health crises and the failure of government action. *The Lancet Regional Health Americas* 39: 100913. <https://doi.org/10.1016/j.lana.2024.100913>
- Riscoti JFC, Sauer IL (2013) An assessment of wind power prospects in the Brazilian hydrothermal system. *Renewable and Sustainable Energy Reviews* 19:742-753. <https://doi.org/10.1016/j.rser.2012.11.010>
- Risso A, Beluco A, Alves RCM (2018) Complementarity roses evaluating spatial complementarity in time between energy resources. *Energies* 11: 1918. <https://doi.org/10.3390/en11071918>
- Rivera JA, Arnould G (2020) Evaluation of the ability of CMIP6 models to simulate precipitation over Southwestern South America: Climatic features and long-term trends (1901–2014). *Atmospheric Research* 241:104953. <https://doi.org/10.1016/j.atmosres.2020.104953>
- Rosa COCS, Costa KA, Christo ES, Bertahone PB (2017) Complementarity of hydro, photovoltaic, and wind power in Rio de Janeiro state. *Sustainability* 9: 1130. <https://doi.org/10.3390/su9071130>
- Rupp DE, Abatzoglou JT, Hegewisch KC, Mote PW (2013) Evaluation of CMIP5 20th century climate simulations for the Pacific Northwest USA. *Journal of Geophysical Research: Atmospheres* 118:10884-10906. <https://doi.org/10.1002/jgrd.50843>
- Sawadogo W, Reboita MS, Faye A, da Rocha RP, Odoulami RC, Olusegun CF, Adeniyi MO, Abiodun BJ, Sylla MB, Diallo I, Coppola E, Giorgi F (2021) Current and future potential of solar and wind energy over Africa using the RegCM4 CORDEX-CORE ensemble. *Climate Dynamics* 57:1647-1672. <https://doi.org/10.1007/s00382-020-05377-1>
- Schmidt J, Cancellara R, Pereira Junior AO (2016) The role of wind power and solar PV in reducing risks in the Brazilian hydro-thermal power system. *Energy* 115: 1748-1757. <https://doi.org/10.1016/j.energy.2016.03.059>
- Sian KTCLK, Sagero P, Kebacho LL, Ongoma V (2025) Dubai's record precipitation event of 16 April 2024 – A diagnosis. *Atmospheric Research* 315: 107924. <https://doi.org/10.1016/j.atmosres.2025.107924>
- Silva AR, Pimenta FM, Assireu AT, Spyrides MHC (2016) Complementarity of Brazil's hydro and offshore wind power. *Renewable and Sustainable Energy Reviews* 56: 413-427. <https://doi.org/10.1016/j.rser.2015.11.045>
- Silva LSO, Silva Junior RS, Lyra RFF, Martins FR, Moura MAL, Leal Junior JBV, Muniz ES, Vasconcelos LN (2024) Avaliação da complementaridade entre os recursos eólico-solar e considerações sobre estabilidade no setor elétrico. *Revista Brasileira de Geografia Física* 17: 1942-1960. <https://doi.org/10.26848/rbgf.v17.3.p1942-1960>
- Sivin DD (2025) Trump: A disaster for health, safety, and environment. *New Solutions: A Journal of Environmental and Occupational Health Policy* 34: 248-252. <https://doi.org/10.1177/10482911241304227>
- Solomon AA, Kammen DM, Callaway D (2016) Investigating the impact of wind-solar complementarities on energy storage requirement and the corresponding supply reliability criteria. *Applied Energy* 168: 130-145. <https://doi.org/10.1016/j.apenergy.2016.01.070>
- Soukissian TH, Karathanasi FE, Zaragkas DK (2021) Exploiting offshore wind and solar resources in the Mediterranean using ERA5 reanalysis data. *Energy Conversion and Management* 237: 114092. <https://doi.org/10.1016/j.enconman.2021.114092>
- Tatebe H, Watanabe M (2018) MIROC MIROC6 model output prepared for CMIP6 CMIP historical. Version 20181212. Earth System Grid Federation. <https://doi.org/10.22033/ESGF/CMIP6.5603>



- Teixeira, L E., Caux J., Beluco, A., Bertoldo, I., Louzada, J. A. S., Eifler, R. C., 2015. Feasibility Study of a Hydro PV Hybrid System Operating at a Dam for Water Supply in Southern of Brazil, *Journal of Power and Energy Engineering*, vol. 3, pp. 70-83.
- Torres RR, Marengo JA (2013) Uncertainty assessments of climate change projections over South America. *Theoretical and Applied Climatology* 112:253-272. <https://doi.org/10.1007/s00704-012-0718-7>
- Tram-Anh Q, Ngo-Duc T, Espagne E, Trinh-Tuan L (2023) A 10-km CMIP6 downscaled dataset of temperature and precipitation for historical and future Vietnam climate. *Scientific Data* 10:257. <https://doi.org/10.1038/s41597-023-02159-2>
- Viviescas C, Lima L, Diuana FA, Vasquez E, Ludovique C, Silva GN, Huback V, Magalar L, Szklo A, Lucena AFP, Schaefer R, Paredes JR (2019) Contribution of variable renewable energy to increase energy security in Latin America: Complementarity and climate change impacts on wind and solar resources. *Renewable and Sustainable Energy Review* 113: 109232. <https://doi.org/10.1016/j.rser.2019.06.039>
- Wieners KH, Giorgetta M, Jungclaus J, Reick C, Esch M, Bittner M, Legutke S, Schupfner M, Wachsmann F, Gayler V, Haak H, de Vrese P, Raddatz T, Mauritsen T, von Storch JS, Behrens J, Brovkin V, Claussen M, Crueger T, Fast I, Fiedler S, Hagemann S, Hohenegger C, Jahns T, Kloster S, Kinne S, Lasslop G, Kornbluh L, Marotzke J, Matei D, Meraner K, Mikolajewicz U, Modali K, Müller W, Nabel J, Notz D, Peters-von Gehlen K, Pincus R, Pohlmann H, Pongratz J, Rast S, Schmidt H, Schnur R, Schulzweida U, Six K, Stevens B, Voigt A, Roeckner E (2019) MPI-M MPI-ESM1.2-LR model output prepared for CMIP6 CMIP historical. Version 20190710. Earth System Grid Federation. <https://doi.org/10.22033/ESGF/CMIP6.6595>
- Wilczak JM, Akish E, Capotondi A, Compo GP (2024) Evaluation and bias correction of the ERA5 reanalysis over the United States for wind and solar energy applications. *Energies* 17:1667. <https://doi.org/10.3390/en17071667>
- Yukimoto S, Kosshiro T, Kawai H, Oshima N, Yoshida K, Urakawa S, Tsujino H, Deushi M, Tanaka T, Hosaka M, Yoshimura H, Shindo E, Mizuta R, Ishii M, Obata A, Adachi Y (2019) MRI MRI-ESM2.0 model output prepared for CMIP6 CMIP historical. Version 20190222. Earth System Grid Federation. <https://doi.org/10.22033/ESGF/CMIP6.6842>
- Zhang W, Zhou T, Ye W, Zhang T, Zhang L, Wolski P, Risbey J, Wang Z, Min S-K, Ramsay H, Brody M, Grimm A, Clark R, Ren K, Jiang J, Chen X, Fu S, Li L, Tang S, Hu S (2025) A year marked by extreme precipitation and floods: Weather and climate extremes in 2024. *Advances in Atmospheric Sciences*. <https://doi.org/10.1007/s00376-025-4540-4>
- Zhou X, Li Y, Xiao C, Chen W, Mei M, Wang G (2025) High-impact extreme weather and climate events in China: Summer 2024 overview. *Advances in Atmospheric Sciences*. <https://doi.org/10.1007/s00376-024-4462-6>

Supplementary Material

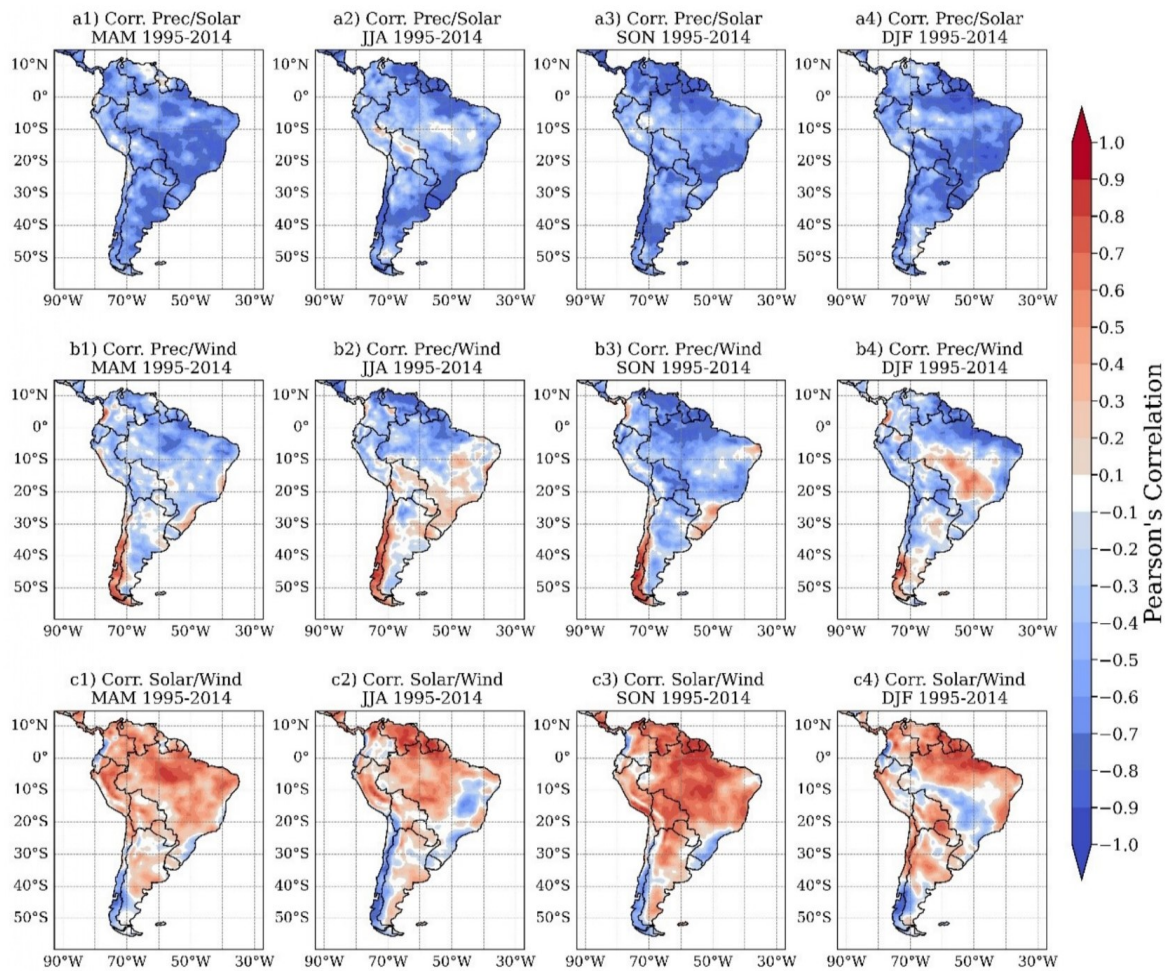


Figure S1: Seasonal complementarity in the historical period based on statistically downscaled CMIP6 climate simulations.

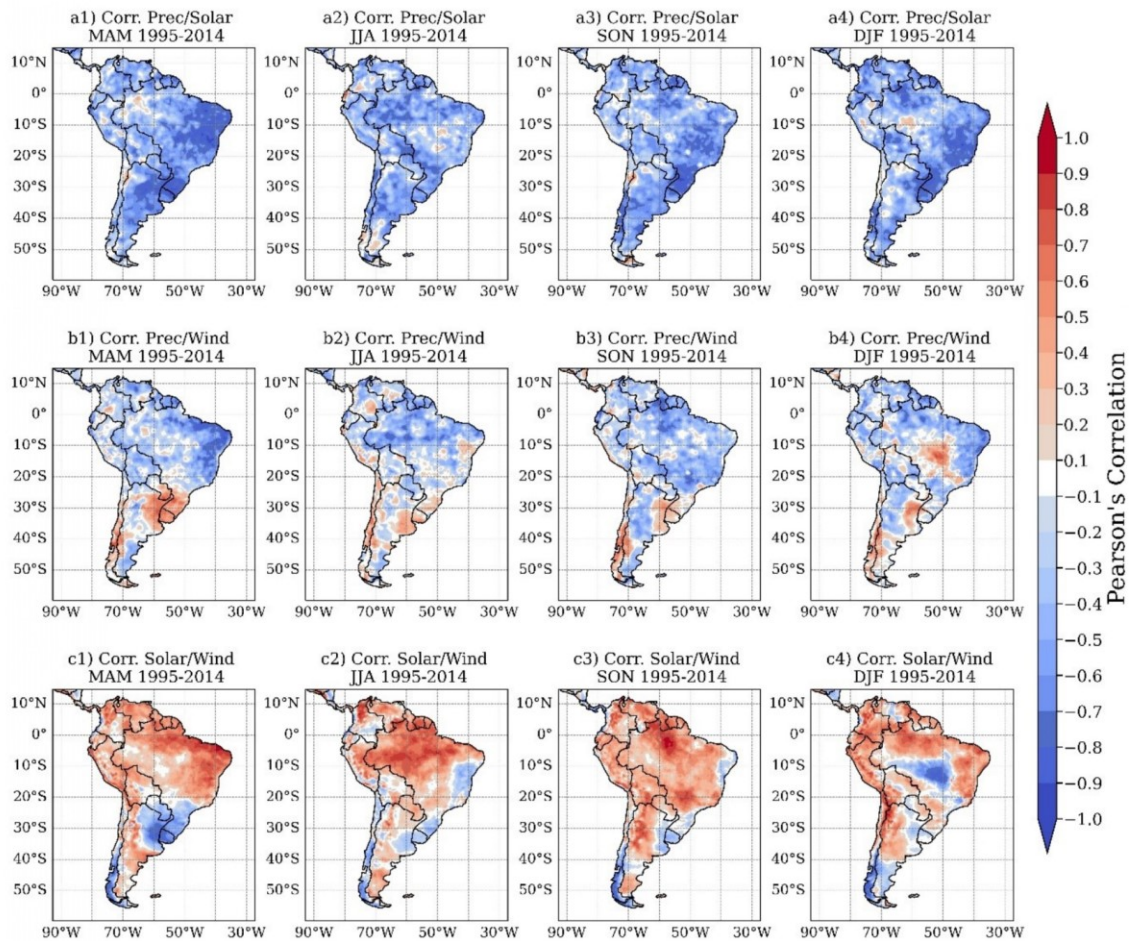


Figure S2: Seasonal complementarity in the historical period based on reference data.

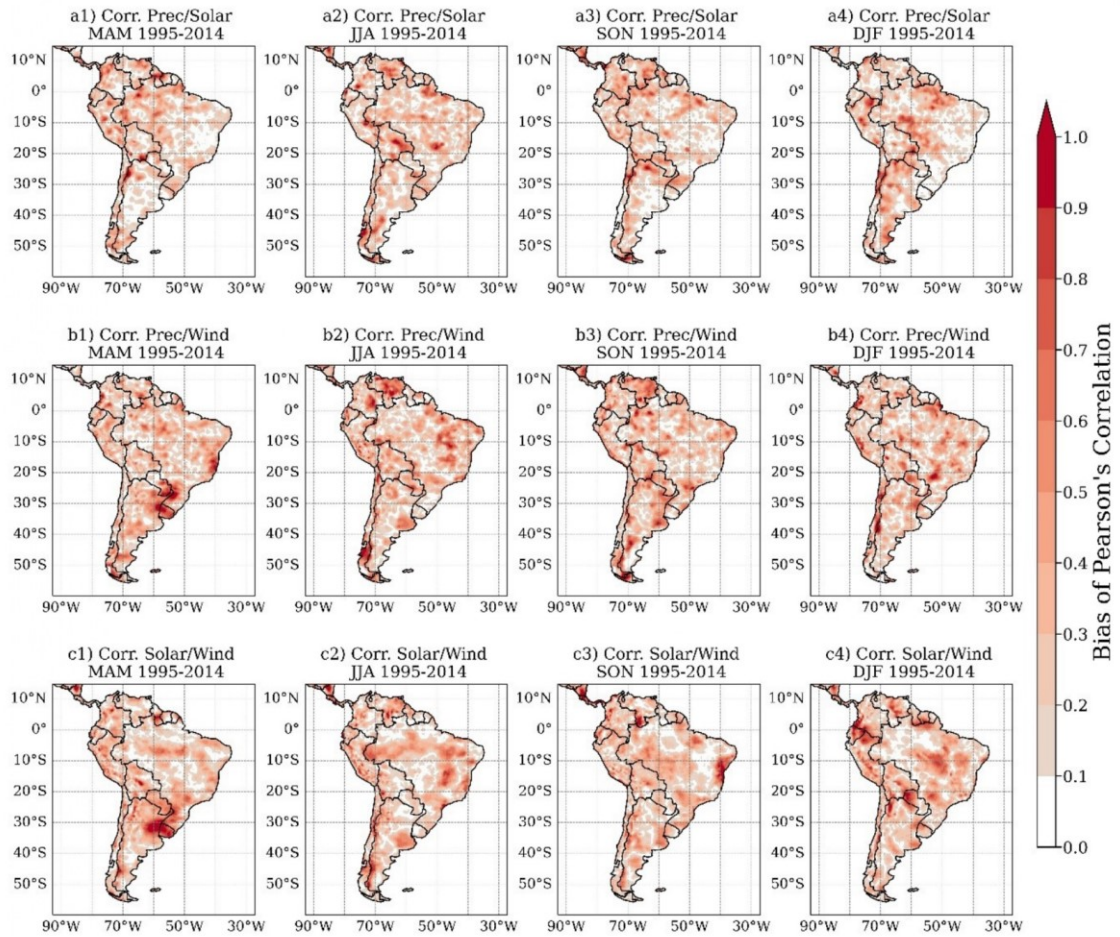


Figure S3: Difference between seasonal complementarity in the historical period based on CMIP6 and reference data.

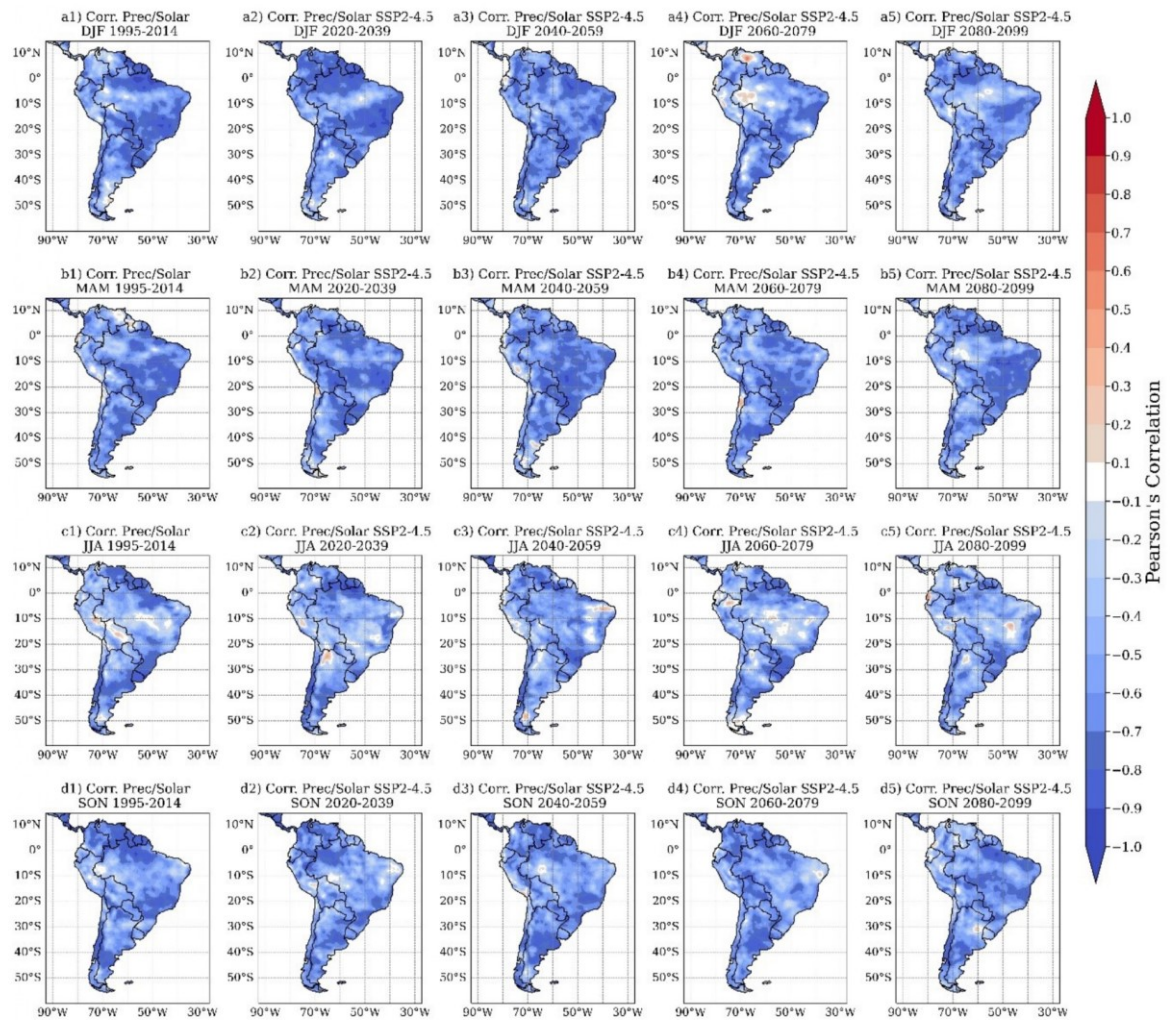


Figure S4: Seasonal correlations between precipitation and global horizontal irradiance anomalies provided by statistically downscaled CMIP6 projections for the historical and future periods under the SSP2-4.5 scenario.

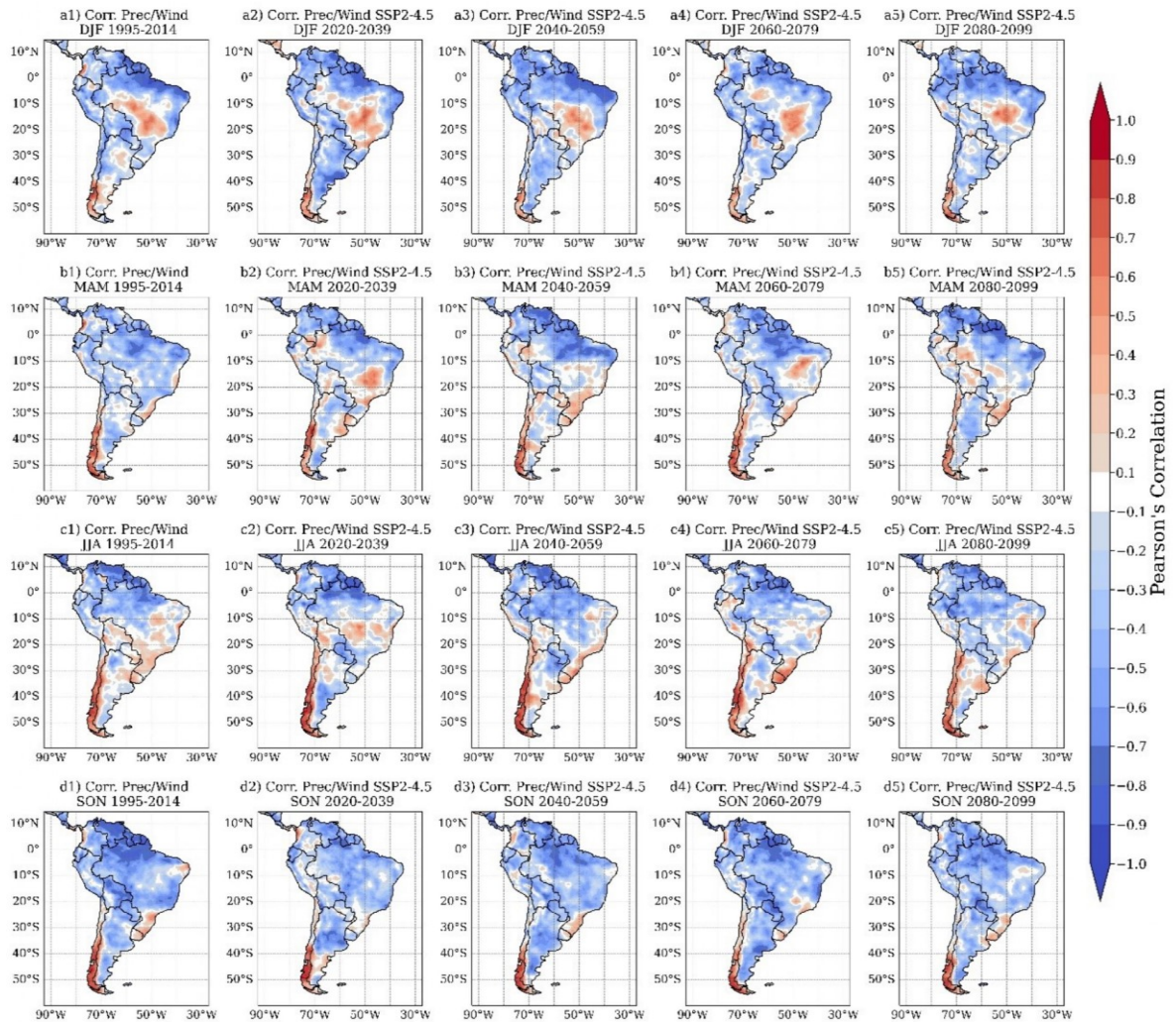


Figure S5: Seasonal correlations between precipitation and wind intensity at 100 m anomalies provided by statistically downscaled CMIP6 projections for the historical and future periods under the SSP2-4.5 scenario.

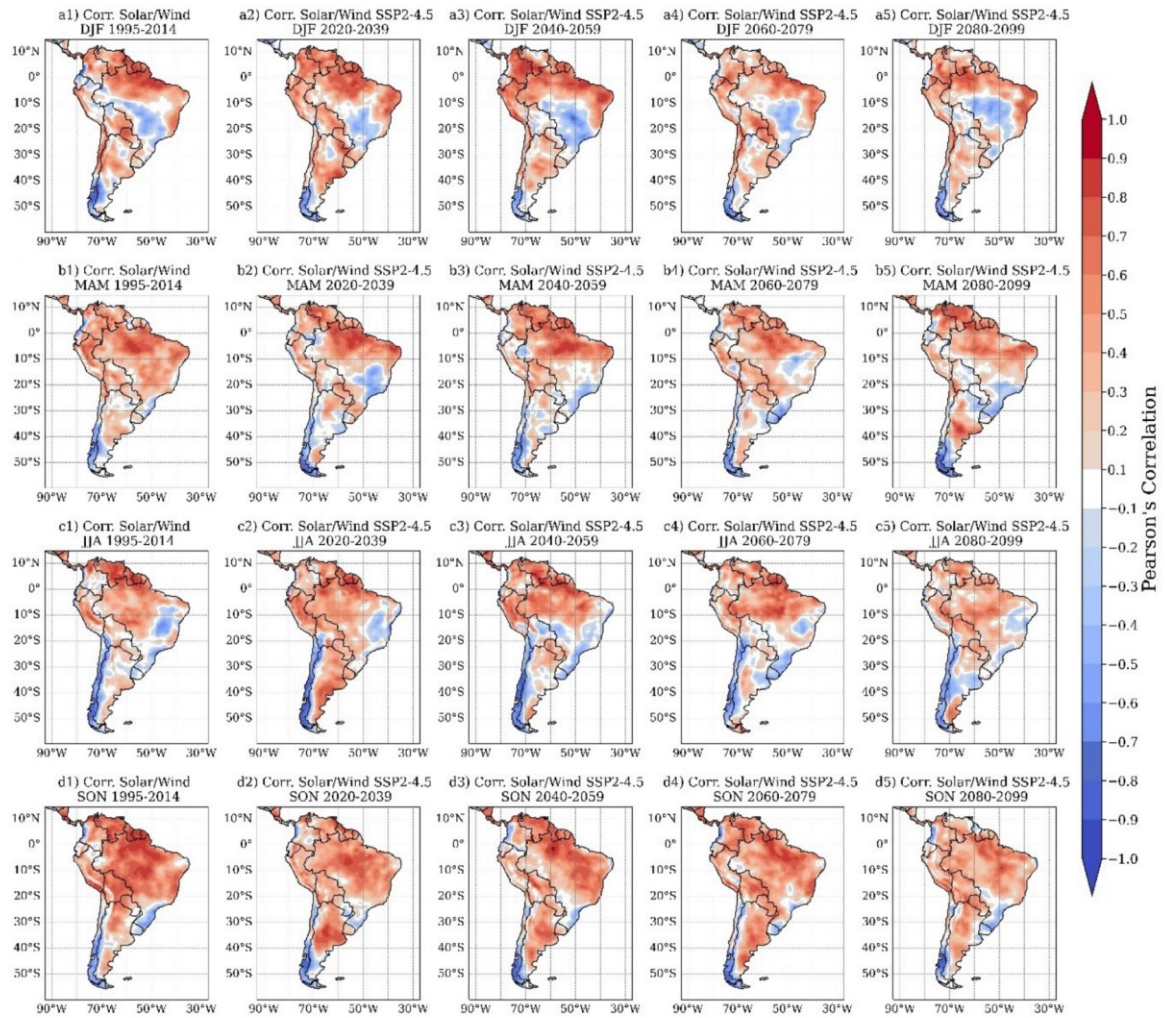


Figure S6: Seasonal correlations between global horizontal irradiance and wind intensity at 100 m anomalies provided by statistically downscaled CMIP6 projections for the historical and future periods under the SSP2-4.5 scenario.

9. GENERAL CONCLUSIONS

This doctoral research analyzed projected changes in key climate variables across South America, particularly Brazil, using simulations and projections from eight CMIP6 global climate models (GCMs). The study focused on precipitation, wind speed at 100 m, wind power density at 100 m, surface solar irradiance, concentrated solar power (CSP), and photovoltaic power (PVP). Statistical downscaling and bias correction were applied using the Quantile Delta Mapping (QDM) method to enhance the accuracy of projections. Overall, the QDM technique reduced systematic biases in CMIP6 models, improving all analyzed variables' seasonal and spatial representation.

Hydrological Droughts

Future projections indicate significant reductions in precipitation across most of the continent, especially during austral spring, with the most pronounced decline under the SSP5-8.5 scenario. While the frequency and intensity of drought events exhibited mixed signals among GCMs, there was strong agreement on droughts' increasing duration and severity throughout the 21st century. Notably, Brazil is expected to experience a higher proportion of moderate and severe droughts, particularly in the Northeast and Midwest regions. These findings emphasize the urgent need for strategic water resource management to mitigate potential energy and agricultural effects.

South American Monsoon Lifecycle

The projected changes in the South American Monsoon System indicate delays in its onset, leading to a shortened rainy season in critical areas. The ensemble suggests a delay of approximately three pentads in monsoon onset across most regions and a two-pentad delay in its demise north of 20°S. These changes are expected to be particularly significant in the South Atlantic Convergence Zone and the Brazilian Amazon, where a statistically significant shortening of the monsoon length is projected in the second half of the 21st century. Such shifts may have profound implications for agriculture, hydropower production, and overall water availability, reinforcing the necessity of adaptive strategies to ensure regional resilience.

Wind Energy Potential

Expanding wind power generation is crucial for South America's transition to a more sustainable energy matrix. Projections indicate a 25-50% increase in wind power density in regions such as Northeast and South Brazil, Argentine Patagonia, northern Venezuela, Uruguay, Bolivia, and Paraguay. The most substantial increases are expected under SSP5-8.5, reinforcing these sectors' growing potential for wind energy expansion. However, individual model projections revealed considerable uncertainties regarding wind intensity anomalies, underscoring the challenges of long-term forecasting. Despite these uncertainties, the study provides the first comprehensive analysis of CMIP6 projections for wind power in South America, offering valuable guidance for energy sector stakeholders.

Solar Energy Potential

The findings indicate spatial and seasonal variations in solar energy generation across South America. For concentrated solar power (CSP), projections suggest that historically favorable regions – such as Northeast Brazil and parts of Chile – will maintain their suitability, with potential 1-6% increases under the SSP5-8.5 scenario. For photovoltaic power (PVP), projected increases range from 1-4%, particularly in the Amazonia, Midwest, and Southeast Brazil. However, in South Brazil, approximately 84% of the projections indicate either a negative or neutral trend, signaling less favorable conditions for solar expansion in this region. These results highlight the importance of region-specific planning to optimize solar energy investments and infrastructure development.

Renewable Resources Complementarity

The complementarity between precipitation, solar radiation, and wind speed is essential to ensuring energy security in South America. Future projections suggest an increase in precipitation-solar complementarity in Midwest and Southeast Brazil during the wet season, whereas declining rainfall in Amazonia may reduce this effect. Precipitation-wind complementarity is expected to strengthen in North and Northeast Brazil, promoting hybrid energy generation during dry periods. Additionally, solar-wind complementarity is projected to increase in northern South America and Northeast Brazil, further supporting the development of hybrid solar-wind systems.

However, challenges remain in balancing the seasonal variability of run-of-river hydropower, particularly in northern Brazil, where reduced water storage capacity may introduce operational constraints.

Study Limitations and Implications for Decision-Making

While this research advances the understanding of climate change impacts on renewable energy in South America through bias-corrected CMIP6 projections at a seasonal scale, several limitations must be acknowledged to contextualize its results and inform their appropriate use by decision-makers. Decision-makers often require spatially and temporally explicit guidance tailored to specific investment horizons, infrastructure lifespans, and energy policies (Illangasingha et al., 2023; Fleming et al., 2025). However, climate projections inherently deal with long-term, probabilistic scenarios rather than deterministic forecasts (Reggiani et al., 2021). This temporal mismatch can lead to misinterpretation or misuse of the data if uncertainty ranges, methodological assumptions and spatial generalizations are not fully understood. Without appropriate contextualization, there is a risk that policymakers may either overestimate the confidence of model-based outputs or dismiss valuable information due to perceived complexity (Moradian et al., 2025).

Furthermore, the analysis presented here is restricted to seasonal averages without exploring finer temporal resolutions such as daily or hourly scales. These higher-resolution scales are critical for evaluating the operational viability of renewable energy systems, particularly regarding the intermittency and ramping behavior of wind and solar power (Esnaola et al., 2024; Yang et al., 2024; Zhang et al., 2024). In addition, the observational datasets used for validation (e.g., reanalysis or gridded climate products) are subject to biases and uncertainties, especially in regions with sparse in situ data, such as parts of the Amazon and Andes. These biases can propagate and lead to erroneous assumptions about the accuracy of GCM projections and bias correction performance (Balmaceda-Huarte et al., 2021). Moreover, extreme events such as heatwaves, heavy precipitation, or wind droughts are not explicitly analyzed despite their significant relevance to energy demand, generation reliability, and system resilience (Antonini et al., 2024). Given the projected intensification of extremes under climate change (IPCC, 2021), their exclusion constitutes a critical research gap to be addressed in future studies.

Also, this study does not incorporate technological progress in wind and solar systems, such as increased hub height for wind turbines or improvements in photovoltaic panel efficiency (Cazzaniga and Rosa-Clot, 2021; Lopes et al., 2022; Zhuo et al., 2025). These advances directly affect capacity factors and energy yield but were not modeled here, potentially underestimating future renewable energy power (Lopes et al., 2022; Satymov et al., 2022; Liu et al., 2023). In addition, hydropower projections were assessed through climate indicators only, without using hydrological models capable of simulating river discharge, reservoir dynamics, or water balance under climate change. Integrating such models is essential for a more accurate evaluation of hydroelectric generation (Almeida et al., 2021; Caceres et al., 2021; de Jong et al., 2021; Serrão et al., 2021). Moreover, biomass energy, a relevant component of South America's renewable energy mix, requires further analysis of how changing climate conditions affect biomass availability, crop yields, and biofuel production efficiency.

Despite the clear benefits of transitioning to renewable energy sources in mitigating greenhouse gas emissions, deploying large-scale wind and solar energy infrastructure can generate significant ecological and social impacts. Wind farms have been associated with noise pollution, landscape fragmentation, and disturbances to avian and bat populations, mainly when installed along migratory routes or near ecologically sensitive areas (Hamed and Alshare, 2022; Karasmanaki, 2022; Msigwa et al., 2022). Similarly, solar PV projects often require large tracts of land, leading to land-use change, habitat loss, and soil degradation (Lambert et al., 2021; Tawalbeh et al., 2021; Hamed and Alshare, 2022).

The Amazon biome, in particular, presents a complex dilemma. While the region holds vast potential for solar energy due to relatively high irradiance in its deforested and degraded areas, installing PV systems may catalyze further deforestation, ecosystem fragmentation, and indirect land-use change (da Silva et al., 2018; Rehbein et al., 2020; Sonter et al., 2020; Usman et al., 2020). Therefore, the expansion of solar infrastructure in this biome must be carefully evaluated through rigorous environmental impact assessments and inclusive planning that prioritizes ecosystem integrity and local livelihoods (Sánchez et al., 2015; Trindade et al., 2022; Hampl, 2024). Another often overlooked aspect of renewable energy development is the environmental footprint of its supply chain – particularly the mining of critical minerals such as lithium, which are essential for solar panels, batteries, and wind turbines (Ali et al., 2017; Sonter et al., 2020; Giglio, 2021).

Beyond energy systems, future work should also focus on the broader socio-environmental consequences of climate change, including its effects on vector-borne disease transmission. Rising temperatures and altered precipitation patterns could expand the habitat suitability for disease-carrying vectors, posing significant public health risks. Furthermore, extreme temperature events, including heatwaves and cold spells, require further investigation to assess their potential impacts on human health, agriculture, and energy demand. By integrating high-resolution climate models, advanced energy system modeling, epidemiological studies, and interdisciplinary approaches, future research can provide even more refined projections and strategic insights to guide sustainable energy planning, public health preparedness, and climate adaptation policies in South America.

10. REFERENCES

Abatan, A. A.; Tett, S. F. B.; Dong, B.; Cunningham, C.; Rudorff, C. M.; Klingaman, N. P.; de Abreu, R. C. Drivers and physical processes of drought events over the state of São Paulo, Brazil. **Climate Dynamics**, 58, 3105-3119, 2022.

Agudelo, J.; Arias, P. A.; Vieira, S. C.; Martínez, J. A. Influence of longer dry seasons in the Southern Amazon on patterns of water vapor transport over northern South America and the Caribbean. **Climate Dynamics**, 52, 2647-2665, 2019.

Ali, S.H.; Giurco, D.; Arndt, N.; Nickless, E.; Brown, G.; Demetriades, A.; Durrheim, R.; Enriquez, M.A.; Kinnaird, J.; Littleboy, A.; Meinert, L.D.; Oberhänsli, R.; Salem, J.; Schodde, R.; Schneider, G.; Vidal, O.; Yakovleva, N. Mineral supply for sustainable development requires resource governance. **Nature**, 543, 367-372, 2017.

Almazroui, M.; Ashfaq, M.; Islam, M.N.; Kamil, S.; Abid, M.A.; O'Brien, E.; Ismail, M.; Reboita, M.S.; Sörensson, A.A.; Arias, P.A.; Alves, L. M.; Tippet, M. K.; Saeed, S.; Haarsma, R.; Doblas-Reyes, F. J.; Saeed, F.; Kucharski, F.; Nadeem, I.; Silva-Vidal, Y.; Rivera, J. A.; Ehsan, M. A.; Martínez-Castro, D.; Muñoz, A. G.; Ali, M. A.; Coppola, E.; Sylla, M. B. Assessment of CMIP6 performance and projected temperature and precipitation changes over South America. **Earth Systems and Environment**, 5, 155-183, 2021.

Almeida, R.M.; Fleischmann, A.S.; Brêda, J.P.F.; Cardoso, D.S.; Angarita, H.; Collischonn, W.; Forsberg, B.; García-Villacorta, R.; Hamilton, S.K.; Hannam, P.M.; Paiva, R.; Poff, N.L.; Sethi, S.A.; Shi, Q.; Gomes, C.P.; Flecker, A.S. Climate change may impair electricity generation and economic viability of future Amazon hydropower. **Global Environmental Change**, 71, 102383, 2021.

Ambrizzi, T.; Reboita, M. S.; da Rocha, R. P.; Llopart, M. The state of the art and fundamental aspects of regional climate modeling in South America. **Annals of the New York Academy of Sciences**, 1436, 98-120, 2019.

Arango-Aramburo, S.; Ríos-Ocampo, J. P.; Larsen, E. R. Examining the decreasing share of renewable energy and growing thermal capacity: the case of South America. **Renewable and Sustainable Energy Reviews**, 119, 109648, 2020.

- Antonini, E.G.A.; Virgüez, E.; Ashfaq, S.; Duan, L.; Ruggles, T.H.; Caldeira, K. Identification of reliable locations for wind power generation through a global analysis of wind droughts. **Communications Earth & Environment**, 5, 103, 2024.
- Arias, P. A.; Ortega, G.; Villegas, L. D.; Martínez, J. Colombian climatology in CMIP5/CMIP6 models: persistent biases and improvements. **Revista de Facultad de Ingeniería**, 100, 75-96, 2021.
- Avila-Diaz, A.; Torres, R. R.; Zuluaga, C. F.; Cerón, W. L.; Oliveira, L.; Benezoli, V.; Rivera, I. A.; Marengo, J. A.; Wilson, A. B.; Medeiros, F. Current and future climate extremes over Latin America and Caribbean: assessing earth system Models from High Resolution Model Intercomparison Project (HighResMIP). **Earth Systems and Environment**, 7, 99-130, 2023.
- Ballarin, A. S.; Sone, J. S.; Gesualdo, G. C.; Schwaback, D.; Reis, A.; Almagro, A.; Wendland, E. C. CLIMBra-Climate change dataset for Brazil. **Scientific Data**, 10, 47, 2023.
- Balmaceda-Huarte, R.; Olmo, M.E.; Bettolli, M.L.; Poggi, M.M. Evaluation of multiple reanalyses in reproducing the spatio-temporal variability of temperature and precipitation indices over southern South America. **International Journal of Climatology**, 41, 5572-5595, 2021.
- Bauer, S.; O'Malia, K.; Prasad, S.; Clark, G.; Behrsin, I. A race to the top Latin America 2023: wind and solar utility-scale buildout gains speed in Brazil, Chile and Colombia, while Mexico falls behind. *Global Energy Monitor*, 2023. Available at: <https://globalenergymonitor.org/report/a-race-to-the-top-latin-america/> (accessed on 05 Apr 2024).
- Bettolli, M. L.; Penalba, O. C. Statistical downscaling of daily precipitation and temperatures in southern La Plata Basin. **International Journal of Climatology**, 38, 3705-3722, 2018.
- Borges, P. A.; Bernhofer, C.; Rodrigues, R. Extreme rainfall indices in Distrito Federal, Brazil: Trends and links with El Niño southern oscillation and Madden–Julian oscillation. **International Journal of Climatology**, 38, 4550-4567, 2018.
- Boulton, C. A.; Lenton, T. M.; Boers, N. Pronounced loss of Amazon rainforest resilience since the early 2000s. **Nature Climate Change**, 12, 271-278, 2022.

- Brazilian Energy Balance. Summary Report 2024 – Reference Year 2023. Energy Research Office (EPE), 2024. Available at: <https://www.epe.gov.br/pt/publicacoes-dados-abertos/publicacoes/balanco-energetico-nacional2024> (accessed on 01 Feb 2025).
- Cacciuttolo, C.; Navarrete, M.; Atencio, E. Renewable wind energy implementation in South America: A comprehensive review and sustainable prospects. **Sustainability**, 16, 6082, 2024.
- Caceres, A.L.; Jaramillo, P.; Matthews, H.S.; Samaras, C.; Nijssen, B. Hydropower under climate uncertainty: Characterizing the usable capacity of Brazilian, Colombian and Peruvian power plants under climate scenarios. **Energy for Sustainable Development**, 61, 217-229, 2021.
- Cannon, A. J.; Sobie, S. R.; Murdock, T. Q. Bias correction of GCM precipitation by Quantile Mapping: How well do methods preserve changes in quantiles and extremes? **Journal of Climate**, 28, 6938-6959, 2015.
- Carvalho, D.; Rocha, A.; Costoya, X.; de Castro, M.; Gómez-Gesteira, M. Wind energy resource over Europe under CMIP6 future climate projections: What changes from CMIP5 to CMIP6. **Renewable Sustainable Energy Reviews**, 151, 111594, 2021.
- Cavalcanti, I. F. A.; Kousky, V. E. Drought in Brazil during summer and fall 2001 and associated atmospheric circulation features. **Revista Climanalise**, 2, 1, 2001.
- Cazzaniga, R.; Rosa-Clot, M. The booming of floating PV. *Solar Energy*, 219, 3-10, 2021.
- Chou, S. C.; Lyra, A.; Mourão, C.; Dereczynski, C.; Pilotto, I.; Gomes, J.; Bustamante, J.; Tavares, P.; Silva, A.; Rodrigues, D.; et al. Evaluation of the Eta simulations nested in three global climate models. **American Journal of Climate Change**, 3, 438-454, 2014.
- Clarke, L.; Eom, J.; Marten, E. H.; Horowitz, R.; Kyle, P.; Link, R.; Mignone, B. K.; Mundra, A.; Zhou, Y. Effects of long-term climate change on global building energy expenditures. **Energy Economics**, 72, 667-677, 2018.
- Coelho, C. A. S.; Oliveira, C. P.; Ambrizzi, T.; Reboita, M. S.; Carpenedo, C. B.; Campos, J. L. P. S.; Tomaziello, A. C. N.; Pampuch, L. A.; Custódio, M. S.; Dutra, L. M. M.; et al. The 2014 southeast Brazil austral summer drought: Regional scale mechanisms and teleconnections. **Climate Dynamics**, 46, 3737-3752, 2016.

- Collazo, S.; Barrucand, M.; Rusticucci, M. Evaluation of CMIP6 models in the representation of observed extreme temperature indices trends in South America. **Climatic Change**, 172, 21, 2022.
- Costa, R. S.; da Costa, G. L.; de Lima, F. J. L.; Gonçalves, A. R.; Martins, F. R.; Pereira, E. B.; Casagrande, M. S. G. Impactos das mudanças climáticas na disponibilidade do recurso energético solar. **Revista Brasileira de Energia**, 26, 39-50, 2020.
- Cuartas, L. A.; Cunha, A. P. M. A.; Alves, J. A.; Parra, L. M. P.; Deusdará-Leal, K.; Costa, L. C. O.; Molina, R. D.; Amore, D.; Broedel, E.; Seluchi, M. E.; Cunningham, C.; Alvalá, R. C. S.; Marengo, J. A. Recent hydrological droughts in Brazil and their impact on hydropower generation. **Water**, 14, 601, 2022.
- Cunha, A. P. M. A.; Zeri, M.; Deusdará-Leal, K.; Costa, L.; Cuartas, L. A.; Marengo, J. A.; Tomasella, J.; Vieira, R. M.; Barbosa, A. A.; Cunningham, C.; Garcia, J. V. C.; Broedel, E.; Alvalá, R.; Ribeiro-Neto, G. Extreme drought events over Brazil from 2011 to 2019. **Atmosphere**, 10, 642, 2019.
- da Rocha, R. P.; Morales, C. A.; Cuadra, S. V.; Ambrizzi, T. Precipitation diurnal cycle and summer climatology assessment over South America: an evaluation of Regional Climate Model version 3 simulations. **Journal of Geophysical Research: Atmospheres**, 114, D10, 2009.
- da Silva, G.D.P.; Branco, D.A.C. Is floating photovoltaic better than conventional photovoltaic? Assessing environmental impacts. **Impact Assessment and Project Appraisal**, 36, 390-400, 2018.
- de Jong, P.; Barreto, T.B.; Tanajura, C.A.S.; Oliveira-Esquerre, K.P.; Kiperstok, A.; Torres, E.A. The impact of regional climate change on hydroelectric resources in South America. **Renewable Energy**, 173, 76-91, 2019.
- de Jong, P.; Barreto, T.B.; Tanajura, C.A.S.; Oliveira-Esquerre, K.P.; Kiperstok, A.; Torres, E.A. The impact of regional climate change on hydroelectric resources in South America. **Renewable Energy**, 173, 76-91, 2021.
- Deng Q.; Alvarado R, Toledo E, Caraguay L. Greenhouse gas emissions, non-renewable energy consumption, and output in South America: the role of the productive structure. **Environmental Science and Pollution Research**, 27, 14477-14491, 2020.

Duffy, P. B.; Brando, P.; Asner, G. P.; Field, C. B. Projections of future meteorological drought and wet periods in the Amazon. **Proceedings of the National Academy of Sciences**, 112, 43, 2015.

Dutta, R.; Chanda, K.; Maity, R. Future of solar energy potential in a changing climate across the world: a CMIP6 multimodel ensemble analysis. **Renewable Energy**, 188, 819-829, 2022.

EPE. Empresa de Pesquisa Energética. Matriz energética e elétrica. Disponível em: <https://www.epe.gov.br/pt/abcdenergia/matriz-energetica-e-eletrica>. Acesso em 05/03/2022.

Esnaola, G.; Ulazia, A.; Sáenz, J.; Ibarra-Berastegi, G. Future changes of global annual and seasonal wind-energy production in CMIP6 projections considering air density variation. **Energy**, 307, 132706, 2024.

Eyring, V., Bony, S., Meehl, G. A., Senior, C. A., Stevens, B., Stouffer, R. J., Taylor, K. E. Overview of the Coupled Model Intercomparison Project Phase 6 (CMIP6) experimental design and organization. **Geoscientific Model Development**, 9, 1937-1958, 2016.

Fernandes, V. R.; Cunha, A. P. M. A.; Pineda, L. A. C.; Leal, K. R. D.; Costa, L. C. O.; Broedel, E.; França, D. A.; Alvalá, R. C. S.; Seluchi, M. E.; Marengo, J. A. Secas e os impactos na região sul do Brasil. **Revista Brasileira de Climatologia**, 28, 561-584, 2021.

Fleming, A.; Fielke, S.; Jakku, E.; Malakar, Y.; Snow, S.; Clarry, S.; Tozer, C.; Darbyshire, R.; Legge, D.; Samson, A.; Prakash, M.; Hunter, T.; Nguyen, V.; Wealands, K.; Dickson, S.; Hennessy, K.; Bonnett, G. Developing climate services for use in agricultural decision making: Insights from Australia. **Climate Services**, 37, 100537, 2025.

Fowler, H. J.; Blenkisop, S.; Tebaldi, C. Linking climate change modelling to impacts studies: Recent advances in downscaling techniques for hydrological modelling. **International Journal of Climatology**, 27, 1547-1578, 2007.

Geirinhas, J. L.; Russo, A. C.; Libonati, R.; Miralles, D. G.; Sousa, P. M.; Wouters, H.; Trigo, R. M. The influence of soil dry-out on the record-breaking hot 2013/2014 summer in Southeast Brazil. **Scientific Reports**, 12, 5836, 2022.

Gernaat, D. E. H. J.; de Boer, H. S.; Daioglou, V.; Yalew, S. G.; Müller, C.; van Vuuren, D.P. Climate change impacts on renewable energy supply. **Nature Climate Change**, 11, 119-125, 2021.

- Giglio, E. Extractivism and its socio-environmental impact in South America. Overview of the “lithium triangle”. **América Crítica**, 5, 47-53, 2021.
- Gilliland, J. M.; Keim, B.D. Position of the South Atlantic Anticyclone and its impact on surface conditions across Brazil. **Journal of Applied Meteorology and Climatology**, 57, 535-553, 2018.
- Gozzo, L. F.; Palma, D. S.; Custodio, M. S.; Machado, J. P. Climatology and trend of severe drought events in the state of Sao Paulo, Brazil, during the 20th century. **Atmosphere**, 10, 190, 2019.
- Guimberteau, M.; Ronchail, J.; Espinoza, J. C.; Lengaigne, M.; Sultan, B.; Polcher, J.; Drapeau, G.; Guyot, J.-L.; Ducharne, A.; Ciaï, P. Future changes in precipitation and impacts on extreme streamflow over Amazonian sub-basins. **Environmental Research Letters**, 8, 014035, 2013.
- Ha, S.; Zhou, Z.; Im, E.-S.; Lee, Y.-M. Comparative assessment of future solar power potential based on CMIP5 and CMIP6 multimodel ensembles. **Renewable Energy**, 206, 324-335, 2023.
- Hamed, T.A.; Alshare, A. Environmental impact of solar and wind energy – A review. **Journal of Sustainable Development of Energy, Water and Environment Systems**, 10, 1090387, 2022.
- Hampl, N. Energy systems for Brazil's Amazon: Could renewable energy improve Indigenous livelihoods and save forest ecosystems? **Energy Research & Social Science**, 112, 103491, 2024.
- Icaza, D.; Borge-Diez, D.; Galindo, S. P. Analysis and proposal of energy planning and renewable energy plans in South America: Case study of Ecuador. **Renewable Energy**, 182, 314-342, 2022.
- Illangasingha, S.; Koike, T.; Rasmy, M.; Tamakawa, K.; Matsuki, H.; Selvarajah, H. A holistic approach for using global climate model (GCM) outputs in decision making. **Journal of Hydrology**, 626, 130213, 2023.
- IPCC – Intergovernmental Panel on Climate Change. Climate change 2021: The physical science basis. Contribution of working group I to the Sixth Assessment Report of the Intergovernmental Panel on Climate Change. Masson-Delmotte V, Zhai P, Pirani A, Connors SL, et al. Eds. Cambridge University Press, 2021.

Jimenez, J.C.; Marengo, J.A.; Alves, L.M.; Sulca, J.C.; Takahashi, K.; Ferrett, S.; Collins, M. The role of ENSO flavours and TNA on recent droughts over Amazon forests and the Northeast Brazil region. **International Journal of Climatology**, 41, 3761-3780, 2021.

Karasmanaki, E. Is it safe to live near wind turbines? Reviewing the impacts of wind turbine noise. **Energy for Sustainable Development**, 69, 87-102, 2022.

Lambert, Q.; Bischoff, A.; Cueff, S.; Cluchier, A.; Gros, R. Effects of solar park construction and solar panels on soil quality, microclimate, CO₂ effluxes, and vegetation under a Mediterranean climate. **Land Degradation & Development**, 32, 5190-5202, 2021.

Lee, T.; Singh, V.P. *Statistical Downscaling for Hydrological and Environmental Applications*, 1st ed.; Taylor & Francis Group: Boca Raton, FL, USA, 2019.

Lima, C. H. R.; AghaKouchak, A. Droughts in Amazonia: Spatiotemporal variability, teleconnections, and seasonal predictions. **Water Resources Research**, 53, 10824-10840, 2017.

Lima, F. J. L.; Gonçalves, A. R.; Costa, R. S.; Martins, F. R.; Pereira, E. B. Variações na frequência de ventos extremos e seu impacto no setor de energia. **Revista Brasileira de Energia**, 26, 3, 2020.

Liu, B.; Ma, X.; Guo, J.; Li, H.; Jin, S.; Ma, Y.; Gong, W. Estimating hub-height wind speed based on a machine learning algorithm: implications for wind energy assessment. **Atmospheric and Chemistry Physics**, 23, 3181-3193, 2023.

Lopes, M.P.C.; Nogueira, T.; Santos, A.J.L.; Branco, D.C.; Pournan, H. Technical potential of floating photovoltaic systems on artificial water bodies in Brazil. **Renewable Energy**, 181, 1023-1033, 2022.

Lovejoy, T. E.; Nobre, C. Amazon tipping point: last chance for action. **Science Advances**, 5, eaba2949, 2019.

Lucena, A. F. P.; Szklo, A. S.; Schaeffer, R.; Souza, R. R.; Borba, B. S. M. C.; Costa, I. V. L.; Pereira Júnior, A. O.; Cunha, S. H. F. The vulnerability of renewable energy to climate change in Brazil. **Energy Policy**, 37, 879-889, 2020.

Maraun, D.; Widmann, M. *Statistical Downscaling and Bias Correction for Climate Research*. Cambridge University Press: Cambridge, UK, 2018.

Marengo, J. A.; Chou, S. C.; Kay, G.; Alves, L. M.; Pesquero, J. F.; Soares, W. R.; Santos, D. C.; Lyra, A. A.; Sueiro, G.; Betts, R.; Chagas, D. J.; Gomes, J. L.; Bustamante, J. F.; Tavares, P. Development of regional future climate change scenarios in South America using the Eta CPTec/HadCM3 climate change projections: Climatology and regional analyses for the Amazon, São Francisco and the Paraná River basins. **Climate Dynamics**, 38, 1829-1848, 2012.

Marengo, J. A.; Torres, R. R.; Alves, L. M. Drought in Northeast Brazil: past, present, and future. **Theoretical and Applied Climatology**, 129, 11891200, 2016a.

Marengo, J. A.; Espinoza, J. C. Extreme seasonal droughts and floods in Amazonia: causes, trends and impacts. **International Journal of Climatology**, 36, 1033-1050, 2016b.

Marengo, J. A.; Alves, L. M.; Alvala, R. C. S.; Cunha, A. P.; Brito, S.; Moraes, O. L. L. Climatic characteristics of the 2010-2016 drought in the semi-arid Northeast Brazil region. **Anais da Academia Brasileira de Ciências**, 90, 1973-1985, 2018.

Marengo, J. A.; Cunha, A. P.; Cuartas, L. A.; Deusdará-Leal, K. R.; Broedel, E.; Seluchi, M. E.; Michelin, C. M.; Baião, C. F. P.; Ângulo, E. C.; Almeida, E. K.; Kazmierczak, M. L.; Mateus, N. P. A.; Silva, R. C.; Bender, F. Extreme drought in the Brazilian Pantanal in 2019-2020: characterization, causes, and impacts. **Frontiers in Water**, 3, 639204, 2021.

Marengo, J. A.; Galdos, M. V.; Challinor, A.; Cunha, A. P.; Marin, F. R.; Vianna, M. S.; Alvala, R. C. S.; Alves, L. M.; Moraes, O. L.; Bender, F. Drought in Northeast Brazil: a review of agricultural and policy adaptation options for food security. **Climate Resilience and Sustainability**, 1, e17, 2022.

Medeiros, F. J.; Oliveira, C. P. Assessment of dry and heavy rainfall days and their projected changes over Northeast Brazil in Coupled Model Intercomparison Project Phase 6 models. **International Journal of Climatology**, 42, 8665-8686, 2022.

Moradian, S.; Gharbia, S.; AghaKouchak, A.; Haghighi, A.T.; Olbert, A.I. Integrated multi-index drought monitoring and projection under climate change. **Atmospheric Research**, 316, 107946, 2025.

Msigwa, G.; Ighalo, J.O.; Yap, P.-S. Considerations on environmental, economic, and energy impacts of wind energy generation: Projections towards sustainability initiatives. **Science of The Total Environment**, 849, 157755, 2022.

Mutz, S. G.; Scherrer, S.; Muceniece, I.; Ehlers, T. A. Twenty-first century regional temperature response in Chile based on empirical-statistical downscaling. **Climate Dynamics**, 56, 2881-2894, 2021.

Nobre, C. A.; Marengo, J. A.; Seluchi, M. E.; Cuartas, A.; Alves, L. M. Some characteristics and impacts of the drought and water crisis in southeastern Brazil during 2014 and 2015. **Journal of Water Resource and Protection**, 8, 252-262, 2016.

Olmo, M. E.; Bettolli, M. L. Statistical downscaling of daily precipitation over southeastern South America: assessing the performance in extreme events. **International Journal of Climatology**, 42, 1283-1302, 2022.

Ortega, G.; Arias, P. A.; Villegas, J. C.; Marquet, P. A.; Nobre, P. Present-day and future climate over Central and South America according to CMIP5/CMIP6 models. **International Journal of Climatology**, 41, 6713-6735, 2021.

Pereira, E. B.; Martins, F. R.; Pes, M. P.; Segundo, E. I. C.; Lyra, A. A. The impacts of global climate changes on the wind power density in Brazil. **Renewable Energy**, 49, 107-110, 2013.

Raven, P. H.; Gereau, R. E.; Phillipson, P. B.; Chatelain, C.; Jenkins, C. N.; Ulloa Ulloa, C. The distribution of biodiversity richness in the tropics. **Science Advances**, 6, eabc6228, 2020.

Reboita, M. S.; Ambrizzi, T. Climate System in a nutshell: an overview for understanding climate change. **International Journal of Development Research**, 12, 53365-53378, 2022.

Reboita, M. S.; da Rocha, R. P.; Dias, C. G.; Ynoue, R. Y. Climate projections for South America: RegCM3 driven by HadCM3 and ECHAM5. **Advances in Meteorology**, 2014, 376738, 2014.

Reboita, M. S.; Dutra, L. M. M.; Dias, C. G. Diurnal cycle of precipitation simulated by RegCM4 over South America: present and future scenarios. **Climate Research**, 70, 39-55, 2016.

Reboita, M. S.; Amaro, T. R.; de Souza, M. R. Winds: Intensity and power density simulated by RegCM4 over South America in present and future climate. **Climate Dynamics**, 51, 187-205, 2018.

Reboita, M. S.; Ambrizzi, T.; Silva, B. A.; Pinheiro, R. F.; da Rocha, R. P. The South Atlantic Subtropical Anticyclone: Present and future climate. **Frontiers in Earth Science**, 7, 8, 2019.

- Reggiani, P.; Todini, E.; Boyko, O.; Buizza, R. Assessing uncertainty for decision-making in climate adaptation and risk mitigation. **International Journal of Climatology**, 41, 2891-2912, 2021.
- Rehbein, J.A.; Watson, J.E.M.; Lane, J.L.; Sonter, L.J.; Venter, O.; Atkinson, S.C.; Allan, J.R. Renewable energy development threatens many globally important biodiversity areas. **Global Change Biology**, 26, 3040-3051, 2020.
- Riahi, K.; van Vuuren, D. P.; Kriegler, E.; Edmonds, J.; O'Neill, B. C.; Fujimori, S.; Bauer, N.; Calvin, K.; Dellink, R.; Fricko, O.; et al. The Shared Socio-economic Pathways and their energy, land use, and greenhouse gas emissions implications: A review. **Global Environmental Change**, 42, 153-168, 2017.
- Rivera, J. A.; Arnould, G. Evaluation of the ability of CMIP6 models to simulate precipitation over Southwestern South America: Climatic features and long-term trends (1901-2014). **Atmospheric Research**, 241, 104953, 2020.
- Ruffato-Ferreira, V.; Barreto, R. C.; Júnior, A. O.; Silva, W. L.; Viana, D. B.; Nascimento, J. A. S.; Freitas, M. A. V. A foundation for the strategic long-term planning of the renewable energy sector in Brazil: hydroelectricity and wind energy in the face of climate change scenarios. **Renewable Sustainable Energy Reviews**, 72, 1124-1137, 2017.
- Sánchez, A.S.; Torres, E.A.; Kalid, R.A. Renewable energy generation for the rural electrification of isolated communities in the Amazon Region. **Renewable and Sustainable Energy Reviews**, 49, 278-290, 2015.
- Satymov, R.; Bogdanov, D.; Breyer, C. Global-local analysis of cost-optimal onshore wind turbine configurations considering wind classes and hub heights. **Energy**, 256, 124629, 2022.
- Schaeffer, R.; Szklo, A. S.; Lucena, P.; Frossard, A.; Borba, M. C.; Soares, B.; Nogueira, P.; Pinheiro, L.; Fleming, F. P.; Troccoli, A. Energy sector vulnerability to climate change: a review. **Energy**, 38, 1-12, 2012.
- Schaeffer, R.; Szklo, A. S.; Lucena, P.; Frossard, A.; Borba, M. C.; Soares, B.; Nogueira, P.; Pinheiro, L.; Fleming, F. P.; Troccoli, A. Adaptação às mudanças climáticas no Brasil: cenários e alternativas. 2015.

Serrão, E.A.O.; Silva, M.T.; Ferreira, T.R.; Ataíde, L.C.P.; Wanzeler, R.T.S.; Silva, V.P.R.; Lima, A.M.M.; Sousa, F.A.S. Large-Scale hydrological modelling of flow and hydropower production, in a Brazilian watershed. **Ecohydrology & Hydrobiology**, 21, 23-35, 2021.

Seth, A.; Fernandes, K.; Camargo, S. J. Two summers of São Paulo drought: origins in the western tropical Pacific. **Geophysical Research Letters**, 42, 10816-10823, 2015.

Silva, M. L.; Oliveira, C. P.; Silva, C. M. S.; Araújo, J. M. Dynamic downscaling of climate simulations and projected changes in tropical South America using RegCM4.7. **International Journal of Climatology**, Early View, 2023.

Solman, S. A.; Blázquez, J. Multiscale precipitation variability over South America: Analysis of the added value of CORDEX RCM simulations. **Climate Dynamics**, 53, 1547-1565, 2019.

Solman, S. A.; Bettolli, M. L.; Doyle, M. E.; Olmo, M. E.; Feijoo, M.; Martinez, D.; Blázquez, J.; Balmaceda-Huarte, R. Evaluation of multiple downscaling tools for simulating extreme precipitation events over southeastern South America: a case study approach. **Climate Dynamics**, 57, 1241-1264, 2021.

Sonter, L.J.; Dade, M.C.; Watson, J.E.M.; Valenta, R.K. Renewable energy production will exacerbate mining threats to biodiversity. **Nature Communications**, 11, 4174, 2020.

Sulca, J.; Vuille, M.; Timm, O. E.; Dong, B.; Zubieta, R. Empirical–statistical downscaling of austral summer precipitation over South America, with a focus on the Central Peruvian Andes and the Equatorial Amazon Basin. **Journal of Applied Meteorology and Climatology**, 60, 65-85, 2021.

Tawalbeh, M.; Al-Othman, A.; Kafiah, F.; Abdelsalam, E.; Almomani, F.; Alkasrawi, M. Environmental impacts of solar photovoltaic systems: A critical review of recent progress and future outlook. **Science of The Total Environment**, 759, 143528, 2021.

Thielen, D.; Schuchmann, K.-L.; Ramoni-Perazzi, P.; Marquez, M.; Rojas, W.; Quintero, J. I.; Marques, M. I. Quo vadis Pantanal? Expected precipitation extremes and drought dynamics from changing sea surface temperature. **PLoS ONE**, 15, e0227437, 2020.

Trindade, A.; Verba, N.; Farias, N.; Ramon, D.; Gyamfi, K.; da Silva, H.; Viana, V. Impact evaluation of solar photovoltaic electrification: Indigenous community case study in Brazilian Amazon. **Environmental and Earth Sciences Proceedings**, 15, 16, 2022.

- Usman, A.; Ameta, S.K.; Tukur, A.; Danjuma, M.S.; Yusuf, T.U.; Hamza, Y.G.; Bolya, K. Overview of the adverse effects of renewable energy sources. **International Journal for Research in Applied Science & Engineering Technology**, 8, 477-486, 2020.
- Vasquez-Arroyo, E.; Silva, F.; Santos, A.; Cordeiro, D.; Marengo, J. A.; Lucena, A. F. P. Climate impacts in the Brazilian energy security: analysis of observed events and adaptation options. **Sustainability in Debate**, 11, 157-176, 2020.
- Washburn, C.; Pablo-Romero, M. Measures to promote renewable energies for electricity generation in Latin American countries. **Energy Policy**, 128, 212-222, 2019.
- Yang, X.; Tao, Y.; Jin, Y.; Ye, B.; Ye, F.; Duan, W.; Xu, R.; Zeng, Z. Time resolution of wind speed data introduces errors in wind power density assessment. **Energy Conversion and Management**, 24, 100753, 2024.
- Zhang, T.; Huang, Y.; Liao, H.; Gong, X.; Peng, B. Short-term power forecasting and uncertainty analysis of wind farm at multiple time scales. **Institute of Electrical and Electronics Engineers Access**, 12, 25129-25145, 2024.
- Zheng, C. W.; Li, X. Y.; Luo, X.; Chen, X.; Qian, Y. H.; Zhang, Z. H.; Gao, Z. S.; Du, Z. B.; Gao, Y. B.; Chen, Y. G. Projection of future global offshore wind energy resources using CMIP6 data. **Atmosphere-Ocean**, 57, 134-148, 2019.
- Zhuo, C.; Wei, L.; Zhangrong, P.; Chenchen, L.; Huiyuan, W.; Junhong, G. Spatiotemporal changes in PV potential and extreme characteristics in China under SSP scenarios. **Energy**, 320, 135215, 2025.
- Zuluaga, C. F.; Avila-Diaz, A.; Justino, F. B.; Martins, F. R.; Ceron, W. L. The climate change perspective of photovoltaic power potential in Brazil. **Renewable Energy**, 193, 1019-1031, 2022.